DEPARTAMENTO DE PSICOLOGÍA DE LA SALUD

Instituto Universitario de Investigación

"Centro de Investigación Operativa" (CIO)

PROYECTO DE TESIS DOCTORAL

2015

COMPUTATIONAL FLUID DYNAMICS of VENTRICULAR CATHETERS for HYDROCEPHALUS

MARCELO GALARZA y VICENTINI

UNIVERSITAS
Miguel
Hernández

DÑA. OLGA PELLICER PORCAR, Doctora en Psicología y profesora del Departamento de Psicología de la Salud, y **DON JOSÉ MARÍA AMIGÓ GARCÍA,** Doctor en Ciencias Físicas, Catedrático de la Universidad y profesor del Departamento de Estadística, Matemáticas e Informática,

CERTIFICAMOS:

Que la Tesis titulada **"COMPUTATIONAL FLUID DYNAMICS of VENTRICULAR CATHETERS for HYDROCEPHALUS"**, presentada por **MARCELO GALARZA**, para optar al grado de Doctor, ha sido realizada bajo nuestra dirección en el Departamento de Psicología de la Salud de la Universidad Miguel Hernández.

Considerando que se trata de un trabajo de investigación original que reúne los requisitos establecidos en la legislación vigente autorizamos su presentación.

Y para que así conste, firmamos el presente certificado en Elche, el 14 de diciembre del 2015.

FDO: DRA. OLGA PELLICER PORCAR

FDO: DR. JOSÉ MARÍA AMIGÓ GARCÍA

UNIVERSITAS
Miguel
Hernández

DON JUAN CARLOS MARZO CAMPOS, Director del Departamento de Psicología de la Salud de la Universidad Miguel

INFORMA:

Favorablemente que la Tesis titulada **"COMPUTATIONAL FLUID DYNAMICS of VENTRICULAR CATHETERS for HYDROCEPHALUS"**, de la que es autor el doctorando MARCELO GALARZA y dirigida por los doctores OLGA PELLICER PORCAR y JOSÉ MARÍA AMIGÓ GARCÍA, tiene la conformidad de este Departamento para que sea depositada y presentada para exposición pública, ya que cumple los requisitos en cuanto a forma y contenido.

Elche, 14 de diciembre de 2015.

FDO: DR. JUAN CARLOS MARZO CAMPOS

UNIVERSITAS
Miguel
Hernández

TESIS DOCTORAL

Departamento de Psicología de la Salud

Instituto Universitario de Investigación

"Centro de Investigación Operativa" (CIO)

2015

Tutores académicos: Dra. Olga Pellicer Porcar (DPS), Dr. José María Amigo García (CIO)

UNIVERSITAS
Miguel
Hernández

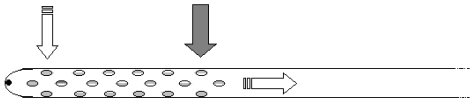

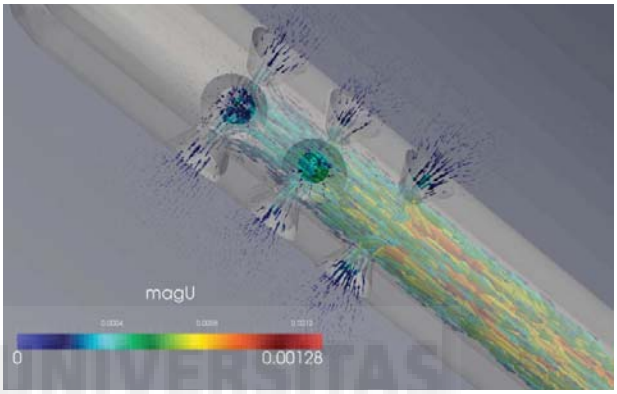

*The richness of **fluid mechanics** is due in large part to a term in the basic equation of the motion of fluids which is nonlinear--i.e., one that involves the fluid velocity twice over. It is characteristic of systems described by nonlinear equations that under certain conditions they become unstable and begin behaving in ways that seem at first sight to be **totally chaotic**.*

Copyright © 1994-2001 Encyclopædia Britannica, Inc. Vol 23:p. 747

UNIVERSITAS
Miguel
Hernández

Dedication:

To the one who suffer in silence, awaiting for your response

Acknowledgements:

To my mentors, Olga, for loyal and unbroken support and José María for unremitting support, limitless time and thoughtful ideas. To Ángel for making most if not *all* the work possible, and to José for his comments at the right time. To my sons Simon and Isabel for their love, and, to my mother Silvia, to my sister Claudia, and to Stefania, all for being there. Finally, to my patients for teaching me relentlessly.

UNIVERSITAS
Miguel
Hernández

CONTENTS

UNIVERSITAS
Miguel
Hernández

Ph.D. DISSERTATION ABSTRACT

Normal-pressure hydrocephalus (NPH) was the first treatable type of dementia ever described. Hakim and Adams described the entity they called normal pressure hydrocephalus in 1965 (Hakim & Adams, 1965). Cerebrospinal fluid shunting for hydrocephalus was the first wide treatment available for the disease. In the following years, an initially uncritical enthusiasm for cerebrospinal fluid (CSF) shunting was gradually dampened because of the underdeveloped shunt technology, low clinical success rates, and frequent complications (Dippel & Habbema, 1993).

The most frequent complication is ventricular catheter obstruction, which may account for 50 to 80% of newly inserted shunts (Bergsneider et al., 2006). Although many factors contribute to this (Harris & McAllister, 2012), the main one is related to flow characteristics of the catheter within the hydrocephalic brain (Harris & McAllister, 2012; Lin, Morris, Olivero, Boop & Sanford, 2003). A landmark study in 2003 addressed the problem of fluid characteristics in ventricular catheters (Lin et al., 2003) by using a 2-D simulation program of computational fluid dynamics (CFD). This study revealed important information related to this dreaded complication. That is, that the major part of the flow occurs through the most proximal catheter´s holes.

Currently, to our knowledge, there is no research that has used simulation software in 3-D CFD to study different models of catheters currently in use, and, new designs of catheters for the treatment of this disease.

So the main objectives of this dissertation are:

- To study flow dynamics in five ventricular catheters models currently in use.
- To create other five new designs of ventricular catheters having different holes distributions and different hole sizes. In order that these variations in the geometric characteristics of catheters significantly alter the liquid mass flow that enters the catheter, avoiding or minimizing the obstruction thereof.
- To study the flow patterns that can be found in the different configurations of ventricular catheters, by using new models of these.
- To establish a set of universal mathematical parameters that can be used to develop new designs of ventricular catheters with improved flow dynamics.

To achieve these objectives, current and new models of ventricular catheters will be studied study by using, never used before for this purpose, a simulation program 3-D computational fluid dynamics. The general procedure for the development of a CFD

model involves incorporating the physical dimensions of the system to be studied into a virtual wire-frame model. The shape and features of the actual physical model are transformed into coordinates for the virtual space of the computer and a CFD computational grid (mesh) is generated. The fluid properties and motion are calculated at each of these grid points. After grid generation, flow field boundary conditions are applied and the fluid's thermodynamic and transport properties are included. At the end, a system of strongly coupled, nonlinear, partial differential conservation equations governing the motion of the flow field are numerically solved. This numerical solution describes the fluid motion and properties.

In conclusion, it is intended to simulate the operation of the CSF flow in five ventricular catheters currently in use and in other 35 new designs ventricular catheters through a system never used before for this purpose. The parameters for the design of new ventricular catheters will be established. These variable parameters along the catheter perforated tip will allow the fluid to enter the catheter more uniformly along its length, thereby reducing the probability of its becoming occluded. This finding will contribute to a better treatment of hydrocephalus, including, dementia complex hydrocephalus.

Key Words:

Dementia complex hydrocephalus. Normal pressure hydrocephalus. Computational fluid dynamics. Ventricular catheters. Flow characteristics.

DISSERTATION OUTLINE

"Remove numeros et omnia evanescunt" (Aurelius Augustinus Hipponensis)

In the field of neurosciences, hydrocephalus occupies a paramount position. Despite being a central nervous system disease known from ancient times, mystery still surrounds this disease. Archetypically, it was a disease associated to newborns and young children; yet, over time, this situation changed. Although it seems that the number of hydrocephalus, globally speaking, is decreasing nowadays, the number of Dementia complex hydrocephalus related to Normal pressure hydrocephalus (NPH) is increasing worldwide. This paradox is due to two reasons: on one hand, the number of abortions due to related or non-related fetal central nervous system malformations is increasing; while, on the other hand, the number of elders and central nervous system age-related diseases is escalating. Both conditions currently present a rising growth.

The fact is, that after analyzing the pertinent literature, and with more than twenty years of clinical experience in the field, I do have more interrogatives than ascertains:

- What is normal pressure hydrocephalus? Categorically, it is a unique entity? Or, it is a compound one?
- Considering intracranial normal pressure, what is normal ICP?
- What is the real percentage of Dementia complex hydrocephalus versus normal pressure hydrocephalus (NPH)? Do we have to consider, within this disease, patients with clinically evident dementia or all those patients with positive neuropsychological testing?
- Is the number of NPH truly ascending? Or, on the contrary, do we diagnose more? And consequently, do we treat more?
- Now, once hydrocephalus is treated, what is the exact percentage of proximal malfunction in Dementia complex hydrocephalus /NPH? It is evident? Are there truly cases of non-responders or, on the other hand, those are wrong diagnoses-false positives cases?
- It is clinically evident a treated failed case of Dementia complex hydrocephalus? -How far we should go on screening tests?

Cold fact is that the absence of Class I studies determine many, if not all, of these questions. So far, the treatment for this disease is pondered by the insertion of a CSF shunt. Now considering all types of hydrocephalus, we do know that shunts, simply, will fail. It is a general rule, other than the exception. Most shunts will get over time, at least, an occluded ventricular catheter.

To follow the aim of this dissertation, exposed in the abstract, in ***Chapter 1*** we will expose the link between hydrocephalus and shunts. The diagnosis of hydrocephalus and its treatment with CSF shunts. In ***Chapter 2***, we will discuss the relationship between shunts and catheters, and, mainly its inherent problems. We will also give an introduction about *Computational fluid dynamics* which is the main system we will use to get our investigations done. ***Chapter 3*** *(Galarza, Giménez, Pellicer, Valero, & Amigó, 2014)* is our first investigational study: it is a 3-D analysis by computational fluid dynamics of ventricular catheters used for the treatment of hydrocephalus. These are current catheters used on an everyday basis. In our second study, ***Chapter 4,*** *(Galarza, Giménez, Valero, Pellicer & Amigó, 2015)* we will present new designs of ventricular catheters for hydrocephalus designed by 3-D computational fluid dynamics with improved flow characteristics. Next, in our third study, ***Chapter 5****, (Galarza, Giménez, Pellicer, Valero, Martínez-Lage & Amigó, 2015)* by using our previous experience with our methodology, we will present the basic cerebrospinal fluid flow patterns that may be found in ventricular catheters prototypes. In addition, in the same chapter, we will investigate the influence of hole geometry on the flow distribution in ventricular catheters *(Giménez, Galarza, Pellicer, Valero, & Amigó, 2015,in publication)* All these empirical studies constitute the previous step of our fifth and last investigational study. In ***Chapter 6,*** *(Galarza, Giménez, Pellicer, Valero, & Amigó, 2015)* we will present the parametric study of the design of ventricular catheters for hydrocephalus. This study is a series of parameters, presented in a mathematical and universal way of what we have found. Also, is a study for the development and construction of future ventricular catheters with improved flow characteristics. Finally, in ***Chapter 7***, we will discuss the major findings of the previous chapters of the dissertation; it will also highlight the foremost conclusions. Still, the main message of this final chapter is to give future perspectives and, precisely, indicate the directions to follow in the path of breaching the general rule: that most shunts will get over time, at least, an occluded ventricular catheter.

Chapter 1:

The link between hydrocephalus and shunts

1.1 Hydrocephalus and subtypes

Hydrocephalus, a term derived from the Greek words “hydro” meaning water and “cephalus” meaning head, is a disorder whose primary characteristic is excessive accumulation of fluid in the brain, with the result in an abnormal widening of spaces in brain called ventricles, causing potentially harmful pressure in brain tissue.

Hydrocephalus is defined according to its pathophysiology. From congenital to dementia complex hydrocephalus there is a wide variety of entities. All responds to disturbances of the CSF within the brain. Yet, among all of them there is no single pathognomonic sign. For example, the most common radiological sign, the ventricular dilation of the brain, is not seen in a specific type of hydrocephalus, in this case, the slit ventricle hydrocephalus, a subtype of hydrocephalus with very small, sometimes even “rigid” ventricles that has been treated before with a CSF shunt, and suffered of overdrainage.

Most typical, though not without exceptions, hydrocephalus can be differentiated in communicating and not communicating. This condition is defined according if there is an anatomical flow obstruction within the ventricular system or at the 4th ventricle outlets ***(Fig 1).***

Congenital pediatric, congenital adult, acute, or secondary chronic (post-infectious, post-trauma or post-hemorrhagic) hydrocephalus was differentiated from idiopathic adult hydrocephalus. At the end, a rigorous definition of hydrocephalus is surprisingly difficult and is becoming more complicated. From a physiological perspective, the finding of enlarged ventricles combined with high ICP represents only one presentation among a variety of disorders ranging from pseudotumor cerebri to low-pressure hydrocephalus to normal-pressure hydrocephalus (Bergsneider et al., 2006).

This last, normal-pressure hydrocephalus (NPH) is characterized by a combination of clinical and radiological findings arising mostly in late adulthood. The mean basal intracranial pressure (ICP) is normal or only mildly elevated in the supine adult. The cardinal symptoms of NPH are gait impairment, dementia, and urinary incontinence. Imaging studies of the brain reveal ventriculomegaly without any marked degree of cortical atrophy.

The Adams and Hakim (Adams, Fisher, Hakim, Ojemann & Sweet, 1965; Hakim, 1964; Hakim & Adams, 1965) description could be considered the first neurological account of primary (idiopathic) normal-pressure hydrocephalus (iNPH) occurring in adult patients. When presenting with clinical symptoms related to dementia it is called Dementia complex hydrocephalus. However, it is surprising that experienced clinicians or pathologists could not detect such a disease for many centuries when the observational method is a key point of medical evaluation (Missori, Paolini & Currà, 2010). Regarding our clinical experience, cognitive decline is just on possible symptom in iNPH. And the one which has the lowest rate of recovery compared to gait and incontinence. All iNPH need to have gait disturbance as minimum while patients can have typical iNPH without any cognitive decline. Typically, these are the ones with best recovery.

Primary (idiopathic) normal-pressure hydrocephalus (iNPH) is distinguished from secondary normal-pressure hydrocephalus (sNPH), whose common causes are subarachnoid hemorrhage, meningitis, and traumatic brain injury (Mori, 2001). A common feature of iNPH and sNPH is that neither involves any obstruction to the flow of CSF within or at the outlet of the ventricular system of the brain (Kiefer & Unterberg, 2012).

We can deduce that, if definition is not straightforward, establishing the real incidence and prevalence is quite impossible. Even though, at least two studies addressed this matter. Using a massive advertising campaign in Norway, Brean and Eide (2008) found an incidence of 5.5 per 100,000 and prevalence of 21.9 per 100,000 for suspected iNPH. Prevalence ranged from 3.3 per 100,000 for people 50 to 59 years of age, to 49.3 per 100,000 for people 60 to 69 years of age, to 181.7 per 100,000 for people 70 to 79 years of age. A recent study of possible symptoms of iNPH found that at least 21.2% of nursing home patients have gait impairment, 9.4% of whom also have dementia and 14.7% of whom also have incontinence (Marmarou, Young & Aygok, 2007). There are no official studies made in Spain. We may assume that the same incidence can be extrapolated to this country.

Regarding its pathophysiology, one theory to explain iNPH is that poor venous compliance, which has been demonstrated in the superior sagittal sinus of iNPH patients (Shprecher, Schwalb & Kurlan, 2008), impairs both cerebrospinal fluid (CSF) pulsations, with secondary flow impairment through the aqueduct, and CSF absorption through arachnoid granulations (Bateman, 2000).

In 2005 the iNPH guidelines were published. This report contained evidence-based guidelines for establishing clinical diagnosis of iNPH, with the intention to facilitate future epidemiological studies of INPH, to promote earlier and more accurate diagnosis, and ultimately to improve treatment outcome. The description of idiopathic normal-pressure hydrocephalus classification included a *probable*, a *possible*, and an *unlikely* category ***(Table 1).***

Table 1.
Description of idiopathic normal-pressure hydrocephalus classification: Probable, possible, and unlikely categories.

Probable NPH
I. History Symptoms should be confirmed by a family member or someone familiar with the person's previous and current condition. a. Insidious vs. acute onset b. Symptoms begin after 40 years old c. Person shows symptoms for at least 3 to 6 months d. No preceding event such as head trauma, intracerebral hemorrhage, meningitis, or other known causes of secondary hydrocephalus. e. Progression over time f. No other neurological, psychiatric, or general medical conditions that can explain the presenting symptoms
II. Brain Imaging a. Ventricular enlargement not completely caused by brain atrophy or congenital enlargement. b. No obvious obstruction to CSF flow c. At least one of the following: 1. Enlargement of the lateral ventricles not entirely caused by brain atrophy. 2. Callosal angle of 40 degrees or more 3. Evidence of altered brain water content, including periventricular signal changes on CT and MRI not attributable to microvascular ischemic changes or demyelination 4. An aqueductal or fourth ventricular flow void on MRI Other brain imaging findings may be supportive of an INPH diagnosis but are not required for a Probable designation 1. A brain imaging study performed before onset of symptoms showing smaller ventricular size or without evidence of hydrocephalus 2. Radionuclide cisternogram showing delayed clearance of radiotracer over the cerebral convexities after 48–72 h 3. Cine MRI study or other technique showing increased ventricular flow rate 4. A SPECT-acetazolamide challenge showing decreased periventricular perfusion that is not altered by acetazolamide

III. Clinical
The classical definition findings of gait/balance disturbance must be present, plus at least one other area of impairment in cognition, urinary symptoms, or both.
Gait/Balance.
At least two symptoms should be present and not due to other conditions.
a. Decreased step height
b. Decreased step length
c. Decreased cadence (speed of walking)
d. Increased trunk sway during walking
e. Widened standing base
f. Toes turned outward on walking
g. Retropulsion (spontaneous or provoked)
h. En bloc turning (turning requiring three or more steps for 180 degrees)
i. Impaired walking balance, as shown by two or more corrections out of eight steps on tandem gait testing
Cognition.
At least two symptoms should be present and not due to other conditions.
a. Psychomotor slowing (increased response latency)
b. Decreased fine motor speed
c. Decreased fine motor accuracy
d. Difficulty dividing or maintaining attention
e. Impaired recall, especially for recent events
f. Executive dysfunction
g. Behavioral or personality changes
Urinary Incontinence.
Either one of the following should be present.
a. Episodic or persistent urinary incontinence not attributable to primary urological disorders
b. Persistent urinary incontinence
c. Urinary and fecal incontinence
Or any two of the following should be present
a. Urinary urgency as defined by frequent feeling of a need to void
b. Urinary frequency as defined by more than six voiding episodes in an average 12-hour period despite normal fluid intake
c. The need to urinate more than two times in an average night

IV. Physiological
CSF opening pressure in the range of 5-18 mm Hg (or 70-245 mm H2O) determined by lumbar puncture or comparable procedure.

Possible INPH

A diagnosis of Possible INPH is based on historical, brain imaging, and clinical and physiological criteria
I. History
Reported symptoms may
a. Have a subacute or indeterminate mode of onset
b. Begin at any age after childhood
c. May have less than 3 mo or indeterminate duration
d. May follow events such as mild head trauma, remote history of intracerebral hemorrhage, or childhood and adolescent meningitis or other conditions that in the judgment of the clinician are not likely to be causally related
e. Coexist with other neurological, psychiatric, or general medical disorders but in the judgment of the clinician not be entirely attributable to these conditions
f. Be nonprogressive or not clearly progressive
II. Brain imaging
Ventricular enlargement consistent with hydrocephalus but associated with any of the following
a. Evidence of cerebral atrophy of sufficient severity to potentially explain ventricular size
b. Structural lesions that may influence ventricular size
III. Clinical
Symptoms of either
a. Incontinence and/or cognitive impairment in the absence of an observable gait or balance disturbance
b. Gait disturbance or dementia alone
IV. Physiological
Opening pressure measurement not available or pressure outside the range required for probable INPH

Unlikely INPH

1. No evidence of ventriculomegaly
2. Signs of increased intracranial pressure such as papilledema
3. No component of the clinical triad of INPH is present
4. Symptoms explained by other causes (e.g., spinal stenosis)

Note. Adapted from "Diagnosing idiopathic normal-pressure hydrocephalus. INPH Guidelines, Part II." by N. Relkin, A. Marmarou, P. Klinge, M. Bergsneider and P.M. Black , 2005, *Neurosurgery, 57*, pp. 6-7. Copyright 2005 by the Congress of Neurological Surgeons.

1.2 Clinical Symptoms of iNPH

There is considerable disparity in the nature, severity, and course of progression of the symptoms of iNPH. The natural history of untreated iNPH has not been well characterized, and it is not clear whether all cases ultimately progress, nor is the time of progression established for the majority of cases. Progression of symptoms is normally expected but may not be uniform over the course of the disease. Symptoms of iNPH in the early stage and late stages of the disease may differ dramatically, as may symptoms in previously treated versus untreated patients. As seen in ***Table 1***, at least two of three components of the so-called classic triad of iNPH need to be present for the diagnosis of iNPH. Gait disturbance tends to be the most readily recognized feature of iNPH, and always has to be present. Yet present in most patients, cognitive disturbances do not occur in all, and the severity of cognitive and motor symptoms does not necessarily correlate at baseline or progress in parallel. Incontinence in iNPH is difficult to distinguish from urinary symptoms associated with other common disorders. The signs and symptoms of iNPH are typically bilateral but may appear lateralized when superimposed on concomitant conditions, such as stroke, nerve radiculopathy, and peripheral neuropathy (Relkin et al., 2005).

As said, cognitive and behavioral manifestations are seen in the majority of patients. Dementia can be present from the initial diagnosis. The severity of cognitive impairments seen in iNPH encompasses a full range from minimally detectable to profoundly severe. The principal cognitive symptoms seen in iNPH are suggestive of a subcortical dementing process, including slowing of thought, inattentiveness, and apathy, as well as encoding and recall problems (Hellström, Klinge, Tans & Wikkelso, 2012; Relkin et al., 2005). True aphasia is unusual in iNPH, although speech output may be disturbed secondary to dysexecutive or motivational problems.

Several neurological conditions may present like iNPH (Bech-Azeddine et al., 2001; Relkin et al., 2005). This is depicted in ***Table 2***. In mild stages, differential diagnosis may be particularly difficult owing to overlap of iNPH-related cognitive impairment with that seen in more prevalent disorders, such as Alzheimer's disease. This overlap occurs because patients with Alzheimer's disease have presenting problems in multiple cognitive domains (Iddon, Pickard, Cross, Griffiths, Czosnyka & Sahakian, 1999).

As iNPH progresses, cognitive impairments may become more generalized and more refractory to treatment. Nevertheless, even in patients with quite advanced dementia may still respond

positively to shunt placement (Bekkelund, Marthinsen & Harr, 1996; Black, 1980). When possible, quantifiable measures of cognitive performance as neuropsychological tests should be used. In this situation, the impairments detected should not be attributable to other conditions such as neurodegenerative disorders, stroke, head trauma, psychoactive medications, or other evident identifiable factors.

Table 2.
Neurological and systemic conditions that may present similarly to idiopathic normalpressure hydrocephalus or present comorbidly.

Neurodegenerative disorders
Alzheimer's disease
Parkinson's disease
Vascular dementia
Cerebrovascular disease
Stroke
Multi-infarct state
Binswanger's disease
Cerebral autosomal dominant arteriopathy, subcortical infarcts, and leukoencephalopathy
Vertebrobasilar insufficiency
Other hydrocephalus disorders
Aqueductal stenosis
Arrested hydrocephalus
Long-standing overt ventriculomegaly syndrome
Noncommunicating hydrocephalus
Other neurodegenerative disorders
Lewy body disease
Huntington's disease
Frontotemporal dementia
Corticobasal degeneration
Progressive supranuclear palsy
Amyotrophic lateral sclerosis
Multisystem atrophy
Spongiform encephalopathy
Infectious diseases
Lyme
Human immunodeficiency virus
Syphilis
Urological disorders
Urinary tract infection
Bladder or prostate cancer
Benign prostatic enlargement

Miscellaneous
B12 deficiency
Collagen vascular disorders
Epilepsy
Depression
Traumatic brain injury
Spinal stenosis
Chiari malformation
arrested hydrocephalus
Wernicke's encephalopathy
Carcinomatous meningitis
Spinal cord tumor

Note. Based on Bech- Azeddine et al. (2001), Relkin et al. (2005) and expert opinion.

Impaired cognitive skills seen in iNPH include most of the time psychomotor slowing, fine motor speed, and fine motor accuracy. While borderline impairment is seen in auditory memory (immediate and delayed), attention concentration, executive function and behavioral or personality changes (Relkin et al., 2005). These deficits are related anatomically to the frontal and temporal lobe. Several imaging studies reports showed these alterations (Hong et al., 2010; Klinge et al., 2008). The locus of dysfunction responsible for dementia in iNPH remains unclear, although the frontostriatal system has been implicated by some investigators (Iddon et al., 1999). Others emphasize the importance of other subcortical structures, including projection fibers passing in proximity to the lateral ventricles (Mataró et al., 2003). Significant correlation with reduced tracer uptake was seen in the mesial frontal and anterior temporal area ***(Fig 2 & 3).*** In fact, anatomical changes of the hippocampus have been demonstrated in both Alzheimer disease and idiopathic normal pressure hydrocephalus (Hong et al. 2010). As well, memory deficits of explicit and implicit type ***(Fig 4 & 5),*** have been demostrated in both conditions (Besson et al., 2014).

1.3 Shunts

The most common accepted treatment for iNPH and the majority of other types of hydrocephalus, is insertion of a ventriculoperitoneal (VP) shunt ***(Fig 6)***. A ventriculoperitoneal (VP) shunt consists of a catheter placed into the ventricles. This is attached to a valve which is connected to a distal catheter. The distal catheter drains the CSF into the peritoneal cavity where it can be absorbed by the body ***(Fig 7)***. There are ventriculoatrial, ventriculopleural, and other types, even less used.

The literature regarding shunts and hydrocephalus is vast. The indication of insertion of a shunt depends strictly on the type of hydrocephalus and the clinical condition of the patient. To sum up, because there are no Class I studies that have addressed the question of comparing operative versus conservative treatment of iNPH, there is insufficient evidence to ascertain the surgical management of iNPH as a standard. Nevertheless, a ventriculoperitoneal (VP) shunt is the main treatment method for all types of hydrocephalus worldwide.

Insertion of a VP shunt is included in the guideline of iNPH (Bergsneider, Black, Klinge, Marmarou & Relkin, 2005) on the basis of a preponderance of the evidence, including well-conducted Class II prospective studies demonstrating acceptable risk-to-benefit ratios in shunted patients (Boon et al. 1998; Børgesen, 1984; Malm et al. 1995; Malm, Kristensen, Fagerlund, Koskinen & Ekstedt, 1995; Malm, Kristensen, Stegmayr, Fagerlund & Koskinen, 2000; Meier, Kiefer & Sprung, 2004; Raftopoulos et al., 1994; Raftopoulos et al., 1996). More recently, the study by Linnea Torsnes et al. provides a detailed review based on 43 publications; it demonstrates a 30-90% success rate from shunt surgery and supports our main point about the shortcomings of diagnoses (Torsnes, Blåfjelldal & Poulsen, 2014).

Endoscopic third ventriculostomy, as an alternative treatment method usually applied in certain cases of obstructive hydrocephalus, may play a role in the treatment of selected iNPH patients. Evidently, most of the experience with this technique comes from the pediatric field (Etus & Ceylan, 2005a; Etus & Ceylan, 2005b) Yet, the benefit of performing endoscopic third ventriculostomy in iNPH cases is relegated to a Class III study (Gangemi, Maiuri, Buonamassa, Colella & De-Divitiis, 2004) The risk-to-benefit ratio must be individualized for each patient with the following issues in mind: 1) shunt-responsive iNPH exists with reasonable certainty, 2) there

are low surgical risks related to comorbidities, and 3) the degree of iNPH-related morbidity warrants the shunt-related risks.

A patient selection should be done prior to consider iNPH treatment. For practical reasons, it is important to identify probable shunt responders in patients diagnosed with iNPH. If the patient is an acceptable candidate for anesthesia, then an iNPH-specific risk-benefit analysis should be performed. In most cases, patients exhibiting negligible symptoms may not be suitable candidates for VP shunt insertion, given the known risks and complications associated with shunting procedures. Hence, in these situations, the indication for treatment of iNPH should be considered closely, given the importance of the possible complications.

Typical *shunt responder* patients were defined by Marmarou, Bergsneider, Relkin, Klinge and Black (2005) ***(Table 3)***.

Table 3.
These are evidence-based neurosurgical practice guidelines for predicting which patients are likely to benefit from shunting. Identifying Shunt-Responsive Patients (Marmarou et al., 2005):

Patient Selection Supplemental Prognostic INPH Tests
•MRI shows no white matter lesions
• Tap test removal of 40 to 50 ml has a positive response
• Prolonged external lumbar drainage over 300 ml
• CSF outflow resistance –infusion tests- (CSF Ro) greater than 18 mm Hg
• CSF-OP in the range of 105 to 190 mm H2O

A typical shunt consists of a catheter placed into the brain ventricles, then connected to a valve which is then connected to a distal catheter. Other than insertion of a VP shunt, the two most commonly used configurations are the ventriculoatrial and ventriculopleural shunts.

The selection of a shunt depends on the type of hydrocephalus and other factors related to non medical situations, like material –hardware- availability; economical, geographical and environmental situations. Contrarily to proximal and distal catheter selection, valve selection is a controversial issue in iNPH and, as well as, in other types of hydrocephalus. The choice of valve type and setting should be based on empirical reasoning and a basic understanding of shunt hydrodynamics (Bergsneider et al., 2005). The phenomenon of “siphoning”, which is defined as CSF overdrainage attributable to the hydrostatic column produced by the shunt catheter, may

become evident in adult patients, and add-on mechanisms were developed to counteract gravity-dependent drainage. These devices are generally called *overdrainage protection systems.* Antisiphon device (ASD) is a special construction system. The ASD is situated in series immediately distal to a standard differential-pressure valve. That is between the valve and the distal catheter. Hence, the most conservative choice is a valve incorporating an ASD, with the understanding that underdrainage, despite a low opening pressure, may occur in a small percentage of patients because of the ASD (Bergsneider et al., 2005; Bergsneider, Peacock, Mazziotta & Becker, 1999). On the basis of the results of retrospective studies, the use of an adjustable valve may be beneficial in the management of iNPH because of the ability to manage both underdrainage and overdrainage problems non-operatively (Zemack & Romner, 2002).

1.4 Shunt Outcome of iNPH

The scales used and the time at which patient outcome is measured are particularly variable throughout the literature. The rates of improvement reported are not identical with the clinical outcome of shunt treatment. Across studies, "improvement rates" and "outcome after shunt" are lumped together when the clinical results of shunting are described (Klinge, Marmarou, Bergsneider, Relkin & Black, 2005).

Moreover, outcome assessment is complex and incorporates many factors, which do not necessarily relate directly to the alleviation of symptoms by the shunt. For example, the judgment of the patient and his or her family is based primarily on regained functional status and/or improved social abilities. These are rarely studied systematically or incorporated into the assessment of shunt outcome (Larsson, Wikkelso, Bilting & Stephensen, 1991). Whereas the assessment of gait and incontinence can be rather simple, assessment of the dementia component is more difficult and may require more sensitive tests than are currently available. Another factor that confounds the assessment of shunt outcome is the risk-to-benefit ratio on an individual patient basis. As mentioned above, it would seem reasonable that with regard to risk, the patient's life expectancy and comorbidity should be taken into consideration. There is a Class II indication that comorbid factors not related to shunt treatment have influenced the patient's clinical outcome and morbidity in long-term studies (Raftopoulos et al., 1996; Savolainen, Hurskainen, Paljarvi, Alafuzoff & Vapalahti, 2002).

Regarding the distal catheter selection the literature is scarce. Main contributions come from pediatric hydrocephalus cases. Discussions addressed the issue of the right length of the catheter

(Couldwell, LeMay & McComb, 1996); and the presence of slits in the distal end of the catheter (Cozzens & Chandler, 1997). Main experience in adults comes from the contributions of Sotelo (Sotelo, Arriada & López, 2005; Sotelo, Izurieta & Arriada, 2001). Sotelo used an open ventriculoperitoneal bypass with a peritoneal catheter for which the cross-sectional internal diameter was 0.51 mm as a distinctive element for flow resistance. It was evaluated for use in the treatment of adult patients with hydrocephalus showing relatively good results. This was partially reflected in the study by Galbarriatu et al. (2013) who suggested that custom-made peritoneal catheters with larger inner diameter could be a good option for the management of low-pressure hydrocephalus.

Now, concerning the proximal catheter selection, the literature is even more sparse. Although the number of patented ventricular catheters is vast, only a few catheters are available on the market. Most important, there is so far no comparative studies investigating different ventricular catheters. We will develop this issue in the next chapter.

Figures Chapter 1

Figure 1. The first figure of this Thesis depicts the Ventricular System of the Human Brain. The arrow is passing through the interventricular foramen from the third ventricle to the lateral ventricle. The interventricular foramen is also known as the Foramen of Monroe.

1. Lateral ventricle,
2. Interventricular foramen,
3. Third ventricle,
4. Midbrain aqueduct,
5. Fourth ventricle,
6. Central ependymal canal.

Note 1. Based on "The Human Central Nervous System. 4th Ed." by R. Nieuwenhuys, J. Voogd and C. Van- Hujzen .

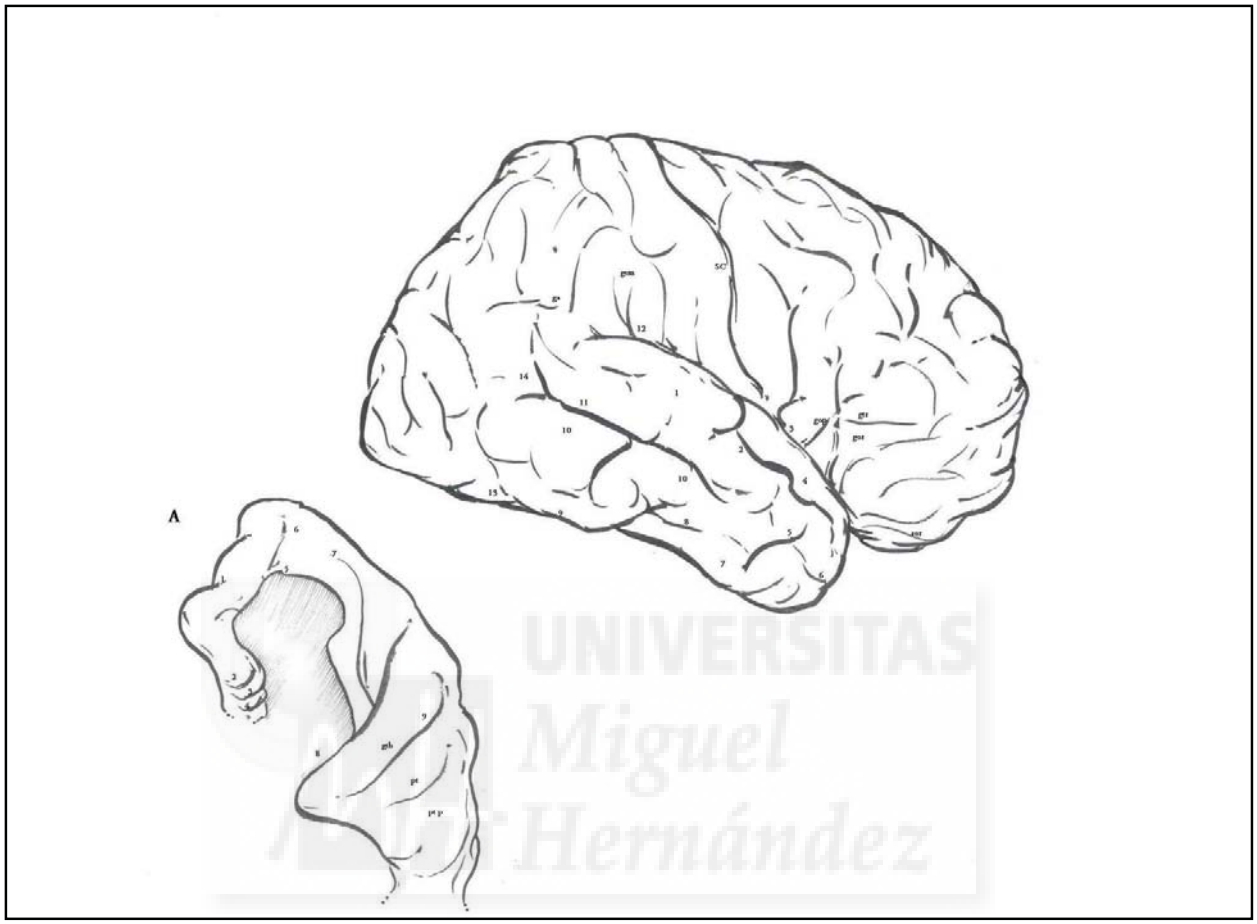

Figure 2. Lateral view of the human brain, with emphasis on the temporal lobe anatomy.

Note 1. SC, Central sulcus; gop, opercular portion of the inferior frontal gyrus; gtr, triangular portion of the inferior frontal gyrus; gor, orbital portion of the inferior frontal gyrus; gsm, supramarginal gyrus; ga, angular gyrus; sor, orbitary gyri and sulci; 1, superior temporal gyrus; 2, superior temporal sulcus; 3, lateral sulcus; 4, superior anterior temporal gyrus; 5, medium anterior temporal gyrus; 6, anterior temporal pole; 7, inferior anterior temporal gyrus; 8, inferior temporal sulcus; 9, inferior posterior temporal sulcus; 10, medium posterior temporal gyrus; 11, superior posterior temporal sulcus; 12, Lateral sulcus posterior part; 13 preoccipital incisura; 14, anterior occipital sulcus. A: superior view of the right temporal lobe, to show the anatomical position of the Heschl transeverse gyri and planum temporal. Pt, planum temporal; ptt, posterior planum temporal; gth, Heschl transverse gyrus. 1, Rhinal sulcus; 2, Uncinate gyrus; 3, band of Giacomini; 4, Ammon horn; 5, Limen insulae; 6, Polar plane; 7, insulae border; 8, Insular plane; 9, temporal transversal sulcus.

Note 2. Based on "The Human Central Nervous System. 4th Ed." by R. Nieuwenhuys, J. Voogd and C. Van- Hujzen .

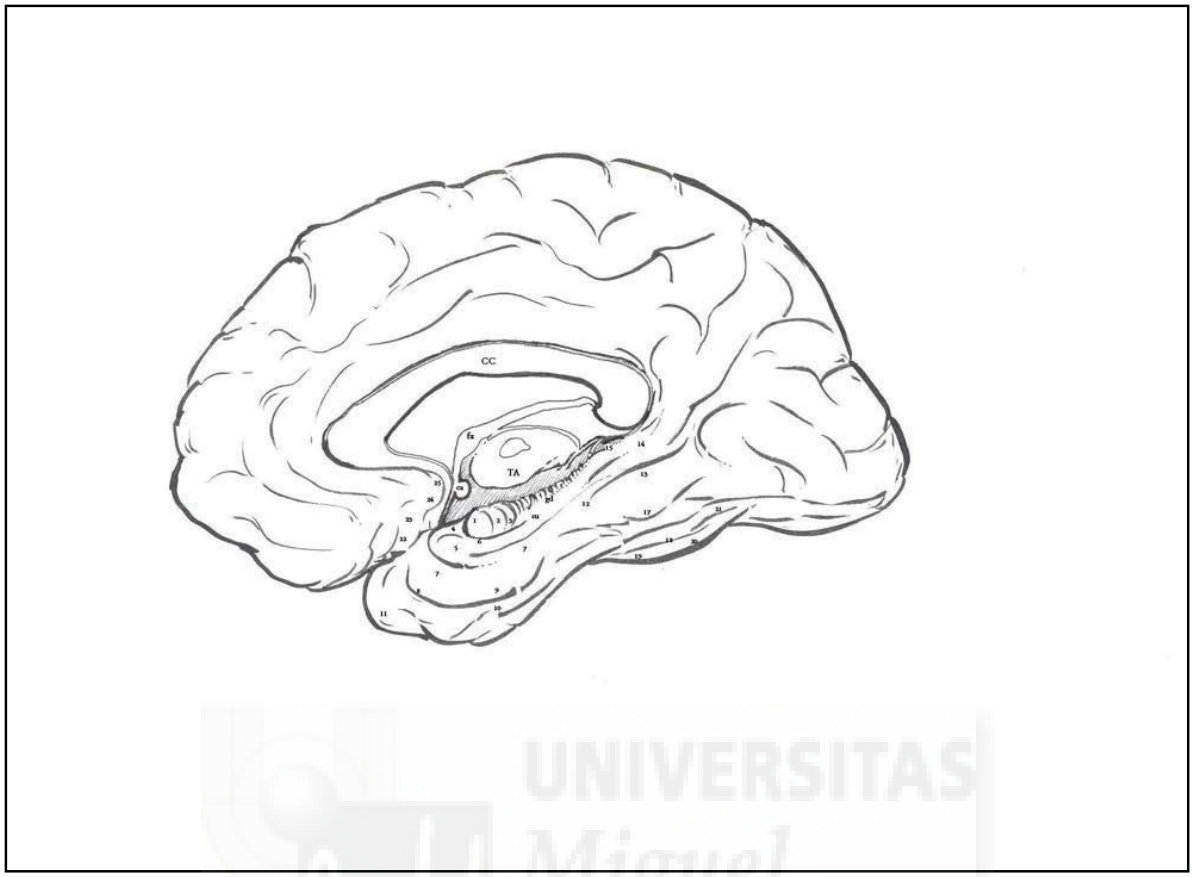

Figure 3. Medial view of the human brain, with emphasis on the temporal lobe anatomy.

Note 1. CC, corpus callosum; TA, thalamus; ca, anterior comisura; fx, Fornix; gd, dentate gyrus; su, subiculum; 1, uncinate gyrus; 2, band of Giacomini; 3, Ammon horn intralimbic gyrus; 4, semilunar gyrus; 5, ambiens gyrus; 6, Uncal incisura; 7, parahippocampal gyrus; 8, rinal sulcus; 9 collateral sulcus; 10 lateral occipitotemporal (fusiform) sulcus; 11, superior temporal gyrus anterior pole; 12, dentate gyrus; 13, anterior calcarine sulcus; 14, Isthmus cingular gyrus; 15, fasciolar gyrus; 16, Indusium griseum; 17, occipitotemporal gyrus medial (lingual); 18, occipitotemporal gyrus lateral (fusiform); 19, occipitotemporal sulcus; 20, inferior temporal gyrus; 21, collateral sulcus; 22, gyrus rectum and anterior para-olfactory sulcus; 23, subcallosal area; 24, posterior para-olfactory sulcus; 25, paraterminal gyrus.

Note 2. Based on "The Human Central Nervous System. 4th Ed." by R. Nieuwenhuys, J. Voogd and C. Van- Hujzen .

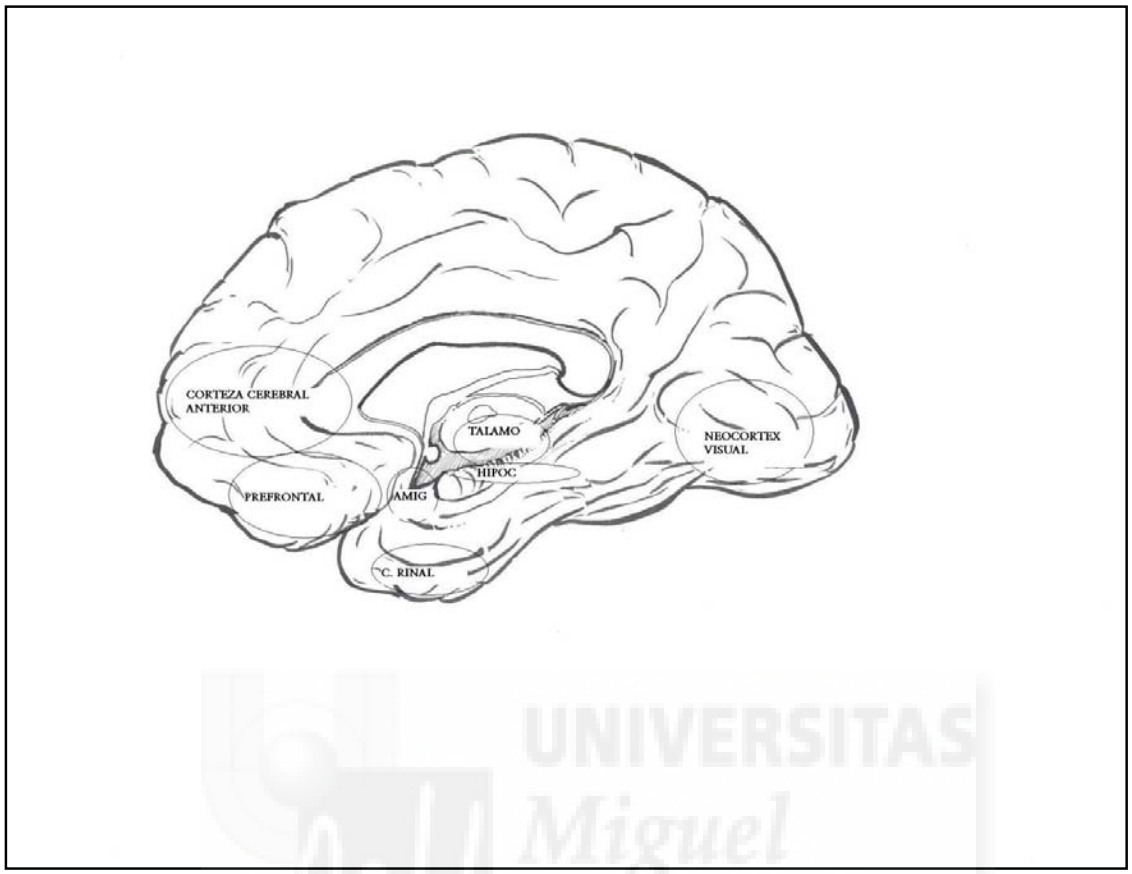

Figure 4. Artistic drawing of a proposed explicit memory neural circuit with anatomical references.

Note. Based on "Behaviorism, cognitivism, and the neuropsychology of memory" by H.L. Petri and M. Mishkin, 1994, *American Scientist*, *82*, 30-37.

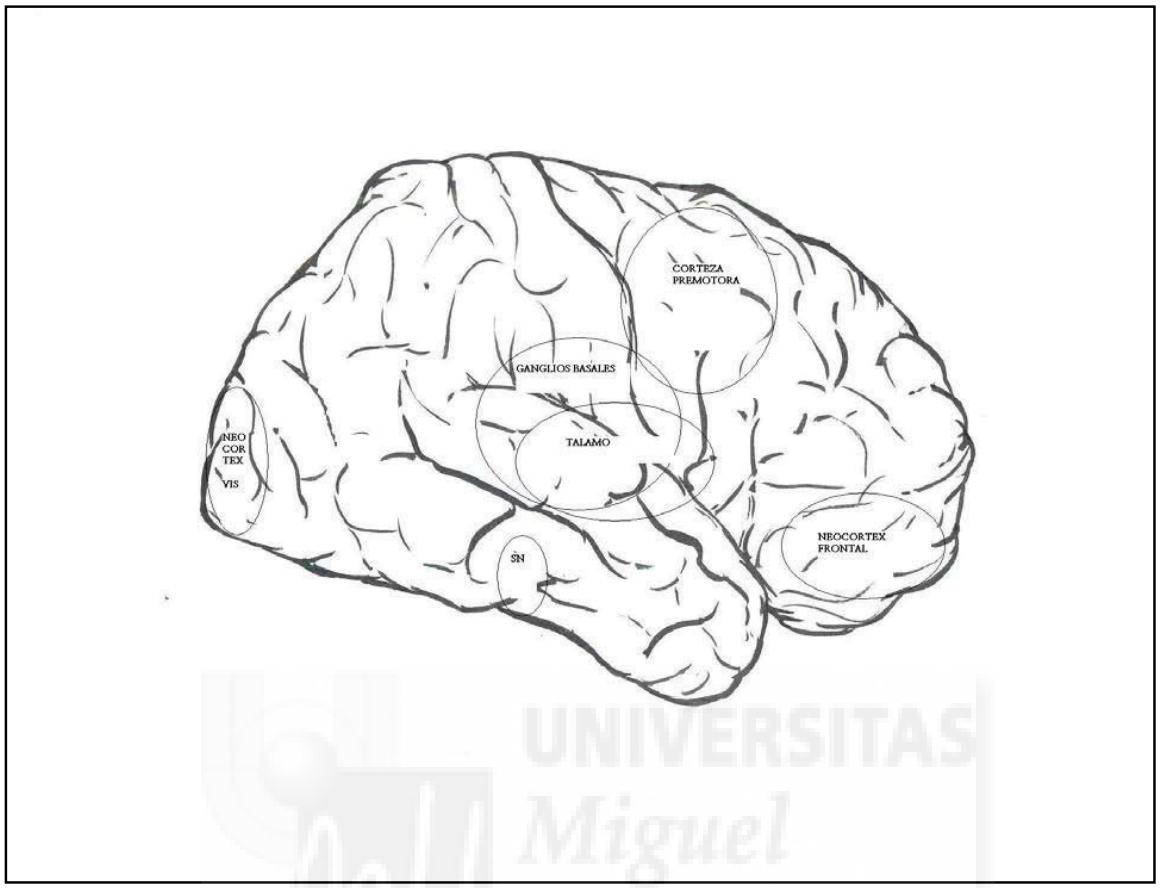

Figure 5. Artistic drawing of a proposed implicit memory neural circuit with anatomical indications *(neocortex vis: neocortex visual; sn: sustancia nigra).*

Note. Based on "Behaviorism, cognitivism, and the neuropsychology of memory" by H.L. Petri and M. Mishkin, 1994, *American Scientist, 82*, 30-37.

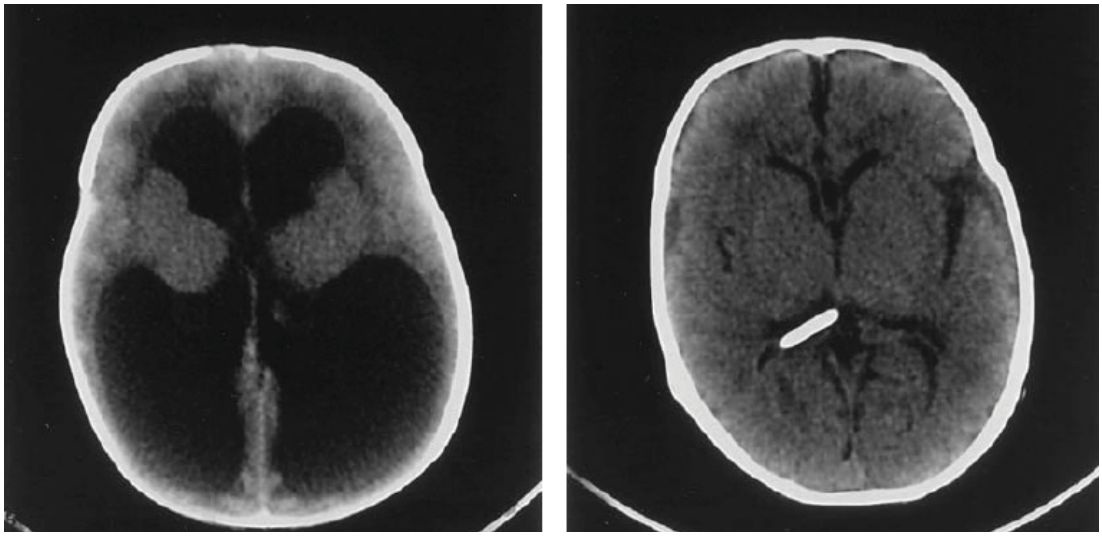

Figure 6. Brain computerized axial tomography (CAT) scans. Axial views.

Note. Hydrocephalus with dilated ventricles and shunted hydrocephalus with collapsed ventricles showing a and ventricular catheter in the occipital horn of the ventricle. This is a case of pediatric hydrocephalus, where you can seen the how the enlarged ventricles disappear while the brain parenchyma expands after shunt insertion. This is not typically seen in cases of iNPH.

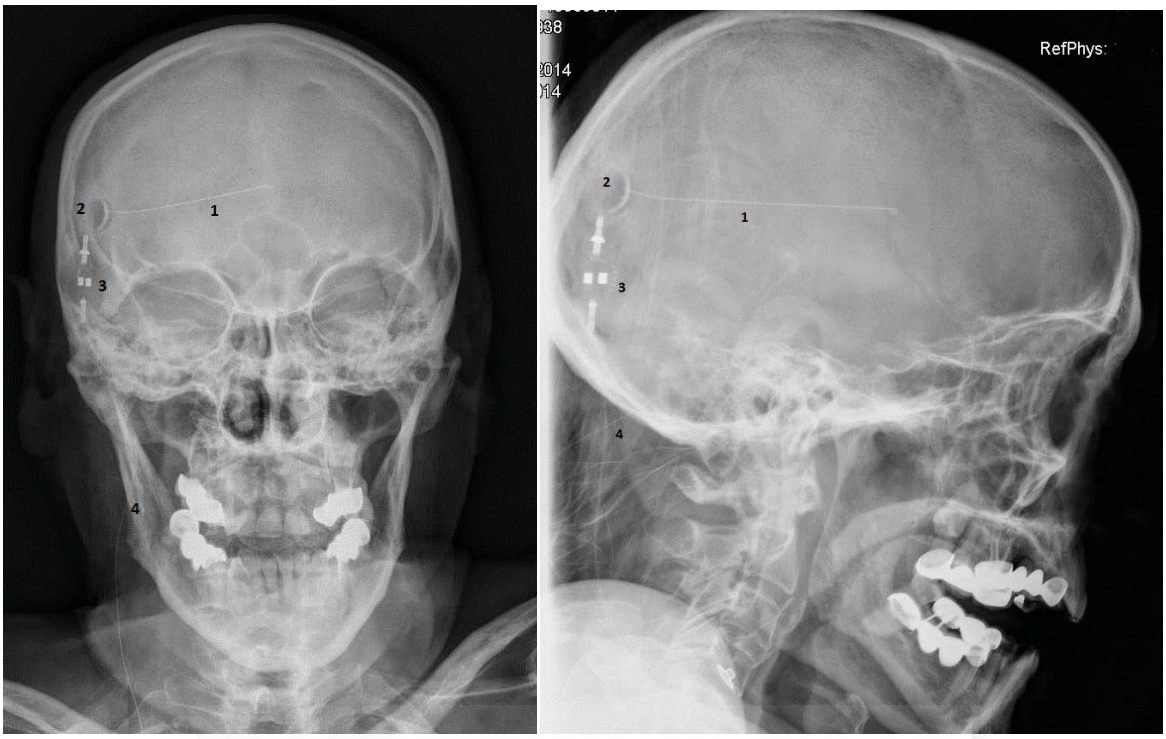

Figure 7. XR cranium.

Note. ap (a), lat (b). Typical shunt components: 1, ventricular catheter; 2, reservoir; 3, valve; 4, distal catheter.

Chapter 2:

Shunts, catheters, problems. *Computational fluid dynamics*

2.1 Types of ventricular catheter

As mentioned previously, most studies address the problems of valve designs and problems related to pressure differences, including overdrainage. Little is mentioned about ventricular catheters (VCs) designs. Currently, there are several available types of ventricular catheters for the treatment of hydrocephalus. The most common designs include silicone elastomer tube with a number of regular holes arranged in 6 or 8 drainage rings, each one with a constant number of holes, typically 2 (opposite with respect to the catheter axis) or 4 (opposite two to two). In most cases, the separation between those rings is identical, although there are designs with varying distances between the drainage rings as well ***(Fig 1).***

Specific types of VC were designed with the purpose of avoiding blockage or obstruction (Kehler, Klöhn, Heese & Glienroth, 2003; Portnoy, 1971), improve CSF flow (Lin, Morris, Olivero, Boop & Sanford, 2003; Thomale et al., 2010), control functionality (Sood, Canady & Ham, 2000), or prevent infections (Winkler et al., 2013).

Adding a peel away covering for VC insertion in order to prevent the holes to get occulded during the brain perforation in its path to the ventricle was developed by Kehler et al. (2003). However, the theoretical advantages attributed to the use of a peel-away sheath to introduce a ventricular catheter could not be confirmed in a randomized study, conducted by the same author (Kheler et al., 2012). They suggested that the proposed role of brain debris in shunt obstructions may be overestimated.

Adding a double catheter for eventual evaluation of VC obstruction and shunt functionality was developed by Sood et al. (2000). Both catheters are joined, so its practical use is limited given that when obstruction occurs it affects both catheters.

Placing inlets or holes in a shorter perforated segment with a closer distance to the VC tip in order to get better flow characteristics were developed by Kaufman and Park (1999) and later by Thomale et al. (2010). The latter author included a laboratory investigation for that purpose.

Adding flanges to the catheter tip was probably the first catheter with a unique design in comparison to the previously available VCs. The Portnoy VC (1971) was used by neurosurgeons for decades, until it was discontinued because of the difficulties for its removal during replacement after catheter obstructions. Although they present a relatively longer survival (Haase & Weeth, 1976), the flanges of the catheter cannot prevent the catheter from being pushed into the brain parenchyma. This is typically seen in children patients of slit ventricle development.

The first catheter being developed with a theoretical basis and constructive laboratory test investigations was the Rivulet VC developed by Lin et al. (2003). By adding "tapering" or progressively smaller holes, they demonstrated in this prototype an equalized flow distribution by fluid dynamics study.

Infection is a serious complication, though most if not all, can be prevented with the proper surgical technique. The incidence of shunt infection has been reported to be as high as 30 to 40 percent (Milhorat, 1972), especially in neonates. More recent studies indicate that acceptable levels are at *5* percent or below. Antibiotic-impregnated, silver-covering ventricular drainage catheters have been developed to prevent or to treat faster this complication (Bayston & Milner, 1981; Winkler et al., 2013).

Also for that purpose, VC made of metal, usually steel, were designed. In the management of shunt infection, the use of ventricular catheters made of silicone rubber for the temporary external drainage of cerebrospinal fluid is usual practice. Nevertheless, the eradication of the primary source of infection may be hindered by the affinity of bacteria to silicone-based material (Birbilis et al., 2013; Vieweg, Kaden & Van Roost, 1996). To our opinion, material construction of VC is of key importance. We will discuss this issue in a fore coming Chapter.

Reported theoretical models of VC include catheters made of electrospun polyurethane (Suresh & Black, 2015), a vibrating device for displacing biological materials (Fox & Norton, 2014), and the development of torsional magnetic microactuators in implantable catheters for removing biological materials (Lee et al., 2011). These prototypes were developed with constructive laboratory investigations with apparent efficacy in an in-vitro environment. There is also a report of a self-cleaning VC prototype without any evidence based support (Ventureyra & Higgins, 1994).

In an attempt to prolong its lifetime, clinical investigations exist for revision of ventricular catheters in situ, included endoscopic recanalization (Pattisapu, Trumble, Taylor, Howard & Kovach, 1999) and intraluminal coagulation (Hudgins & Boydston, 1998). Laboratory investigations for revision of ventricular catheters in situ by using ultrasonic cavitation has been reported (Ginsberg, Drake, Peterson & Cobbold, 2006).

2.2 Anatomy and positioning of a ventricular catheter

There is more literature regarding the accurate placement of a catheter in the ventricle. Most contributions coming from the pediatric hydrocephalus field (Kauffman & Park, 1999; Tuli, O'Hayon, Drake, Clarke & Kestle, 1999). Once again, most studies are retrospective of Class III type. Typical VC placements include the occipital and frontal horns of the ventricles. The best catheter placement, as determined by intraoperative imaging, should leave the tip of the ventricular catheter within the anterior horn of the lateral ventricle, anterior to the choroid plexus lying along the floor of the ventricle. Alternative location for shunt positioning include placement within the occipital horn, well posterior to the glomus of the choroid plexus at the ventricular atrium (Milhorat, 1972). For surgical feasibility, the occipital horn probably is the most common location in permanent placement of VP shunts. Yet, this is changed accordingly to the type of patient and other factors, such as previous shunt history. The length of the VC to leave within the ventricle varies according to the location and patient. Most typical include a 5 cm VC when inserted frontally and 7 to 10 cm when inserted occipitally. This situation will directly influence the length of the perforated section of the VC. We will discuss it in coming *Chapter 3 and 4*.

It has been demonstrated that long term VP shunt function or failure due to irreversible malfunction is directly influenced by the position of the ventricular catheter tip (Albright, Haines & Taylor, 1988). Ideal points for positioning the ventricular catheter tip are superior to the foramen of Monro and in the center of the lateral ventricle body. Early shunt revision may be required for patients in whom the catheter tip contacts the ventricle wall or is located in the septum pellucidum (Yamada, Kitagawa & Teramoto, 2013). There is a rating of the catheter position, where the catheter position is rated in a centralized manner in regard to the 2 cm tip of the perforated part of the catheter (Schaumann & Thomale, 2013).

Devices based on supposing that a convex of skull matches to a sphere, in which the foramen of Monro is the center, a perpendicular direction from the surface of the sphere to inside always directs toward the center, have been developed to accurately insert a VC. Reports of devices for successful placement include those of Ghajar (1985), Schaumann and Thomale (2013) and Yamada et al. (2012).

More recently, placement of VC by using intraoperative imaging guidance, both in children and adults has been reported with variable results (Crowley, 2014; Hermann, Capelle, Tschan & Krauss, 2012; Janson, Romanova, Rudser & Haines, 2014; Levitt et al., 2012; Lind, Tsai, Lind & Law 2009; Whitehead, 2013; Wilson, Stetler, Al-Holou & Sullivan, 2013).

So, by examining different ventricular catheter positions we may encounter variable dispositions of the anatomical situation within the ventricle. As seen, the positioning of the VC holes is of critical importance. From a trajectory from the occipital horn, the tip of the VC may contact the septum pellucidum, and the proximal part of the VC may contact the choroid plexus of the atrium part of the ventricle ***(Fig 2)***. This situation may predispose early VC obstruction. Other similar situation is seen from a trajectory from the frontal horn ***(Fig 3)***, where the most proximal VC inlets are seen already within the brain parenchyma. After evaluating these situations we deduce that there are, as a general rule, three different parts with anatomical importance, of the VC within the ventricle ***(Fig 4)***. The most distal part, the medium part and the most proximal part, that is the one closer to the outlet part of the shunt system. These three different parts of the VC may influence, specifically, in the CSF flow within the catheter.

2.3 Problems

After discussion of the different types of ventricular catheters, anatomical dispositions and ventricular locations, we conclude that a shunt insertion is not without problems. Other than the exception, it is closer to being the rule. CSF diversion procedures are among the most common neurosurgical procedures performed worldwide. All neurosurgeons, with formal training, have done shunt insertions or revisions in their lifetime. Consider that, nearly half of shunt related surgeries are revisions of previous insertions. Overall, the most frequent cause of shunt failure in pediatric hydrocephalus is ventricular catheter obstruction, which may account for 50 to 80% of newly inserted

shunts (Drake et al., 1998; Drake, Kestle & Tuli, 2000a; Drake, Kestle & Tuli, 2000b; Hirsch, 1992).

Other complications include infections, malpositioning of the ventricular or distal catheter, disconnection and migrations, but these latter are directly related to the surgical technique during shunt placement, and contrarily to the first and main, can be avoidable to some extent. As mentioned before, main experience comes from the pediatric scenario (Schuhmann et al., 2005; Drake, Kestle & Tuli, 2000b).

Once a ventricular catheter is blocked, the usual technique is to replace it. Though, because of the attachment of the brain tissue or choroid plexus or both to the catheter, its removal can produce from minimal to devastating hemorrhage, because of tear forces. Several techniques have been developed to avoid this occurrence (Boop et al. 2007; Brownlee, Dold & Myles, 1995; Gnanalingham et al., 2005; Hudgins & Boydston, 1998; Martínez-Lage, López, Poza & Hernández, 1998; Sagan, Kojder & Madany, 2005; Whitfield, Guazzo & Pickard, 1995;Yamamoto, Oka, Nagasaka & Tomonaga, 1994).

To some extent, improvements over time were seen. The amount of shunt failures attributable to infection has probably decreased over the years (Enger, Svendsen & Wester, 2003; Faillace, 1995). Several investigators have suggested that surgical skill, technological advances, or specific operative techniques can lower shunt failure rates (Boon et al., 1998; Cochrane & Kestle, 2002; Hirsch, 1992; Kestle, Milner & Drake, 1999). Nevertheless, not all studies have shown a difference, (Di-Rocco, Marchese & Velardi, 1994; Drake et al., 1998; Drake et al., 2000a; Drake et al., 2000b) and there is no convincing evidence that overall shunt failure rates are falling.

The difficulty in recognizing shunt failure in normal-pressure hydrocephalus, a condition much more prevalent in adults than in children, is another aspect to discuss. The value of overnight monitoring of intracranial pressure has been tested for this and other common causes of malfunction in children (Schuhmann et al., 2008) and adults (Czosnyka et al., 2007; Stephensen et al., 2005). Shunt failure may go unrecognized for months or years in this group, thus delaying diagnosis of malfunctioning shunts. As an

example, Williams, Razumovsky and Hanley (1998) evaluated 28 patients with normal-pressure hydrocephalus whose response to shunt insertion was absent or temporary. Twenty-two of them (~80%) exhibited partial or complete shunt obstruction. Nonfunctioning shunts in patients with normal intracranial pressure may be relatively asymptomatic, and malfunction may be missed.

Taking in consideration the cohort of patients with treated iNPH, in this group delayed morbidity from a CSF shunt may arise from seizures, shunt obstruction, infection, subdural fluid collection, overdrainage headaches, and shunt underdrainage, sometimes disclosed with failure to clinically improve despite a patent shunt (Bergsneider et al., 2005). Estimates of complication incidences for the treatment of idiopathic normal pressure hydrocephalus indicate: intracerebral hematoma, 3% (Black, 1980); subdural hematoma, 2–17% (Black, 1980; Zemack & Romner, 2002; Boon et al., 1998; Krauss et al., 1996); shunt infection, 6% (Zemack & Romner, 2002); seizure, 3–11% (Black,1980; Hughes, 1978) and, finally, shunt malfunction including VC obstruction (3 to 5 yr), 20% (Malm et al., 2000; Raftopoulos, 1996; Williams et al., 1998)

Although shunt malfunction still has the highest complication rate in this particular group of iNPH, from the perspective of permanent morbidity, the most important complication to consider is the subdural hematoma. According to expert opinion, the proportion of VC obstruction in the shunt malfunction group is not as high as the proportion of valve failure in the iNPH cohort (Schuhmann, personal communication, 2015). The other “complications” listed above may result in prolonged or repeated hospitalizations, but in general, patients recover completely. The ultimate outcome may not be negatively affected, but the management of iNPH symptoms can be delayed.

For many years, the cause of subdural hematoma has been attributed to “siphoning.” It is well known that negative ICP values are generated by gravity-dependent drainage (Bergsneider et al., 2005). Multiple valve designs have been developed through the years including antisiphon devices, flow-limiting designs, and gravitational valves (Bergsneider et al., 2005; Chapman, Cosman & Arnold, 1990) to counteract siphoning, none of which have been shown to prevent, radically, the incidence of subdural

hematomas or hygromas. Some experts state that in patients requiring CSF diversion, adjustable valves (Bergsneider et al., 2005; Zemack & Romner, 2002) maximize the likelihood of both attaining a positive clinical response and avoiding or reversing complications. However, recent randomized multicentre studies showed that gravitational and adjustable valves have considerably decreased overdrainage, including subdural hematoma, and hygromas (Lemcke et al., 2013; Delwel et al., 2013).

On the other hand, a rather simple device described by Sotelo et al. (2005), such as an open catheter, complied with most hydrokinetic parameters imposed by a bypass connection between the ventricular and peritoneal cavities in humans; while it also complied with the physiological ideal of continuous CSF flow and drainage according to CSF production. The occlusion rate was significantly lower than that with conventional valve shunts.

Shunt troubles have a medical cost. The study by Patwardhan and Nanda (2005), showed that, after all, ventriculoperitoneal shunts constitute a significant medical problem, in terms of both urgency of treatment and economic costs, which approximate $1 billion for the United States for a single year, if only admissions that list a shunt-related procedure as a primary diagnosis are counted. Nonetheless, according to expert opinion, this study underestimates the value by at least 50% (McAllister II, personal communication). More recently, the study by Simon et al. (2008) disclosed similar disproportionate share of hospital days and healthcare cost. To our knowledge there are no similar studies considering cost and NPH shunt treatment.

Other than shunt procedures, which represent a significant health care expenditure, approximately half of the cost associated with VP shunt procedures were spent on shunt revisions. The study by Wu, Green, Wrensch, Zhao and Gupta (2007), in the state of California, disclosed 32% of that population –all type of hydrocephalus- with VP shunts experienced a surgical complication, reminding us that the current treatment for hydrocephalus is unsatisfactory for a large proportion of patients.

A case-control study looking at patients treated for a shunt failure compared with those who did not experience a shunt failure being developed for further estimation of the financial impact and "real world" costs associated with a shunt failure episode is still to be determined (Shannon et al., 2011). As far we know, there are no studies of this type in Europe and Spain.

After analyzing all factors, it is evident that obstruction of the proximal end of the shunt system or ventricular catheter blockage is a common cause of shunt malfunction in all types of hydrocephalus. Although some hold responsible collapsed ventricles for increasing the threat of proximal shunt malfunction, others attempt to optimize the neurodevelopmental function of patients with hydrocephalus by maximizing their cerebral mantle using programmable valves. Regarding catheter tip location, the goal is to keep it away from obstructing biological agents such as the choroid plexus, ependymal, glial, and other brain tissues. Given that the mean inlet size (perforated length) of a ventricular catheter is 1.5 to 2 cm and that the mean intraventricular distance available for frontal horn placement is less than 1.6 cm, it is very difficult to place a catheter so that the inlets or holes are directed away from the choroid plexus (Kaufman & Park, 1999; Lin et al., 2003). The depicted figures illustrate a personal series of representative cases disclosing occluded ventricular catheters ***(Figs 5 to 10).***

In sum, progress in preventing ventricular catheter failures has not been made over the last several decades. Any improvements made in shunt materials or insertion techniques have been overshadowed by biological and other factors (Del-Bigio, 1998; Stein & Guo, 2008). Avoiding shunt malfunctions, and other reasons resulting in shunt revisions, is a minimal requirement nowadays.

This situation emphasizes the need for a better technology for the treatment of hydrocephalus.

2.4 *Computational Fluid Dynamics*

Our study investigates current in use and prototypes of ventricular catheters for the treatment of hydrocephalus, by using simulation studies, in particular Computational Fluid Dynamics (CFD) in three-dimensional (3D). Our main theoretical reference is coming from the book of Versteeg and Malalasekra (2007).

Computational fluid dynamics or CFD is the analysis of systems involving fluid flow, heat transfer and associated incidents such as chemical reactions by using computer-based simulation. The technique is especially powerful and covers a wide range of industrial and non-industrial application fields. Some examples are: aerodynamics of aircraft and vehicles; hydrodynamics of ships; power plant: combustion in internal combustion engines and gas turbines; turbomachinery: flows inside rotating passages or diffusers; electrical and electronic engineering: cooling of equipment including microcircuits; chemical process engineering such as mixing and separation or polymer moulding; external and internal environment of buildings: wind loading and heating/ventilation; environmental engineering: distribution of pollutants and effluents; in hydrology and oceanography: flows in rivers, estuaries, oceans, etc.; meteorology: weather prediction; and finally, biomedical engineering to study, but not restricted, blood flows through arteries and veins, CSF circulation, among others applications in the medical field (Lin et al., 2003; Linninger et al., 2007).

The ultimate aim of developments in the CFD field is to provide a capability comparable with other computer-aided engineering tools such as stress analysis. The main reason why CFD has lagged behind is the tremendous complexity of the underlying behavior, which precludes a description of fluid flows that is at the same time economical and sufficiently complete. The availability of affordable high-performance computing hardware and the introduction of user-friendly interfaces have led to a recent upsurge of interest, and CFD has entered into the wider industrial community since the 1990s.

The investment costs of a CFD capability are not undersized, but the total expenditure is not normally as great as that of a high-quality experimental facility. Moreover, there are several distinctive advantages of CFD over experiment-based approaches to fluid systems design, for example: substantial reduction of lead times and costs of new

designs; ability to study systems where controlled experiments are difficult or impossible to perform (e.g. very large systems); ability to study systems under hazardous conditions at and beyond their normal; performance limits (e.g. safety studies and disaster scenarios); and, basically unlimited level of detail of results. The variable cost of an experiment, in terms of facility hire and/or person hour costs, is comparative to the number of information points and the number of configurations tested. In contrast, CFD systems can produce exceedingly large volumes of results at practically no added expense, and it is affordable to perform parametric studies, for instance to optimize equipment functionality, such as our cases of ventricular catheter flows.

CFD systems are structured around the numerical algorithms that can undertake fluid flow problems. In order to provide straightforward access to their solving capabilities commercial CFD packages include user interfaces to input problem parameters and to examine the results. Hence all systems contain three main elements: *(i)* a pre-processor, *(ii)* a solver and *(iii)* a post-processor.

Pre-processing consists of the input of a flow problem to a CFD program by means of an operator-friendly interface and the following transformation of this input into a form appropriate for use by the solver. The user activities at the pre-processing stage involve: definition of the geometry of the region of interest (ROI): the computational domain; grid generation – the sub-division of the domain into a number of smaller, non-overlapping sub-domains: a grid (or mesh) of cells (or control volumes or elements); selection of the physical and chemical characteristics that need to be modeled; definition of fluid properties; specification of appropriate boundary conditions at cells which coincide with or touch the domain boundary.

The solution to a flow problem (velocity, pressure, temperature etc.) is defined at nodes inside each cell. The accuracy of a CFD solution is governed by the number of cells in the grid. Overall, the larger the number of cells, the better the solution accuracy. Both the accurateness of a solution and its cost in terms of necessary computer hardware and calculation time are dependent on the fineness of the grid. Optimal meshes are often non-uniform: finer in areas where large variations occur from point to point and coarser in regions with relatively little change. Efforts are under way to develop CFD systems

with an adaptive meshing capability. Ultimately such programs will routinely refine the grid in areas of rapid variations. A substantial amount of basic development work still needs to be done before these techniques are robust enough to be incorporated into commercial CFD systems. At the present time it is still up to the skills of the CFD user to design a grid that is a suitable compromise between desired accuracy and solution cost. It is worthy to note, that over 50% of the time spent in industry on a CFD project is committed to the definition of the domain geometry and grid generation.

Regarding the solver step, there are three distinct streams of numerical solution techniques: finite difference, finite element and spectral methods. Our fundamental interest is the finite volume method, a singular finite difference formulation that is central to the most well-established CFD systems. In outline the numerical algorithm consists of the following steps: integration of the governing equations of fluid flow over all the (finite) control volumes of the domain; discretization – conversion of the resulting integral equations into a system of algebraic equations; solution of the algebraic equations by an iterative method; concerning the post-processor stage, as in pre-processing, a huge amount of development work has recently taken place in the post-processing field. Due to the increased popularity of engineering workstations, many of which have exceptional graphics capabilities, the leading CFD packages are now equipped with versatile data visualization tools. These usually include: domain geometry and grid display; vector plots; line and shaded contour plots; 2-D and 3-D surface plots; particle tracking; view manipulation (translation, rotation, scaling etc.); color post-script output. More recently these facilities may also include animation for dynamic result display, and in addition to graphics all systems produce trusty alphanumeric output and have data export facilities for further manipulation external to the code. As in many other branches of computer-aided engineering, the graphics output capabilities of CFD systems have developed the communication of ideas to the non-specialist. In recent years, thanks to the ever-growing capability of computers and the maturity of Computational Multiscale Modeling (CMM), a different approach is emerging specifically developed for high-performance application that is the Materials by Design (MbD) approach (McDowell & Story, 1998). MbD consists in designing the structure of a material at a subscale in order to make this material, or the body made of

this material, the best-suited for a specific application. Prospective applications in medicine have been reported (Fachinotti et al., 2015).

In solving fluid flow problems we need to be aware that the underlying physics is complex and the results generated by a CFD system are at best as good as the physics, and chemistry as well, implanted in it and at worst as good as its operator. Elaborating on the latter issue first, the user of a system must have skills in a number of areas. Prior to setting up and running a CFD simulation there is a stage of identification and formulation of the flow problem in terms of the physical and chemical characteristics that need to be considered. Other typical decisions that might be needed are whether to model a problem in two or three dimensions.

In the last decade, CFD systems were incorporated to the medical scenario. So far CFD studies in the biomedical engineering field include, but are not limited to, blood flows simulation through arteries and veins, CSF flow in brain anatomy and brain malformations, and 2-D ventricular catheter flow. Now, regarding the possibility to simulate hydrocephalus, it is important to recognize that mathematical modeling of hydrocephalus combines basic physics and materials science with a refined abstraction of brain properties (Clarke & Meyer, 2007). This implies that serious limitations in the utility of these models exist, and progress in eliminating them has been slow if not null. We will discuss this issue in *Chapter 3*.

2.5 Aims and hypothesis of the present Thesis

The overview of the literature presented in this and the previous chapter has shown that flow in ventricular catheters play an important, if not the key role in the field of hydrocephalus surgically treated with shunts. Yet, what is evident, as well, is that there are some important gaps and contradictory results in the medical literature regarding this topic. To address them, by using current simulation methods, we designed and performed a total of four studies. Each study, performed in sequential way, had the following aims and hypothesis:

Study 1

By taking as a model the landmark study by Lin et al. (2003) who addressed the problem of fluid characteristics in ventricular catheters by using a 2-D simulation program of computational fluid dynamics (CFD), the aim of this study is to study five current commercially available ventricular catheter designs by using computational fluid dynamics (CFD), though this and for the first time, in three-dimensional (3D) automated designs. The general procedure for the development of a CFD model involves incorporating the physical dimensions of the system to be studied into a virtual wire-frame model. The shape and features of the actual physical model are transformed into coordinates for the virtual space of the computer and a CFD computational grid (mesh) is generated. The fluid properties and motion are calculated at each of these grid points. After grid generation, flow field boundary conditions are applied and the fluid's thermodynamic and transport properties are included. At the end, a system of strongly coupled, nonlinear, partial differential conservation equations governing the motion of the flow field are numerically solved. This numerical solution describes the fluid motion and properties. We will calculate the total fluid mass flows into the catheter's holes. Our hypothesis is that most commercially available ventricular catheters have an abnormally increase flow distribution pattern.

Study 2

After study the three-dimensional flow patterns of five commercially available VC, the aim of this study is to design five VC prototypes with equalized flow characteristics. By

means of CFD in three-dimensional (3-D) automated models we will compare the fluid-mechanical results with our previous study of currently in use VC. The general procedure for the development of a CFD model calls for transforming the physical dimensions of the system to be studied into a virtual wire-frame model which provides the coordinates for the virtual space of a CFD mesh. The incompressible Navier-Stokes equations, a system of strongly coupled, nonlinear, partial differential conservation equations governing the motion of the flow field, are then solved numerically. The hypothesis is that by varying the number of drainage holes and the ratio hole/segment, we will improve flow characteristics in five prototypes of VC. We expect that new catheter designs with variable hole diameter, number of holes, and ratio hole/segment along the catheter allow the fluid to enter the catheter more uniformly along its length, thus reducing the chance that the catheter becomes occluded.

Study 3

Based on our previous studies by computational fluid dynamics (CFD) of the three-dimensional (3-D) flow in ventricular catheters (VC), the aim of the present study is to investigate basic flow patterns in VC prototypes. Once again, we will develop a CFD model calls for transforming the physical dimensions of the system to be studied into a virtual wire-frame model which provides the coordinates for the virtual space of a CFD mesh, in this case, several VC. Six new designs of VC, e.g. with novel hole configurations, can be then readily modelized, and the corresponding flow pattern computed in an automated way. In addition, we will use purposely modified VCs for benchmark experimental testing. Our hypothesis is that there are at least three distinct types of flow pattern in prototypes models of VC: Specifically we will try to show how to equalize and reverse the flow pattern through the different VC drainage segments by choosing appropriate parameters. In our opinion the flow pattern in prototype catheters is determined by the number of holes, the hole diameter, the ratio hole/segment and the distance between hole segments.

Study 4

In this paper we focus on analyzing the effects that tilt holes as well as conical holes have on the flow distribution and shear stress. We will proceed with 3D computational

simulations to study the effect of the hole geometry on the cerebrospinal fluid flow through the VC. All the simulations will be done using the OpenFoam toolbox. In particular, three different groups of models will be investigated by varying tilt angles of holes, inner and outer diameters of the holes and inter-segment distances. Our hypothesis is that there are flow differences between conical holes instead of cylindrical holes with a direct influence on the flow distribution and the shear stress. While tilting the holes may affect the shear stress without influencing the flow distribution.

Study 5

By using our previous studies and methodology, to better understand the flow pattern of CSF catheters, the aim of the present study is to carry out a parametric study via numerical models of ventricular catheters. The parameters chosen are the number of drainage segments, the distances between them, the number and diameter of the holes on each segment, as well as their relative angular position. As an end result, our common hypothesis is to formulate general mathematical principles for ventricular catheter design. These principles can help to develop new catheters with homogeneous flow patterns, thus possibly extending their lifetime.

Figures Chapter 2

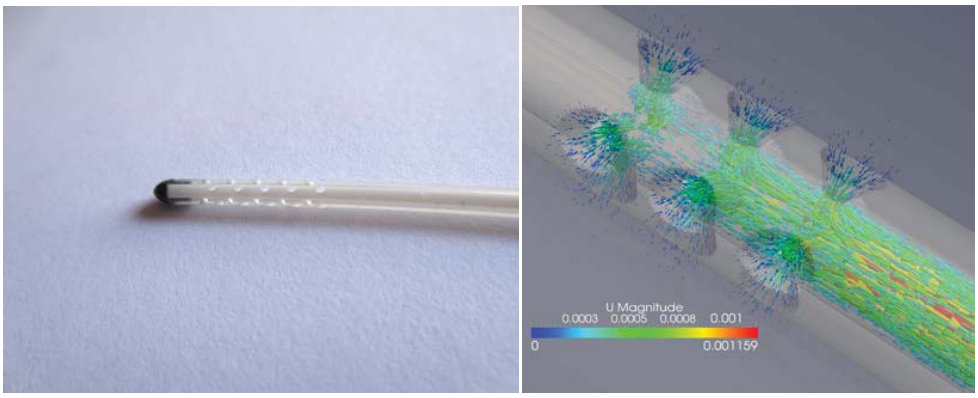

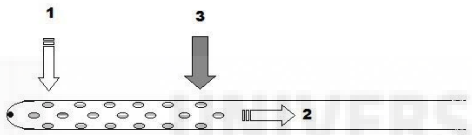

Figure 1. The first figure of this Chapter illustrates a typical ventricular catheter.

Note. A ventricular catheter model from Sophysa® is depicted on the top. Next to it is depicted one of our studied ventricular catheters and its computational fluid dynamics with three-dimensional flow imaging. Below there is an schematic illustration about the fluid dynamics in a typical ventricular catheter: 1, fluid flow entering in the distal holes; 2, distal fluid flow within the catheter in its final direction; 3, fluid flow entering in the most proximal holes. This is the usual occlusion site.

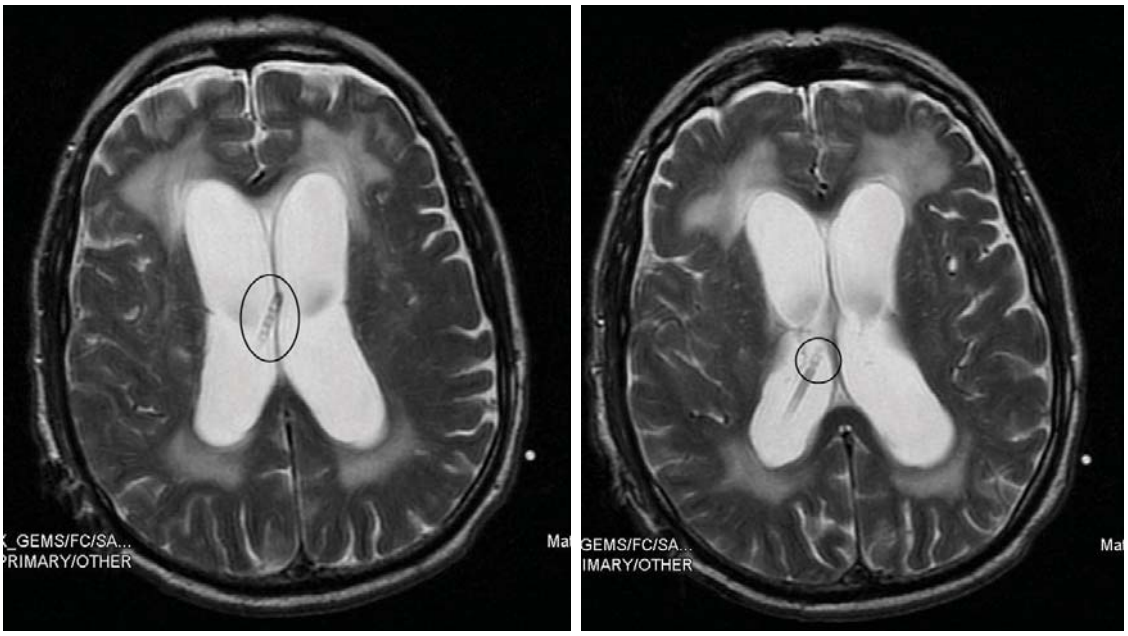

Figure 2. Brain MRI scans. Axial views.

Note. Hydrocephalus with a shunt. Ventricular catheter with evident open inlets in the occipital horn of the brain, shows its most distal part in contact with the septum pellucidum, while the most proximal are directly in contact with the choroid plexus.

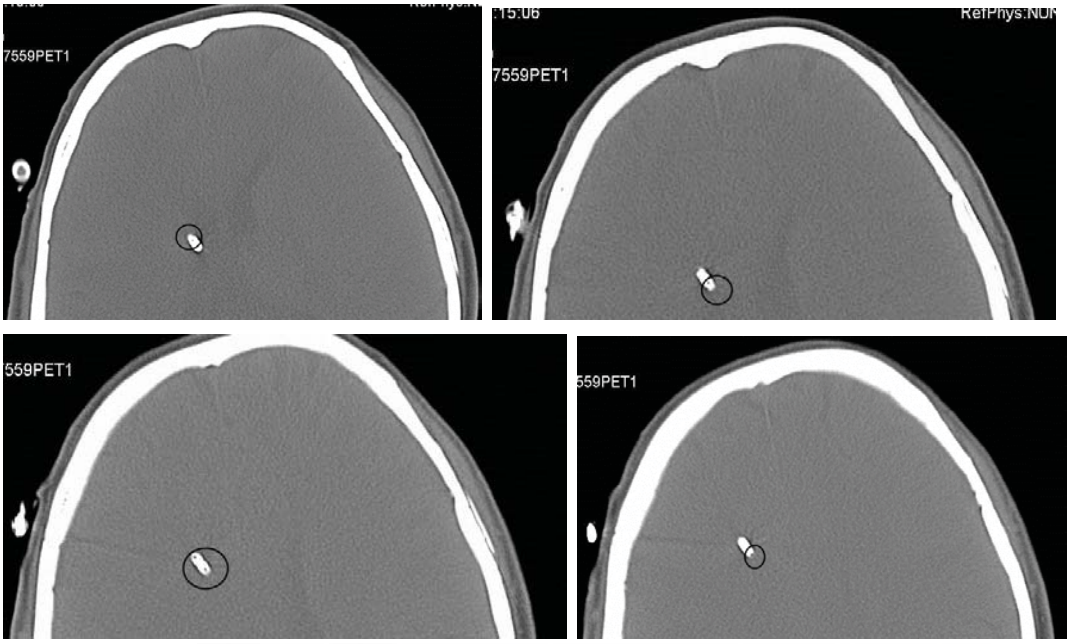

Figure 3. Brain CAT scans. Axial views.

Note. Shunted hydrocephalus with collapsed ventricles and ventricular catheter placed in the frontal horn with evident opening of the inlets. The holes of the ventricular catheter at the most proximal part are embedded in the brain.

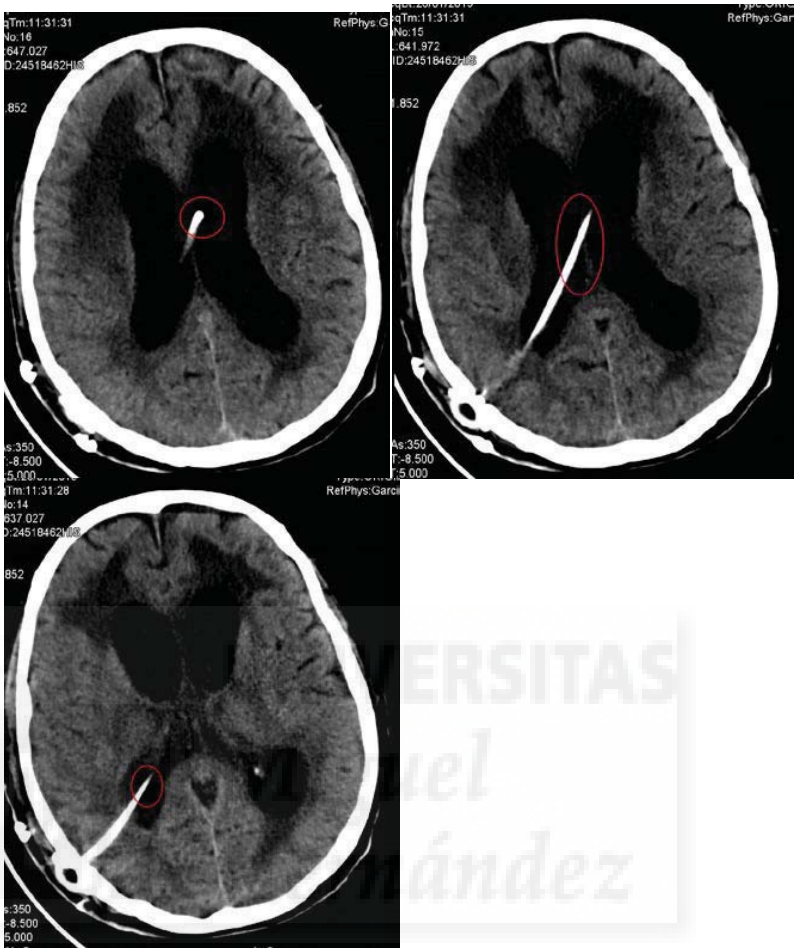

Figure 4. Brain CAT scans. Axial views.

Note. Hydrocephalus with a shunt and a ventricular catheter inserted in the occipital horn of the cerebrum. We deduce that there are *three different parts of the catheter*: a distal part in contact with the septum pellucidum, a medial part within the ventricle, a proximal part, in contact with the choroid plexus and brain. The usual perforated or inlet section of the catheter is within the distal and medial part of it, yet, it is not excluding a potential occlusion of the VC.

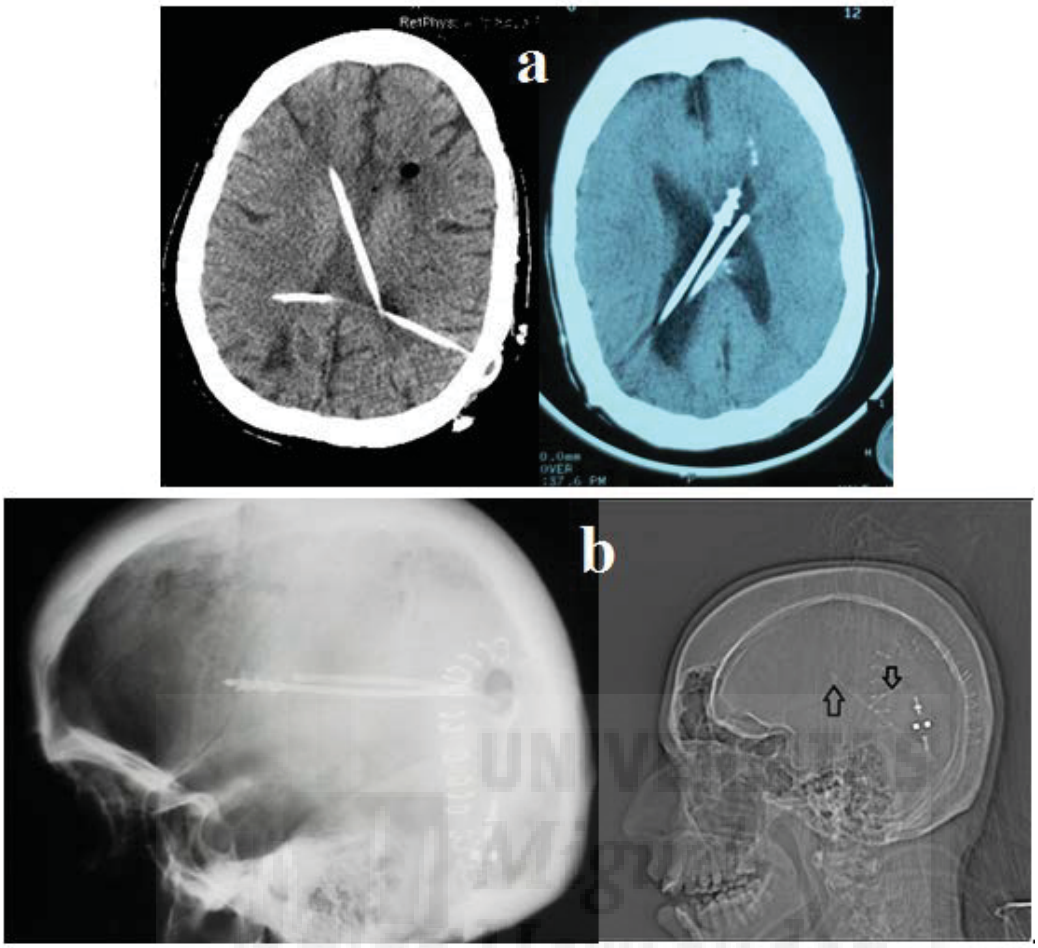

Figure 5. Cases with lost ventricular catheters due to shunt malfunction.

A) Brain CAT scans. B) Lateral XR cranium.

Note. a) Brain CAT scans, axial views b) Lateral XR disclosing several cases of lost ventricular catheters after revision. Some catheters can get lost during revision, while others, like the Portnoy catheter seen in two of these cases, cannot get removed during revision. Trying to remove these catheters is highly risky because of the potential hemorrhage due to tearing forces.

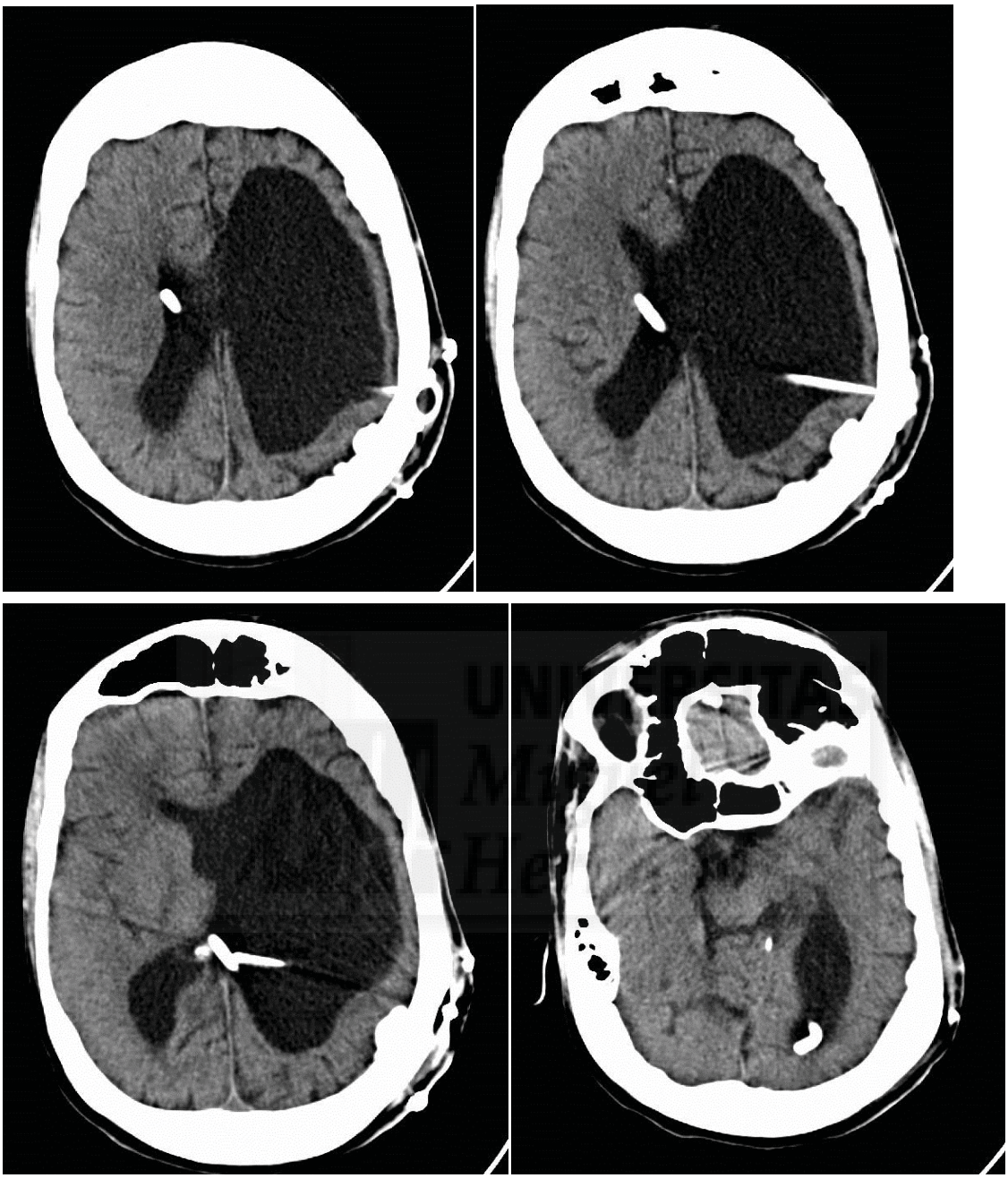

Figure 6. Brain CAT scans, axial views showing a case of lost ventricular catheter in the temporal horn.

Note. Shunted hydrocephalus with a partially functional ventricular catheter in the left lateral ventricle the brain.

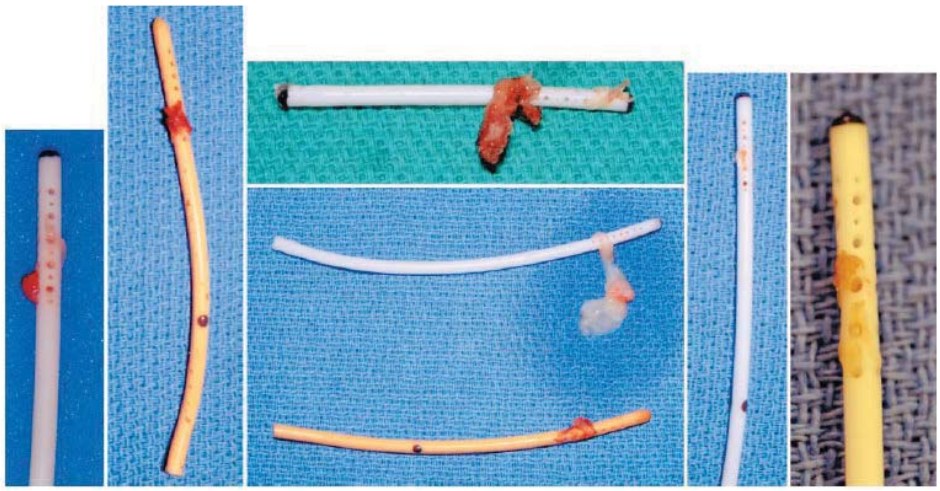

Figure 7. A series of removed ventricular catheters showing occlusion at the most proximal part of it.

Note. This photograph is unique and takes consideration about the aim of our dissertation. Taken from "Computational and experimental study of proximal flow in ventricular catheters. Technical note." By J. Lin, M. Morris, W. Olivero, F. Boop and R.A.Sanford, 2003, *Journal of Neurosurgery, 99*, 426-431.

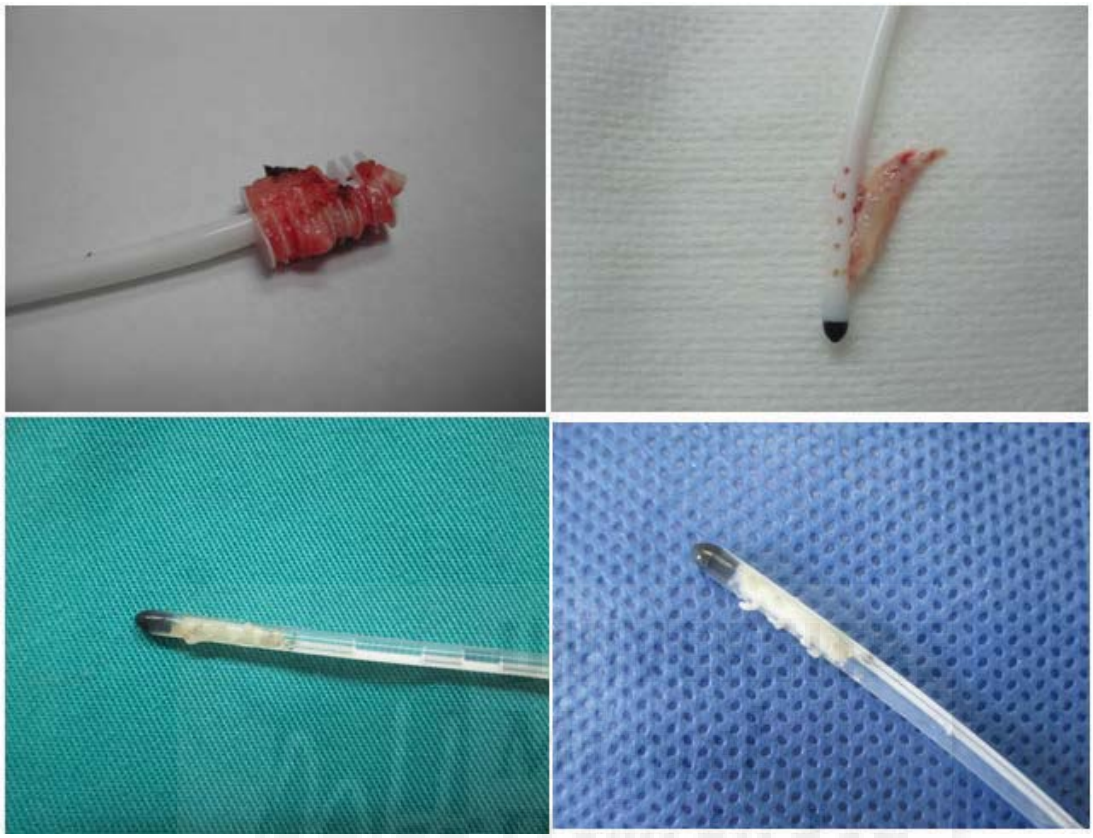

Figure 8. A series of removed ventricular catheters with total occlusion due to brain tissue and choroid plexus.

Note. The first photograph depicts a Portnoy catheter with brain embedded in its flanges. Other cases mainly disclosed brain tissue obstructing the perforated part of the catheter.

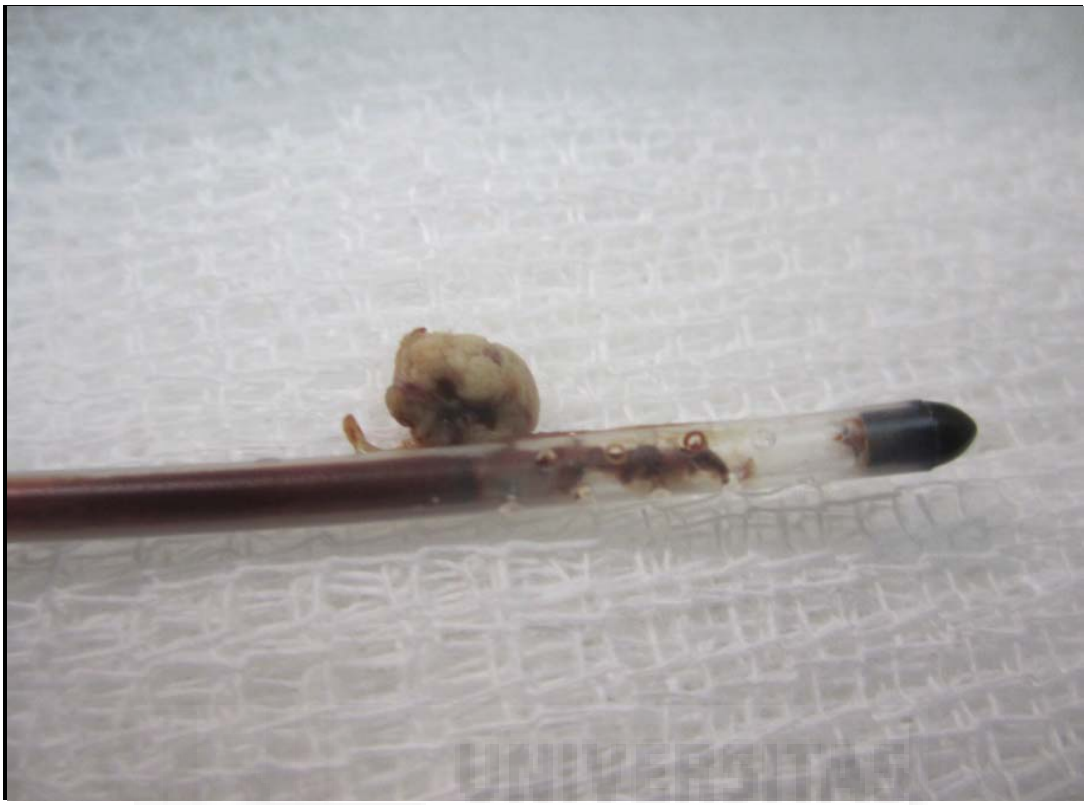

Figure 9. Removed ventricular catheters with total and partial occlusion showing remnants of hemorrhage.

Note. The depicted cases show removed catheters with blood remnants. This occurrence happens due to brain tissue and choroid plexus tearing during removal. Consequences in these cases can be catastrophic, not saying lethal.

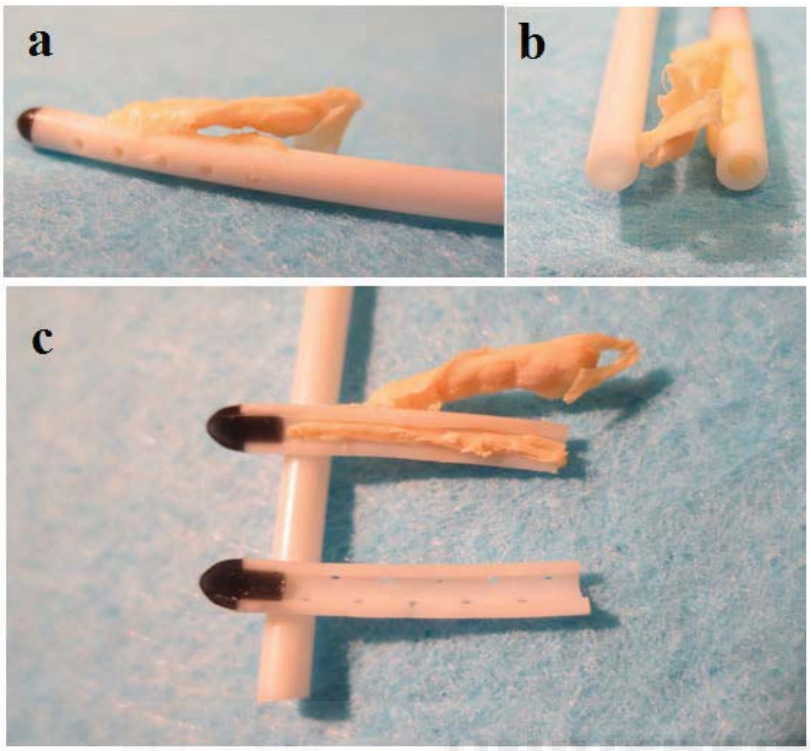

Figure 10. A case of a totally occluded ventricular catheter due to brain tissue. We cut it at the most proximal hole and disclosed a complete occlusion at that level with a persisting patent rest of the catheter. Thereafter, we did split the occluded catheter in half lengthwise to verify visually where exactly luminal blockage occurred.

Note. a) A case of totally occluded ventricular catheter due to brain tissue; b) Complete occlusion at the most proximal hole in the ventricular catheter; c) Brain tissue infiltrated the holes only on one side. The brain tissue infiltrated the holes completely on one side, while the other side was quite free.

Chapter 3:

Study 1. Computational fluid dynamics of ventricular catheters used for the treatment of hydrocephalus: a 3-D analysis

INTRODUCTION

Although the description of hydrocephalus could be found in ancient civilizations; its basic treatment, consisting of internal cerebrospinal fluid (CSF) drainage was first described in early 1900. The concept of valves and flow regulation was stated by the procedure reported by Payr (1908) in which he used venous valves to divert CSF from the ventricles to the venous sinuses. In 1929, Davidoff (citado en Bergsneider et al., 2006) stated that in hardly a single condition such as hydrocephalus, have cures been so elusive or so often wrecked on purely mechanical obstacles. 25 years later, in 1952 Nulsen and Spitz, working in conjunction with John Holter, the father of a child with hydrocephalus, reported the successful use of a ventriculojugular shunt (Drake & Sainte-Rose, 1995), bringing cerebrospinal fluid shunts into existence as an effective treatment for hydrocephalus. Since then, countless children and adults have received treatment for this disease, often resulting in symptomatic recovery and improvement in development and functional ability. Nonetheless, in the following years, the initial enthusiasm for cerebrospinal fluid shunting weakened because of the underdeveloped shunt technology, low clinical success rates, and frequent complications (Drake & Sainte-Rose, 1995; Drake et al., 2000b; Sainte-Rose et al., 1991; Tuli et al., 2000). As stated in an honest and critical review paper (Bergsneider et al., 2006) by current experts in the field, Davidoff's phrase "so often wrecked on purely mechanical obstacles" was predictive. Nowadays, the mechanical obstacle of shunt failure remains the rule, not the exception, in the management of hydrocephalus. More than 30% of new shunts fail within 1 year (Drake et al., 1998). Probably less than one third of new shunts survive 10 years without revision (Sainte-Rose et al., 1991). In some large pediatric neurosurgery services, the ratio of shunt revisions to placement of new shunts is 2.5:1 (Tuli et al., 2000). Authors of a recent randomized controlled multicenter study have

shown that a half century of research in shunt valve design has produced little if any improvement in the rate of shunt survival (Drake et al., 1998).

The most frequent cause of shunt failure is ventricular catheter obstruction, which may account for 50 to 80% of newly inserted shunts (Drake & Sainte-Rose, 1995; Drake et al., 1998; Sainte-Rose et al., 1991; Tuli et al., 2000). That is in the pediatric population. Although many factors contribute to this (Bergsneider et al., 2006; Harris & McAllister, 2012), the main one is related to fluid flow characteristics of the catheter within the hydrocephalic brain (Bergsneider et al., 2006; Ginsberg, Sum & Drake, 2000; Lin et al., 2003; Sainte-Rose et al., 1991).

A landmark study in 2003 addressed the problem of flow characteristics in ventricular catheters (Lin et al., 2003) by using a 2-D simulation program of computational fluid dynamics (CFD). This study revealed important information related to this common complication. Both the computational and experimental data in this study showed that more than 80% of the flow into the catheter occurs at the two most proximal sets of holes. CFD is an engineering tool used to calculate fluid flow, provides a means to analyze different flow patterns. For a 3D model of the domain to be studied and for specified rates of flow, CFD software calculates flow with greater spatial and temporal resolution than that achieved with specific MRI studies (real-time phase-contrast magnetic resonance) and also displays pressures, flow structures, stresses, and pressure waves. Its current application in medicine includes modeling of hemodialysis (Clark, Van-Canneyt & Verdonck, 2012) and urinary (Frawley & Geron, 2009) catheters, among others.

Our objective was to study current ventricular catheter designs by using a 3-D CFD models. This will produce a visual image of the flow field and results will be integrated to evaluate mass flow rates, velocities and shear stress values.

MATERIAL AND METHODS

Five commercially available ventricular catheters were studied. Models were taken from figures from the factory models (Medtronic Inc.) and current in use catheters. Model 1 *(Figure 1, image a)* consisted of a VC of 4 rows of 8 holes distributed in 16 mm from tip to last hole; model 2 *(Figure 1, image b)* of 4 rows of 4 holes distributed in 8 mm from tip to last hole, and model 3 (*Figure 1, image c)* consisted of 4 rows of 6 tapered

holes distributed in 10 mm from tip to last hole simulating the current Rivulet catheter; model 4 *(Figure 1, image d)* of 4 rows of 3 holes distributed in 7.5 mm from tip to last hole; model 5 *(Figure 1, image e)* of 4 rows of 4 holes distributed in 24 mm from tip to last hole. The placement of the drainage holes across samples was designed to mimic the current in use catheter by maintaining the distance between each hole (approximately 500 μm in models 1 to 4) and the number of hole rows (4 in total). The drainage hole size of the ventricular catheter, with holes that varied from 500 μm (model 1; 2 and 4; 5), and from 282 to 975 μm in diameter (model 3). The internal diameter was 1.2 to 1.5 mm and external diameter was 2.1 to 2.5 mm depending of the model.

Catheter and hydrocephalus modeling

The hole distribution in model 1; 2; 4 and 5 is intercalated in two and two rows, so there are 6 to 16 internal flow segments to calculate *(Figure 2, image a)*. In model 3 the hole distribution is strictly parallel in four rows, so there are 6 flow segments to calculate *(Figure 1, image c)*, but also in model 4; while there are 16 segments in model 1, and 8 segments in model 2 and 5. The CFD calculation considered flow distribution evolution in time (secs) and flow rate (cm^3/day) in each flow segment. The last time flow distribution in 16, 8 and 6 flow segments was calculated considering flow percentage. The shear stress behavior was calculated considering max shear stress (N/m^2) in time evolution in seconds.

Normative data for CSF volumes and characteristics was taken from excellent discussions have been provided by Drake and Saint Rose (1995), Hakim (1969), Harris and McAllister (2012), Schley, Billingham, and Marchbanks (2004) and Sood, Kim, Ham, Canady and Greninger (1993) in an effort to understand the pathophysiology of hydrocephalus. Total CSF volume is approximately 150 to 450 ml according to age, body habitus and gender. While the internal spinal cerebral CSF (within the ependyma) is 150 to 280cc, the normal ventricles have a normal volume of approximately 25 to 30 cc. Ventricle volumes in hydrocephalus can reach 50 to 300 cc (Drake & Sainte-Rose, 1995; Hakim, 1969; Schley et al., 2004). The volume capacity of our ventricle model was of 60 cc. The geometric model of the hydrocephalus followed a rigid cylinder of 85mm of length and 15mm of radius. In sagittal and axial sections, the geometric model followed to approximate the lateral ventricular space of hydrocephalus *(Figure 2, image b)*. CSF production is about 500cc/day, and 60% is produced by the plexus and the rest

by the brain surrounding ependyma. It is similarly reabsorbed through the venous system. Pulsatile variation of the systolic cardiac cycle (in) and diastolic (out) can vary by up to 20% the volume of the ventricle. According to clinical experience, a ventricular catheter drains about 50 to 300 cc/day, depending to the treated hydrocephalus that is about 10% of what is produced. The drainage volume of our catheter model was of 100 cc. The normal ventricular pressure is ranging between 12 to 18 cmH2O, and in cases of normal pressure hydrocephalus numbers are similar. The CSF has a specific gravity of 1007, compared with the surrounding brain 1047. Same numbers were used in our model.

Ventricular catheter designing

To simulate fluid flow in a space, we created 3D models of ventricular catheters based on current commercially available models based from actual geometric shapes or from images or measurements that define the actual boundaries of that space. In order to design the solid geometry of the ventricular catheters we have used Salome (version 6.6.0). Salome is a general graphical environment for numerical computing using spatially discretised, mesh-based methods like finite element or finite volume method. The environment contains separate working modes for geometry creation or manipulation (Geometry), meshing (Mesh), solver management (Supervisor), post-processor (Post-Pro), and communication module (MED). The software is open source software under GNU Lesser General Public License (LGPL).

The physical space is converted to a mathematic model—that is, a series of interconnected points or nodes that define the space. The number of nodes determines the resolution of the model and the length of time needed for computation. The mathematic model, if displayed graphically, appears as a mesh. The physical characteristics of the fluid and its flow volume per unit time (boundary conditions) are specified. The grid-generation utility snappyHexMesh is used to discretize the computational domain with unstructured hexahedral boundary-fitted mesh. The grid generator allows cutting out unnecessary parts not related to the region of interest and closing the computational domain by defining inlet, outlet, and wall boundaries to finally define the region of interest on which CFD will be applied, as shown in *Figure 2 (image b).* SnappyHexMesh is a utility provided with OpenFoam (see below), which has the ability to produce meshes for complex geometries with small effort, providing finer grids in areas where they are needed, in our case, in catheter holes and the output

area. The numbers of grid nodes or hexahedrons have been chosen as a reasonable compromise between better accuracy and shorter computational time of subsequent simulations.

CFD Calculation

OpenFOAM® (Open Field Operation and Manipulation) CFD Toolbox is a free, open source CFD software package produced by OpenCFD Ltd. It has a large user base across most areas of engineering and science, from both commercial and academic organizations. OpenFOAM has an extensive range of features to solve anything from complex fluid flows involving chemical reactions, turbulence and heat transfer, to solid dynamics and electromagnetics.

The governing equations for CFD calculation are the 3D incompressible unsteady Navier-Stokes equations written in conservative form for mass and momentum. Our 3D model is assuming to be a steady, incompressible, laminar flow of a Newtonian fluid. The numerical simulations are running by using the software OpenFOAM® v2.1.1. According to our case, we have used the icoFoam solver in order to perform the numerical integration of the equation.

The software OpenFOAM® 2.1.1 was applied to solve the physiologic pulsating flow in our model. The simulation was performed by setting the kinematic viscosity of water equal to $0.75 \times 10^{(-6)}$ m2/s. Boundary conditions are required to complete the setting of the problem, we therefore need to specify boundary conditions on all our boundary faces. The velocity field at the inlet *(Figure 2, image b)* is adjusted in order to achieve a constant inflow of 100 cc/day and, for consistency, the pressure is zero gradient. On the rest of ventricular and catheter walls, which are considered rigid, we applied the non-slip and non-penetration conditions (i.e., all velocity components at the catheter walls were set to zero). The pressure is specified zero gradient since the flux through the wall is zero. For the outlet, you can set the desired pressure, which in our experiments is equal to 15 cmH2O, and a zero gradient condition on velocity is specified. The flow was computed with a time step of 0.025 seconds for a time interval of 0.3 seconds. The time step was found to be sufficient from the point of view of accuracy. The results corresponding to the last, third cycle were considered independent from the initial conditions and used for the flow analysis.

RESULTS

A flow vector design of model 1 to 5 of standard ventricular catheter from 3D CFD modelling is shown in *Figures 3 to 7.*

The scale on the down side of each model demonstrates that most flow vectors are concentrated in the two most proximal holes; while most of the holes were scarcely or not used *(Figures 3-7, image a).*

Flow velocities can then be calculated into mass flow rates and designed in flow distribution rates. The simulations showed velocity patterns changing in all catheters. Sagittal images showed larger velocities in the proximal holes canal than in the distal ones in all models *(Figures 3-7, image b).* The flow distribution evolution showed that flow rate in catheter segments reaches baseline after 0.05 sec in most models. Last time flow distribution is depicted in *Figures 3-7, image c*; where the flow is indicated in each catheter segment (group of holes).

Velocity flow evolution showed consistent results in all models. These images showed regions of localized above-average velocities ("jets") in latest holes phases with proximal flow with some exception in model 3 and 4. The AP and LR components of the velocity vectors (in-plane or x and y components) showed the same patterns in all models *(Fig. 3-7, image d).* These jets had velocities of 0.19 cm/s at peak proximal flow, more than twice the velocity in the caudal holes in all models.

Velocity peak evolution showed variable results. At the peak volume flow rate, velocity components in models 1, 2, 3 and 4 had a down peak clear jet pattern at t= 0.05 sec. *(Fig. 3-7, image e).* However, the velocity component in model 5 had a clear jet pattern of uniform descent velocity *(Figure 7, image e).* Highest velocity peaks were seen in models 2 and 5. Yet, these jet patterns were seen for all catheters in plane velocity components in any axial plane chosen for t= 0.05, 0.010, 0.25, or 0.30 seconds.

Ventricular catheter wall shear stress can be seen in *Figures 3-7, image f.* While shear stress peak evolution reached highest values at 0.02 sec in time, reaching baseline at 0.10 sec *(Figures 3-7, image g),* for most catheter models. Highest values were seen in most proximal holes.

Specifically, using the CFD model, we calculated that 75% of the total fluid mass flows into the most four proximal holes of a 16-segment (segments 13 to 16) catheter (model 1). From 58 to 68% flows into the two most proximal sets of holes (segments 7 and 8) within an eight-segment catheter (model 2 and 5); 44% flows into the two medial sets of holes (segments 3 and 4) within a six-segment/24-hole catheter (model 3); while 51% flows into the two most proximal sets of holes (segments 5 and 6) within a six-segment/12-hole catheter (model 4). This relation is depicted in *Figures 3-7, image c.*

DISCUSSION

We evaluated the fluid dynamics of five commercially available catheters to evaluate flow factors of proximal shunt malfunction. We found that flow distribution follows a similar pattern in most ventricular catheters, stating that occlusion may occur without differences in all of them, occurring at the proximal inlets, with some uniformity in model 3 (Rivulet type).

The results of this study agree with the previous report on CFD in ventricular catheters by Lin et al. (2003). They also studied ventricular catheter designs by using in addition a 2D water table experiments, and 3D automated testing apparatus together with an actual catheter. They developed a new model by placing the largest hole distally, stating that this change would decrease the probability of occluding the entire catheter when only its tip is blocked. This was partially reflected in our study. Also, as most studies of shunts components (valves and catheters) for the treatment of hydrocephalus, there is no clinical comparative data. Nonetheless, our study is purely mathematical (simulation) and our results can only be compared with previous reports in which 3-D flow studies have been obtained, thus far not possible.

Hydrocephalic domain

For the hydrocephalic area, we used the simple model of a cylinder. Our hydrocephalus model does not reproduce the pathologic anatomy of any individual or any group of patients. Rather, it essential characteristics are within the range of what is found in patients. Our model is simplified in several ways. Some ventricular structures, such as the third ventricle and choroid plexus, were not included in the model. These may affect CSF flow, but their absence in our model did not invalidate the flow patterns observed in hydrocephalus treated with ventricular catheter shunts. Model boundaries were

assumed rigid and immobile, even if the ventricles and choroid plexus in vivo are known to move with the pulsating CSF. In an idealized model of hydrocephalus, the systolic-diastolic cardiac cycle had the effect of increasing CSF pressure gradients and the complexity of flow patterns. In fact, hydrocephalus alone is a sufficient cause for hyperdynamic CSF flow (Penn, Basati, Sweetman, Guo & Linninger, 2011). The extent of this shift is directly affected by medical conditions such as type of hydrocephalus, arachnoidal adhesions, previous hemorrhage or infection, and so forth (Sood, Lokuketagoda & Ham, 2005; Sood et al., 2004). However, MR imaging-based measurements of the CSF flow direction and lateral ventricle volume size in healthy and hydrocephalic cases, as well as the results of computer modeling of fluid dynamics lead to conclude that the directional pattern and magnitude of CSF flow in patients with hydrocephalic may be an indication of the disease state (Penn et al., 2005). Yet, according to clinical experience and several authors (Bergsneider et al., 2006; Hakim, 1969; Penn et al., 2011), ventricular deflections tend to be minimal such in cases of hydrocephalus, of normal pressure type for example. So the assumption of rigidity and immobility seems justified in our model. These displacements of the ventricles, if they occur in unoperated patients with hydrocephalus, may increase CSF pressures and magnitudes above the levels that we found (Penn et al., 2005; Penn et al., 2011; Sood et al., 2005; Stein & Guo, 2008). The assumption of plug flow at model ends did not likely affect simulated flow patterns because the region of study was relatively far from the ends. Also, starting CSF flow simulations from a nonphysical rest seems justified because periodic flow patterns stabilized after 2–3 cycles. Precise CSF pressure gradients through the cardiac cycle have not, to our knowledge, been reported. Penn et al. (2005) did a precise monitoring of pressure before and during the development of hydrocephalus and did not detect pressure gradients between the ventricle, brain, and subarachnoid space. This was true for long-term measurements over weeks and for real-time measurements that allowed accurate assessment of pulse pressures. They stated that theories predicting pressure gradients greater than the resolution of these sensors (0.5 mm Hg) across brain tissue have to be reevaluated. Yet this may not reflect real cases. Our idealized mathematic model allowed full control of study parameters, avoiding the problem of individual variations found in typical patient group studies.

Ventricular catheter domain and CFD results

Although there are various commercially available ventricular catheters intended to prevent the occlusion of the catheter, such as the modification by adding flanges and slots (Portnoy, 1971), none of these features has clinically proven to alter proximal shunt revision rates (Haase & Weeth, 1976; Lin et al., 2003). The exact mechanism of ventricular catheter occlusion is not precise but certainly includes various factors (Ginsberg et al., 2000; Harris et al., 2010; Harris et al., 2011; Harris & McAllister, 2012) including obstruction caused by normal brain cells or by pathological cells (Harris & McAllister, 2011; Harris & McAllister, 2012)

Cases of gross post-operative cerebrospinal fluid leakage along a ventricular catheter were reported. The CSF appeared to leak through the perforations of the ventricular catheter, as well as at the site of penetration of the ventricular wall (Prasad, Madan, Buxi, Renjen & Vohra, 1991). In narrow ventricles, we assume that catheter perforations that are located also in the tissue might be a risk for CSF shunt obstruction. As Thomale et al. (2010) stated fewer amounts of perforations in the catheters with equal flow features might decrease this risk when catheters can be implanted with adequate precision. This was seen in our study, where shear stress and flow rate was somewhat equally distributed in catheter models with fewer holes. On the other side, conditions of the catheter itself may alter flow as well. There appears to be some increase in resistance of CSF shunt catheters as they age, altering flow dynamics. In addition, the use of straight connectors within a CSF shunt system increases the resistance to flow of artificial CSF within the shunt system. The increase in resistance appears to be related to the duration of implantation and the length of the catheter and inversely related to the diameter of the catheter. This increase in resistance may be related to sterile shunt malfunction. The addition of straight connectors was associated with a significant increase in resistance in comparison with catheters without connectors (Cheatle, Bowder, Agrawal, Sather & Hellbusch, 2012). Although done in LPS, but applicable to VPS in essential, application of Poiseuille's law and Bernoulli's principle to the experimental design shows that the volume of flow is directly proportional to the sum of the pressure head and the vertical drop and inversely proportional to the length of the catheter. The flow rate through the standard catheter lengths was abnormally high (Mukerji, Cahill, Rodrigues, Prakash & Strachan, 2009).

We found shear stress numbers in this study in lesser values compared to those in the experimental study by Harris and McAllister (2012). As the authors suggest, hole´s size

change the shear stress numbers in only small portions of the total ventricular catheter lumen (Harris & McAllister, 2012). Our study was purely mathematical so shear stress numbers were minor. Harris and McAllister previous results on flow through catheter lumen indicate that a raise in flow, therefore shear stress, at these levels increases cells adhesion (Harris et al., 2010). Their study suggests cell adhesion generally decreases with increasing holes diameter under flow conditions and stated the need to examine how hole diameter impacts inflammatory-based shunt obstruction (Harris & McAllister, 2012). Although we did not modeling cell adhesion, we acknowledge that findings may be cell type-dependent, but we may also speculate that elevated shear stress played a specific role in each hole flow. A finding relevant to the debate on catheter obstruction is the position we observed in flow distribution. Flow velocities were clearly elevated at the level of the two most proximal hole distribution but were very low at the most distal ones. Yet, a blockage may develop in any portion of the proximal flow of ventricular catheter, but it will conduct fluid until the latest hole segment is not occluded. In such cases, our results disclose that flow patterns at the level of latest hole segment is not uniform, suggesting that blockage formation at that level will be abnormally higher, but also implying that trigger mechanisms other than local flow velocity changes should be sought.

Harris and McAllister (2011) and Lin et al. (2003) reported the only studies to date that have observed the effect of hole size. The first reported that flow and blockage are greatest in the holes farthest from the catheter tip and hypothesized that this was due to uneven flow distribution through the holes. While Harris and McAllister specifically studied VC occlusion adhesion factors, their results implied no clear dependencies between adhesion and proximity to the catheter tip but rather a dependency on how the holes were oriented in the flow system. This may imply that flow distribution is not the only factor in VC occlusion, and, as Harris and McAllister stated adhesion may be also influenced by gravity. Certainly, obstruction that occurs distal to the catheter tip in vivo may be caused by other factors, including holes being positioned outside of the ventricle (Thomale et al., 2010). While our study specifically addresses the flow patterns in various VC, it does not reproduce long standing, compound, multiple VC obstruction factors.

Additional CFD studies may help determine the effect of specific anatomic abnormalities on CSF flow patterns. The effect result of ventricular dimensions, of

pressure changes, of heart rate, and of cells and element forms on CSF flow are need to be determined. All these pressing issues can be safely studied with engineering mathematic models. The CSF flow through the holes followed a non homogenous pattern in all models, distributed predominantly in most proximal holes. Finally, we need to evaluate the optimal size and extent of hole dimensions, hole segment and ventricular catheter lumen to normalize CSF flow dynamics. Future work is guaranteed.

Legends to Figures:

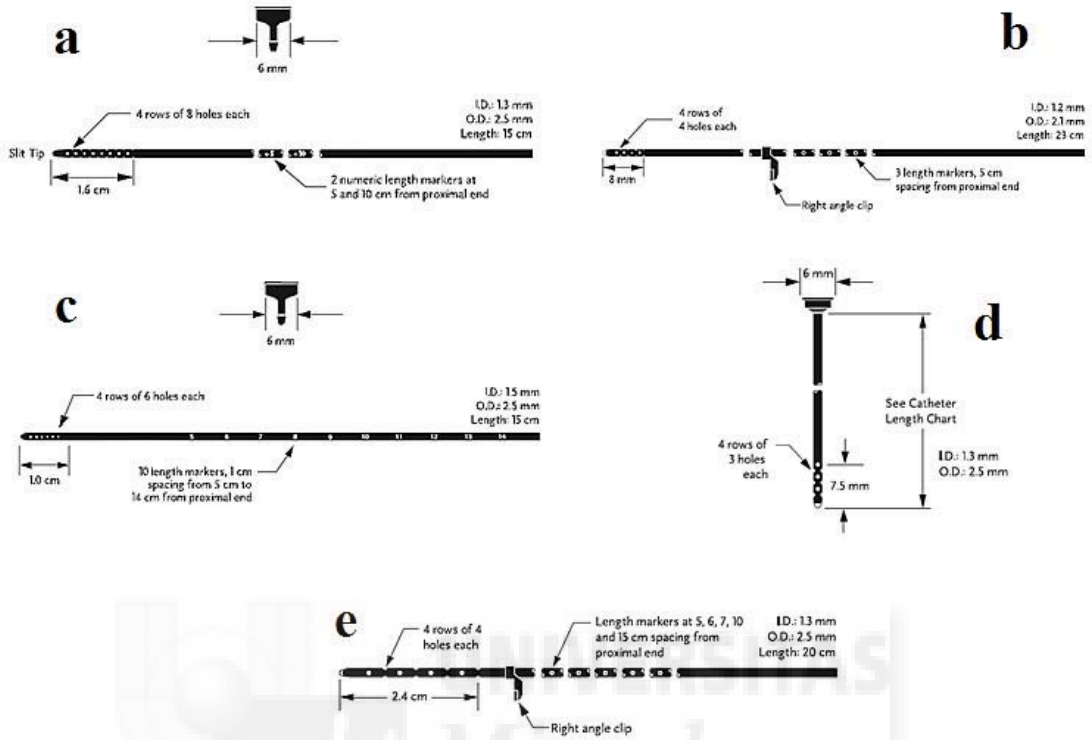

Figure 1. Five different models of current in use ventricular catheters used for CFD from Medtronic Catalogue**.**

Note. a) Innervision Snap Shunt Ventricular Catheter Kit. Included: innervision ventricular catheter, standard, barium impregnated, 15 cm; snap assembly reservoir base, burr hole, 6 mm, shallow depth; stainless steel stylet (not shown). b) Ventricular Catheter (small, 8 mm. flow holes and barium impregnated, 23 cm.). Included with product: right angle clip; stainless steel stylet (not shown). c) Rivulet Snap Shunt Ventricular Catheter Kit. Included with product: snap assembly reservoir base; stainless steel stylet (not shown). d) CSF-Snap Shunt Ventricular Catheter (standard barium impregnated). Included with product: unitized snap assembly reservoir base, burr hole, 6 mm, shallow depth; stainless steel stylet (not shown). e) Ventricular Catheter (standard, large flow holes, extra length markers, barium impregnated, 20 cm). Included with product: right angle clip; stainless steel stylet (not shown).

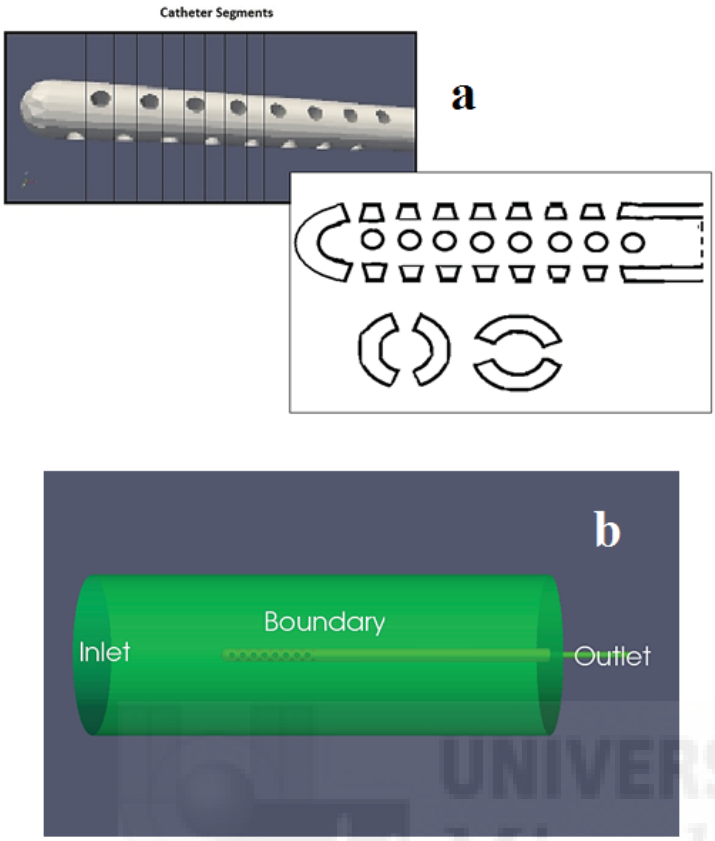

Figure 2. Mathematical model used in this study.

Note. a) Segmental distribution of inlets used for CFD calculation in ventricular catheters; b) The mathematic model as a mesh on which CFD was applied. Inlet, outlet, and wall boundaries used to define the region of interest.

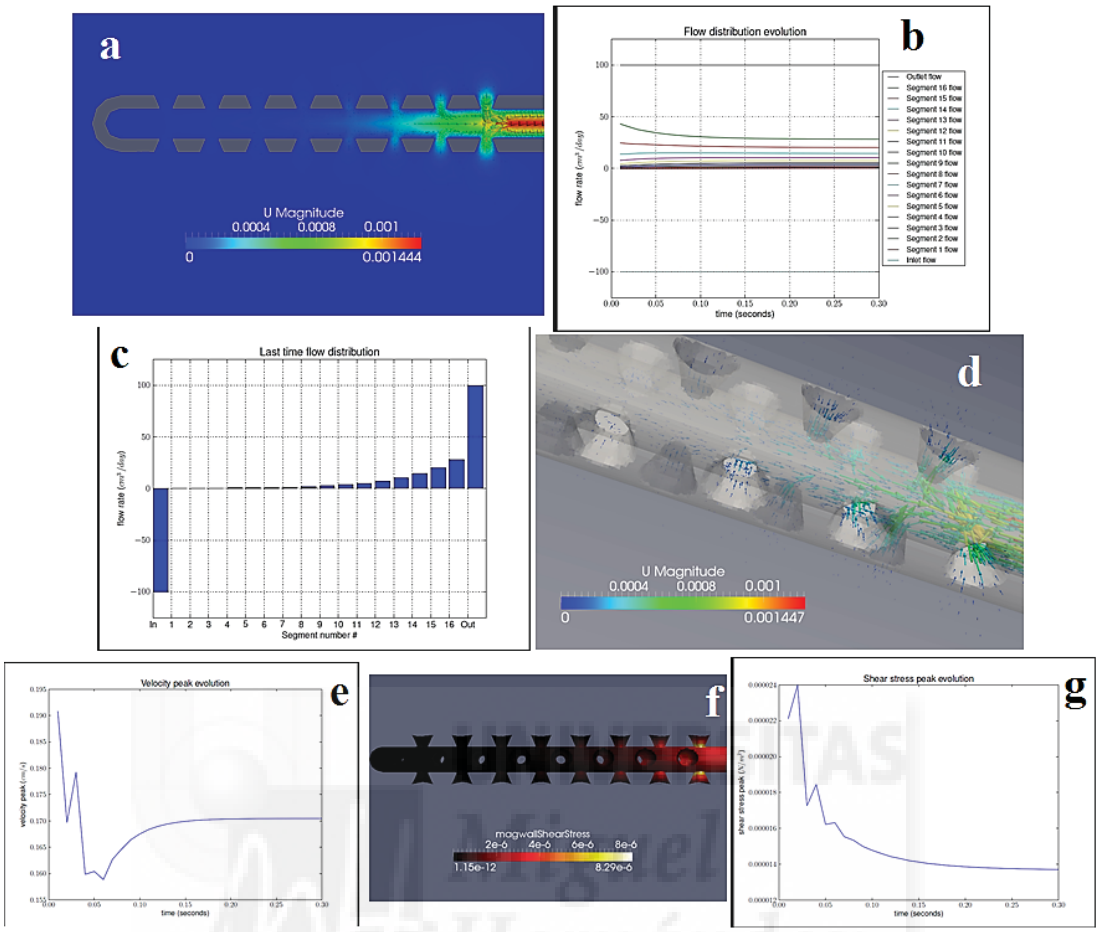

Figure 3. CFD results of a 3-D simulation of Catheter model 1.

Note. a) Flow velocity imaging of a 16-segment/32-hole catheter; b) Flow distribution evolution according to flow rate in time. Segments (group of holes) 13 to 16 have substantial flow comparing to the others holes; c) Flow bar distribution graph depicting flow rate in each segment. 75% of the flow is running through the four most proximal segments; d) 3D imaging representation of model 1 catheter showing regions of localized above-average velocities ("jets") in latest holes phases with proximal flow; e) Velocity peak components in models 1 catheter had a down peak clear jet pattern at t_0.05 sec.; f) Imaging depiction of magnitude shear stress in catheter model 1 with highest values at most proximal segments; g) Shear stress peak evolution graph. According to time, highest values were reached at 0.02 sec reaching baseline at 0.10 sec.

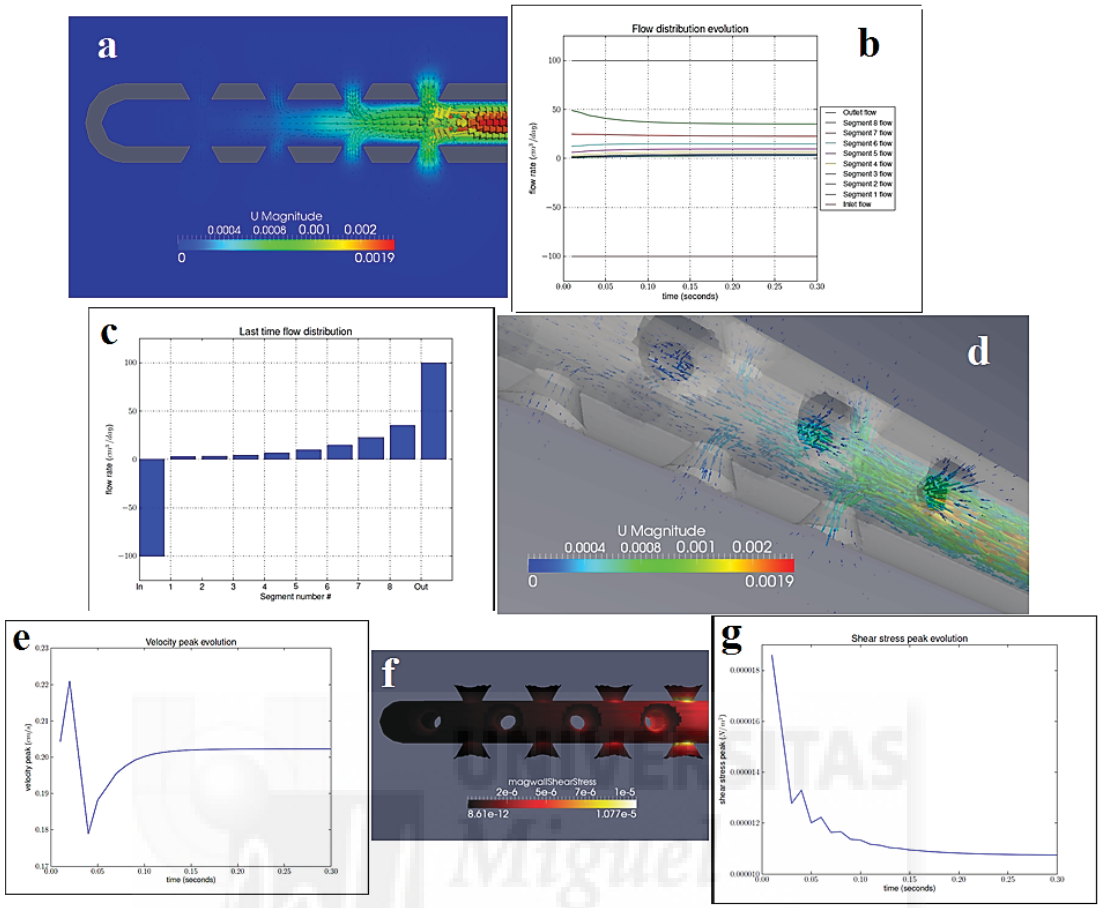

Figure 4. CFD results of an 8-segment/16-hole distributed in 8 mm (catheter model 2).

Note. See text for analysis.

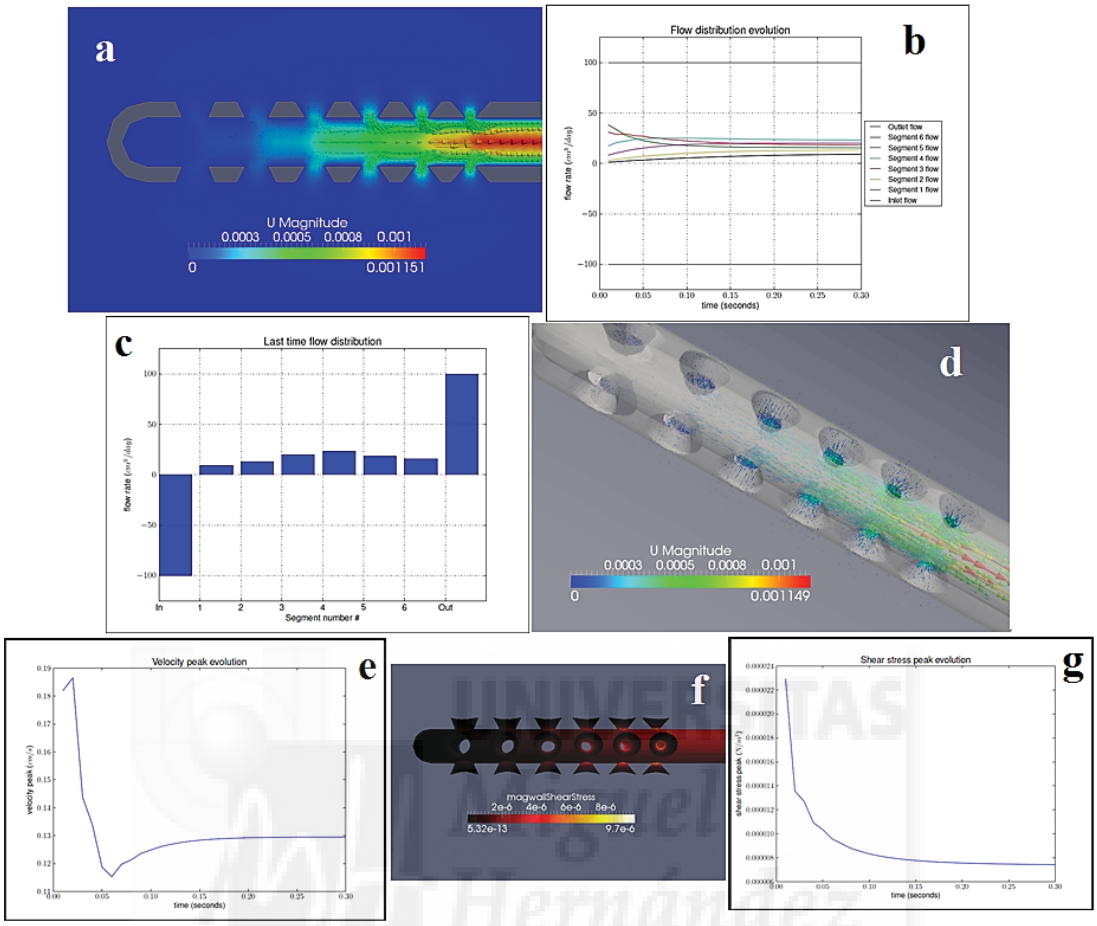

Figure 5. CFD results of an 6-segment/24-hole (catheter model 3-Rivulet type).

Note. See text for analysis.

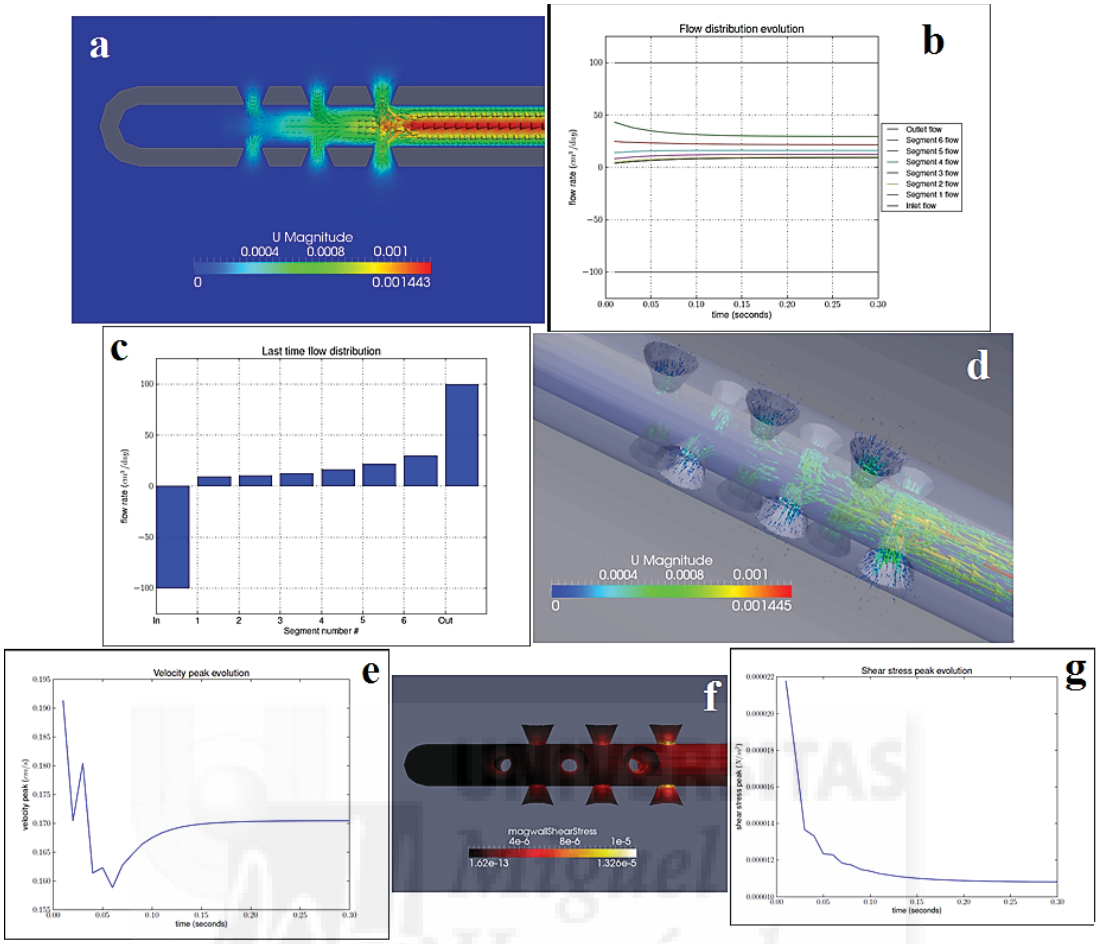

Figure 6. CFD results of an 6-segment/12-hole (catheter model 4).

Note. See text for analysis.

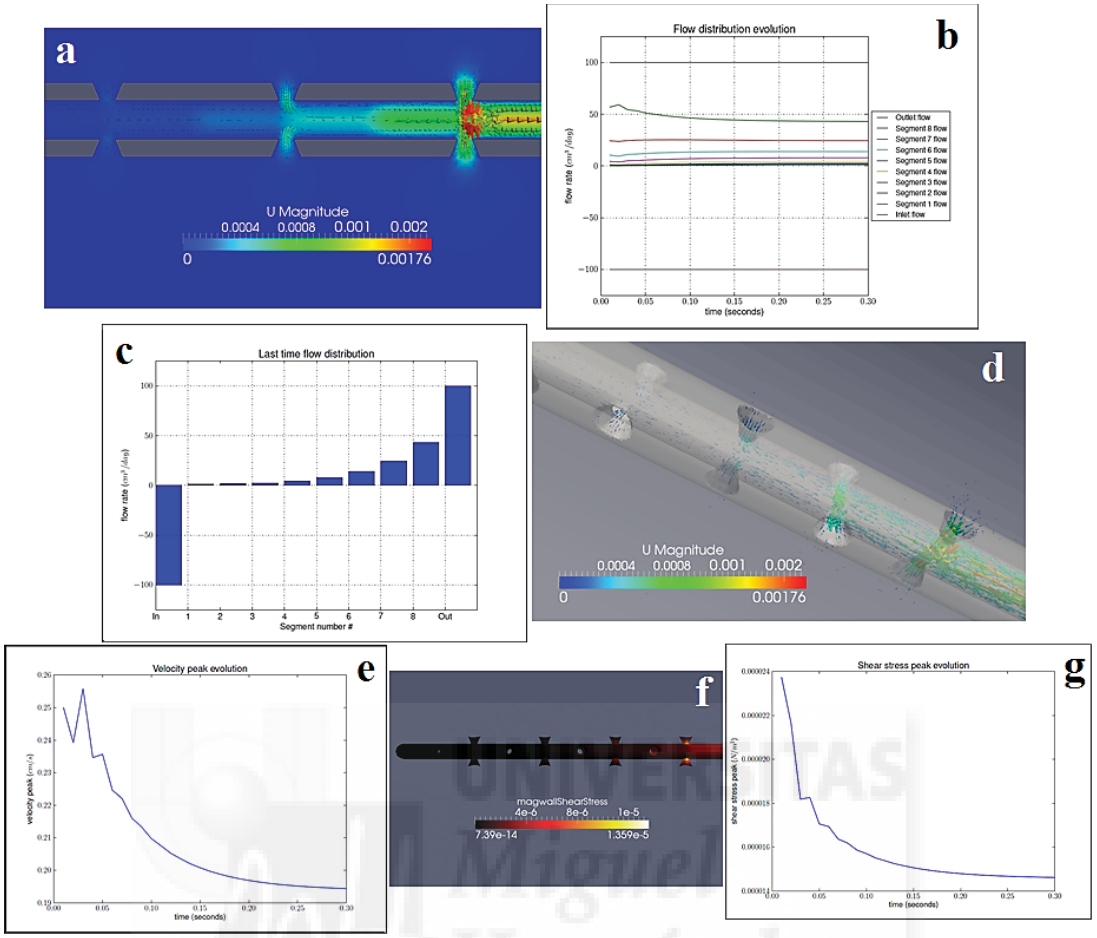

Figure 7. CFD results of an 8-segment/16-hole distributed in 24 mm (catheter model 5).

Note. See text for analysis.

Chapter 4:
Study 2. New designs of ventricular catheters for hydrocephalus

INTRODUCTION

In our initial study (Galarza, Giménez, Valero, Pellicer & Amigó, 2014) we analyzed the fluid dynamics of five currently used VC models to evaluate flow factors of proximal shunt malfunction. We found that the flow distribution follows a similar pattern in all VC considered. Specifically, from 50 to 75% of the cerebrospinal fluid flows into proximal sets of inlets of current commercially available 12 to 32-hole catheters, the flow being most uniform for the model Rivulet. We concluded that occlusion is most likely to occur at the proximal inlets in those VC. Our results agree with the landmark application of 2-D CFD to VC by Lin et al. (2003). In addition, they also resorted to 2-D water table experiments, and 3D automated testing apparatus together with an actual catheter.

It is well known that the most frequent cause of shunt failure is ventricular catheter obstruction, which may account for 50 to 80% of newly inserted shunts (Drake et al., 1998; Drake & Sainte-Rose, 1995; Sainte-Rose et al., 1991; Tuli et al., 2000). Although many factors contribute to this (Bergsneider et al., 2006; Harris et al., 2010; Harris et al., 2011; Harris & McAllister, 2012) the main one is related to fluid flow characteristics of the catheter within the hydrocephalic brain (Ginsberg et al., 2000; Lin et al., 2003; Sainte-Rose et al., 1991; Tuli et al., 2000). Numerical simulation is widely applied in everyday engineering studies to solve efficiently a wide variety of physical and technical problems. In particular, CFD is a numerical method to calculate the flow of compressible and incompressible fluids even with complicate geometries, thus

providing a handy tool for design optimization. Given a 3D model of the system to be studied, and the initial and boundary conditions, the CFD software calculates the resulting flow with greater spatial and temporal resolution than that achieved with specific MRI studies (real-time phase-contrast magnetic resonance) and also displays other flow characteristics like pressures, flow structures, stresses, and pressure waves. We recently presented results of 3-D CFD in five models of commercially available VC, disclosing similar results for the CSF flow in all models (Galarza et al., 2014).

Our present objective is to study five new ventricular catheter designs by means of 3-D CFD. This produces a visual image of the fluid velocity field and the results can be integrated to evaluate flow and shear stress values.

MATERIAL AND METHODS

Five prototypes of ventricular catheters are studied in this paper. Models were designed based on currently in use catheters. Model 1 *(Figure 1, image a)* consists of a VC of 3 segments of 4 holes distributed along 6 mm from tip to last segment; Model 2 *(Figure 1, image b)* consists of 2 segments of 6 holes and 1 segment of 3 holes distributed along 6 mm from tip to last segment; Model 3 *(Figure 1, image c)* consists of 2 segments of 6 holes and 2 segments of 3 holes distributed along 7.5 mm from tip to last segment; Model 4 *(Figure 1, image d)* consists of 4 segments of 6 holes distributed along 7.5 mm from tip to last segment; and Model 5 *(Figure 1, image e)* has the same hole configuration as Model 4 but they differ in the hole sizes *(Table 1)*. In all models the internal diameter of the catheter (its lumen) is 1.5 mm and the external diameter 2.5 mm. Furthermore, all holes are tapered (or conical), i.e., modeled by truncated cones. The greatest diameter, corresponding to the external side of the catheter, is always 0.50

mm. The smallest diameter, corresponding to the internal side of the catheter, ranges from 0.20 to 0.35 mm depending on the model and segment. The inter-segment distance is 1.5 mm in all models. See *Table 1* for more details.

Catheter and hydrocephalus modeling

The methodology follows our initial study (Galarza et al., 2014). Thus, the VC is located in a cylindrical cavity with rigid walls which models the ventricle. An inlet and outlet centered on the bases of the cylinder allow simulating the drainage of cerebrospinal liquid. This cavity is large enough (as compared to the length of the perforated catheter segment) not to influence the flow in the proximity of the holes, which is the flow we are most interested in. The holes of the VC are grouped on cross planes, each plane at a constant distance from each other. We refer to each group of holes as a row or a segment. These segments total three or four, depending on the model, each segment containing a varying number of holes symmetrically disposed in the angular direction. Furthermore, the holes of the VC are aligned in the longitudinal direction if consecutive segments contain the same number of holes. A CFD model is used then to calculate the so-called stationary (i.e., time independent) values of the velocity and pressure fields in the whole domain of the fluid, as well as the flow (in cm^3/day) through each flow segment, and the maximal shear stress (N/m^2) in seconds. These stationary values are reached after a transient phase during which the flow evolves from the initial state, defined by the initial conditions of the CFD model, to the steady state. We come back to this point below.

Broad normative data for CSF characteristics and volumes was taken from first-rate considerations that have been provided by Drake and Saint Rose (1995), Hakim (1969), Harris and McAllister (2011), Schley et al. (2004) and Sood et al. (1993). The drainage

flow of our catheter model was set equal to 100 cm^3/day. This being the case, the graphical representations of the stationary flows through the hole segments *(Figures 2 to 6, images b and c)* can also be read as percentages. The normal ventricular pressure ranges from 12 to 18 cmH2O, which may resemble cases of normal pressure hydrocephalus. We have used 12 cmH2O. The CSF has a specific gravity of 1007, compared to 1047 for the surrounding brain. The same numbers were used in our model. Other specific normative data can be taken from our previous study (Galarza et al., 2014).

Ventricular catheter designing

To simulate the flow of the CSF through the new ventricular catheters, we created 3D numerical models based on the actual geometric shapes of commercially available models, or on images and dimensions of their actual boundaries. The solid geometry of the VC was generated with Salome (version 7.3.0) GNU Lesser General Public License (LGPL). This numerical and graphical environment contains separate working modules for geometry creation or manipulation (Geometry), meshing (Mesh), solver management (Supervisor), post-processor (Post-Pro), and communication module (MED).

The physical space is converted to a series of interconnected points or nodes which define the computational domain. The number of nodes determines the resolution of the model and the time needed for computation. The mathematic model, if displayed graphically, appears as a mesh. The physical characteristics of the fluid and its initial and boundary conditions are specified. The grid-generation utility snappyHexMesh is used to discretize the computational domain with unstructured hexahedral boundary-fitted mesh. The grid generator allows cutting out unnecessary parts not related to the

region of interest and delimiting the computational domain by means of the inlet, outlet, and cavity solid boundaries. The result is the region of interest in which CFD will be applied. SnappyHexMesh is a utility provided with OpenFoam (see below), which has the ability to produce meshes for complex geometries. In particular, it generates finer grids on curved surfaces and boundaries, such as the internal and external surfaces of the catheter (including tip and holes).

CFD Calculation

OpenFOAM® (Open Field Operation and Manipulation) is a free, open source CFD Toolbox software package produced by OpenCFD Ltd. The governing equations for CFD calculation are the 3D incompressible unsteady Navier-Stokes equations written in conservative form for mass and momentum. The numerical simulations were run with the version OpenFOAM® v2.2.2. In our case we used the icoFoam solver to integrate numerically the incompressible Navier-Stokes equations. As explained above, the fluid-mechanical variables change with time at the beginning, till the flow reaches a steady phase (the stationary regime) just because the boundary conditions are time-independent. Note that the initial, unsteady phase is a numerical artefact due to the use of the general ("unsteady") Navier-Stokes equations. Needless to say, we are only interested in the stationary regime.

The simulation was performed by setting the kinematic viscosity of CSF equal to 0.75 x 10^{-6} m^2/s, the kinematic viscosity of water at body temperature. Boundary conditions were specified on all our boundary surfaces. The velocity field at the cavity inlet was adjusted in order to achieve a constant inflow of 100 cm^3/day and, for consistency, the pressure was zero gradient. On the rest of the ventricle and catheter walls, which were considered rigid, non-slip and non-penetration conditions were chosen (i.e., all velocity

components at the solid walls were set to zero). The pressure was specified to have zero gradient there because the flux through the wall is zero.

At the cavity outlet, the pressure was set equal to 15 cmH2O, or 20.41 mmHg (2721 $Pa=N/m^2$), and a zero gradient condition on the velocity was specified as well. The flow was computed with a time step of 0.005 seconds during a time interval of 0.3 seconds, long enough to reach stationarity. The time step was found to be sufficiently small from the point of view of accuracy. The results used for the flow analysis corresponds to the stationary regime, thus guaranteeing that the results are independent of the initial conditions.

The images were displayed by using ParaView 4.1.0.

RESULTS

Vector representations of the flow fields of the VC Models 1 to 5 resulting from 3D CFD are shown in *Figures 2 to 6, image a*, respectively. The scale below each model makes evident that the flow vectors are equally concentrated in all holes and the fluid velocities are there similar in each model, which discloses that all holes are uniformly draining the CSF. Fluid velocities can then be converted into flows and distributions of flow per segment. The simulations also demonstrate that the velocity patterns are different in all catheters. Sagittal images display moderate larger velocities in the distal holes than in the proximal ones in Models 1, 2, 3. This relation is inverted in Model 4 and reaches uniformity in Model 5 *(Figures 2 to 6, image b).*

The evolution of the flow distribution shows that the flow through the catheter segments reaches stationarity after 0.05s in most models. The stationary flow distribution is

depicted in *Figures 2 to 6, image c,* in cm^3/day, where the flow is indicated in each catheter segment. The inlet flow through each segment of each catheter, as well as the inlet flow per unit area through each segment and the total sum of inlet segment flows are shown in *Table 1***.**

Three-D images show stationary flow in all models. These images reveal regions of localized above-average velocities in most holes with a uniform pattern in all new models. The antero-posterior and left-right components of the velocity vectors, depicted in three dimensions, show the same pattern in all models *(Figures 2 to 6, image d).*

Figures 2 to 6, image e, show the time evolution of the velocity peak in Models 1 to 5, respectively. This variable drops very fast from its initial value to its minimum, and then converges slowly to its stationary value. Once again we point out that the physically relevant data correspond to stationary flow results.

VC wall shear stress imaging can be seen in *Figures 2 to 6, image f.* The shear stress peaks converge to their stationary values in a, basically, decreasing monotonic way for all catheter models *(Figures 2 to 6, image g).* Highest values are seen in Models 1, 2 and 3, while the lowest value is seen in Model 4.

Using our CFD methodology we calculated that the flows through the segments distribute evenly in these five CV prototypes. Still, Models 1, 2 and 3 have a distal to proximal decreasing flow. Model 4 has an inverse flow to the previous ones, that is, a distal to proximal increasing flow, while Model 5 has a constant flow over the segments. These relations are depicted in *Figures 2 to 6, image b*.

DISCUSSION

We evaluated the fluid dynamics of five new VC models to estimate flow factors of proximal shunt malfunction.

This paper is basically based in three previous studies of currently in use VCs. According to Galarza et al. (2014), the CSF flow through the holes follows a non homogeneous pattern in all models studied, the flow being predominantly concentrated in the most proximal holes. This renders the other holes useless. In the first application of CFD to VC, Lin et al. (2003) developed a new model by placing the largest holes distally. They state that this change would decrease the probability of occluding the entire catheter when only its tip is blocked. We have incorporated this idea by varying the number of holes in the segments and possibly also their external and/or internal diameter. Quite recently, the significance of the number of holes for the proper function of the VC was addressed by Thomale et al. (2010). Both VCs (Thomale and Rivulet) are currently in use.

Let us underline at this point that, at variance with Lin et al. (2003), the results reported in this paper are only based on (three-dimensional) flow simulations, hence they are entirely mathematical. Thus, our results can only be compared with other 3-D flow results, so far not available.

Our first prototype, a 12-hole VC, shows a distal to proximal decreasing stationary flow distribution in three segments *(Figure 2, image c)*, a velocity peak evolution reaching stationarity at 0.15 seconds *(Figure 2, image e)*, and a high shear stress *(Figure 2, image g).*

The second prototype, a 15-hole VC, also shows a distal to proximal decreasing stationary flow distribution in three segments *(Figure 3, image c*), a velocity peak

evolution reaching stationarity at 0.15 seconds (*Figure 3, image e)*, and a high shear stress (*Figure 3, image g).*

The third prototype, a 18-hole VC, shows a distal to proximal decreasing stationary flow distribution in 4 segments (*Figure 4, image c),* a slower velocity peak evolution (*Figure 4, image e*), and the highest shear stress (*Figure 4, image g).*

The 24-hole VC of 4 segments, our fourth prototype, shows a proximal to distal decreasing stationary flow distribution that is similar to most commercially available VC *(Figure 5, image c*), a homogeneous velocity peak evolution *(Figure 5, image e),* and the lowest value of shear stress *(Figure 5, image g).*

The tapered 24-hole VC of 4 segments, our fifth prototype, shows the most uniform stationary flow distribution *(Figure 6, image c),* a relatively faster velocity peak evolution (*Figure 6, image e)*, and a low value of shear stress (*Figure 6, image g).*

All of them show better flow characteristics, according to 3-d CFD results, than commercially available, currently in use VC.

In order to evaluate CFD in VC we developed a hydrocephalus paradigm. Our hydrocephalus domain is an idealized mathematical model that allows full control of study parameters, avoiding the problem of individual variations found in typical patient group studies. This hydrocephalus model does not reproduce the pathologic anatomy of any individual or any group of patients. Rather, its characteristics are within the range of what is found in all patients. Still we simplified the hydrocephalic area by modeling it as cylinder. The reason and method for this can be found in our previous paper (Galarza et al., 2014) and in references (Penn et al., 2005; Penn et al., 2011; Sood et al., 2004; Sood et al., 2005; Stein & Guo, 2008).

The ICP value we have taken for our hydrocephalus model may be criticized. In fact, the concept that a “normal” CSF pressure is a defining feature of INPH has been criticized (Bradley, 2000; Bret, Guyotat & Chazal, 2002). In patients with INPH, the CSF-OP measured by lumbar puncture in the lateral recumbent position averages 11 +/- 3.3 mm Hg (150 +/- 45 mm H2O) but may fall between 4.4 and 17.6 mm Hg (60–240 mm H2O) (Relkin et al., 2005). In large series by Eide (2006), the static ICP was normal in all patients (mean ICP 7.6 ± 4.8 mmHg). As in other papers cited in this manuscript, there is no specific numbers. In any event, our mathematical model takes a single value for analysis calculation.

Thomale et al. (2010) were the first researchers to address the importance of the number of holes for the performance of VC. Other important contributions regarding the VC design came from the Harris and McAllister group (Harris et al., 2010; Harris et al., 2011; Harris & McAllister, 2011; Harris & McAllister, 2012). In the 4- as well as in the 6-hole catheters of Thomale’s design, the drainage is balanced and functional through every single perforation, at variance with the 16-hole catheter. They visualize the highest possible values for drainage through all perforations in the 4-hole catheter, and stated that the draining capacity of this type of catheter is limited. However, an additional reserve draining capacity of the distal perforations of the 6-hole catheter in the low and high flow experiments is demonstrated in their study. Thus, the 6-hole catheter was chosen for clinical evaluation. They decided to use a lower number of perforation holes based on calculations showing that additional holes become useless when the total area of perforation exceeds the area of the intraluminal diameter of the VC. They stated that the use of more than two holes, theoretically, did not enhance the amount of drainage through the catheter. This is true, from a hydrodynamic standpoint, only when there is a constant pressure. Certainly, a condition not reflected in

hydrocephalus. This information has been pointed out, partly, in the paper by Ginsberg et al. (2000), who disputed that one remaining patent perforation increased the draining pressure of no more than 0.5 cmH2O to permit flow and those three holes have the same pressure flow correlation as 32 holes in a ventricular catheter (Ginsberg et al., 2000; Harris & McAllister, 2011). This is not reflected in our study, which aims at the influence of the hole diameter and the number of holes per VC segment on the flow distribution per segment. This factor helps redistribute the pressure flow along the VC, as we disclosed it in the shear stress curves *(Figure 2 to 6, images f and g).*

On the other hand, we entirely agree with Thomale et al. (2010) when they state that a reason to include more perforations in VC than actually needed might be the high probability of placing some holes intraventricularly by freehand puncturing. Thus, the amount of perforation holes is simply related to the narrow precision of how ventricular catheters are routinely implanted.

In narrow ventricles we assume that catheter perforations that are located also in the tissue might be a risk for CSF shunt obstruction. The CSF appears to leak through the perforations of the ventricular catheter, as well as at the site of penetration of the ventricular wall (Prasad et al., 1991). As Thomale et al. (2010) showed a smaller number of holes in the catheters with equal flow characteristics might decrease this risk when catheters can be implanted with adequate precision. This was seen in our previous study, where shear stress and flow rate was somewhat equally distributed in catheter models with fewer holes. For this reason we sought VC with the adequate number of holes, specifically the precise number of holes per segment. Rather than changing the number and hole dimensions of the VC, there are various commercially available ventricular catheters intended to prevent the occlusion of the catheter, such as the modification by adding flanges and slots (Portnoy, 1971). Yet, these features have not

been clinically proven to diminish rates of proximal shunt malfunction (Lin et al., 2003; Haase & Weeth, 1976). Although this is seen in daily practice, most studies of shunts and catheters for the treatment of hydrocephalus are clinical non-comparative studies, hence there is no blunt experimental data.

Still, the precise mechanism of ventricular catheter occlusion is not known but it certainly includes other than the valve design (Drake & Sainte-Rose, 1995; Sainte-Rose et al., 1991; Tuli et al., 2000; Schley et al., 2004), hindrance caused by normal brain or pathological cells (Bergsneider et al., 2006; Harris & McAllister, 2012; Harris et al., 2011; Harris et al., 2010; Ginsberg et al., 2000; Harris & McAllister, 2011).

The number of holes in the VC is important, but a blockage may develop in any portion of the proximal flow of the VC, and it will conduct fluid until the latest hole is not occluded. The results of our previous study revealed that, in most commercially available VC, the flow is elevated at the most proximal segment, suggesting that blockage formation at that level will be abnormally higher. Given that blockage may begin in any of the VC segments, this also implies that trigger mechanisms other than local flow velocity changes should be sought. Harris and McAllister previous results on flow through catheter lumen indicate that a raise in flow, therefore shear stress, increases cells adhesion (Harris et al., 2010). Their study suggests that cell adhesion generally decreases with increasing hole diameter under flow conditions and stated the need to examine how hole diameter impacts inflammatory-based shunt obstruction (Harris & McAllister, 2012). Although we did not model cell adhesion, we acknowledge that findings may be cell type-dependent, but we may also speculate that elevated shear stress played a specific role in each hole flow. As previously pointed out (Galarza et al., 2014), we found much smaller shear stress numbers than in the experimental study by Harris and McAllister (2012). As the authors suggest, the hole

size changes the shear stress numbers in only small portions of the total VC lumen (Harris & McAllister, 2012). As Galarza et al. (2014), the present study is entirely mathematical, so shear stress numbers are lower.

Other than the precise number of holes per segment of VC, we sought the precise hole dimension to conduct fluid. Harris and McAllister (2011) and Lin et al. (2003) reported the only studies to date that have observed the effect of hole size. Harris and McAllister specifically studied VC occlusion adhesion factors and their results implied no clear dependencies between adhesion and proximity to the catheter tip but rather a dependency on how the holes were oriented in the flow system. This may entail that flow distribution is not the only factor in VC occlusion, and, as they stated, adhesion may be also influenced by gravity. Certainly, obstruction that occurs distally to the catheter tip in vivo may be caused by other factors, including holes being positioned outside of the ventricle (Thomale et al., 2010). It is important to point out that our study specifically addresses the flow patterns in five new prototypes of VC, and it does not reproduce multiple compound, long standing VC occlusion factors.

Additional CFD studies may help determine the effect of specific anatomic abnormalities on CSF flow patterns. Other factors, such as the effect result of ventricular dimensions, of pressure changes, of heart rate, and of cells and element forms on CSF flow still need to be investigated. Some of these factors can be safely studied with engineering mathematic models

After assessment of diverse prototypes of VC, we disclosed that flow pattern depends on certain parameters. It is determined by the number of holes, the hole diameter, the ratio hole/segment and the distance between hole segments. We will elaborate this concept in an upcoming report.

In this study, we found that flow distribution follows a specific pattern according to the number of holes per catheter segment and to the hole size(s) of the VC. In regard to these new models, we may state that they are less prone to occlusion because of the improved flow pattern.

Conclusion

With our designs we obtain a homogeneous flow pattern, similar to the Rivulet catheter, but without necessarily varying the diameters of the holes. The third prototype of 18-hole VC shows a distal to proximal decreasing stationary flow distribution in 4 segments with a slower velocity peak, which makes it, theoretically, less prone to proximal obstruction. The new method resorts to varying the number of holes in the VC segments. Instead of a fixed number of holes per segment, as in the current VC designs (including the Rivulet model), we propose that the number of holes per segment can vary, being higher in the distal segments (the farthest to the valve) and lower in proximal segments. Thus, our design has the same advantage as the catheter Rivulet (flow uniformity) but without the disadvantage of using very small holes. We must add that our numerical study is based on three-dimensional models, which allows studying properties that cannot be studied with two-dimensional models. Examples of the latter are the flow behavior when (a) the segments rotate independently, (b) holes are randomly clogged, or (c) the dimension of the cavity that models the ventricle varies. Prospect studies are assured.

Table 1.
CV characteristics and flow volumes in five prototypes. Lengths in cm. Areas in cm^2. Flows in cm^3/day.

	Model 1	Model 2	Model 3	Model 4	Model 5
Number of holes / Number of segments	12 / 3	15 / 3	18 / 4	24 / 4	24 / 4
No. of holes per segment	[4, 4, 4]	[6, 6, 3]	[6, 6, 3, 3]	[6, 6, 6, 6]	[6, 6, 6, 6]
Distance from each segment to the tip	[3, 4.5, 6]	[3, 4.5, 6]	[3, 4.5, 6, 7.5]	[3, 4.5, 6, 7.5]	[3, 4.5, 6, 7.5]
External radius of the holes in the same segment	[0.5, 0.5, 0.5]	[0.5, 0.5, 0.5]	[0.5, 0.5, 0.5, 0.5]	[0.5, 0.5, 0.5, 0.5]	[0.5, 0.5, 0.5, 0.5]
Internal radius of the holes in the same segment	[0.28, 0.24, 0.2]	[0.3, 0.25, 0.25]	[0.3, 0.25, 0.25, 0.2]	[0.25, 0.25, 0.25, 0.25]	[0.35, 0.3, 0.25, 0.2]
Total sum of hole areas per segment	[0.99, 0.72, 0.5]	[1.7, 1.18, 0.59]	[1.7, 1.18, 0.59, 0.38]	[1.18, 1.18, 1.18, 1.18]	[2.31, 1.7, 1.18, 0.75]
Inlet flow through each segment	[35.77, 35.18, 28.8]	[35.75, 34.89, 29.11]	[28.7, 28.05, 23.42, 19.58]	[12.3, 16.49, 26.21, 44.74]	[19.43, 23.09, 29.08, 28.14]
Inlet flow per unit area through each segment	[36.3, 48.6, 57.3]	[21.07, 29.61, 49.42]	[16.92, 23.81, 39.75, 51.93]	[10.44, 14.0, 22.25, 37.97]	[8.42, 13.61, 24.69, 37.32]
Total sum of inlet segment flows	99.74362	99.74448	99.74189	99.74362	99.74448

Legends to Figures:

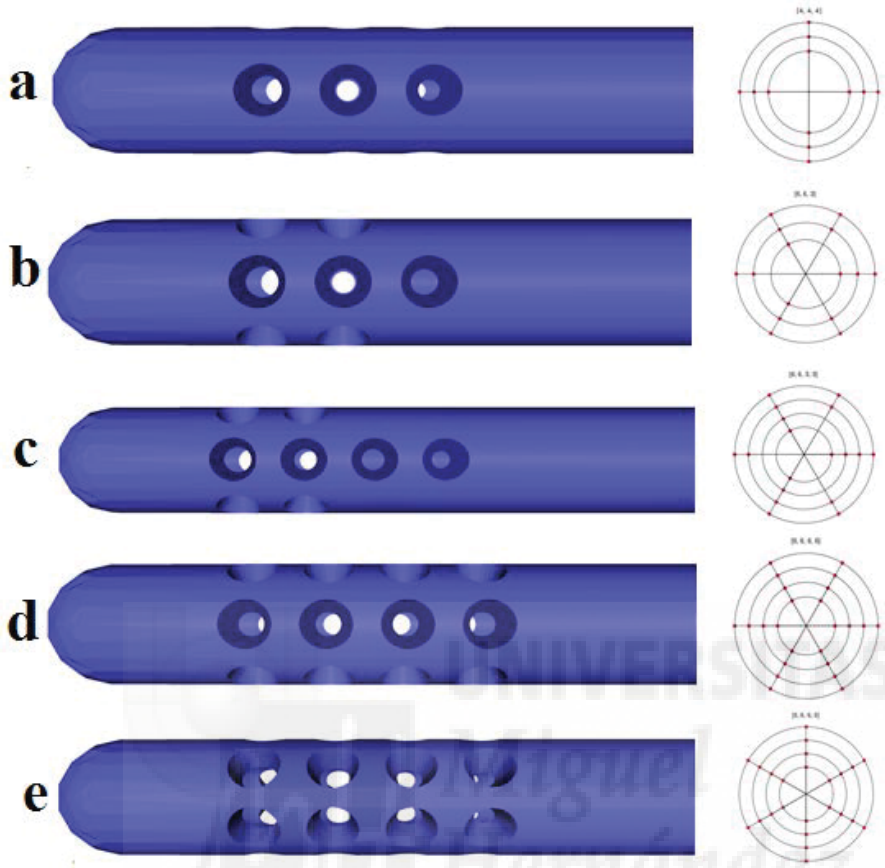

Figure 1. New models of VC for the treatment of hydrocephalus based on 3-D CFD studies.

Note. The target design shows the distribution and number of the holes according to the VC segment. All holes are conic, i.e., their surfaces are doubly truncated cones. a) Model 1 consists of a VC of 3 segments of 4 holes distributed in 6 mm from tip to last hole; b) Model 2 consists of 2 segments of 6 holes and 1 segment of 3 holes; c) Model 3 consists of 2 segments of 6 holes and 2 segments of 3 holes distributed in 7.5 mm from tip to last hole; d) Model 4 consists of 4 segments of 6 holes; e) Model 5 consists of 4 segments of 6 holes.

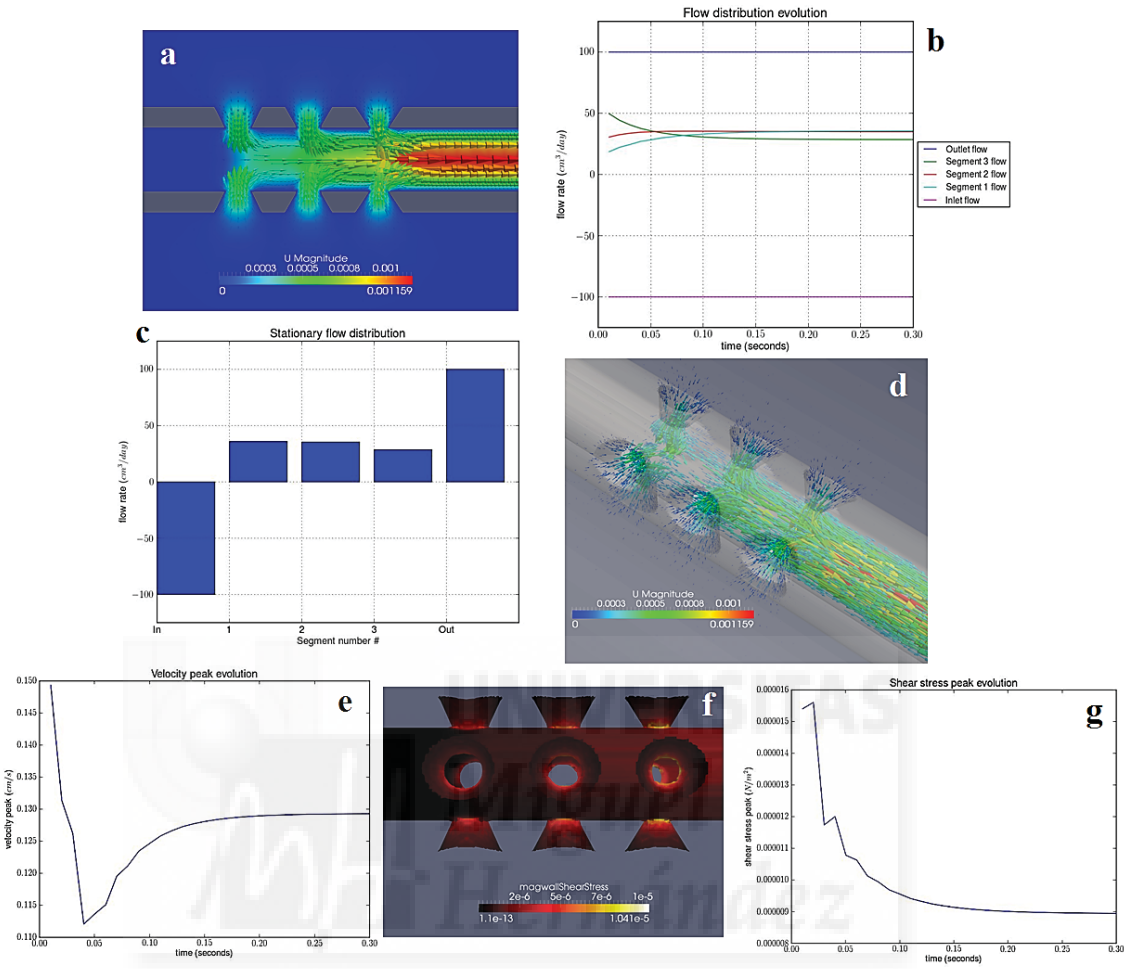

Figure 2. CFD results in prototype Model 1.

Note. a) Fluid velocity imaging of a longitudinal cross section; b) Time evolution of the flow per segment. The stationary flows per segment are roughly evenly distributed; c) Bar diagram of the stationary flows per segment; d) 3D representation of the velocity through the holes and inside the catheter; e) Time evolution of the fluid velocity peak; stationarity is reached after approximately 0.20 sec.; f) Imaging depiction of the shear stress in the hole walls, with equally distributed values at all segments; g) Time evolution of the shear stress peak; stationarity is consistently reached after some 0.20 sec.

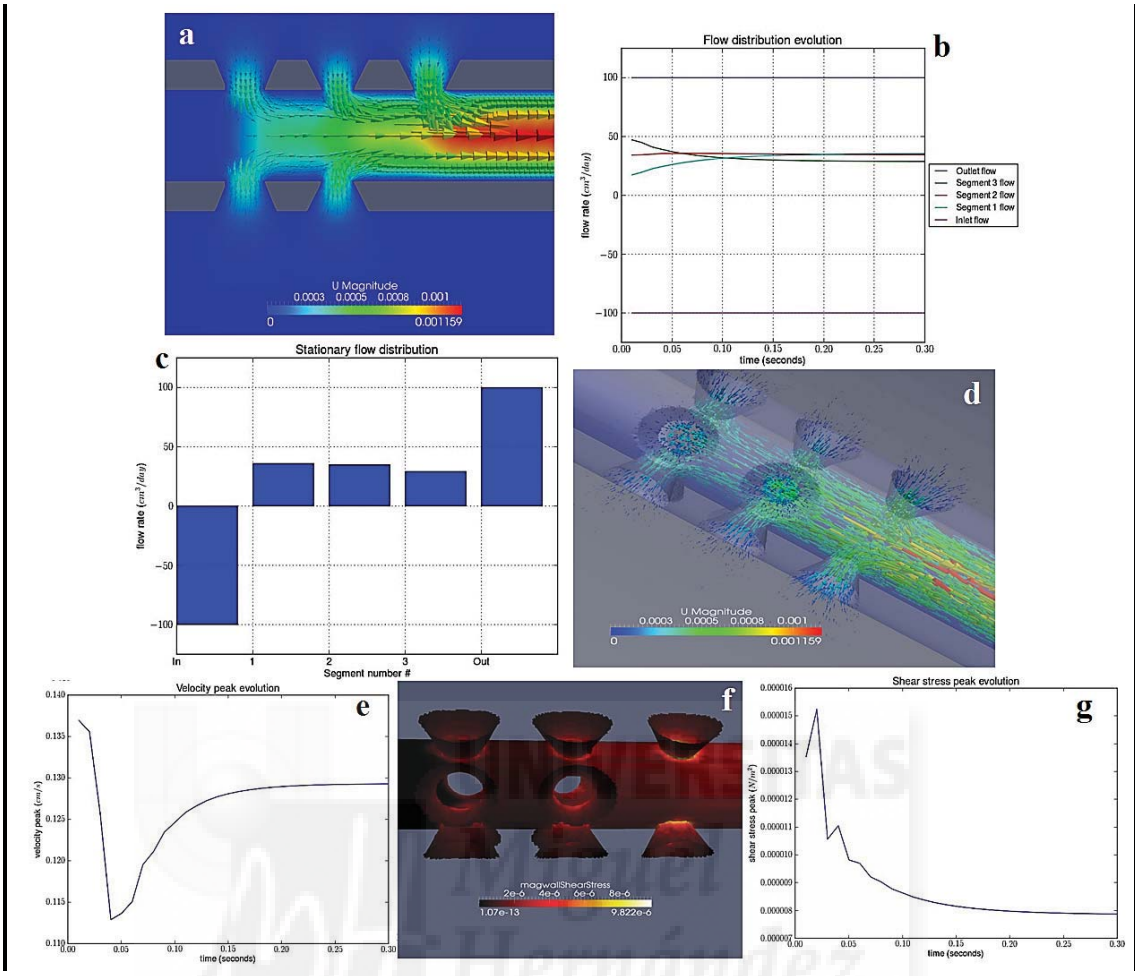

Figure 3. The following panels refer CFD results in prototype Model 2.

Note. a) Fluid velocity imaging of a longitudinal cross section; b) Time evolution of the flow per segment. The stationary flows per segment are roughly evenly distributed; c) Bar diagram of the stationary flows per segment; d) 3D representation of the velocity through the holes and inside the catheter; e) Time evolution of the fluid velocity peak; f) Imaging depiction of the shear stress in the hole walls; g) Time evolution of the shear stress peak.

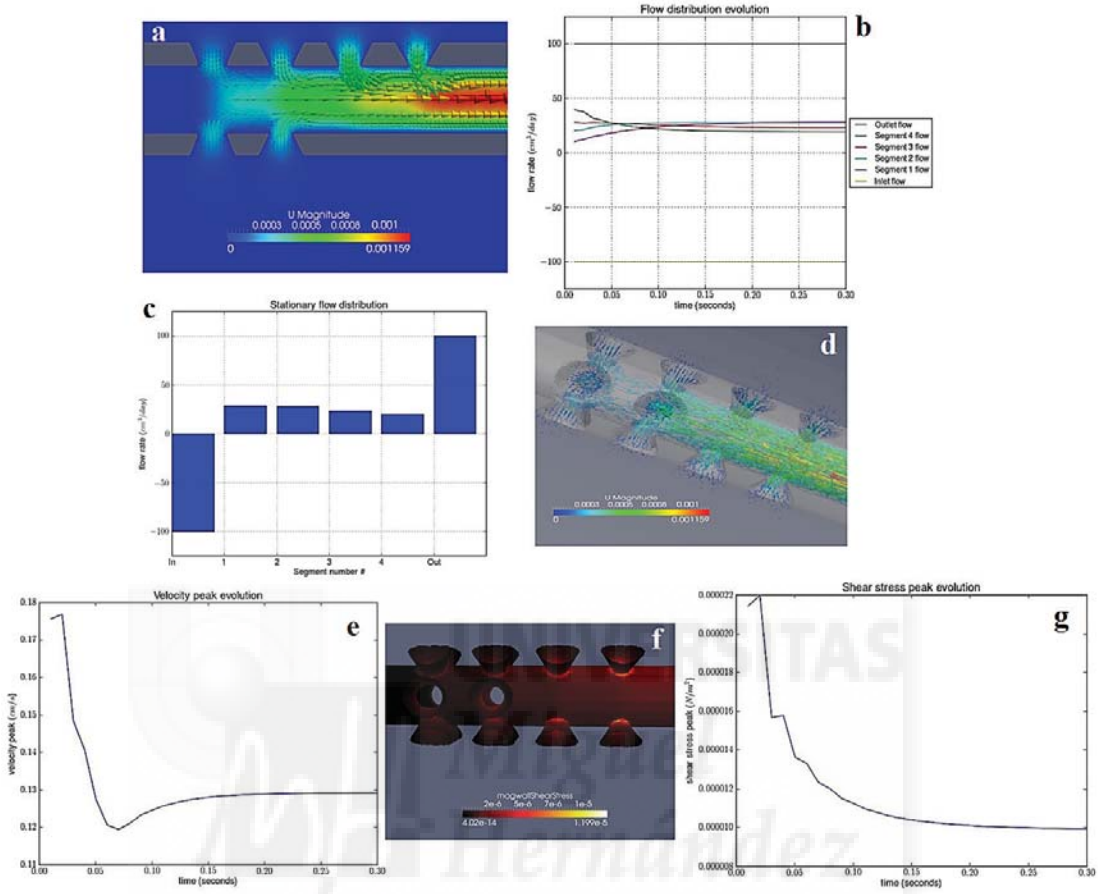

Figure 4. The following panels refer CFD results in prototype Model 3.

Note. a) Fluid velocity imaging of a longitudinal cross section; b) Time evolution of the flow per segment; c) Bar diagram of the stationary flows per segment; d) 3D representation of the velocity through the holes and inside the catheter; e) Time evolution of the fluid velocity peak; f) Imaging depiction of the shear stress in the hole walls, with equally distributed values at all segments; g) Time evolution of the shear stress peak.

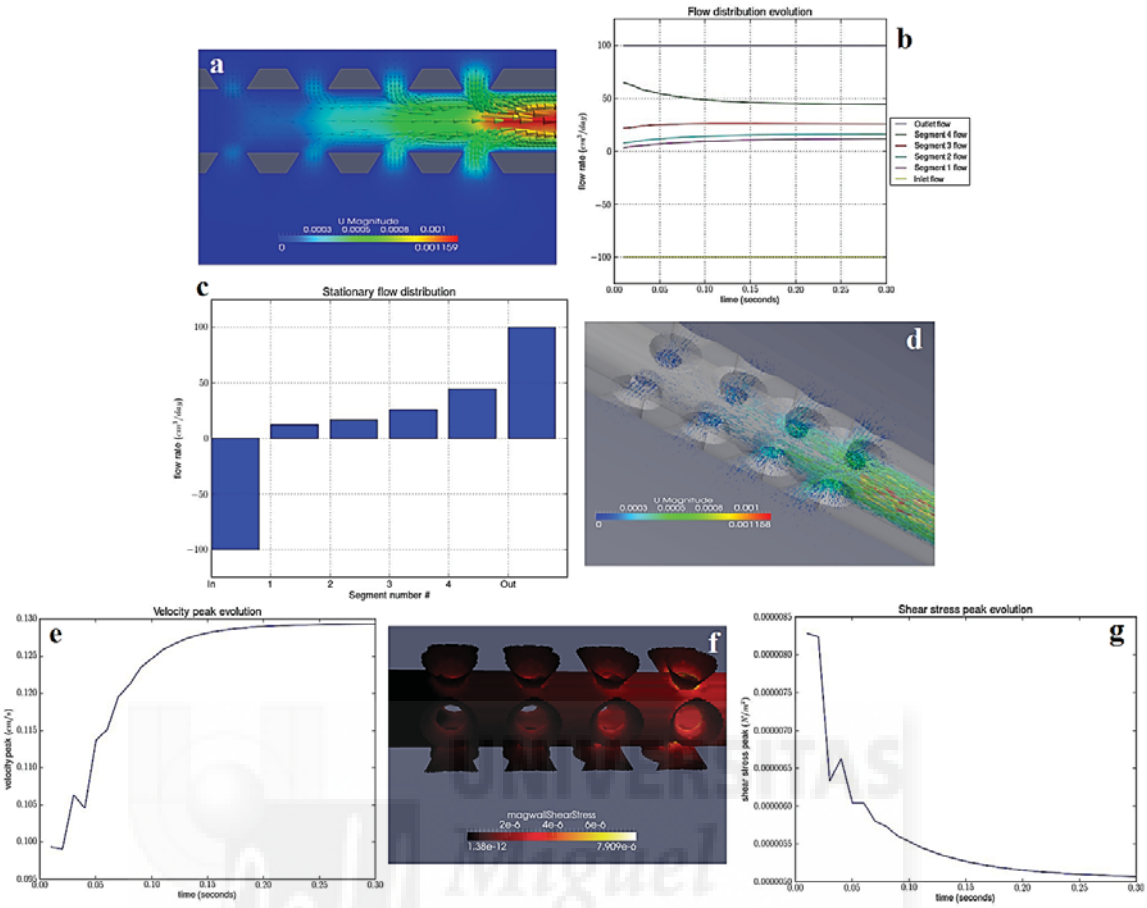

Figure 5. The following panels refer CFD results in prototype Model 4.

Note. a) Fluid velocity imaging of a longitudinal cross section; b) Time evolution of the flow per segment; c) Bar diagram of the stationary flows per segment; d) 3-D representation of the velocity through the holes and inside the catheter; e) Time evolution of the fluid velocity peak; f) Imaging depiction of the shear stress in the hole walls, with equally distributed values at all segments; g) Time evolution of the shear stress peak.

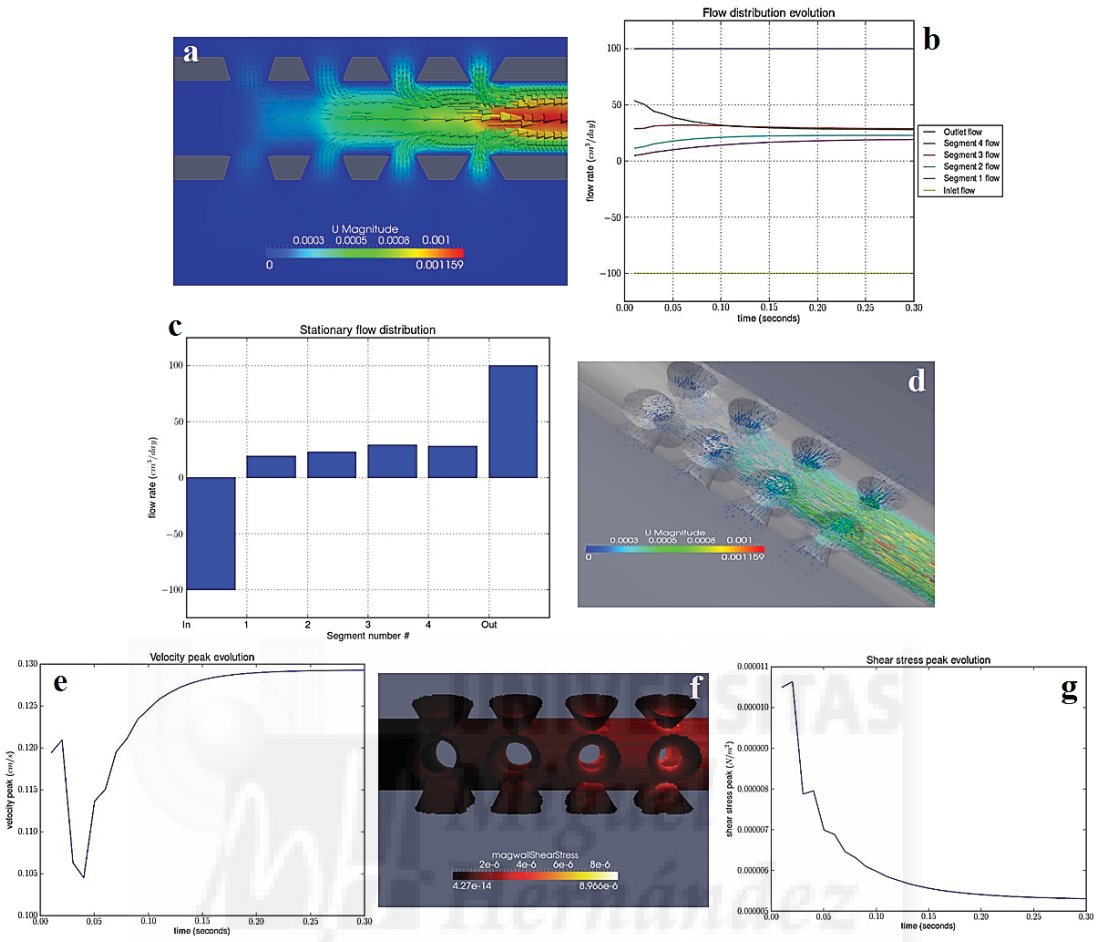

Figure 6. The following panels refer CFD results in prototype Model 5.

Note. a) Fluid velocity imaging of a longitudinal cross section; b) Time evolution of the flow per segment. The stationary flows per segment are roughly evenly distributed; c) Bar diagram of the stationary flows per segment; d) 3-D representation of the velocity through the holes and inside the catheter; e) Time evolution of the fluid velocity peak; stationarity is reached after approximately 0.15 sec.; f) Imaging depiction of the shear stress in the hole walls, with equally distributed values at all segments; g) Time evolution of the shear stress peak; stationarity is consistently reached after some 0.12 sec.

UNIVERSITAS
Miguel
Hernández

Chapter 5:
Study 3. Basic Cerebrospinal Fluid Flow Patterns in Ventricular Catheters Prototypes

INTRODUCTION

It is well known that the most frequent cause of shunt failure is ventricular catheter obstruction, which may account for 50 to 80% of newly inserted shunts (Bergsneider et al., 2006; Drake et al., 1998; Drake & Sainte-Rose, 1995; Sainte-Rose et al., 1991; Tuli et al., 2000). Although many factors contribute to this (Bergsneider et al., 2006; Harris et al., 2010; Harris et al., 2011; Harris & McAllister, 2012; Prasad et al., 1991), the main one is related to fluid flow characteristics of the catheter within the hydrocephalic brain (Ginsberg et al., 2000; Lin et al., 2003; Prasad et al., 1991; Sainte-Rose et al., 1991; Tuli et al., 2000). In a previous study (Galarza et al., 2014) we analyzed the fluid dynamics of five currently used VC models to evaluate flow factors of proximal shunt malfunction. We found that the flow distribution follows a similar pattern in all VC considered. Current catheter designs were studied by means of 3-D CFD. This produced a visual image of the fluid velocity field and the results were integrated to evaluate flow and shear stress values. Indeed, the CSF flow through the holes follows a non-homogeneous pattern in currently in use VC models, the flow being predominantly concentrated in the most proximal holes. This renders the other holes useless.

Currently there are several types of ventricular catheter to drain CSF. The most common designs include 6 or 8 drainage rings, also called drainage segments, with each one of these rings consisting of a constant number of holes, typically 2 (in opposition with

respect to the catheter axis) or 4 (in opposition two to two). In most cases, the separation between the drainage rings is identical, although there are designs which vary the distances between them. As the McAllister group stated (Harris & McAllister, 2011; Harris & McAllister, 2012), the size of the holes, the distance between each hole, the hole rugosity, and the number of holes may all be significant for obstruction.

In the first application of CFD to VC research, Lin et al. (2003) developed a new model by placing the largest holes distally, which is called the Rivulet catheter. They state that this change would decrease the probability of occluding the entire catheter when only its tip is blocked. One of the primary failure sites of current shunt devices is in and surrounding the holes of the ventricular catheter. We take into account this point in the new designs by varying the number of holes in the different drainage rings and sometimes as well their external and/or internal diameter. The relevance of the number of holes for the proper function of the VC was addressed by Thomale et al. (2010), a conclusion being that fewer perforations in the catheters with equal flow features might decrease obstruction when catheters can be implanted with adequate precision.

Simulation is broadly applied on a daily basis in engineering studies to resolve competently a large diversity of physical and technical situations. CFD is a numerical simulation method to calculate the flow of compressible and incompressible fluids even with complicate geometries, thus providing a practical instrument for design optimization. To simulate the fluid flow in a space, we create 3-D models of ventricular catheters based on the actual geometric shape of commercially available models and on images or measurements that define the actual boundaries of that space (Galarza et al., 2014). In order to design the solid geometry of the ventricular catheters we use a general graphical environment for numerical computing which implements partially discretised, mesh-based methods like finite element or finite volume. Specifically, the governing

equations for this CFD calculation are the 3-D incompressible unsteady Navier-Stokes equations written in conservative form for mass and momentum.

By using simulation and CFD, in Galarza, Giménez, Pellicer, Valero and Amigó (2015) we presented five new VC models with homogenous flow characteristics. In that study we disclosed that flow patterns depends on certain parameters. Our present objective is to describe basic flow characteristics, according to those parameters, that can be found in VC prototypes. Our conclusions follow from the solutions, after analyzing several models, of the corresponding 3-D CFD models and from benchmark testing from specifically modified VCs.

MATERIAL AND METHODS

Six prototypes of ventricular catheters were studied in this paper. Several models were analyzed before choosing distinctive types. Models were designed based on currently in use catheters and on our ideas. Model 1 *(Figure 1, images a and b)* consisted of a VC of 4 segments each with 6 holes distributed along 7.25 mm from tip to last segment; Model 2 *(Figure 2, images a and b)* consisted of 4 segments alternating 6 holes with 4 holes, distributed along 8.75 mm from tip to last segment; Model 3 *(Figure 3, images a and b)* consisted of 2 adjacent segments with 6 holes and 2 adjacent segments with 4 holes distributed along 8.75 mm from tip to last segment; Model 4 *(Figure 4, images a and b)* consisted of 3 segments with 5 holes distributed along 9.25 mm from tip to last segment; and Model 5 *(Figure 5, images a and b)* had the same hole configuration and hole sizes than Model 4 but the holes were distributed along 7.25 mm from tip to last segment instead; Model 6 *(Figure 6, images a and b)* consisted of a VC of 3 segments of 6, 3 and 3 holes respectively distributed along 7.25 mm from tip to last segment. In

all models the internal diameter of the catheter (its lumen) was 1.5 mm and the external diameter 2.5 mm. All holes were tapered (or conical), i.e., modeled by truncated cones. The greatest diameter of the holes, corresponding to the external side of the catheter, was always 0.50 mm. Their smallest diameter, corresponding to the internal side of the catheter, ranged from 0.18 to 0.35 mm depending on the model and segment. The inter-segment distance varied from 1 to 2.5 mm depending on the model. See *Table 1* for more details.

Catheter and hydrocephalus modeling

Our 3-D model was assumed to be a steady, incompressible, laminar flow of a Newtonian fluid. The methodology followed our previous studies (Galarza et al., 2014; Galarza et al., 2015). Thus, the VC was located in a cylindrical cavity with rigid walls which modeled the ventricle. An inlet and outlet centered on the bases of the cylinder allow simulating the drainage of cerebrospinal liquid. This cavity was large enough (as compared to the length of the perforated catheter segment) not to influence the flow in the proximity of the holes, which was the flow we were most interested in. The holes of the VC were grouped on cross planes, each plane being thus parallel to each other. As before, we referred to each group of holes as a drainage ring or a segment. Depending on the model, there were three or four segments, where each segment contained a varying number of holes symmetrically disposed in the angular direction. Furthermore, the holes of the VC were aligned in the longitudinal direction if consecutive segments contained the same number of holes. A CFD model was used then to calculate the so-called stationary (i.e., time independent) values of the velocity and pressure fields in the whole domain of the fluid, as well as the flow (in cm^3/day) through each flow segment. These stationary values were reached after a transient phase during which the flow evolves from the initial state, defined as the steady state.

Broad normative data for CSF characteristics and volumes were taken from our first study. This being the case, the graphical representations of the stationary flows through the hole segments *(Figures 1 to 6, images c and d)* can also be read as percentages. Values used in our model resembled normal pressure hydrocephalus and specific gravity of CSF (Galarza et al., 2014; Galarza et al., 2015).

Ventricular catheter designing

To simulate the flow of the CSF through the new ventricular catheters, we created 3-D numerical models based on the actual geometric shapes of commercially available models, or on images and dimensions of their actual boundaries. The solid geometry of the VC was generated with Salome (version 7.3.0) GNU Lesser General Public License (LGPL). The physical space was converted the computational domain. The number of nodes determined the resolution of the model and the time needed for calculation. The grid-generation utility snappyHexMesh was used to discretize the computational domain with unstructured hexahedral boundary-fitted mesh. The grid generator allowed cutting out redundant parts not related to the region of interest and delimiting the computational area by means of the inlet, outlet, and cavity solid limits. The result was the region of interest (ROI) in which CFD was applied.

CFD Calculation

The numerical simulations were run with the version OpenFOAM® (Open Field Operation and Manipulation) v2.2.2. In our case we used the icoFoam solver to combine numerically the incompressible Navier-Stokes equations. The fluid-mechanical variables changed with time at the beginning, until the flow reached a steady phase or the stationary regime, just because the boundary conditions were time-independent. The

initial, unsteady phase was a numerical artifact due to the use of the general -"unsteady"- Navier-Stokes equations. Our only interest was the stationary regime.

As Galarza et al. (2014) and Galarza et al. (2015), boundary conditions were specified on all our boundary surfaces. The velocity field at the cavity inlet was adjusted in order to achieve a constant inflow of 100 cm^3/day and, for consistency, the pressure was zero gradient. On the rest of the ventricle and catheter walls, which were considered rigid, non-slip and non-penetration conditions were chosen meaning that all velocity components at the solid walls were set to zero. At the cavity outlet, the pressure was set equal to 15 cmH2O, or 11 mmHg (1471 Pa=N/m^2), and a zero gradient condition on the velocity was specified as well. The flow was computed with a time step of 0.005 seconds during a time interval of 0.3 seconds, long enough to reach stationarity. The time step was found to be sufficiently small from the point of view of accuracy. The simulation was performed by setting the kinematic viscosity of CSF equal to 0.75 x 10^{-6} m^2/s, the kinematic viscosity of water at body temperature (37ºC). The results used for the flow analysis corresponded to the stationary regime, thus guaranteeing that the results were independent of the initial conditions. The images were obtained by using ParaView 4.1.0.

Benchmark testing

For experimental testing we choose commercially available silicone VC (Medtronic PS) that resembled our prototype models. Each catheter has ten drainage segments, each one consisting of two holes. We modified their segments by adding holes with the punching technique or by closing segments with crystal glue. A water vase and Indian ink were used for the injection flow technique. This experimental validation is based and, to a certain extent follows the Lin et al. (2003) and Thomale et al. (2010) studies.

RESULTS

Vector representations of the flow fields of the VC Models 1 to 6 resulting from 3D CFD are shown in *Figures 1 to 6, image e,* respectively. These images revealed regions of localized above-average velocities in most holes, with a distinctive pattern, in all prototypes. Fluid velocities could then be converted into flows and distributions of flow per segment. The simulations also demonstrated that the velocity patterns were different in all catheters *(Figures 1 to 6, image c).* Again, flow rate bar images exhibited higher values in the distal hole segments than in the proximal ones in Models 5 and 6. This relation was inverted in Models 1 and 2 and reached uniformity in Models 3 and 4. Inlet flow through each segment of every catheter, as well as the inlet flow per unit area, and the total sum of inlet segment flows are listed in *Table 1.*

The stationary flow distribution is depicted in *Figure 1 to 6, image d,* in cm^3/day, where the flow was indicated in each catheter segment. The evolution of the flow distribution showed that the flow through the catheter segments reached stationarity after 0.1s in most models.

Using our CFD methodology we disclosed that the flow through the hole segments were distributed in three distinctive patterns in these VC prototypes.

Basic flow distributions

Type "A" flow pattern is seen in Model 1 and 2 *(Figure 7, image a).* Our first prototype, a 24-hole VC, showed a distal to proximal increasing stationary flow distribution in four segments with an axial rotation between segments. Its holes were non-tapered and distributed over a distance of 7.25 mm from its tip. The second prototype, a 20-hole VC, also showed a distal to proximal increasing stationary flow distribution in four

segments, with no rotation between them, yet with a more homogeneous flow pattern compared to Model 1. Its two distal segments had holes slightly larger, and were distributed over a distance of 8.75 mm from its tip.

Type "B" flow pattern is seen in Model 3 and 4 *(Figure 7, image b).* The third prototype, a 20-hole VC, showed a distal to proximal uniform stationary flow distribution in 4 segments with no axial rotation. Its two distal segments had holes slightly larger, had two more holes, and were distributed over a length of 8.75 mm from its tip. At this point, we lessen the number of segments in our fourth prototype, a 15-hole VC with 3 segments, with axial rotation, and tapered holes distributed over a distance of 9.25 mm from its tip. This VC also showed a proximal to distal uniform stationary flow distribution similar to Model 3.

Type "C" flow pattern is observed in Models 5 and 6 *(Figure 7, image c).* Our fifth prototype, a tapered 15-hole VC with 3 segments, showed a slight distal to proximal decreasing stationary flow distribution. Its segments were rotated in axial plane, and arranged within a shorter distance of 7.25 mm from its tip. Our last prototype, a 12-hole VC, showed the most distal to proximal decreasing stationary flow distribution in three segments with an axial rotation between segments. Only its last segment had three holes slightly smaller, Segments were distributed over a distance of 7.25 mm from its tip. These observations are clearly displayed in *Figures 1 to 6, images c and d.*

Benchmark testing results

Modified VCs used for this part of the test resembled our designed CFD catheters Models 1, 3 and 6. Video examination after ink injections into the water vase facilitated the analysis of the functionality of segment holes in these modified ventricular catheters. Representative images of ink stained water draining into the different

catheters segments are depicted in *Figure 8.* Initial ink flow was considered representative. Again, as in the CFD study, three distinct patterns were disclosed.

DISCUSSION

In this report, by studying the flow obtained with 3-D CFD in diverse prototype models of VC we disclosed three types of CSF flow patterns. Models 1 and 2 have a distal to proximal increasing flow or Type "A" flow pattern. Model 1 has the same number of holes per segment, while Model 2, with an uneven number of holes per segment, has a more homogenous flow. In Model 3 we obtain an even more uniform flow pattern, by changing the hole distribution, while in Model 4 we remove a whole segment, and choose the same number of holes in the remaining segments, the holes being smaller than in Model 3. Models 3 and 4 exhibit a flat flow distribution over the segments or Type "B" flow pattern. Models 5 and 6 have an inverse flow pattern to Model 1 and 2, that is, a distal to proximal decreasing flow, or Type "C" flow pattern. Model 5 is the same as Model 4, but the perforated section span a shorter length. In Model 6 we add holes to the most distal segment *(Figure 7).*

In our first report (Galarza et al., 2014), we disclosed that, specifically, from 50 to 75% of the CSF flows into proximal sets of inlets of current commercially available 12 to 32-hole catheters, the flow being most uniform for the model Rivulet. In fact, this study agreed with the milestone application of 2-D CFD to VC by Lin et al. (2003), developers of the Rivulet catheter. The ventricular catheter typically uses 32 holes arranged in 4 rows to permit CSF outflow from the ventricular space, but the number and size of the holes varies somewhat with the manufacturer. As Harris and McAllister (2011) pointed, and to our knowledge, there is no literature explaining why 32 holes is

the standard number, or why the number of holes varies among catheters. The drainage hole size of most ventricular catheters is roughly 500 μm, and in the Rivulet type is from 975 to 282 μm in diameter in the most proximal part. Although the latter has a more homogenous flow, the small diameter of the most proximal holes makes it disadvantageous when compared to common VC. This hole has the highest stress during flow circulation (Galarza et al., 2014), so it might be more liable to be occluded by cells or other elements (Harris & McAllister, 2011; Harris & McAllister, 2012; Prasad et al., 1991). Up to now, the size of the holes has been studied by 3 groups of researchers: Lin et al. (2003), McAllister group (Harris et al., 2011; Harris & McAllister, 2011) and ours, and we basically agreed with the data interpretation. Harris and McAllister study, focused on form elements, suggests that cell adhesion generally decreases with increasing hole diameter under flow conditions and stated the need to examine how hole diameter impacts inflammatory-based shunt obstruction (Harris et al., 2011; Harris & McAllister, 2012). They let us know also, that typical catheter holes are made by a pneumatic pin and die-punching technique (Harris & McAllister, 2012), thus producing partially conical holes. We simulated the same kind of holes, but varying the inner diameter in several models.

After considering several models, we designed six VC prototypes and reported their flow patterns in this paper. Some of them present a homogeneous flow pattern, similar to the Rivulet catheter, but other than varying the diameters of the holes, the new method resorts to varying the number of holes in the VC segments or rings. We propose that the number of holes per segment may be variable, being higher in the distal segments (the farthest to the valve) and lower in proximal segments. Some of these designs have the same benefit as the catheter Rivulet, namely, flow uniformity, but without the disadvantage of using very small holes. We may infer that type “C” flow

pattern will prolong the catheter lifetime the most because the flow rate is highest at the distal segment, i.e., upstream of the other segments. Indeed, if the lumen of the catheter gets clogged at the distal segment, this will not impair the drainage capability of the catheter as it happens with the type "A" flow pattern if the lumen gets clogged at the proximal segment.

As Thomale et al. (2010) showed a smaller number of holes in the catheters with equal flow characteristics might decrease this risk when catheters can be implanted with adequate precision. This was seen in our previous study, where shear stress and flow rate was somewhat equally distributed in catheter models with fewer holes. Thomales´ VC has six to 16 perforation holes and the total distance from the tip to the distal margin of the most proximal perforation measures from 6.4 to 15.4 mm. Nevertheless, the short length of the perforated section makes it crucial to insert the VC within the ventricle with utmost precision, so far not possible in everyday practice in most neurosurgical centers. Although our longest perforated section is less than 10 mm, the purpose of this study is essentially to report flow patterns, other than make direct comparisons among VC. Others features in ventricular catheters intended to prevent the occlusion of the catheter, such as adding flanges and slots (Portnoy, 1971), have not been clinically proven to diminish rates of proximal shunt malfunction (Haase & Weeth, 1976; Lin et al., 2003). Other efforts focused on methods to inhibit tissue infiltration during insertion of the VC (Kehler, Klöhn, Heese & Gliemroth, 2003), but comparative results are still lacking.

Main contributions regarding the VC design came from the Harris and McAllister group (Harris et al., 2010; Harris et al., 2011; Harris & McAllister, 2011; Harris & McAllister, 2012). But probably, Thomale et al. (2010) were the first investigators to address the significance of the number of holes for the performance of VC. They stated that the use

of more than two holes, theoretically, did not enhance the amount of drainage through the catheter. This is true, from a hydrodynamic standpoint, only when there is a constant pressure; indeed, a condition not fulfilled in hydrocephalus. This information has been pointed out, partly, in the paper by Ginsberg et al. (2000) who disputed that one remaining patent perforation increased the draining pressure by no more than 0.5 cmH2O to permit flow and, in fact, only three holes have the same pressure flow correlation as 32 holes in a ventricular catheter (Ginsberg et al., 2000; Harris & McAllister, 2011). This is not reflected in our study, which disclosed the influence of the hole diameter and the number of holes per VC segment on the flow distribution per segment.

In some of our prototypes we varied the distance between hole segments either by shortening or elongating them. Overall, the closer the distance, the more uniform the flow obtained. However, as Harris and McAllister (2011, 2012) found, contact between like cells may cause inhibition of proliferation and growth, and cell proliferation may decrease with small distances between holes. Yet on the other hand, epithelial cells have been shown to link across holes suggesting that contact inhibition may be slowed if the proximity of the neighboring holes is extremely small. We cannot make further conclusions to this respect, except that shortening the segment distance, as in Model 4 and 5, changes the flow pattern from a “B” to a “C” type. While rotating the axial plane of the segments, as in Model 1 and 2, makes no flow changes.

It is important to point out that our study specifically address the flow patterns in distinct prototypes of VC, and it does not reproduce other occlusion factors related to the type of shunt valve, cells and CSF elements forms, and the type of hydrocephalus. As in our previous studies, our hydrocephalus model does not reproduce the pathologic anatomy of any individual or any group of patients. To a certain extent, its

characteristics are within the range of what is found in all patients. We shortened the hydrocephalic region by modelling it as cylinder. The reason and method for this can be found in our previous papers (Galarza et al., 2014; Galarza et al., 2015) and in references (Penn et al., 2005; Penn et al., 2011; Sood et al., 2004; Sood et al., 2005; Stein & Guo, 2008).

Most studies of shunts and catheters for the treatment of hydrocephalus are clinical non-comparative studies hence there is little blunt experimental data (Bergsneider et al., 2006; Drake et al., 1998; Stein & Guo, 2008; Thomale et al., 2010). Nonetheless, numerical simulation is widely applied in everyday engineering studies to solve efficiently a wide variety of physical and technical problems. In particular, CFD is a numerical method to calculate the flow of compressible and incompressible fluids even with complicate geometries, thus providing a handy tool for design optimization. Given a 3D model of the system to be studied, and the initial and boundary conditions, the CFD software calculates the resulting flow with greater spatial and temporal resolution than that achieved with real-time phase-contrast magnetic resonance studies, displaying also other flow characteristics like pressures, flow structures, stresses, and pressure waves. Some of these factors can be safely studied with engineering mathematic models. Our numerical study is based on three-dimensional models, which allows studying properties that cannot be studied with the previous two-dimensional models.

Our physical experimental testing may be criticized, given that the benchmark testing was done in modified VCs and not in specific fabricated VC prototypes. Still, the images obtained were similar to those obtained by CFD analysis. As a general comment, let us put forward right away that our study is theoretical in the sense that it based on computational fluid dynamics. Numerical methods allow to study many different complex scenarios and to obtain quantitative results in a time span and with an

accuracy that would be unfeasible with an experimental set up. Once the most promising solutions have been identified, they are experimentally validated. This is the approach followed by the industry because of the savings in time and money, and this is a good methodology in science as well. In our case, we have focused on definite aspects of the ventricular catheter flow, a situation not well known to most neurosurgeons. Specific experimental testing is not an objective of our study at the present stage since it requires prototype fabrication and a measurement set up. Further research is in progress.

Conclusion

In this study, we found that the flow distribution follows specific patterns according to the number of holes per catheter segment, the hole size, and the distances between hole segments along the VC. In regard to these prototypes, we may infer that VC with a type "C" flow pattern will be less prone to occlusion because the flow distribution shows a decreasing pattern from distal to proximal segments. Still, this hypothesis requires experimental testing with specific fabricated VC prototypes, not modified VCs; and certainly, with clinical validation studies.

Legends to Figures:

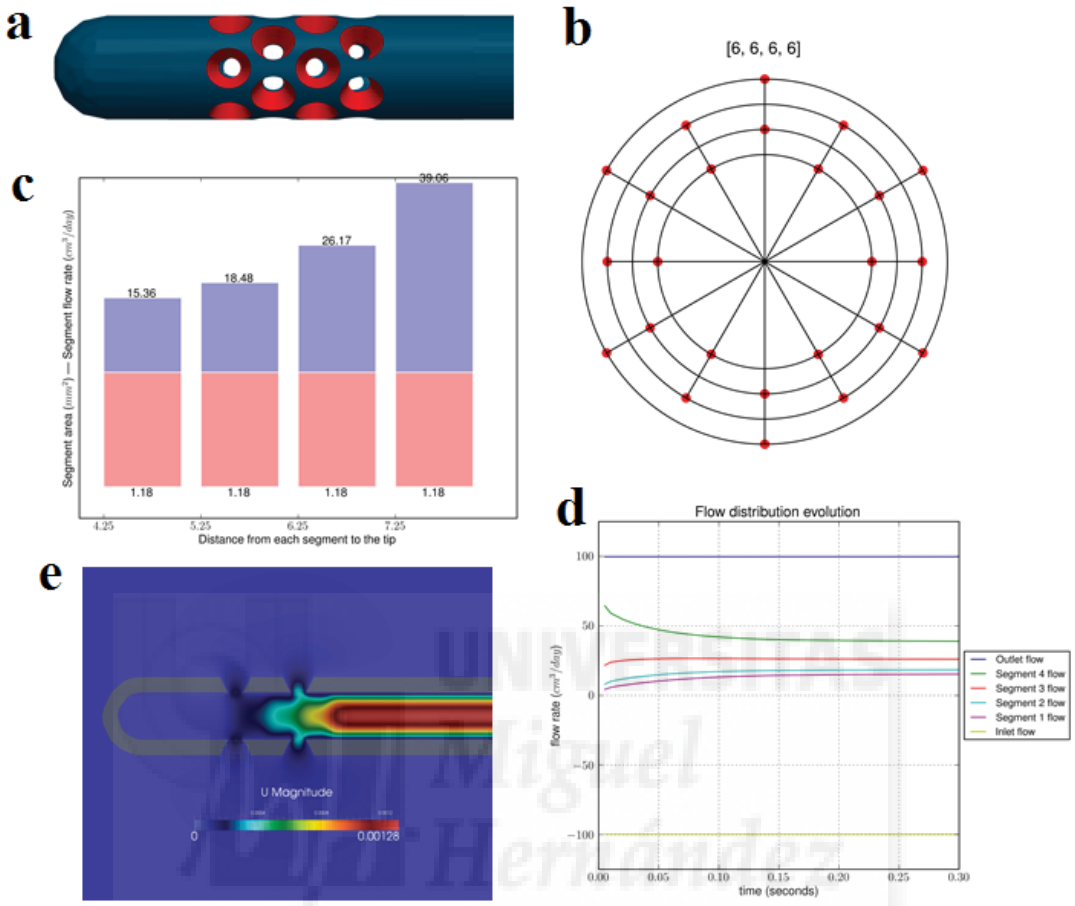

Figure 1. The following panels refer CFD results in prototype Model 1.

Note. a). New models of VC for the treatment of hydrocephalus based on 3-D CFD studies. All holes are conic, i.e., their surfaces are doubly truncated cones. External radius of the holes in the same segment is 0.5 cm in all catheters, while the internal varies according to VC type. The target design shows the distribution of the holes according to the VC segment; b). Bar diagram of the stationary flows per segment with their segment drainage area. The stationary flows per segment are not evenly distributed, and they follow an increasing pattern from distal to proximal; c). Flow time evolution per segment, reaching uniformity after 0.1s; d). Fluid velocity imaging of a longitudinal cross section of the VC; e) Representation of the flow velocity through the holes and inside the catheter.

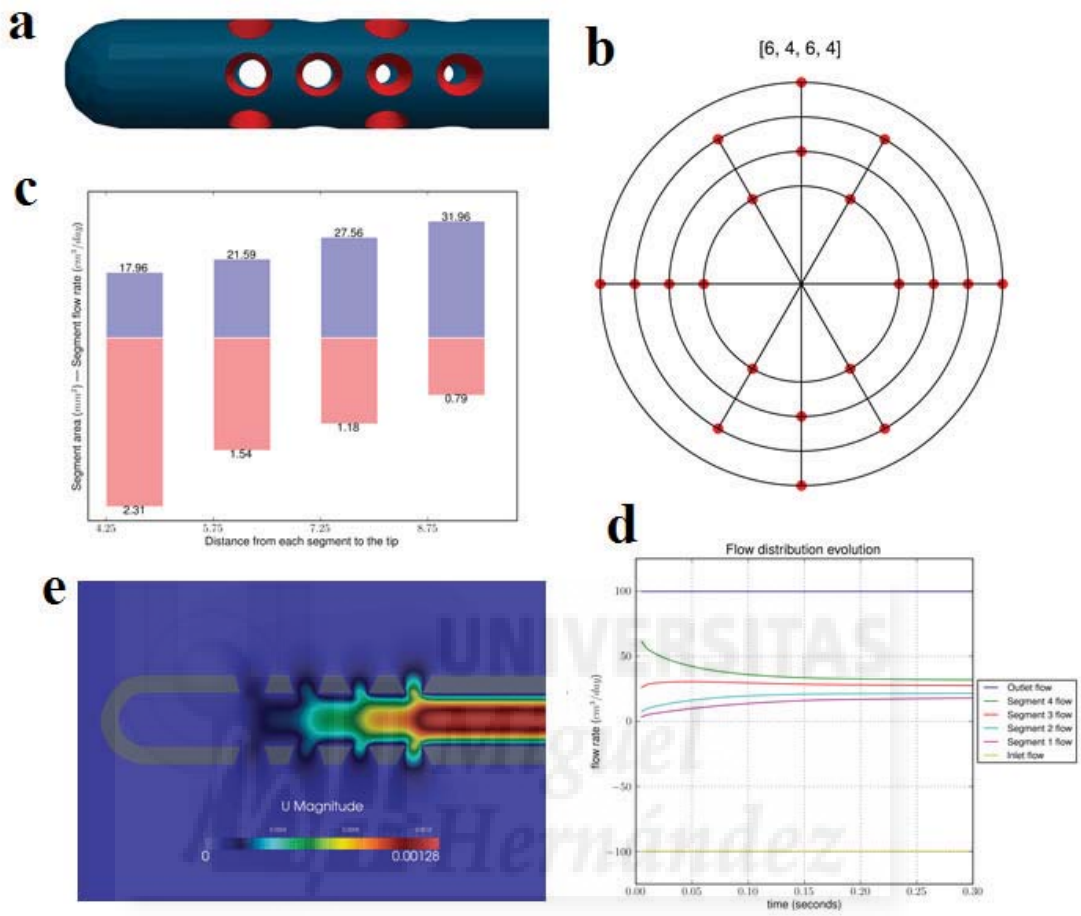

Figure 2. The following panels refer CFD results in prototype Model 2.

Note. The stationary flows per segment are not evenly distributed, and they follow anincreasing pattern from distal to proximal. See the section Results in the text.

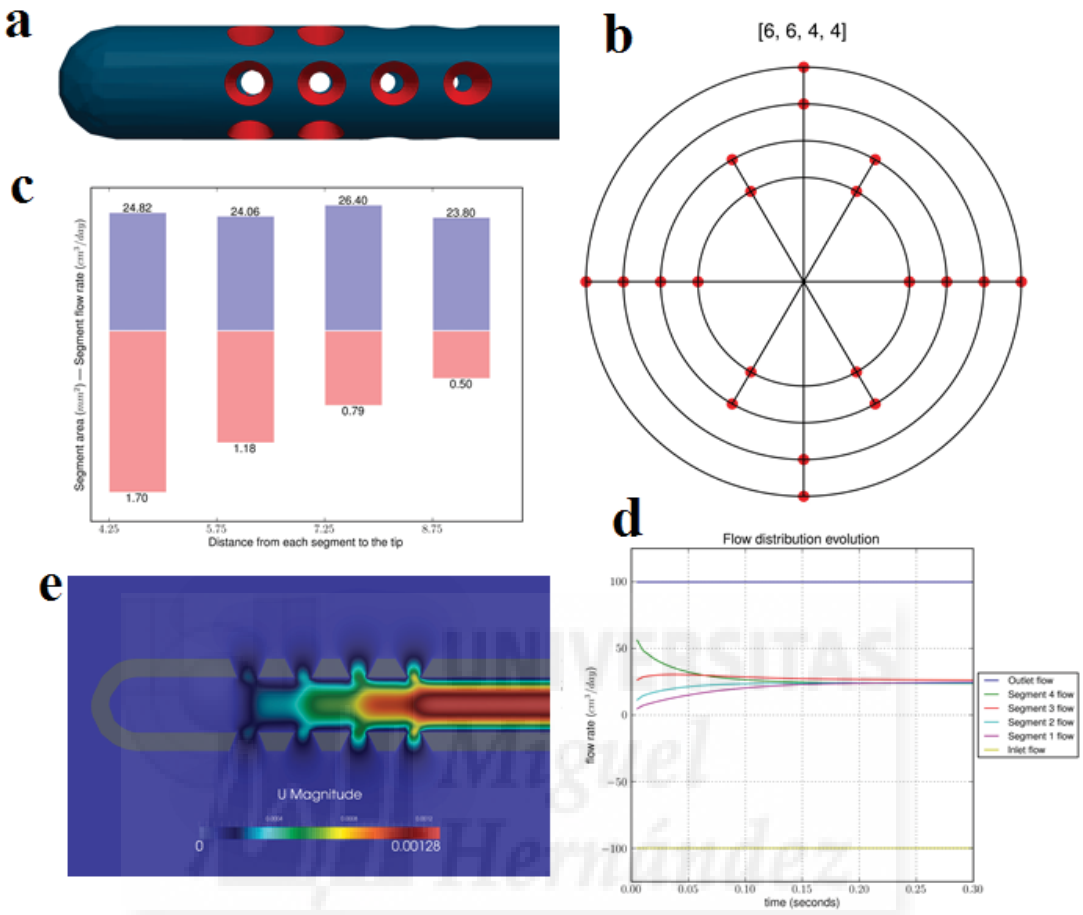

Figure 3. The following panels refer CFD results in prototype Model 3.

Note. The stationary flows per segment are somewhat evenly distributed. See the section Results in the text.

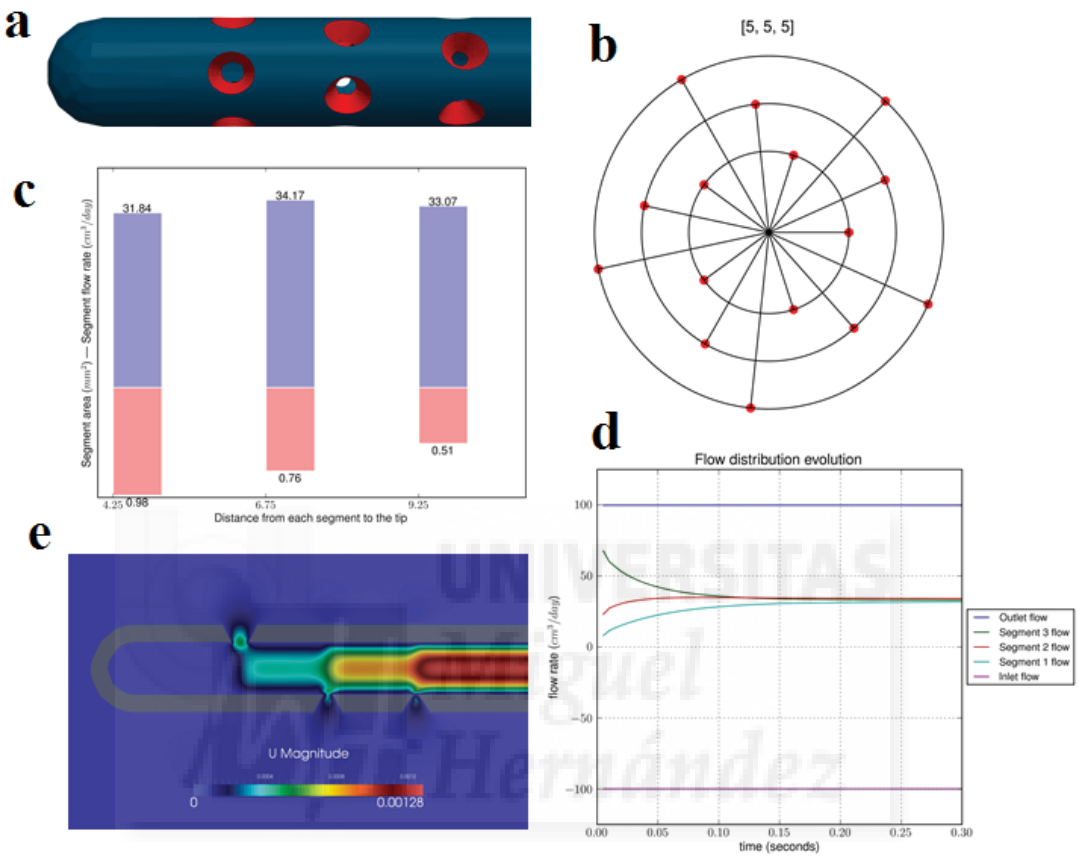

Figure 4. The following panels refer CFD results in prototype Model 4.

Note. The stationary flows per segment are quite evenly distributed. See the section Results in the text.

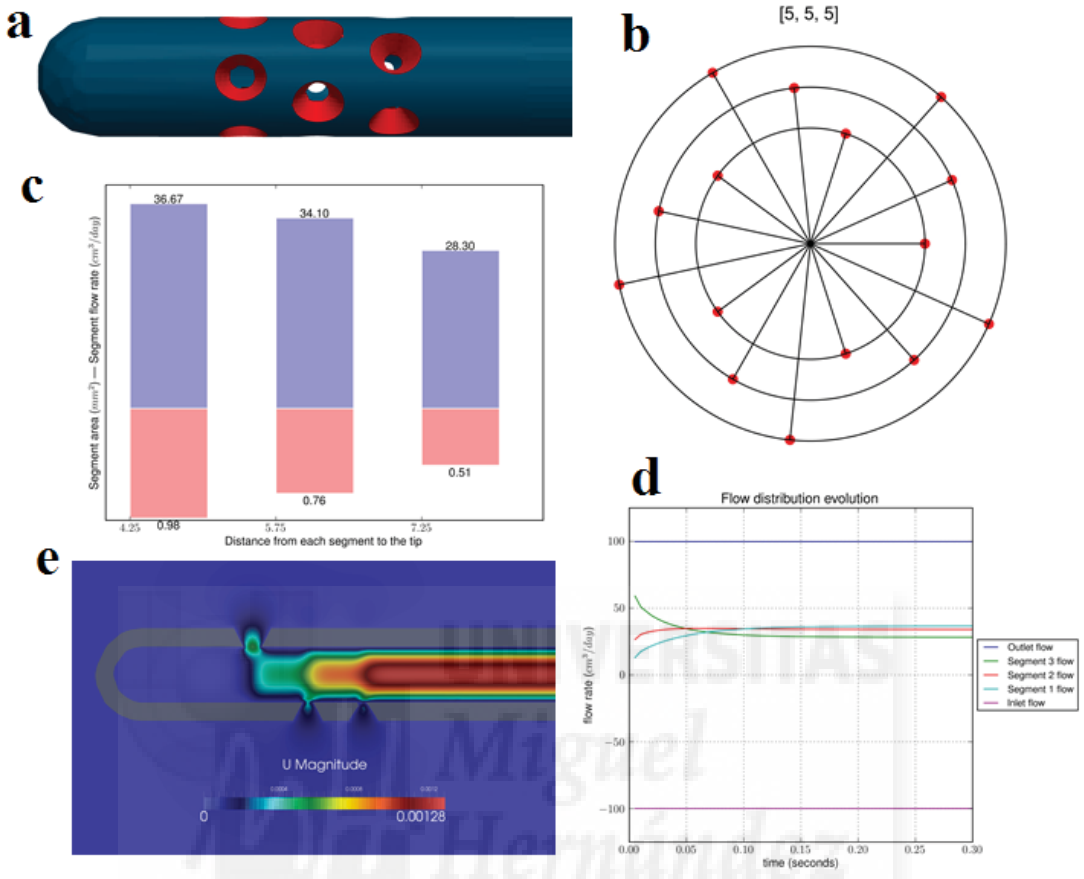

Figure 5. The following panels refer CFD results in prototype Model 5.

Note. The stationary flows per segment are not evenly distributed, and they follow a decreasing pattern from distal to proximal. See the section Results in the text.

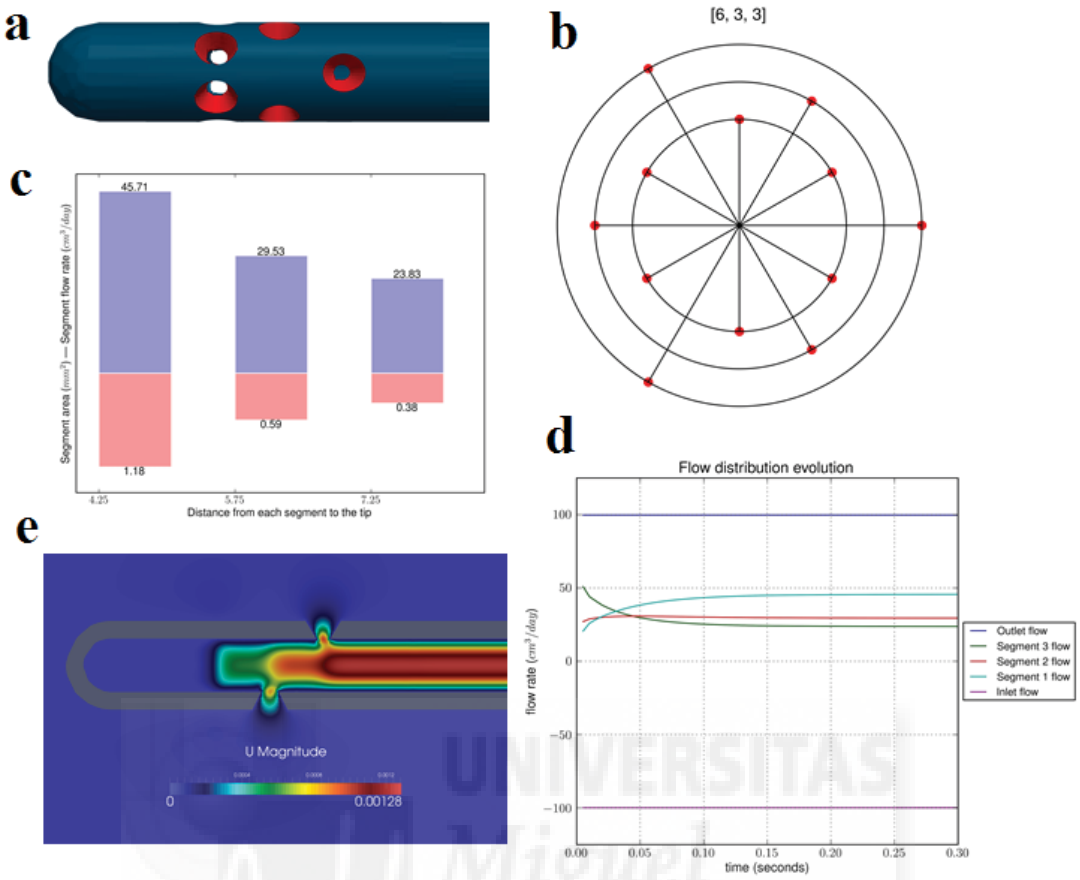

Figure 6. The following panels refer CFD results in prototype Model 6.

Note. The stationary flows per segment are not evenly distributed, and they follow a decreasing pattern from distal to proximal. See the section Results in the text.

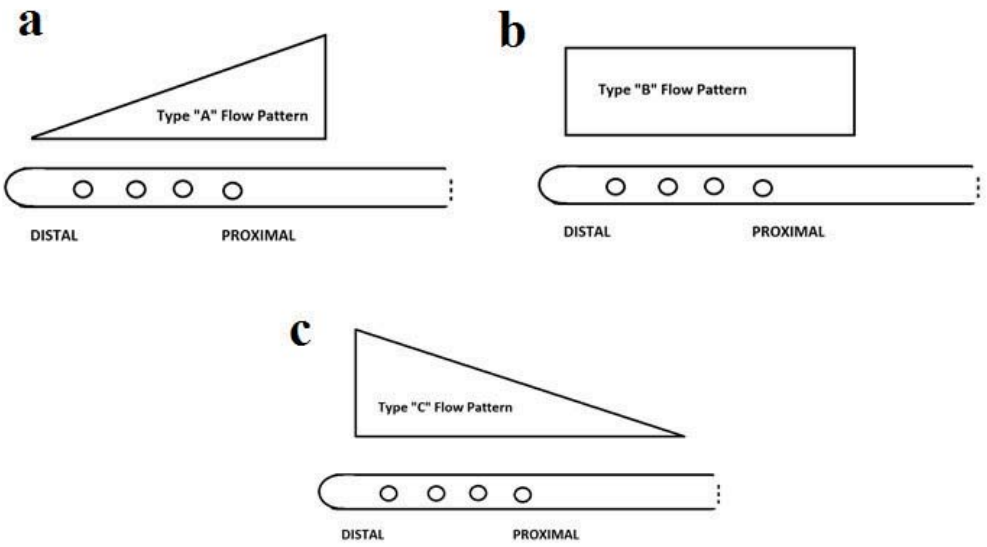

Figure 7. Cerebrospinal Fluid Flow Patterns in Ventricular Catheters Prototypes.

Note. Basic design showing a Type “A” Flow pattern (a), a Type “B” Flow pattern (b) and a Type “C” Flow pattern (c).

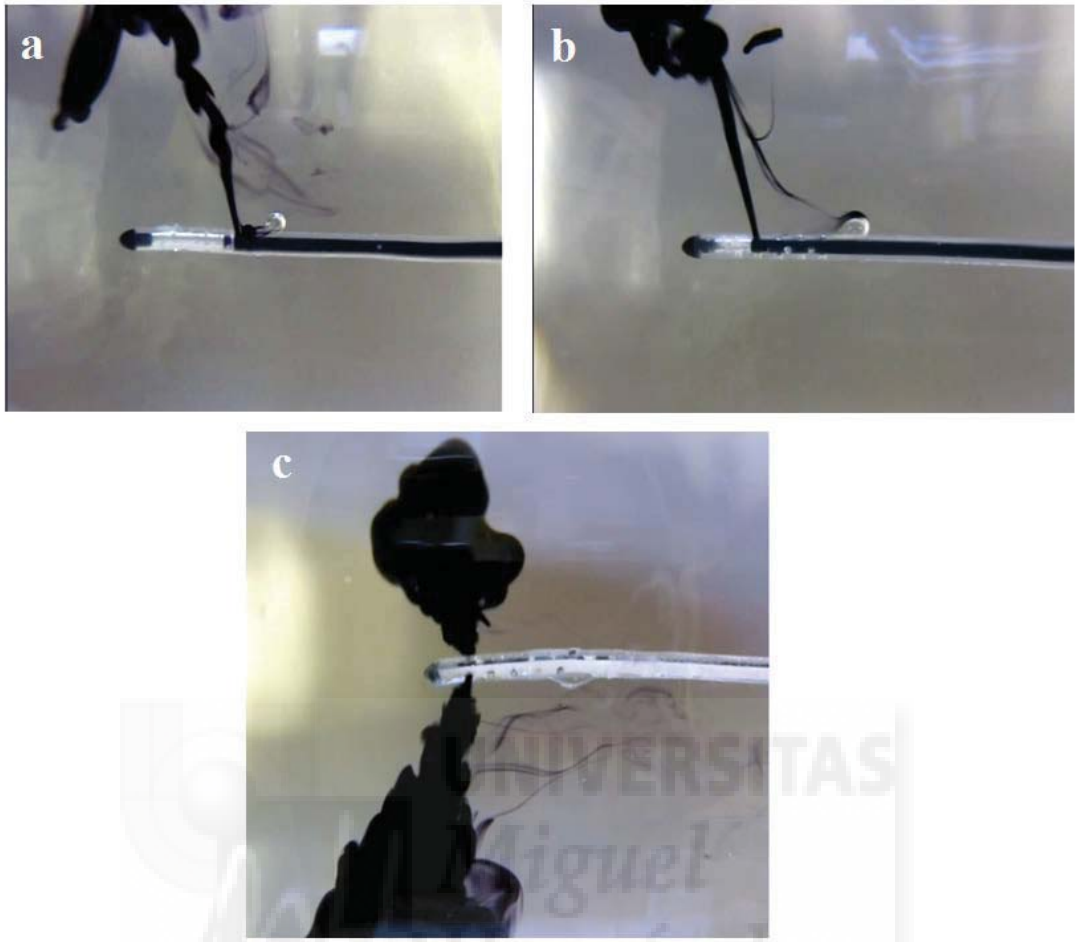

Figure 8. Benchmark Testing Results of Cerebrospinal Fluid Flow Patterns in real modified Ventricular Catheters.

Note. Modified catheter showing a Type “A” Flow pattern, where Indian ink is initially flowing from the most proximal holes (a), another VC showing a Type “B” Flow pattern, where Indian ink is initially flowing from the medium segments holes (b), and a third one showing a Type “C” Flow pattern, where Indian ink is initially flowing from the most distal VC holes (c).

Table 1.

VC characteristics and flow volumes in six new models, determining three types of flow pattern. Lengths in mm. Areas in mm^2. Flows in cm^3/day.

	Model 1	Model 2	Model 3	Model 4	Model 5	Model 6
Number of holes/Number of segments	24 / 4	20 / 4	20 / 4	15 / 3	15 / 3	12 / 3
Flow Pattern Type	A	A	B	B	C	C
No. of holes per segment	[6, 6, 6, 6]	[6, 4, 6, 4]	[6, 6, 4, 4]	[5, 5, 5]	[5, 5, 5]	[6, 3, 3]
Distance from each segment to the tip	[4.25, 5.25, 6.25, 7.25]	[4.25, 5.75, 7.25, 8.75]	[4.25, 5.75, 7.25, 8.75]	[4.25, 6.75, 9.25]	[4.25, 5.75, 7.25]	[4.25, 5.75, 7.25]
Internal radius of the holes in the same segment	[0.25, 0.25, 0.25, 0.25]	[0.35, 0.35, 0.25, 0.25]	[0.3, 0.25, 0.25, 0.2]	[0.25, 0.22, 0.18]	[0.25, 0.22, 0.18]	[0.25, 0.25, 0.2]
Total sum of hole areas per segment	[1.18, 1.18, 1.18, 1.18]	[2.31, 1.54, 1.18, 0.79]	[1.7, 1.18, 0.79, 0.5]	[0.98, 0.76, 0.51]	[0.98, 0.76, 0.51]	[1.18, 0.59, 0.38]
Inlet flow through each segment	[15.36, 18.48, 26.17, 39.06]	[17.96, 21.59, 27.56, 31.96]	[24.82, 24.06, 26.4, 23.8]	[31.84, 34.17, 33.07]	[36.67, 34.1, 28.3]	[45.71, 29.53, 23.83]
Inlet flow per unit area through each segment	[13.04, 15.68, 22.22, 33.15]	[7.78, 14.02, 23.39, 40.7]	[14.63, 20.42, 33.61, 47.35]	[32.43, 44.95, 64.97]	[37.35, 44.86, 55.6]	[38.8, 50.13, 63.22]
Total sum of inlet segment flows	99.0697	99.07315	99.07661	99.07488	99.07488	99.07402

UNIVERSITAS
Miguel
Hernández

Chapter 5 (cont.):

Study 4. Influence of hole geometry on the flow distribution in ventricular catheters for hydrocephalus

Introduction

The most common treatment for hydrocephalus is the insertion of a cerebrospinal fluid shunt system. The shunt system comprises three parts: distal catheter, shunt valve and ventricular catheter. The standard ventricular catheter (VC) is a flexible tubing with a number of holes placed symmetrically around several transversal sections or "drainage segments" which is inserted in one of the ventricles to extract the excess fluid. The valve regulates the pressure and so the outlet flow. Up to 80% of all shunt malfunctions are caused by obstruction of the VC. The most common cause of VC obstruction is the adhesion of cells and macromolecules to the walls of the catheter which, in turn, is due to a variety of factors, including wrong placement of the catheter and the material used. But some of the most important factors are inherent to the geometric configuration of the catheter since it determines the flow characteristics (Bergsneider et al., 2006; Drake et al., 1998; Drake & Sainte-Rose, 1995; Harris et al., 2010; Harris et al., 2011; Harris & McAllister, 2012; Sainte-Rose et al., 1991; Tuli et al., 2000).

In (Galarza et al., 2014; Galarza, Giménez, Pellicer, Valero, Martínez-Lage and Amigó, 2015; Galarza, et al., 2015a), the authors studied the effect of some parameters variation on the flow distribution by using three-dimensional computational fluid dynamics (CFD). These parameters included the hole size but not its geometry (cylindrical vs conical holes) nor its angular position (perpendicular vs tilted) with respect to the wall.

In this paper we fill this gap and show that both geometrical features are relevant as well for the flow characteristics.

Methods

CFD software

A numerical model consists of three basic steps regarding its performance: pre-processing, solving process, and post-processing. In the pre-processing the computational domain and the meshing of the model are built, and the initial and boundary conditions are fixed. Next, a suitable numerical scheme is implemented to solve the governing equations of the model. Lastly, in the post-processing, a correct analysis and visualization of the data are required to ensure a proper discussion of the results.

It is therefore customary in CFD to use numerous software tools to carry out a numerical experiment. The core of our simulations was OpenFOAM®, which is the acronym of Open Source Field Operation and Manipulation. OpenFOAM® is an open-source CFD software based on C++ that contains a toolbox for tailored numerical solvers. The algorithm implemented in OpenFOAM® uses the Finite Volume Method on unstructured meshes (see Versteeg and Malalasekra, 2007; Ferziger and Peric, 2001). OpenFOAM® includes pre-processing and post-processing capabilities such as snappyHexMesh and ParaFoam for meshing and visualization, respectively. We also used other open-source software that provide pre-processing and post-processing tools for CFD and numerical simulations such as Salome and ParaView. Salome (version 7.3.0) was mainly used to build the geometry of the different models, and ParaView (version 4.1.0) to display some of the images.

Flow domain

The structural and geometric complexity of the ventricles prevents from implementing an accurate computational model. On the other hand, we are only interested in the CSF flow pattern in the proximity of the CV. For this purpose it suffices that the flow domain of all our models is a catheter inserted into a cylinder through one of its bases, as in *Figure 1*. To comply approximately with the standard ventricle volume, the cylinder is 85mm long and its diameter is 30mm. The inner diameter and outer diameter of the catheter are 1.5mm and 2.5mm, respectively, and the part of the catheter inside the cylinder has a length of 60mm. The assumption that both the cylinder and the catheter are rigid and straight is a natural simplification that implies no significant differences in the results.

The computational domain was created bottom-up with Salome and converted to a stereolithography to be linked to the snappyHexMesh utility for the generation of the mesh. An unstructured grid based on hexahedral meshes was generated. Mesh cells are the atomic elements on which the physics of the flow is solved, and hexahedral meshes give more accurate solutions, especially when the grid lines are aligned with the flow. Refined meshes around the holes were created to capture all relevant flow features under study.

Governing equations

Our model is governed by the incompressible Navier-Stokes equations given by:

$$\frac{\partial \mathbf{u}}{\partial t} + \mathbf{u} \cdot \nabla \mathbf{u} - \nu \Delta \mathbf{u} + \nabla p = \mathbf{0} \qquad (1)$$

$$\nabla \cdot \mathbf{u} = 0 \qquad (2)$$

where u and p stand for the velocity field and the pressure, respectively, v denotes the kinematic viscosity of the CSF (v = 7.5 x 10^{-7} m^2/s), and t the time. The equation (2) reflects the incompressibility constraint, in particular, the inlet flow is equal to the outlet flow. Needless to say, the Reynolds number is very low in our case, so the flow is laminar.

We integrated numerically the coupled system (1) and (2) by means of the icoFoam solver, which is based on the so-called PISO algorithm and implemented in OpenFOAM®. The icoFoam code is inherently transient, requiring an initial condition and boundary conditions. The flow was computed as long a time till stationary had set in. The convergence of the solver was highly successful, except in a few cases which were solved by refining the mesh to avoid skewed cells.

Initial and boundary conditions

All non-stationary CFD problems require initial and boundary conditions, these being necessary to specify the initial values of all the flow variables at all points in the computational domain. The initial and boundary conditions described in the paragraph below were deemed of the based of (Galarza et al., 2014; Galarza et al.,2015; Schley, Billingham, and Marchbanks, 2004).

At the inlet boundary (the left cylinder base in *Figure 1*), the velocity field was adjusted to achieve a constant inflow of 100 cm^3/day, and the pressure was taken as zero gradient. At the outlet boundary (the intersection of the VC lumen with the right cylinder base) the pressure was fixed to 15cm H_2O (=1471Pa) and a zero gradient condition was set on the velocity. The conditions at the wall boundaries were nonslip for the the velocity and zero gradient for the pressure. On the rest of the computational domain the initial velocity was taken to be zero and the pressure 15cm H_2O.

Description of the models

Before going into the models we shall briefly explain the terminology used later on for the elements of the catheter. *Figure 2* displays a VC with three drainage segments which will be always numbered from the tip to the valve (left-to-right). Drainage segments are also called hole segments or just segments. We refer to the closest segment to the tip of the catheter as the distal segment. Similarly, the proximal segment stands for the closest segment to the valve. Three types of holes can be distinguished in *Fig. 2*: cylindrical (segment 1), conical (segment 2) and tilted (segment 3), where in the latter case the holes could in turn be cylindrical or conical. In a conical hole, the largest (resp. smallest) diameter is the outer (resp. inner) diameter with respect to the VC lumen, and its surface area will be called the outer (resp. inner) area of the hole. We will refer to the sum of the outer and inner areas of all holes located on the same drainage segment as the drainage outer area and the drainage inner area of that segment, respectively.

Although relative rotations of the drainage segments do not change the flow rate distribution per segment (Galarza et al., 2014; Galarza, Giménez, Pellicer, Valero and Amigó, 2015; Galarza, et al., 2015a), it is convenient to rotate contiguous segments to achieve a higher mechanical stability, especially when they are very close. For a better visualization of the images though, we did not always follow this recommendation in our models.

For studying the effect of different hole shapes on the flow, we divided the models into the three groups described below. All models have the following common feature: 3 drainage segments with 4 holes each.

Group I consists of three models (see *Figure 3* and *Table 1*), each model having one drainage segment with all its holes tilted 45 degrees from the vertical (see *Figure 2*). The segments are located at 4mm/10mm/16mm from the tip.

Group II consists of three models (see *Figure 4* and *Table 2*) each model having one drainage segment with all its holes being conical. The drainage segments are located as in Group I.

Group III consists of 4 models, each model differing from the other in that the middle segment is shifted. But before dealing with the issue of how to choose inter-segment distances, we shall discuss how to fix the diameters of the holes to get a more even flow distribution. In view of the results obtained with Group II, it seems appropriate to consider catheters in which the drainage outer area decreases from the distal segment to the proximal segment. Numerical simulations show that, indeed, it is suitable to take exponentially decreasing drainage outer areas. This being the case, we are going to adopt the following criterion for selecting drainage outer areas. Suppose that we want to design a catheter with N segments numbered left-to-right by i, $1 \leq I \leq N$, with a certain number of holes each one. Let A_i be the drainage outer area of the segment i, and let d_i be the distance from the center of the segment i to the tip of the catheter. We first set the areas A_1 and A_N ($A_1 \geq A_N$) of the distal and proximal segments, respectively, as well as the positions of all segments, i.e. d_1, $d_{2,\ldots,}$ d_N. The outer areas A_i of the intermediate segments, $1 < i < N$, is then calculated by the mathematical formula

$$A_i = A_1 e^{\lambda(d_i - d_1)}; \quad \lambda = \frac{1}{d_N - d_1} \ln\left(\frac{A_N}{A_1}\right). \tag{3}$$

Observe that this formula is suitable provided that $A_1 \geq A_N$ (or equivalently, $\lambda \leq 0$), i.e., when the drainage outer area of the distal segment is equal or greater than the drainage outer area of the proximal segment.

Bearing in mind this general criterion, we have considered four configurations in Group III (see *Figure 5* and *Table 3*) to analyze numerically how different inter-segment distances affect the flow rate distribution.

Results

The main scope of this study was to analyze the distribution of the flow rate and mean shear stress per segment for the different models. All the results are shown in *Figures 6–15,* each one having the same description. In the upper part there are two bar graphs depicting the flow rate per segment (left), and the mean shear stress on the walls of all holes of the same segment (right). In the lower part the shear stress distribution on the inner wall and hole of the catheter is color coded, the darker the color, the higher the shear stress. In all models, the flow is given in cm^3/day and the shear stress in μPa. Since the total inflow (and so the total outflow) is 100cm^3/day, the results for the segments flow can also be considered as flow percentages. Also in all models, the inner diameter of the holes is 0.5 mm.

Group I: Influence of the hole tilt

Results of the Group I are displayed in *Figures 6, 7* and *8*. They show the effect of segments with tilted holes. We may assert that no significant differences in the segment flow rates emerged between the three models tested, although we should note that this holds because the distance between the segments is large (4mm in this case). In fact, according to (Galarza et al., 2015a), the closer the segments are, the more sensitive is

the flow rate with respect to the tilt angle. On the contrary, important differences were found for the mean shear stress. In particular, when tilted holes are included in any segment, the mean shear stress is reduced approximately 20%.

The numerical simulations also disclosed (not shown here) that the higher the tilt angle, the lower the mean shear stress. However, tilt angles higher than 45 degrees might cause mechanical stability problems.

Group II: Influence of conical holes

Figures 9, 10 and *11*, show the effect of segments with conical holes (models 4, 5 and 6, respectively). It is worth observing that conical holes boost the "sink effect" by increasing the flow passing through them. In our numerical experiments, the flow growth rates obtained when cylindrical holes are replaced by conical holes were approximately the following: 35% at the distal segment (Model 4), 45% at the middle segment (Model 5) and 35% at the proximal segment (Model 6). Moreover, at the same time that the segment flow rate increases with conical holes, the mean shear stress per segment is also slightly reduced. Thus, if the conical holes are properly placed in the catheter, they will increase the segment flow rate and decrease the mean shear stress.

Group III. Influence of conical holes with varying inter-segment distance

The most significant conclusion from this group is that constant inter-segment distances is not the best arrangement. Indeed, the results of the numerical experiments shown in *Figures 12–15* clearly indicate that, in a three-segment catheter configuration, the distribution of the segment flow rates improves (i.e., gets more uniform) as the middle segment shifts from left to right. This suggests that a segment distribution with diminishing distances from the distal position to the proximal position is a better choice than keeping constant the inter-segment distances.

Discussion

In this study we evaluated the fluid dynamics of several VC prototypes to analyze flow factors related specifically to the hole geometry. These results will contribute to better understand the fluid-mechanical causes of VC malfunction in hydrocephalus, thus possibly helping to prolong the VC lifetime. Indeed, hydrocephalus is being treated with a shunt system which drains CSF from the cerebral ventricles, but its significant failure rate has caused engineers and neurosurgeons to query its design. The most common failure site is the ventricular catheter due to occlusion by debridement, cells, and brain tissue (Bergsneider et al., 2006; Drake et al., 1998; Drake & Sainte-Rose, 1995; Harris et al., 2010; Harris et al., 2011; Harris & McAllister, 2012; Sainte-Rose et al., 1991). According to the literature (Bergsneider et al., 2006; Drake et al., 1998; Drake & Sainte-Rose, 1995; Harris et al., 2010; Harris et al., 2011; Harris & McAllister, 2012; Lin, Morris, Olivero, Boop & Sanford, 2003), the flow distribution and the shear stress play an important role in such an adhesion of particles to walls. In turn, the flow distribution and the shear stress are determined by the geometric configuration of the catheter. Let us remind that the shear stress is a measure of the force of friction from a fluid acting on a body in the path of the fluid. The experimental evidence shows that the closest holes to the valve in a VC (i.e., belonging to the most proximal segments) are the primary sites of blockage. Of course, obstruction in the proximal perforated area in vivo may be caused also by other reasons, including holes being positioned outside the ventricle. Interestingly, manufacturers have barely altered the number of holes and their placement over the last 60 years (Harris & McAllister, 2011, Harris & McAllister, 2012). There are no overtly accessible records indicative of why the number of holes, the size of each hole, and the distance between segments were so chosen (Harris & McAllister, 2011). Historically, the general consensus has been that the number and size

of the holes were chosen to facilitate an adequate flow from the ventricular space, but recent studies suggest that perhaps fewer holes are required for this (Ginsberg, Sum, Drake, & Cobbold, 2006; Thomale et al., 2010). The first study of VCs that varied the drainage hole size was done by Lin et al. in 2003. They concluded that a gradual decrease in hole diameter from the catheter tip would modify the mass flow rate distribution and would hypothetically reduce the probability of occlusion. Yet, this latter key conclusion was not tested. Notably, the shear stress through a hole depends on its size, a factor known to control cell adhesion in other functions (Zhu et al., 2008).

The only study today that have specifically addressed the influence of the hole size on cell adhesion was done by Harris and McAllister (2011). As the VC of the shunt system is made of poly (dimethyl)siloxane (PDMS), they designed several PDMS samples, designed to mimic the current clinical catheter, with holes that varied in diameter. The number of holes was so chosen that the bulk flow rate and total hole surface area were equal across all samples. The holes were cylindrical or conical holes according to the punching fabrication method used. Analysis of the data using linear regression suggested that the relationship between one cell type (astrocyte) adhesion and hole size was more linear than the relationship between other cell type (macrophage) adhesion and hole size. Their results implied a dependency on how the holes were oriented in the flow system, and suggested that the flow distribution is not the only factor in adhesion. Another factor that may influence adhesion is gravity. They concluded that the cell type adhesion has a strong dependency on the hole size (and most probably on the shear stress as well), and therefore these relationships should be considered in future studies. However, in their study, the shear stress was calculated assuming that the volumetric flow rate through each hole and the hole diameter remained constant. Furthermore, they propose to interpret the shear stress values only as approximations, because the

volumetric flow rate per hole was not measured in their study and, moreover, it probably varies with the distance to the catheter tip, see suggested by Lin et al. (2003). As we used mathematical modeling and numerical simulation, our values are more accurate in that point.

Our models are based on “clean water”, so it might differ slightly from reality since the CSF contains cells and macromolecules. It is important to stress that our main purpose is not so much the search of precise data results, but rather the discussion of how the flow distribution and shear stress vary with the variation of the hole diameters and tilt angles of the holes. As said above, the flow distribution is the key factor in VC obstruction.

Pursuant to our next study about parametric patterns (Galarza et al., 2015b), the basic principles of the segment flow distribution behavior can be summarized as follow:

- Relative rotations of the drainage segments around the axis of the catheter and rigid translations of all the segments along the catheter do not change the flow distribution.

- The flow distribution pattern depends on the inter-segment distances in a sensitive way. In particular, one can transfer fluid mass from right to left just by scaling down the inter-segment distances (and viceversa).

- A lower number of segments as well as a lower number of holes per segment favor a more uniform flow distribution pattern, but the mean shear stress increases.

In view of the results in this paper, to the above principles we should add the following:

- A decreasing distribution of outer diameters of holes (while keeping the inner diameters fixed) also causes transfer of fluid mass from the proximal perforated area to the distal one.

- The flow distribution is not much affected by the hole tilt when the distance between segments is large, however it has a positive effect on the mean shear stress distribution. On the contrary, tilted holes can have a considerable influence when the drainage segments are close enough.

Conclusions

Current commercially available VCs are very often designed with no other guideline than geometrical symmetry. But the difficulties caused by their short mean lifetime require a more rigorous approach. In this regard, further work is needed to design new prototypes with (i) an even (or a decreasing) segment flow distribution pattern, (ii) holes as large as possible, (iii) shear stress as low as possible, and (iv) technical simplicity of manufacturing. The Rivulet model (Lin et al., 2003) was designed to attain a more uniform flow distribution than previous designs, but it also has the disadvantage of having too small hole diameters in the most proximal segments. The present work suggests an alternative solution by combining the use of conical holes (fixing the inner diameter and varying the outer diameter) and tilted holes. It is noteworthy that technically simple changes, which might be overlooked at first sight, become relevant to achieve better designs.

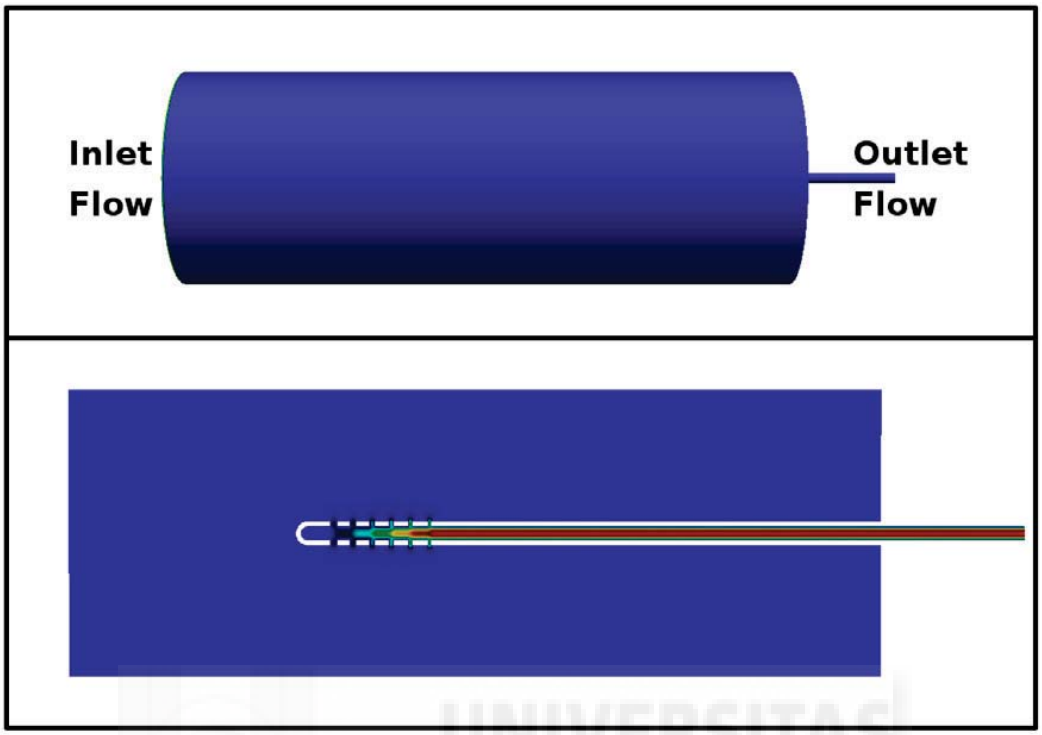

Figure 1: Flow domain. Upper panel: The three-dimensional computational domain in all numerical simulations. Lower panel: A two-dimensional slice of the computational domain.

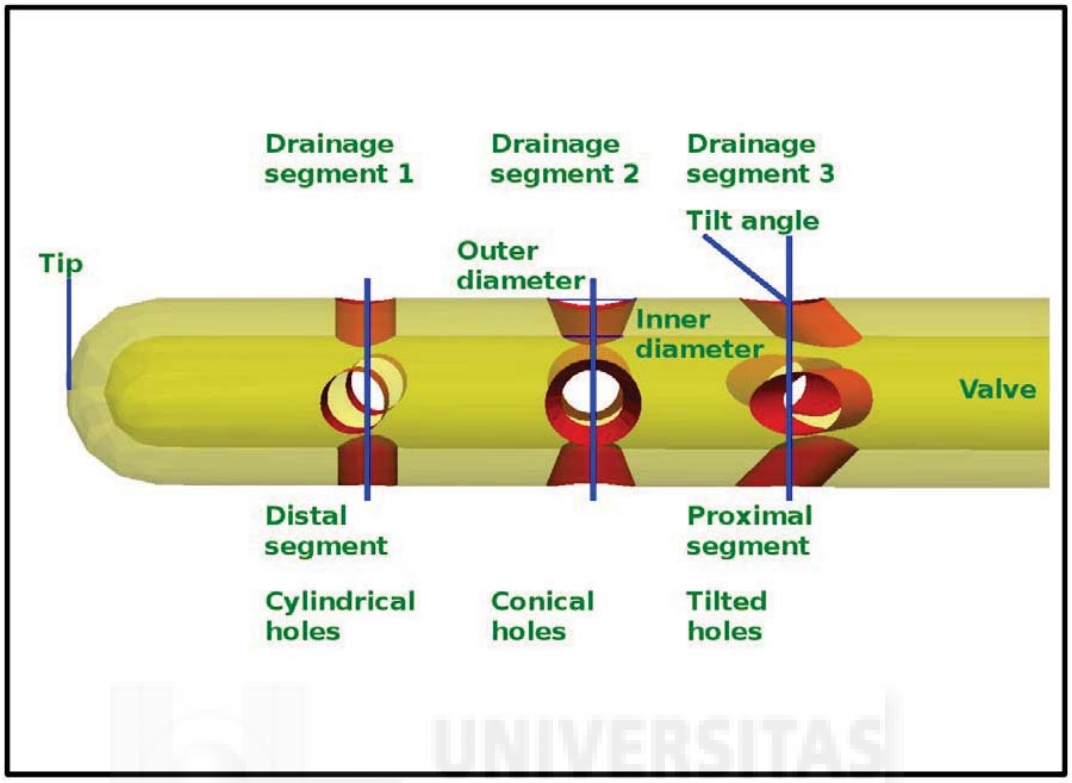

Figure 2: Elements of a catheter. Schematic representation of the component parts of the catheter used throughout the paper.

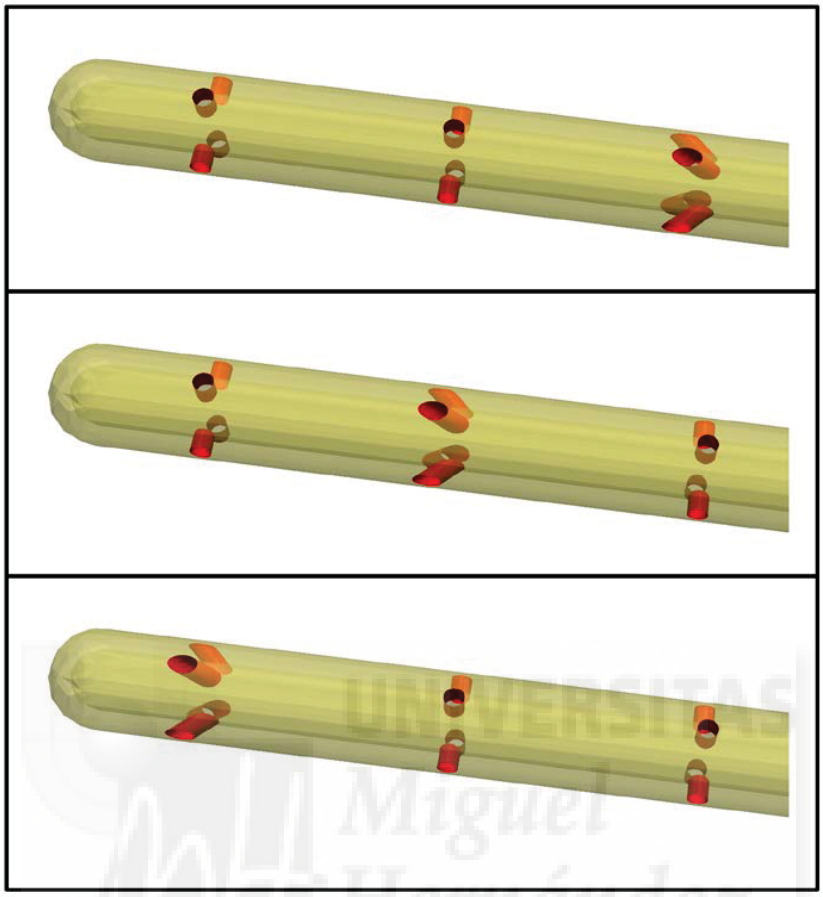

Figure 3: Group I: Models 1, 2 and 3 (from top to bottom). Three-dimensional computational designs of the VCs in Group I. Each model has two segments with vertical holes and one segment with tilted holes.

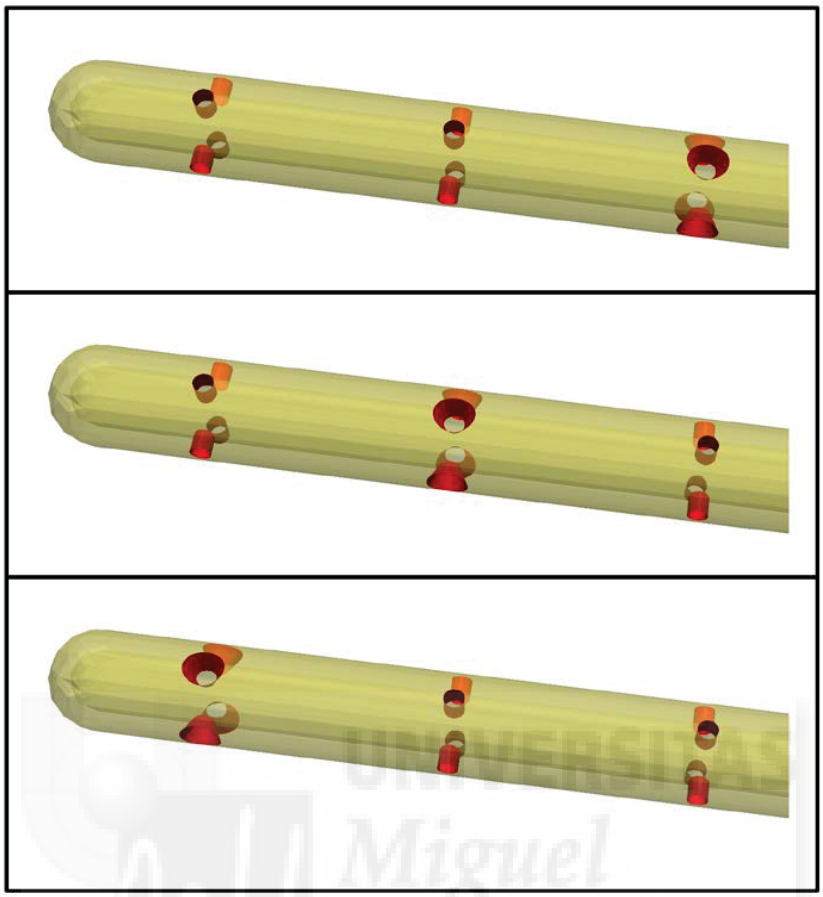

Figure 4: Group II: Models 4, 5 and 6 (from top to bottom). Three-dimensional computational designs of the VCs in Group II. Each model has two segments with cylindrical holes and one segment with conical holes.

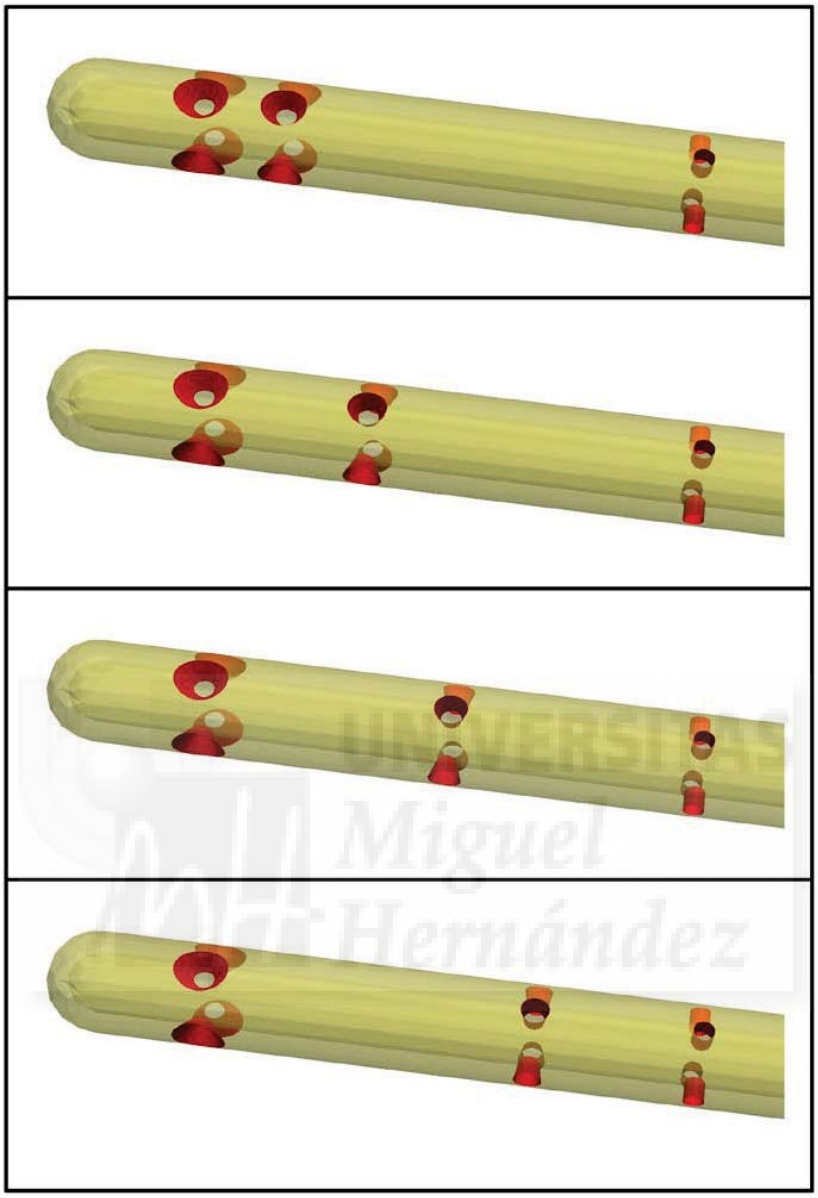

Figure 5: Group III: Models 7, 8, 9 and 10 (from top to bottom). Three-dimensional computational designs of the VCs in Group III. The position of the middle segment is shifted from left to right.

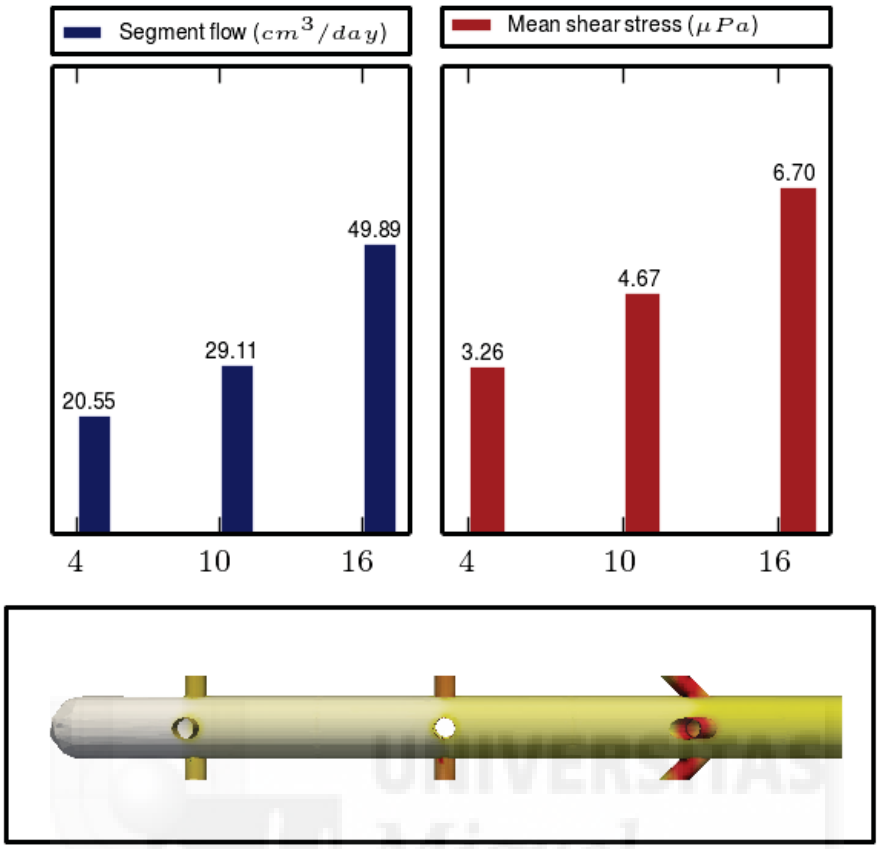

Figure 6: Results of Model 1

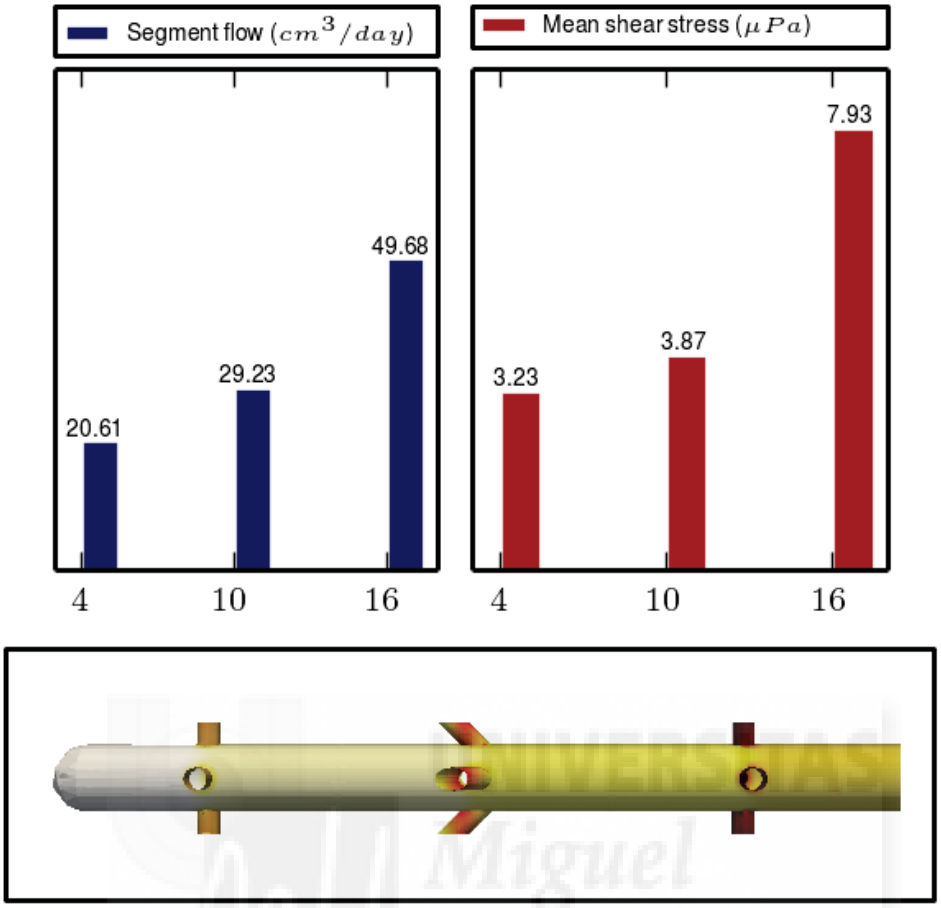

Figure 7: Results of Model 2

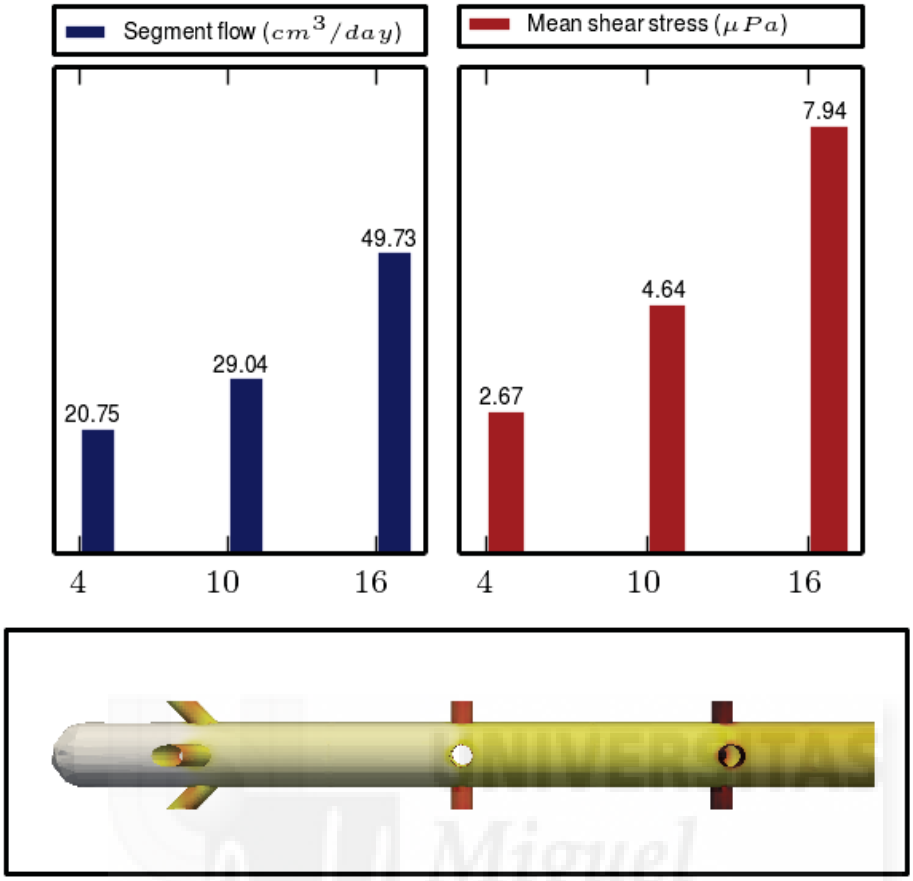

Figure 8: Results of Model 3

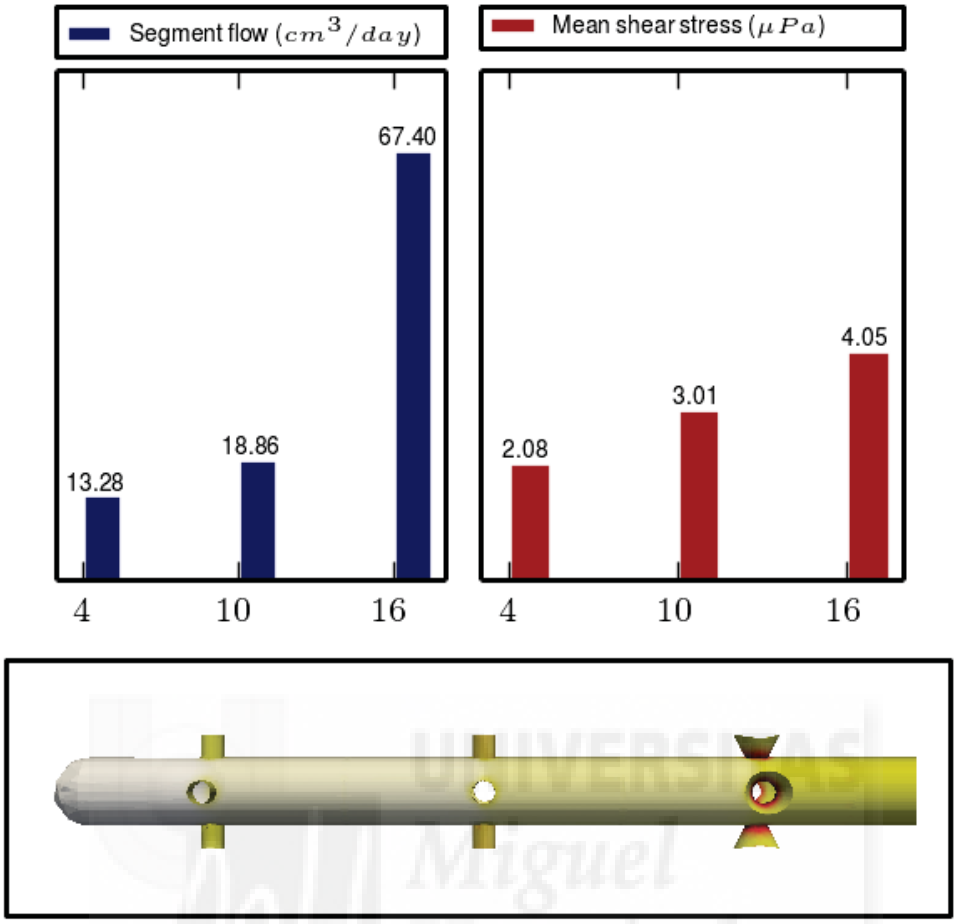

Figure 9: Results of Model 4

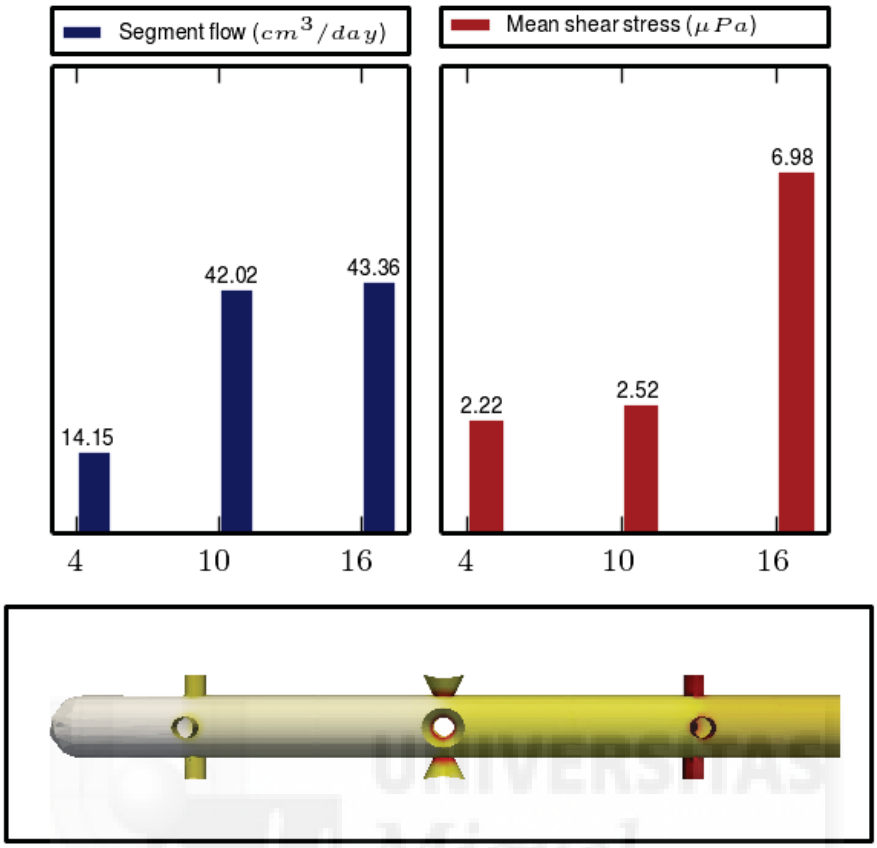

Figure 10: Results of Model 5

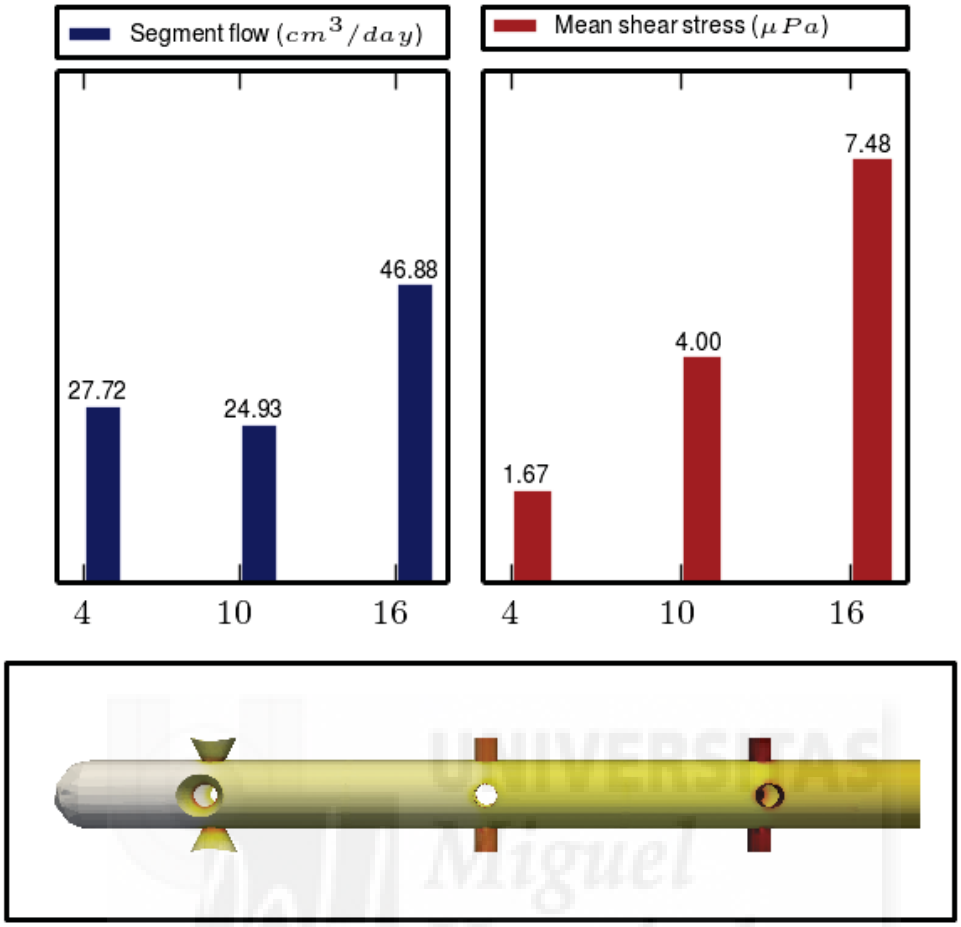

Figure 11: Results of Model 6

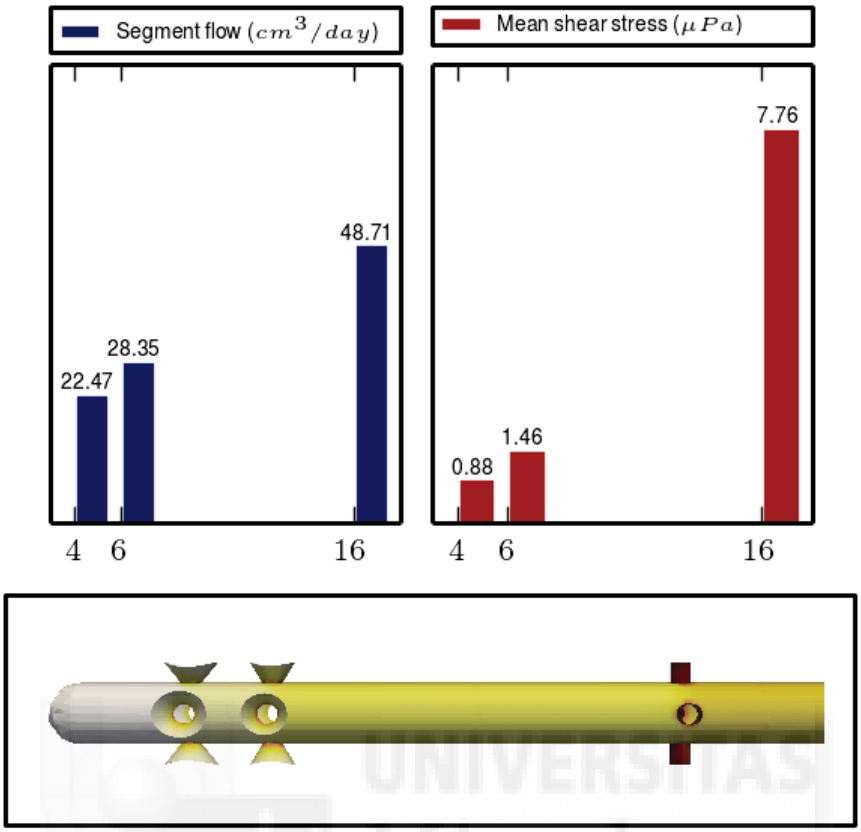

Figure 12: Results of Model 7

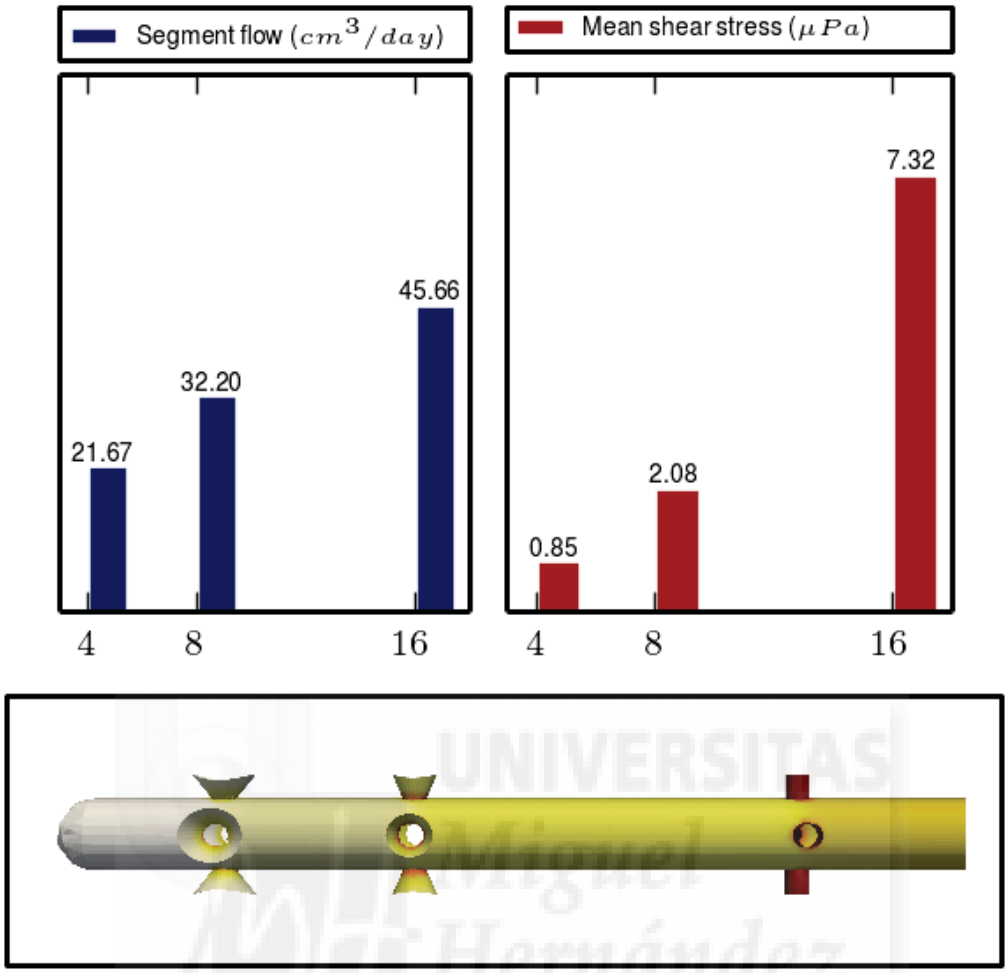

Figure 13: Results of Model 8

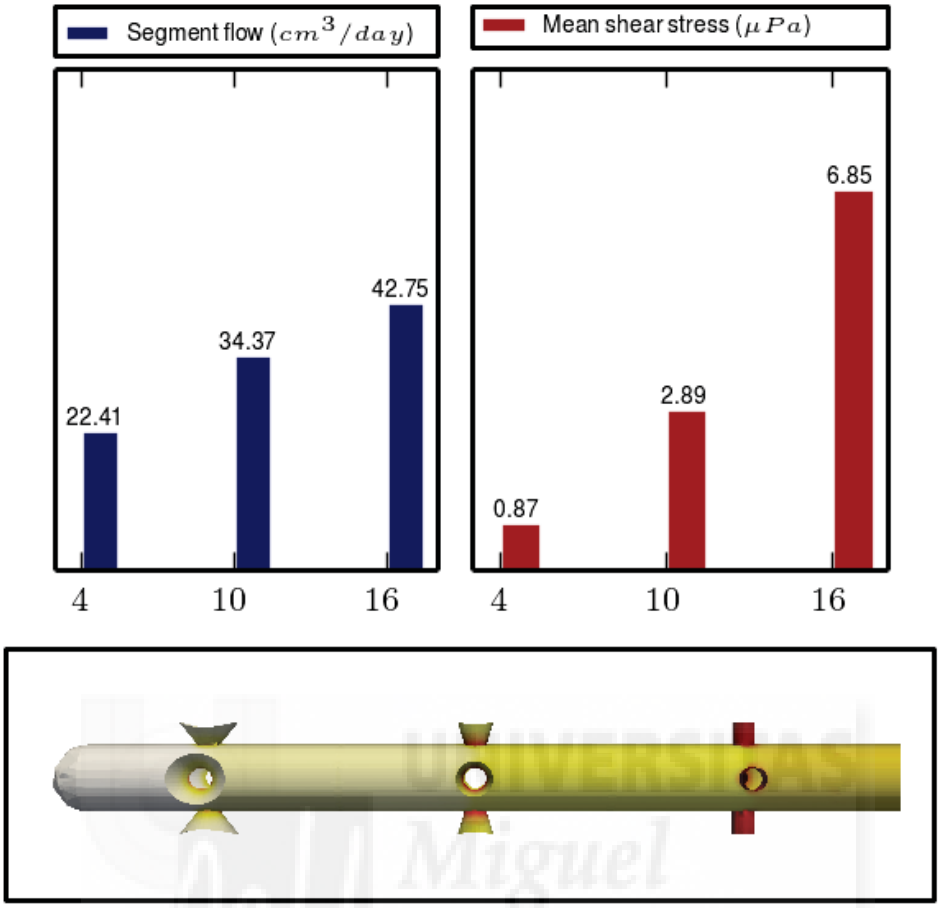

Figure 14: Results of Model 9

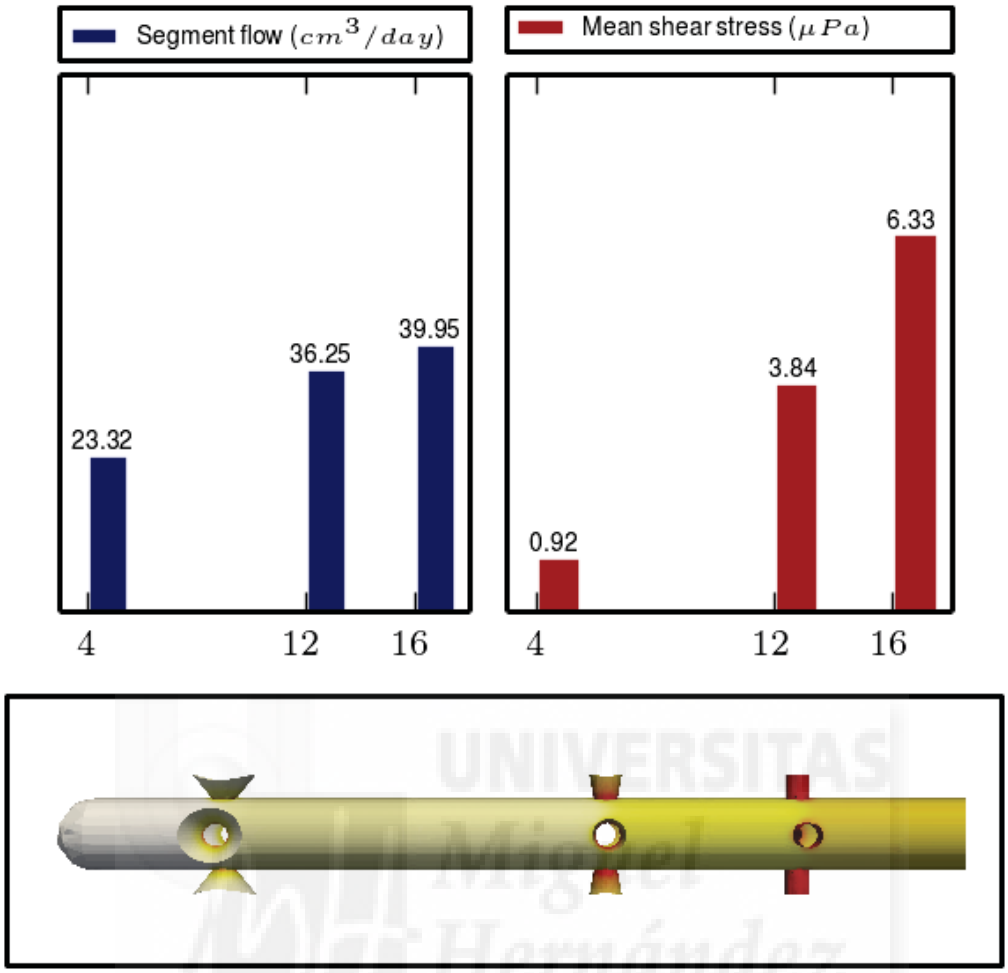

Figure 15: Results of Model 10

Tables Study 4

Table 1: Geometrical parameters of the VCs in Group I. Each entry in the table displays the corresponding measure in the following order: [distal segment, middle segment, proximal segment]. Lengths are given in millimeters and angles in degrees.

	Outer diameter	Inner diameter	Tilt angle
Model 1	[0.5, 0.5, 0.5]	[0.5, 0.5, 0.5]	[0.0, 0.0, 45.0]
Model 2	[0.5, 0.5, 0.5]	[0.5, 0.5, 0.5]	[0.0, 45.0, 0.0]
Model 3	[0.5, 0.5, 0.5]	[0.5, 0.5, 0.5]	[45.0, 0.0, 0.0]

Table 2: Geometrical parameters of the VCs in Group II. Each entry in the table displays the corresponding measure in the following order: [distal segment, middle segment, proximal segment]. Lengths are given in millimeters and angles in degrees.

	Outer diameter	Inner diameter	Tilt angle
Model 4	[0.5, 0.5, 1.0]	[0.5, 0.5, 0.5]	[0.0, 0.0, 0.0]
Model 5	[0.5, 1.0, 0.5]	[0.5, 0.5, 0.5]	[0.0, 0.0, 0.0]
Model 6	[1.0, 0.5, 0.5]	[0.5, 0.5, 0.5]	[0.0, 0.0, 0.0]

Table 3: Geometrical parameters of the VCs in Group III. Each entry in the table displays the corresponding measure in the following order: [distal segment, middle segment, proximal segment]. Lengths are given in millimeters.

	Outer diameter	Inner diameter	Distance to the tip
Model 7	(1.3, 1.1, 0.5)	[0.5, 0.5, 0.5]	[4.0, 6.0, 16.0]
Model 8	[1.3, 0.94, 0.5]	[0.5, 0.5, 0.5]	[4.0, 8.0, 16.0]
Model 9	[1.3, 0.8, 0.5]	[0.5, 0.5, 0.5]	[4.0, 10.0, 16.0]
Model 10	[1.3, 0.68, 0.5]	[0.5, 0.5, 0.5]	[4.0, 12.0, 16.0]

UNIVERSITAS
Miguel
Hernández

Chapter 6:
Study 5. Parametric study of the design of ventricular catheters for hydrocephalus

INTRODUCTION

Hydrocephalus is a medical condition characterized by an excessive accumulation of cerebrospinal fluid (CSF) in the ventricles of the brain. Nowadays the most common treatment for hydrocephalus involves the insertion of a cerebrospinal fluid shunt in one of the ventricles. The main components of a typical shunt system are a ventricular catheter (VC), a controlling valve, and a distal catheter that diverts the excess of CSF to a body cavity. The standard VC is a long and thin tube made of a silicone elastomer, just a few millimeters across, with a number of tiny holes punctured equidistantly around some transversal sections which we call *drainage segments* or simply *segments*. For a given extraction pressure at the valve, the volumetric flow rate is determined by the number of holes per drainage segment and the cross section of the holes, i.e, by the total drainage area. Between 50% and 80% of all shunt malfunctions occur because of obstruction of the VC (Bergsneider et al., 2006; Harris & McAllister, 2011; Sainte- Rose et al., 1991). This occurrence, which is produced by cells and macromolecules present in the CSF, can have serious consequences, even death. VC obstruction is due to a variety of factors (Bergsneider et al., 2006; Harris & McAllister, 2012), including a wrong placement of the catheter. Of all such factors, the flow characteristics play certainly an important role, if not the crucial one. In 2003, in the first application of two-dimensional computational

fluid dynamics (CFD) to VC research, Lin et al. (2003) disclosed that the flow in conventional catheters is predominantly concentrated in the holes closest to the valve, rendering the other holes useless. Ten years later, using software that reproduces accurately the intrincate geometry of a real catheter, we analyzed the three-dimensional fluid dynamics of VC models to evaluate flow factors of shunt malfunction (Galarza et al., 2014).

The most common VC designs have between 12 and 32 holes of the same size, allotted in 6 or 8 drainage segments with the same number of holes (2 or 4). Thus, the holes are situated in pairs opposite on each segment and, furthermore, they are lined up in the longitudinal direction. The Rivulet VC (Lin et al., 2003) features a tapered hole configuration, i.e., holes of different sizes, the smallest holes being located proximally and the largest ones distally. As usual, here and hereafter "proximal" stands for nearest to the valve, while "distal" means the contrary, i.e., nearest to the tip of the catheter. In all these standard designs the drainage segments are separated a constant distance from each other. As for the hole diameter, in most VC it is roughly 500 μm (the exact value depends on the manufacturer), while it ranges from 975 μm (distal holes) to 282 μm (proximal holes) in the Rivulet catheter. According to our three-dimensional numerical simulations in stationary regime (Galarza et al., 2014), between 50% and 75% of the CSF volume flows through proximal holes in a cohort of commercially available catheters, the most even distribution per segment corresponding to the Rivulet model. As Harris and McAllister state (2011, 2012), the size of the holes, the distance between them, the hole irregularity, and the number of holes may all be significant to obstruction. This was partially shown in our second study (Galarza et al., 2015) where we developed VC prototypes with more homogenous flow patterns than currently in use VCs.

Interestingly, most studies and designs regarding shunt systems are aimed at valve devices (Drake et al., 1998), while clinical studies comparing different VCs are still lacking as of this writing. Moreover, there is no reason beyond technical simplicity, why most VC manufacturers produce only standard designs. Bearing in mind this situation, we have studied the dependence of the flow in VCs on the hole configuration as characterized by specific parameters. These comprise (i) the distances between the drainage segments, (ii) the number of holes per segment, (iii) the number of segments, and (iv) their relative angular position. Because of the sheer number of combinations of these parameters and the computational cost of each simulation, our parametric study covers a limited number of relevant cases, yet sufficient to provide a qualitative picture. The results led us to propose some general principles which allow achieving diverse flow patterns, in particular, uniform patterns and patterns with a higher flow rate at the distal segments. These principles, specifically, are intended as guidelines for designing VCs less prone to flow obstruction-related failures.

METHODS

We considered several prototypes of VCs, some of them we called below Models 1 to 12, whose geometrical characteristics are listed in *Table 1*. In all these models, the outer diameter of the catheter is 2.5 mm, and the inner diameter is 1.5 mm. Ventricular catheter holes can be annular or conical, according to the fabrication method. In our cases, the holes are conical with the same outer diameter (1 mm); their inner diameter though changes in general from model to model, and hence so does the drainage area of each model too.

The corresponding *stationary*, 3-D fluid-mechanical problem, with the CSF being modelized by water at body temperature, was solved with the software OpenFoam ® *(http://www.openfoam.org/download/)*. All flow rates are henceforth volumetric (cm^3/day); as a matter of fact, these values are very close to the mass flow rates if the mass unit is taken to be 1 gram because the density of water at 37 ºC is 0.99 g/ cm^3.

Since the catheters are depicted with the tip on the left, all properties involving a direction (like segment numbering, increase or decrease of flows per segment, and inter-segment distances) are meant in the distal-to-proximal direction.

Catheter and hydrocephalus modeling

Our 3D model was assumed to be a steady, incompressible, laminar flow of a Newtonian fluid. The hole distribution in our models varied as segments. The CFD calculation considered flow distribution evolution in time (seconds) and flow rate (cm^3/day) in each flow segment. The last time flow distribution flow segment was calculated considering flow percentage. In addition, the shear stress behavior was calculated considering max shear stress (N/m^2) in time evolution in seconds.

Thus, the VC was located in a cylindrical cavity with rigid walls which modeled the ventricle. An inlet and outlet centered on the bases of the cylinder allow simulating the drainage of cerebrospinal liquid. This cavity was large enough (as compared to the length of the perforated catheter segment) not to influence the flow in the proximity of the holes, which was the flow we were most interested in. The holes of the VC were grouped on cross planes, each plane being thus parallel to each other. As before, we referred to each group of holes as a drainage ring or a segment. These figures are depicted in our first paper (Galarza et al., 2014). Depending on the model, there were three to nine segments, where each segment contained a varying number of holes

symmetrically disposed in the angular direction. In some models, the holes of the VC were aligned in the longitudinal direction if consecutive segments contained the same number of holes. A CFD model was used then to calculate the so-called stationary (i.e., time independent) values of the velocity and pressure fields in the whole domain of the fluid, as well as the flow (in cm^3/day) through each flow segment. These stationary values were reached after a transient phase during which the flow evolves from the initial state, defined by the initial conditions of the CFD model, to the steady state. We further explain this point below.

Broad normative data for CSF characteristics and volumes was taken from first-rate considerations that have been provided by Drake and Sainte-Rose (1995), Hakim (1969), Harris and McAllister (2011, 2012), Schley et al. (2004) and Sood et al. (1993). The drainage flow of our catheter model was set equal to 100 cm^3/day. This being the case, the graphical representations of the stationary flows through the hole segments can also be read as percentages. Values used in our model resembled normal pressure hydrocephalus and specific gravity of CSF. Total CSF volume is approximately 150 to 450 ml according to age, body habitus and gender. While the internal spinal cerebral CSF (within the ependyma) is 150 to 280 cc, the normal ventricles have a normal volume of approximately 25 to 30 cc. Ventricle volumes in hydrocephalus can reach 50 to 300 cc (Drake & Sainte-Rose, 1995; Harris & McAllister, 2011; Schley et al., 2004). The volume capacity of our ventricle model was of 60 cc. The geometric model of the hydrocephalus followed a rigid cylinder of 85mm of length and 30mm of diameter. In sagittal and axial sections, the geometric model followed to approximate the lateral ventricular space of hydrocephalus.

CSF production is about 500cc/day, and 60% is produced by the plexus and the rest by the brain surrounding ependyma. It is similarly reabsorbed through the venous system.

Pulsatile variation of the systolic cardiac cycle (in) and diastolic (out) can vary by up to 20% the volume of the ventricle. According to clinical experience, a ventricular catheter drains about 50 to 300 cc/day, depending to the treated hydrocephalus that is about 10% of what is produced. The drainage volume of our catheter model was of 100 cc. The normal ventricular pressure is ranging between 12 to 18 cmH2O, and in cases of normal pressure hydrocephalus numbers are similar. The CSF has a specific gravity of 1007, compared with the surrounding brain 1047. Same numbers were used in our model.

Ventricular catheter designing

To simulate the flow of the CSF through the new ventricular catheters, we created 3D numerical models based on the actual geometric shapes of commercially available models, or on images and dimensions of their actual boundaries. The solid geometry of the VC was generated with Salome (version 7.3.0) GNU Lesser General Public License (LGPL). This numerical and graphical environment contained separate working modules for geometry creation or manipulation (Geometry), meshing (Mesh), solver management (Supervisor), post-processor (Post-Pro), and communication module (MED). The physical space was converted to a series of interconnected points or nodes which defined the computational domain. The number of nodes determined the resolution of the model and the time needed for computation. The mathematic model, if displayed graphically, appeared as a mesh. The physical characteristics of the fluid and its initial and boundary conditions were specified. The grid-generation utility snappyHexMesh was used to discretize the computational domain with unstructured hexahbedral boundary-fitted mesh. The grid generator allowed cutting out unnecessary parts not related to the region of interest and delimiting the computational domain by means of the inlet, outlet, and cavity solid boundaries. The result was the region of interest in which CFD was applied. SnappyHexMesh is a utility provided with

OpenFoam ® (see below), which has the ability to produce meshes for complex geometries. In particular, it generates finer grids on curved surfaces and boundaries, such as the internal and external surfaces of the catheter (including tip and holes).

CFD Calculation

OpenFOAM® (Open Field Operation and Manipulation) is a free, open source CFD Toolbox software package produced by OpenCFD Ltd. The governing equations for CFD calculation were the 3D incompressible unsteady Navier-Stokes equations written in conservative form for mass and momentum. The numerical simulations were run with the version OpenFOAM® v2.2.2. In our case we used the icoFoam, a transient solver for incompressible laminar flow, to integrate numerically the Navier-Stokes equations. As explained above, the fluid-mechanical variables changed with time at the beginning, till the flow reached a steady phase (the stationary regime) just because of the boundary conditions were time-independent. Note that the initial, unsteady phase was a numerical artifact due to the use of the general ("unsteady") Navier-Stokes equations. Needless to say, we were only interested in the stationary regime.

The simulation was performed by setting the kinematic viscosity of CSF equal to 0.75 x 10^{-6} m^2/s, the kinematic viscosity of water at body temperature. Boundary conditions were specified on all our boundary surfaces. The velocity field at the cavity inlet was adjusted in order to achieve a constant inflow of 100 cm^3/day and, for consistency, the pressure was zero gradient. On the rest of the ventricle and catheter walls, which were considered rigid, non-slip and non-penetration conditions were chosen (i.e., all velocity components at the solid walls were set to zero). The pressure was specified to have zero gradient there because the flux through the wall was zero.

At the cavity outlet, the pressure was set equal to 15 cmH2O, or 11 mmHg (1471 Pa=N/m^2), and a zero gradient condition on the velocity was specified as well. The flow was computed with a time step of 0.005 seconds during a time interval of 0.3 seconds, long enough to reach stationarity. The time step was found to be sufficiently small from the point of view of accuracy. The results used for the flow analysis corresponded to the stationary regime, thus guaranteeing that the results were independent of the initial conditions. As previously, the images were displayed by using ParaView 4.1.0.

The ICP value we have taken for our hydrocephalus model may be criticized. In fact, the concept that a "normal" CSF pressure is a defining feature of idiopathic normal pressure hydrocephalus (INPH) has been criticized (Bradley, 2000; Bret et al., 2002). In patients with INPH, the CSF-OP measured by lumbar puncture in the lateral recumbent position averages 11 +/- 3.3 mm Hg (150 +/- 45 mm H2O) but may fall between 4.4 and 17.6 mm Hg (60–240 mm H2O) (Relkin et al., 2005). In large series by Eide, the static ICP was normal in all patients (mean ICP 7.6 ± 4.8 mmHg) (Eide, 2006). As in other papers cited in this manuscript, there is no specific numbers. In any event, our mathematical model takes a single value for analysis calculation.

VC Model characteristics

Model 1 consists of 3 drainage segments located at 4.75/5.75/7.25 mm from the tip with 6, 4 and 2 holes, respectively; these locations change to 4.75/7.25/10.25 mm in Model 2, and to 4.75/8.75/13.25 mm in Model 3. The inner diameters of the holes are the same (0.5 mm) in these models. The velocity field can then be integrated into flow rates per segment. The segment drainage area (mm^2), which is the total inner area of the

holes per segment, is shown below the velocity fields. Corresponding segments have the same drainage area in these three models.

Model 4 has 6 drainage segments located at 4.25 mm from the tip, with tapered holes (max. 0.35mm; min.0.15mm), each segment separated 2 mm respectively from each other; the intersegment distance decreases in Model 5, and present a disposition “in pairs” in Model 6. Note that, contrarily to Models 1-3, the distance between the proximal and distal segment is the same (10 mm). As the inner diameter of the holes varies, the corresponding drainage area per segment follows *Eq. 1*.

Models 7 to 9 have 3 drainage segments with same number of holes in the distal and medium segment, while presenting 2, 4, and 6 holes in the proximal segment, respectively. The distances from the distal and proximal segment to the tip are the same across these models (4.25 and 7.25 mm). The inner hole diameter in the distal and medium segment is constant (0.3, 0.25 mm, respectively) in three models, while the inner hole diameter of the proximal segment varies according to the presenting number of holes and follows *Eq. 1*.

In the last group we wanted to disclose the effect of the number of segments in catheters. For that purpose, Model 10 to 12 consists of 9, 5 and 3 segments respectively. While, the distance from the proximal segment to the tip is 16.25 mm in all three models, they have the same inter-segment distance. In these prototypes, the distal and proximal segments have 6 and 3 holes; and the inside radius of the holes in those segments is the same (0.3 and 0.2 mm). Yet, we varied the number of medium segments, keeping the same number of holes (n=4). In the medium segments, the inner holes diameters are based on the results of *Eq. 1*.

As we evaluated the effect of number of segments specifically, we assessed the overall flow rate per segment with a hole perforated at the catheter tip. To conclude we calculated the relative angular rotations of the segments. As expected, effects on the flow rate distribution were no observable or negligible.

VENTRICULAR CATHETER MODELS

To study the variation of the flow with the parameters mentioned above, we have considered different groups of VC models, called Groups 1 to 5 hereafter. Let us point out right away that the only practical way to deal with such a huge manifold of possibilities is to change one, possibly two parameters at a time. Thus, in Group 1 we changed the inter-segment distance in a uniform manner while keeping the other parameters fixed. In Group 2 we changed the inter-segment distance in a non-uniform manner, taking the Rivulet catheter as a reference. This amounts to benchmarking new tapered hole configurations against the current standard design. The catheters of Groups 3 and 4 implement changes in the number of holes per segment and segments, respectively. Finally, Group 5 is dedicated to check possible effects of relative segment rotations.

To exclude the drainage area of the segments from the set of parameters, the drainage areas of the distal segment, A_1, and the proximal segment, A_N, were conveniently chosen in each group, while the drainage areas of the remaining segments, A_i $(1 < i < N)$, were set according to the mathematical formula

$$A_i = A_1 exp(\lambda(d_i - d_1)), \qquad \text{(Eq. 1)}$$

where d_i is the distance from the segment i $(1 \leq i \leq N)$ to the tip of the catheter, and

$$\lambda = \frac{1}{d_N - d_1} ln\left(\frac{A_N}{A_1}\right).$$

Observe that this procedure is suitable provided that $A_1 \geq A_N$ (or, equivalently, $\lambda \leq 0$), i.e., whenever the drainage area of the distal segment is equal or greater than the drainage area of the proximal segment.

A few further geometrical characteristics were kept fixed throughout. In all our models the outer diameter of the catheter is 2.5 mm, and the inner diameter is 1.5 mm. Although not necessary, the holes are conical to account for the usual punch fabrication method. Their outer diameter is 1 mm in all models; their inner diameter, though, changes in general from model to model so that the drainage area of each segment complies with *Eq. 1*. Since a rigid translation of the drainage segments is inconsequential for the flow rate distribution, we fixed to 4.25 mm the distance d_1 from the distal segment to the tip. All flow rates are volumetric and measured in cm^3/day.

The corresponding stationary, 3-D fluid-mechanical problems were solved with the software OpenFoam (see *Supplementary Materials* for details). The resulting velocity fields were then integrated into flow rates per segment and visualized. The segment drainage area (mm^2), which is the total inner area of the holes per segment, is shown in the figures below the segment flow**.**

Of the many models evaluated in each group, we have selected three representatives of Groups 1–4 to illustrate the results. All properties involving a direction (like segment numbering, increase or decrease of flow rates per segment, and inter-segment distances) are meant in the distal-to-proximal direction, i.e., left-to-right in the pertinent figures. The part of the catheter between the distal and the proximal segment will be called the perforated area.

Each of the Models 1, 2, and 3 (Group 1) has three segments with 6, 4 and 2 holes, respectively, at constant distance from each other. As we go from Model 1 to Model 3, the inter-segment distance, and thereby the length of the perforated area, grows uniformly *(Figure 1).* See *Table 1* for their geometrical characteristics. Note that *Eq. 1* assigns the same drainage area to corresponding segments in the three models. The results show that the flow is concentrated in the distal segment in Model 1, evenly distributed among the three segments in Model 2, and concentrated in the proximal segment in Model 3.

Each of the Models 4, 5, and 6 (Group 2) has 6 drainage segments with 4 holes each of decreasing sizes *(Figure 2).* This time the distribution of inter-segment distances is varied without changing the length of the perforated area. Distinctively, the inter-segment distances are constant in Model 4, which represents the Rivulet catheter; decrease in Model 5; and features an arrangement in pairs ("stripe configuration") in Model 6. See *Table 1* for the definite characteristics. Model 5 exhibits the most uniform distribution of flow rates per segment in this group.

The fluid-mechanical results with Models 7, 8, and 9 (Group 3) illustrate the impact of the number of holes per segment of a VC. All these models have three segments at the same locations with the same number of holes in the distal and middle segment (6 and 4), whereas the proximal segment has 2, 4, and 6 holes, respectively *(Table 1).* The graphical results in *Figure 3* show that the differences among the three flow rate patterns are rather marginal. In any case, observe that all patterns are decreasing. The same variation of the number of holes in the middle segment yields a mixed impact on the flow rate pattern (not shown).

Models 10, 11, and 12 (Group 4) have a different number of segments (9, 5, and 3) along the same perforated area, the other geometric characteristics being the same in corresponding segments. Model 11 is obtained from Model 10 by removing every second segment, and the same applies to Model 12 with respect to Model 11. Furthermore, the distal segment has 6 holes, the proximal segment 2 holes, and the remaining segments 4 holes. Other geometrical details are summarized in *Table 1*. We see in *Figure 4* that Models 10 and 11 (the two designs with most segments) have increasing flow rate patterns (the steeper the more segments), while Model 12 (the one with only three segments) has a uniform pattern.

Numerical simulations not reported above lead also to the following result: there is practically no difference in the flow rate per segment if a hole is perforated at the VC tip.

Finally, in Group 5, we also checked that the relative angular rotations of the segments have, as previously avowed, no observable effects on the flow rate distribution.

PARAMETRIC STUDY

Clinical praxis demonstrates that a catheter design with a constant number of holes per drainage segment, like in the currently in use VCs, favors obstruction. This being the case, we proposed in to vary the number of holes per segment to improve the flow rate pattern over the perforated area (Galarza et al., 2015). Variation of other parameters, like inter-segment distances and the inner diameter of the holes, proved to be convenient as well. In the previous section it was evidenced that the flow rate

through the drainage segments depends on the hole configuration in a well-defined way. We elaborate further on in the following subsections. As mentioned before, Models 1 to 12 are representatives of many others which were also considered in our parametric study. The properties described above and the conclusions drawn below are common to all of them.

Flow rate dependence on an uniform inter-segment distance distribution

Models 1, 2 and 3 have 3 segments, each model with constant inter-segment distances. In these models we were able to change the flow rate pattern solely by prolonging or shortening uniformly the inter-segment distance, while keeping constant the number of holes per segment and their sizes (i.e., the segment drainage areas). Specifically, Model 1, with the shortest inter-segment distance, displays a *decreasing flow rate pattern*, i.e., the flow rate per segment takes decreasing values. Model 2 has a *uniform flow rate pattern*, i.e., the distribution of the flow rate per segment is constant. And Model 3, with the longest inter-segment distances, shows an *increasing flow rate pattern*, i.e., the distribution of the flow rate per segment takes increasing values. In sum, the flow rate pattern can be changed and even reversed by adjusting the inter-segment distances in the way done in Group 1. This was previously evidenced in our third study about basic flow patterns (Galarza et al., 2015b). Theoretically Model 1 has the best flow rate pattern because the highest flow rate occurs at the distal segment, that is, farthest away from the typical occlusion site of a VC (Harris & McAllister, 2011). Indeed, if the lumen of the catheter gets clogged in the proximal segment(s), then the drainage capability of the whole system results partially or even fully disabled because the obstruction happens downstream of the other segments. In practice, however, the short length of the perforated section requires an accurate catheter placement within the ventricle. This, so far, is not feasible in most neurosurgical scenarios.

Flow rate dependence on a non-uniform inter-segment distance distribution

To assess the influence of a non-uniform variation of the inter-segment distances (Group 2), the Rivulet catheter (Model 4) was taken as reference. The main feature of this model is their tapered hole configuration: it has a fixed number of holes per segment and decreasing hole sizes (as measured by the inner diameter). Ideally, the proximal segment should have the least flow rate (shear stress) value to reduce the chance of obstruction (Harris & McAllister, 2012).

The flow rates obtained with our VC Model 4 agrees with the results of Lin et al. (2003). They developed a VC with constant inter-segment distances and hole sizes diminishing progressively, and claimed that this VC design would lower the probability of occluding the entire catheter.

By varying the inter-segment distance, as in Model 5 and 6, a more uniform flow rate pattern can be achieved, the most uniform distribution of flow rates per segment occurring in Model 5.

Flow rate dependence on the number of holes per segment

In Group 3 we varied the number of holes of the segments, while keeping constant the drainage area of the segments (which requires adjusting the inner hole diameters). Purposely, Models 7, 8, and 9 implement this variation at the proximal segment, the critical one from the point of view of obstruction. The results show a minor influence of the number of holes there. We conclude that, in this case, the choice of the number of holes at the proximal segment should be based on the relation between the hole size and the probability of obstruction, then the more holes the smaller their size.

Harris and McAllister (2011) and Lin et al. (2003) reported the only studies to date on the effect of the hole size. Harris and McAllister studied specifically the adhesion factors of VC occlusion. From their results no clear relation between adhesion and proximity to the catheter tip follows but rather a dependency on how the holes are oriented in the flow. This could entail that the flow rate distribution is not the only factor in VC occlusion, and, as they state, adhesion might be also influenced by gravity. Furthermore, obstructions that occur in the proximal segments *in vivo* can be caused by other factors, including holes being positioned outside the ventricle (Ginsberg et al., 2000; Thomale et al., 2010).

The impact of the number of holes in VCs was described by Thomale et al. (2010). According to these authors, fewer holes overall, with equal flow characteristics might decrease obstruction when catheters can be implanted with adequate precision.

In sum, the smaller the diameter of a hole, (i) the more prone to become occluded by debris or cells, and (ii) the higher the shear stress of the fluid flowing through it (Harris & McAllister, 2012).

Flow rate dependence on the number of segments

In this case, when the number of segments increases, the total drainage area also increases and, consequently, the flow rate per segment decreases by constant pressure. This was addressed by Ginsberg et al. (2000) and then by Thomale et al. (2010); although, they compared the number of holes rather than the number of segments. In our case, the direct comparison between the different models is complex because the drainage area per segment is not constant but follows the law given in *Eq. 1*. In this situation, a way to proceed is to calculate the cumulative flow rate distribution.

According to the results in *Table 1*, given two models as in Group 4 the model with less segments has a higher cumulative rate flow at the distal and common intermediary segments. This is a consequence of the fact that few segments over a given perforated area lead to a more uniform flow, see *Figure 4.*

GENERAL PRINCIPLES FOR VC DESIGN

From the numerical facts summarized in the previous sections, a number of general principles can be derived.

Principle 1. The flow rate pattern depends on the inter-segment distances in a sensitive way. Indeed, starting with a configuration with an increasing/decreasing flow rate pattern and equal inter-segment distances, one can reverse the pattern just by scaling down or up the inter-segment distances, respectively. Clearly, the uniform flow rate pattern is achieved at some intermediary stage.

Therefore, according to *Principle 1* the distribution of the flow rate per segment is strongly influenced by the inter-segment distance distribution. As an additional remark, the inter-segment distance should be larger than 1 mm because of mechanical stability. Further considerations, like the VC material and the size of the particles present in the CSF, may increase that distance.

The following principle condenses the results obtained with the models of Group 2. For completeness, we have added the principle behind the tapered hole configurations (Lin et al., 2003):

Principle 2. A decreasing distribution of hole diameters levels off the increasing flow rate pattern produced by equally spaced segments with holes of the same size. A decreasing inter-segment distance distribution uniforms further the flow rate pattern.

Principle 3. The number of holes at the proximal segment has no significant influence on the flow rate pattern.

Principle 4. A small number of segments over a given perforated area favors a uniform flow rate pattern, provided that the drainage areas of the segments follow *Eq. 1*.

Principle 5. Relative rotations of the drainage segments around the axis of the catheter do not change the flow rate pattern.

In conclusion, an adequate choice of a few parameters according to the *Principles 1 to 5* allows achieving all three flow rate patterns: increasing, constant or decreasing. The increasing one, which is precisely the flow rate pattern of most standard VCs, enhances the possibility of obstruction and, therefore, must be disregarded. A quantitative formula for a distribution of the drainage area per segment guaranteeing a relatively homogeneous flow rate pattern was given in *Eq. 1*.

LEGENDS TO FIGURES

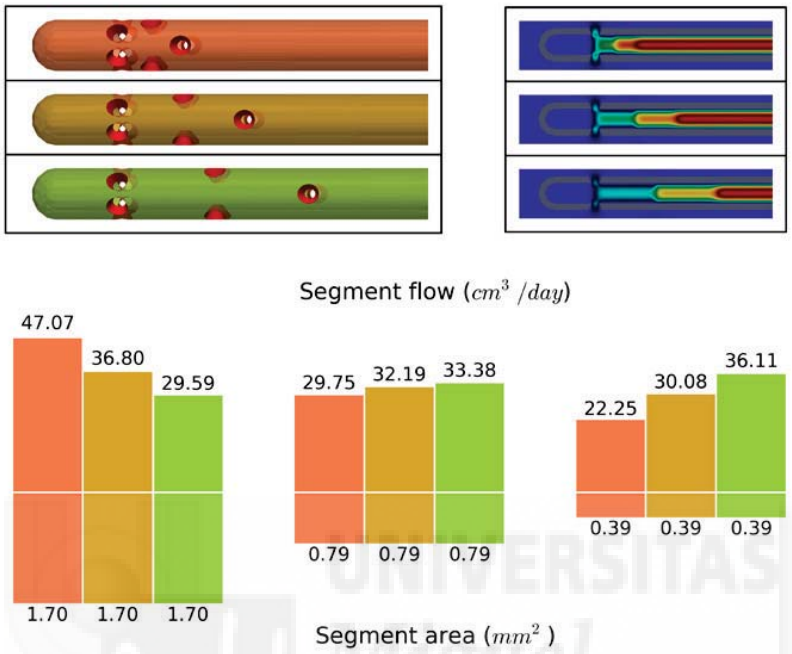

Figure 1. The following panel refers CFD results in VC prototypes 1, 2, 3 of Group 1. It is evident three different patterns of flow in each model.

Note. Group 1, Models 1, 2, and 3 of ventricular catheters with three segments of 6, 4 and 2 holes with the inter-segment distance increasing uniformly. CFD imaging for each catheter is shown on the left. They have the same drainage area to corresponding segments. The results show that the flow is concentrated in the distal segment in Model 1, evenly distributed among the three segments in Model 2, and concentrated in the proximal segment in Model 3.

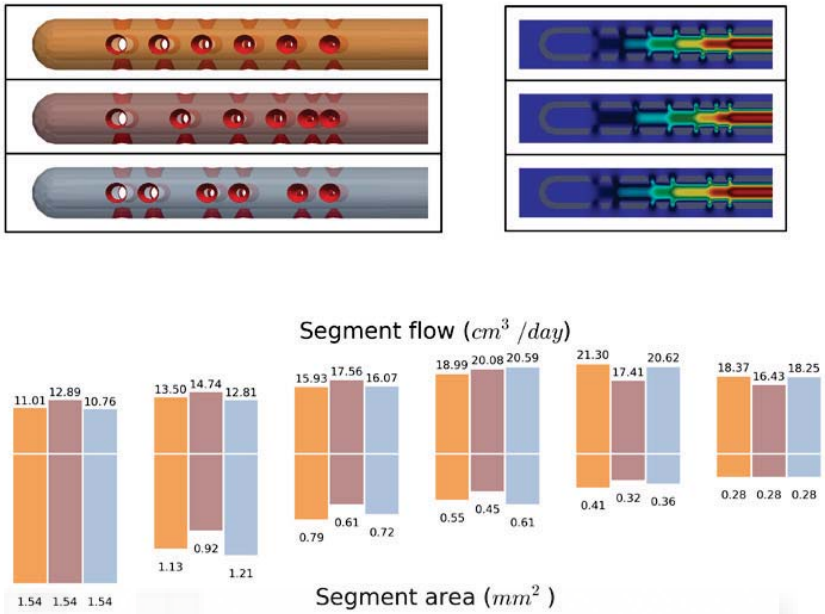

Figure 2. The following panel refers CFD results in VC prototypes 4, 5, 6 of Group 2.

Note. Group 2, Models 4, 5, and 6, has 6 drainage segments with 4 holes each of decreasing sizes (tapered). The inter-segment distances are constant in Model 4, decrease in Model 5; and shows a "stripe configuration" in Model 6. Overall, Model 5 discloses the most consistent distribution of segment flow rate.

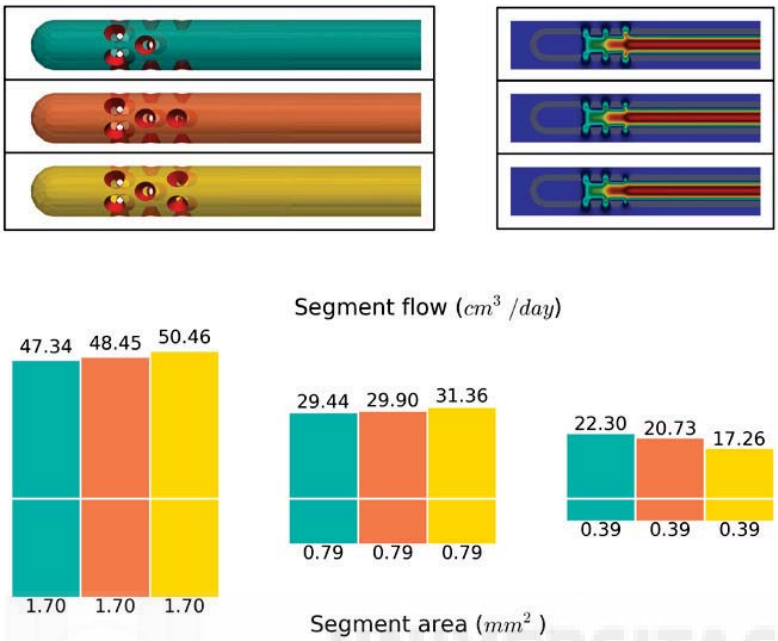

Figure 3. The following panel refers CFD results in VC prototypes 7, 8, 9 of Group 3.

Note. Group 3, Models 7, 8, and 9, have three segments with the same number of holes in the distal (n=6) and middle (n=4) segment, but the proximal segment has 2, 4, and 6 holes, respectively. The differences among the segment flow rate patterns are fairly minor in all three catheters. Yet all patterns are decreasing. The same variation of the number of holes in the middle segment showed similar results (not shown).

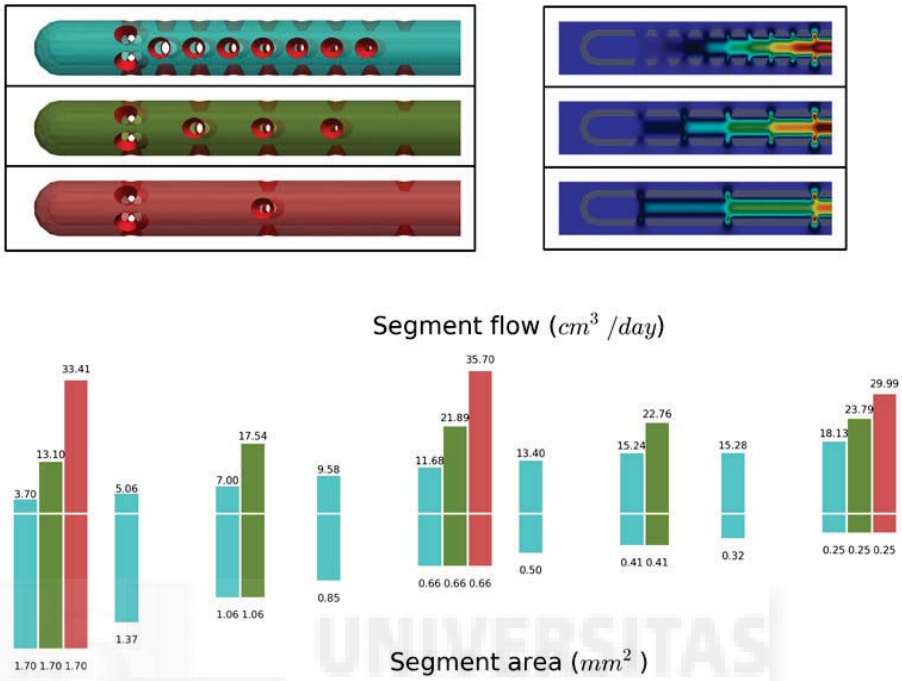

Figure 4. The following panel refers CFD results in VC prototypes 10, 11, 12 of Group 4. It shows the main finding according to the number of segments in different models.

Note. In Group 4, Models 10, 11, and 12, catheters have a different number of segments along the same perforated area. Geometrical features are summarized in *Table I*. The two designs with most segments, Models 10 and 11 have increasing flow rate patterns, while the catheter with three segments, Model 12, has a uniform pattern.

Table 1.

Numerical characteristics and Computational Fluid Dynamics results in twelve Models of ventricular catheter prototypes distributed in four Groups according to parametric results.

Catheter 1 Group 1.-(a)	
Number of holes / Number of segments	12 / 3
Number of holes per segment	[6, 4, 2]
Distance from each segment to the tip	[4.25, 5.75, 7.25]
Outside radius of the holes in the same segment	[0.5, 0.5, 0.5]
Inside radius of the holes in the same segment	[0.3, 0.25, 0.25]
Inside diameter of the catheter (I.D.)	1.5
Outside diameter of the catheter (O.D.)	2.5
Total sum of hole areas per segment	[1.7, 0.79, 0.39]
Inlet flow through each segment	[47.07, 29.75, 22.25]
Inlet flow per unit area through each segment	[27.75, 37.88, 56.67]
Total sum of inlet segment flows	99.07488
Catheter 2 Group 1.-(b)	
Number of holes / Number of segments	12 / 3
Number of holes per segment	[6, 4, 2]
Distance from each segment to the tip	[4.25, 7.25, 10.25]
Outside radius of the holes in the same segment	[0.5, 0.5, 0.5]
Inside radius of the holes in the same segment	[0.3, 0.25, 0.25]
Inside diameter of the catheter (I.D.)	1.5

Outside diameter of the catheter (O.D.)	2.5
Total sum of hole areas per segment	[1.7, 0.79, 0.39]
Inlet flow through each segment	[36.8, 32.19, 30.08]
Inlet flow per unit area through each segment	[21.69, 40.99, 76.61]
Total sum of inlet segment flows	99.07488

Catheter 3 Group 1.-(c)

Number of holes / Number of segments	12 / 3
Number of holes per segment	[6, 4, 2]
Distance from each segment to the tip	[4.25, 8.75, 13.25]
Outside radius of the holes in the same segment	[0.5, 0.5, 0.5]
Inside radius of the holes in the same segment	[0.3, 0.25, 0.25]
Inside diameter of the catheter (I.D.)	1.5
Outside diameter of the catheter (O.D.)	2.5
Total sum of hole areas per segment	[1.7, 0.79, 0.39]
Inlet flow through each segment	[29.59, 33.38, 36.11]
Inlet flow per unit area through each segment	[17.44, 42.5, 91.96]
Total sum of inlet segment flows	99.07834

Catheter 4 Group 2.-(a)

Number of holes / Number of segments	24 / 6
Number of holes per segment	[4, 4, 4, 4, 4, 4]
Distance from each segment to the tip	[4.25, 6.25, 8.25, 10.25, 12.25, 14.25]
Outside radius of the holes in the same segment	[0.5, 0.5, 0.5, 0.5, 0.5, 0.5]
Inside radius of the holes in the same segment	[0.35, 0.3, 0.25, 0.21, 0.18, 0.15]
Inside diameter of the catheter (I.D.)	1.5

Outside diameter of the catheter (O.D.)	2.5
Total sum of hole areas per segment	[1.54, 1.13, 0.79, 0.55, 0.41, 0.28]
Inlet flow through each segment	[11.01, 13.5, 15.93, 18.99, 21.3, 18.37]
Inlet flow per unit area through each segment	[7.15, 11.94, 20.29, 34.27, 52.31, 64.98]
Total sum of inlet segment flows	99.10858

Catheter 5 Group 2.-(b)

Number of holes / Number of segments	24 / 6
Number of holes per segment	[4, 4, 4, 4, 4, 4]
Distance from each segment to the tip	[4.25, 7.25, 9.75, 11.75, 13.25, 14.25]
Outside radius of the holes in the same segment	[0.5, 0.5, 0.5, 0.5, 0.5, 0.5]
Inside radius of the holes in the same segment	[0.35, 0.27, 0.22, 0.19, 0.16, 0.15]
Inside diameter of the catheter (I.D.)	1.5
Outside diameter of the catheter (O.D.)	2.5
Total sum of hole areas per segment	[1.54, 0.92, 0.61, 0.45, 0.32, 0.28]
Inlet flow through each segment	[12.89, 14.74, 17.56, 20.08, 17.41, 16.43]
Inlet flow per unit area through each segment	[8.37, 16.09, 28.88, 44.26, 54.1, 58.1]
Total sum of inlet segment flows	99.10685

Catheter 6 Group 2.-(c)

Number of holes / Number of segments	24 / 6
Number of holes per segment	[4, 4, 4, 4, 4, 4]
Distance from each segment to the tip	[4.25, 5.75, 8.5, 10.0, 12.75, 14.25]
Outside radius of the holes in the same segment	[0.5, 0.5, 0.5, 0.5, 0.5, 0.5]
Inside radius of the holes in the same segment	[0.35, 0.31, 0.24, 0.22, 0.17, 0.15]
Inside diameter of the catheter (I.D.)	1.5

Outside diameter of the catheter (O.D.)	2.5
Total sum of hole areas per segment	[1.54, 1.21, 0.72, 0.61, 0.36, 0.28]
Inlet flow through each segment	[10.76, 12.81, 16.07, 20.59, 20.62, 18.25]
Inlet flow per unit area through each segment	[6.99, 10.61, 22.2, 33.86, 56.79, 64.55]
Total sum of inlet segment flows	99.10771

Catheter 7 Group 3.- (a)

Number of holes / Number of segments	12 / 3
Number of holes per segment	[6, 4, 2]
Distance from each segment to the tip	[4.25, 5.75, 7.25]
Outside radius of the holes in the same segment	[0.5, 0.5, 0.5]
Inside radius of the holes in the same segment	[0.3, 0.25, 0.25]
Inside diameter of the catheter (I.D.)	1.5
Outside diameter of the catheter (O.D.)	2.5
Total sum of hole areas per segment	[1.7, 0.79, 0.39]
Inlet flow through each segment	[47.34, 29.44, 22.3]
Inlet flow per unit area through each segment	[27.91, 37.49, 56.78]
Total sum of inlet segment flows	99.08179

Catheter 8 Group 3.- (b)

Number of holes / Number of segments	14 / 3
Number of holes per segment	[6, 4, 4]
Distance from each segment to the tip	[4.25, 5.75, 7.25]
Outside radius of the holes in the same segment	[0.5, 0.5, 0.5]
Inside radius of the holes in the same segment	[0.3, 0.25, 0.18]
Inside diameter of the catheter (I.D.)	1.5

Outside diameter of the catheter (O.D.)	2.5
Total sum of hole areas per segment	[1.7, 0.79, 0.39]
Inlet flow through each segment	[48.45, 29.9, 20.73]
Inlet flow per unit area through each segment	[28.56, 38.07, 50.92]
Total sum of inlet segment flows	99.08093
Catheter 9 Grupo 3.- (c)	
Number of holes / Number of segments	16 / 3
Number of holes per segment	[6, 4, 6]
Distance from each segment to the tip	[4.25, 5.75, 7.25]
Outside radius of the holes in the same segment	[0.5, 0.5, 0.5]
Inside radius of the holes in the same segment	[0.3, 0.25, 0.14]
Inside diameter of the catheter (I.D.)	1.5
Outside diameter of the catheter (O.D.)	2.5
Total sum of hole areas per segment	[1.7, 0.79, 0.39]
Inlet flow through each segment	[50.46, 31.36, 17.26]
Inlet flow per unit area through each segment	[29.74, 39.93, 46.72]
Total sum of inlet segment flows	99.0792
Catheter 10 Group 4.- (a)	
Number of holes / Number of segments	36 / 9
Number of holes per segment	[6, 4, 4, 4, 4, 4, 4, 4, 2]
Distance from each segment to the tip	[4.25, 5.75, 7.25, 8.75, 10.25, 11.75, 13.25, 14.75, 16.25]
Outside radius of the holes in the same segment	[0.5, 0.5, 0.5, 0.5, 0.5, 0.5, 0.5, 0.5, 0.5]
Inside radius of the holes in the same segment	[0.3, 0.33, 0.29, 0.26, 0.23, 0.2, 0.18, 0.16, 0.2]
Inside diameter of the catheter (I.D.)	1.5

Outside diameter of the catheter (O.D.)	2.5
Total sum of hole areas per segment	[1.7, 1.37, 1.06, 0.85, 0.66, 0.5, 0.41, 0.32, 0.25]
Inlet flow through each segment	[3.7, 5.06, 7.0, 9.58, 11.68, 13.4, 15.24, 15.28, 18.13]
Inlet flow per unit area through each segment	[2.18, 3.7, 6.62, 11.28, 17.57, 26.66, 37.43, 47.5, 72.14]
Total sum of inlet segment flows	99.07574

Catheter 11 Group 4.- (b)

Number of holes / Number of segments	20 / 5
Number of holes per segment	[6, 4, 4, 4, 2]
Distance from each segment to the tip	[4.25, 7.25, 10.25, 13.25, 16.25]
Outside radius of the holes in the same segment	[0.5, 0.5, 0.5, 0.5, 0.5]
Inside radius of the holes in the same segment	[0.3, 0.29, 0.23, 0.18, 0.2]
Inside diameter of the catheter (I.D.)	1.5
Outside diameter of the catheter (O.D.)	2.5
Total sum of hole areas per segment	[1.7, 1.06, 0.66, 0.41, 0.25]
Inlet flow through each segment	[13.1, 17.54, 21.89, 22.76, 23.79]
Inlet flow per unit area through each segment	[7.72, 16.59, 32.94, 55.9, 94.65]
Total sum of inlet segment flows	99.08093

Catheter 12 Group 4.- (c)

Number of holes / Number of segments	12 / 3
Number of holes per segment	[6, 4, 2]
Distance from each segment to the tip	[4.25, 10.25, 16.25]
Outside radius of the holes in the same segment	[0.5, 0.5, 0.5]
Inside radius of the holes in the same segment	[0.3, 0.23, 0.2]

Inside diameter of the catheter (I.D.)	1.5
Outside diameter of the catheter (O.D.)	2.5
Total sum of hole areas per segment	[1.7, 0.66, 0.25]
Inlet flow through each segment	[33.41, 35.7, 29.99]
Inlet flow per unit area through each segment	[19.7, 53.7, 119.31]
Total sum of inlet segment flows	99.09475

Group 4.- Cumulative Segment Flow Table

Distance from each segment to the tip (*mm*)								
4.25	5.75	7.25	8.75	10.25	11.75	13.25	14.75	16.25
Cumulative flow in each segment (*cm3*/*day*)								
3.70	8.76	15.76	25.34	37.02	50.42	65.66	80.95	99.08
13.10		30.64		52.53		75.29		99.08
33.41				69.11				99.08

UNIVERSITAS
Miguel
Hernández

Chapter 7:

Main findings and future perspectives

The studies presented in the preceding chapters have shown that CSF flow through ventricular catheters, either currently existing or prototypes models can be accurately simulated by means of three-dimensional CFD. Furthermore, these studies disclosed CSF specific flow patterns within the ventricular catheter. Also, we have carried out a parametric study via computational dynamics of several models. The parameters were the number of drainage segments, the distances between them, their relative angular position, and the number and diameter of the holes on each segment. In consequence we have formulated general principles for designing new ventricular catheters. These principles can help develop new catheters with homogeneous flow patterns, thus possibly extending their lifetime. What follows is a short description and conclusion of the previous chapters and a general reflection upon their implications.

1. Summary of main findings

1.2 Study 1

The most common treatment for hydrocephalus remains the ventriculoperitoneal shunt. Yet, the most frequent complication is ventricular catheter obstruction, which may account for 50–80% of newly inserted shunts. Although many factors contribute to this, the main one is related to flow characteristics of the catheter within the hydrocephalic brain. A landmark study by Lin, Morris, Olivero, Boop & Sanford, 2003 addressed the problem of fluid characteristics in a ventricular catheter using a two-dimensional

simulation program of computational fluid dynamics (CFD). They found an unequally distribution of flow through the studied catheter, where most of the holes were useless.

In our first study, the authors have studied five current commercially available ventricular catheter designs using CFD in three dimensional automated designs. The models studied were a catheter of 12 holes, two of 16, one of 24 (Rivulet) and another of 32 holes. The specific objective of this first study was to investigate the flow pattern in these catheters.

In this study it was disclosed that most of the total mass of liquid flows in most proximal holes of the catheters. 75% of the flow flows into the two most proximal holes of the catheters of 12, 16 and 32 holes. Some flow uniformity, with a 50% flow in the most proximal holes, has been observed in the catheter of 24 holes or Rivulet type.

The authors conclude that most commercially available ventricular catheters have an abnormally increase flow distribution pattern.

1.2.Study 2

Based on a landmark study by Lin, Morris, Olivero, Boop & Sanford, 2003 of the two-dimensional flow in ventricular catheters (VC) via computational fluid dynamics (CFD), we studied in a previous paper (Galarza M, Giménez A, Valero J, Pellicer O, Amigó JM, 2014) the three-dimensional flow patterns of five commercially available VC. We found that the drainage of the cerebrospinal fluid (CSF) mostly occurs through the catheter's most proximal holes. In this second paper we designed five VC prototypes with equalized flow characteristics. We studied five prototypes of VC by means of CFD in three-dimensional (3-D) automated models and compare the fluid-mechanical results with our previous study of currently in use VC. The general

procedure for the development of a CFD model calls for transforming the physical dimensions of the system to be studied into a virtual wire-frame model which provides the coordinates for the virtual space of a CFD mesh. By varying the number of drainage holes and the ratio hole/segment, we improved flow characteristics in five prototypes of VC. Models 1, 2 and 3 have a distal to proximal decreasing flow. Model 4 has an inverse flow to the previous ones, that is, a distal to proximal increasing flow, while Model 5 has a constant flow over the segments. These new five catheter designs with variable hole diameter, number of holes, and ratio hole/segment along the catheter allowed the fluid to enter the catheter more uniformly along its length.

1.3.Study 3

By using the methodology from our previous studies, the aim of the third study was to investigate basic flow patterns in VC prototypes. As previously, the general procedure for the development of a CFD model called for transforming the physical dimensions of the system to be studied into a virtual wire-frame model which provides the coordinates for the virtual space of a CFD mesh, in this case, a VC. New designs of these, e.g. with novel hole configurations, could be then readily modelized, and the corresponding flow pattern computed in an automated way. The authors also used purposely modified VCs for benchmark experimental testing in a water vase and Indian ink injection. Three distinct types of flow pattern in prototypes models of VC were obtained by varying specific parameters of the catheter design, like the number of holes in the drainage segments and the distance between them. The patterns disclosed were ascending, homogenous, and descending. We disclosed how to equalize and reverse the flow pattern through the different VC drainage segments by choosing appropriate parameters.

The authors concluded that the flow pattern in prototype catheters is determined by the number of holes, the hole diameter, the ratio hole/segment and the distance between hole segments. Hence, the application of basic design principles may help to develop new ventricular catheters with better flow circulation, thus reducing the possibility of becoming occluded.

1.4.Study 4

In this study we focused on analyzing the effects that tilt holes as well as conical holes have on the flow distribution and shear stress. We have carried out 3D computational simulations to study the effect of the hole geometry on the cerebrospinal fluid flow through the VC. Once again, all the simulations were done using the OpenFoam^{tm} toolbox. In particular, three different groups of models were investigated by varying tilt angles of holes, inner and outer diameters of the holes and inter-segment distances. Conical holes instead of cylindrical holes were found to have a strong influence on the flow distribution and to lower slightly the shear stress. Tilt holes did not involve flow distribution changes when segments are sufficiently separated, but the mean shear stress was certainly reduced. The authors present new results about the behavior of the fluid flow through VC depending on the hole geometry that complete the earlier work on this topic.

1.5. Study 5

After having found three distinctive types of flow pattern in several prototypes models of VC, to better understand the flow pattern, we have carried out a parametric study via numerical models of ventricular catheters. The parameters chosen were the number of

drainage segments, the distances between them, the number and diameter of the holes on each segment, as well as their relative angular position. As a result, the authors formulated a series of general principles for ventricular catheter design.

Principle 1. The flow rate pattern depends on the inter-segment distances of the perforated section of the VC in a sensitive way. In fact, one can reverse the pattern just by scaling down or up the inter-segment distances.

Principle 2. A decreasing distribution of hole diameters levels off the increasing flow rate pattern produced by evenly spaced segments with holes of the same size.

Principle 3. The number of holes at the proximal segment has no significant influence on the flow rate pattern.

Principle 4. A small number of segments over a given perforated area supports a uniform flow rate pattern, considering that the drainage areas of the segments follow *Equation 1*.

$$A_i = A_1 exp(\lambda(d_i - d_1)), \qquad \text{(Eq. 1)}$$

Principle 5. Relative rotations of the drainage segments around the axis of the catheter do not modify the flow rate pattern.

The authors provided a quantitative formula for a distribution of the drainage area per segment guaranteeing a relatively homogeneous flow rate pattern *(Eq. 1).*

UNIVERSITAS
Miguel
Hernández

Precautionary Conclusions

Many cold facts, lead us to assert that the findings included in this dissertation have to be treated with caution. Although the neurological line of investigation by Salomon Hakim and Raymond Adams (1965) defined the foremost characteristics of iNPH, it also uncovered a number of unclear areas about the pathogenesis that are yet to be elucidated. Dementia complex hydrocephalus, hydrocephalus itself, is still an unclear entity.

Several caveats should be emphasized. While our studies described basic design principles which may help to develop new catheters with better flow circulation, the whole aim is reducing the possibility of catheter occlusion. Still, this hypothesis requires experimental testing with definite fabricated VC prototypes, and not purposefully modified VCs such as the ones used in our third study. On the other hand, unquestionably, the hypothesis needs clinical validation studies.

On the other hand, the methodology used in all our studies was a powerful mathematical simulation system. Hence, the possibility to have introduced some bias in the samples is reduced to near zero. Therefore, we can generalize the results of this dissertation to all ventricular catheter models used for the treatment of hydrocephalus.

This dissertation is almost completely theoretical. This is the first step in an upcoming pathway. We need to develop and test the new VC prototypes. Eventually, these new catheters will get obstructed over time. However, we do know nowadays, that currently in use ventricular catheters will get obstructed in the future. This happens in approximately 50% of newly inserted VC within the first two years. It is imperative to study how to design and to develop new ventricular catheters with improved characteristics.

Future perspectives

The thorough triad of symptoms in idiopathic adult hydrocephalus was described by French neurologists in 1950; yet, at the same time, there were reports from some American physicians. They summarized the clinical picture characterized by progressive walking, cognitive, and urinary impairment, which for the first time were confirmed with the radiological picture of enlarged ventricles. When Salomon Hakim and Raymond Adams in 1965 described six adult patients with hydrocephalus, no more than three were primary hydrocephalus patients. These authors described the triad of gait, urinary and cognitive impairment as a clinical norm of patients affected by iNPH. Thus far, the relevant result was the responsiveness of these patients to lumbar tap test and shunt surgery. In conclusion, the breakthrough discovery of idiopathic adult hydrocephalus followed a medley methodology in which many distinguished worldwide physicians contributed to putting the pieces in place. Bearing in mind this situation, the finding of a definitive treatment for this entity may also lay in interdisciplinary collaboration.

Interdisciplinarity involves the combining of two or more academic disciplines into one common research project. The term interdisciplinary is applied to describe studies that use methods and insights of several established scientific or traditional fields of study. Interdisciplinarity engages several people with the objective of connecting and integrating diverse academic fields, professions, or technologies, by keeping their specific perspectives, in the pursuit of a common assignment. It is about creating something new by crossing boundaries, and thinking across them. Interdisciplinary

programs usually arise from new research developments, such as nanotechnology, which cannot be addressed without combining the approaches of two or more disciplines. Examples include quantum information processing, an amalgamation of quantum physics and computer science; bioinformatics, combining molecular biology with computer science; and our methodology: applied medical CFD, a combination of hydrodynamics, computer engineering and medical science. Noteworthy, that in our team all participants in this interdisciplinary venture were trained in traditional disciplines, so we have learned to appreciate differing of perspectives and methods. Archetypically, some ventures may also take place from a shared conviction that a single traditional discipline is unable or unwilling to deal with an important problem. In this particular case, the frequency of ventricular catheter obstructions in shunted hydrocephalus.

There are two key factors concerning VC functionality. One is flow characteristics. Many models of catheters for the treatment of hydrocephalus were designed in this interdisciplinary project. This so-called ventricular catheter is a standard-size, flexible tubing with a number of holes placed symmetrically around several transversal sections or “drainage segments”. Although a typical shunt system is composed with three parts, and the typical shunt malfunction occurs at the VC, most studies and research projects regarding shunt systems were proposed at valve devices. Whilst clinical studies comparing different VCs are still absent at the present time. Moreover, there is no reason beyond technical simplicity, why most VC manufacturers produce only classic designs. Then again, there are myriads of patented models of VC. Some of them seems completely useless from a clinical and practical point of view. While others, most of them are useless from a hydrodynamic point of view. Three-dimensional computational

dynamics in our project shows that most of the fluid volume flows through the drainage segment closest to the valve, or anatomically speaking, to the limit between the brain and the ventricle filled with CSF. This fact raises the likelihood that those holes and then the lumen get clogged by the cells and macromolecules present in the cerebrospinal fluid, as well, the ventricle can collapse for CSF drainage and the ventricle ependyma or directly the brain can embed the catheter. Both situations can provoke malfunction of the whole system. Standard VC is made of silicone elastomer and its resistance to heat, high flexibility and biocompatibility makes it well suited for in vivo implantation use. Yet, silicone elastomer is a rubber material and this condition certainly has implication in the attraction or adhesion of the cells and forms elements to the catheter.

Adhesion factor is the other key factor to consider when dealing with VC functionality. Cells and bacteria strongly adhere to the VC directly affecting its function. Nowadays, coated or impregnated catheters with antibacterial substances are currently in use for decreasing shunt infection rates. On the other hand, anti-adherent materials or processes are used at the moment in the medical industry, for the most part in metal prosthesis for the skeleton. Noteworthy, that any anti-adherent processes is an extreme high temperature process and, possibly cannot get implemented in silicone or other rubber materials. Plasma technology, based on a simple physical principle, might be an option. Physical matter changes its state when energy is supplied to it: solids become liquid, and liquids become gaseous. If even more energy is supplied to a gas, it is ionized and goes into the energy-rich plasma state, the fourth state of matter. The anti-adherent effect occurs solely due to plasma polymerization on the cast surface. Henceforth, material properties, such as silicone and other plastics, polytetrafluoroethylene (PTFE or Teflon^{tm}), or other materials with same characteristics need to be addressed. In all

these, we have to consider biocompatibility, immune response, altered physical properties and degradation process.

Once resolved the flow factors in ventricular catheters, as we assume we did in this study, we need to name the hitherto anonymous construction material with anti-adherent characteristics. But, that is another chapter yet to be written.

Murcia, Spain, 2015

REFERENCES

Adams, R.D., Fisher, C.M., Hakim, S., Ojemann, R.G. & Sweet, W.H. (1965). Symptomatic occult hydrocephalus with ‘‘normal’’ cerebrospinal-fluid pressure. A treatable syndrome. *The New England Journal of Medicine, 273*, 117–126.

Albright, A.L., Haines, S.J. & Taylor, F.H. (1988). Function of parietal and frontal shunts in childhood hydrocephalus. *Journal of Neurosurgery, 69*, 883–886.

Bateman, G.A. (2000). Vascular compliance in normal pressure hydrocephalus. *American Journal of Neuroradiology, 21*, 1574–1585.

Bayston, R. & Milner, R.D.G. (1981). Antimicrobial activity of silicone rubber used in hydrocephalus shunts, after impregnation with antimicrobial substances. *Journal of Clinical Pathology, 34*, 1057-1062.

Bech-Azeddine, R., Waldemar, G., Knudsen, G.M., Hogh, P., Brahn, P., Wildschiodtz, G., Gjerris, F., Paulson, O.B. & Juhler, M. (2001). Idiopathic normal pressure hydrocephalus: Evaluation and findings in a multidisciplinary memory clinic. *European Journal of Neurology, 8*, 601–611.

Bekkelund, S., Marthinsen, T. & Harr, T. (1996). Reversible dementia in idiopathic normal pressure hydrocephalus: A case report. *Scandinavian Journal of Primary Health Care, 17*, 22–24.

Bergsneider, M., Black, P.M., Klinge, P., Marmarou, A. & Relkin, N. (2005). Surgical management of idiopathic normal-pressure hydrocephalus. *Neurosurgery, 57*, 29-39.

Bergsneider, M., Egnor, M.R., Johnston, M., Kranz, D., Madsen, J.R., McAllister, J.P., Stewart, C., Walker, M.L. & Williams, M.A. (2006). What we don’t (but should) know about hydrocephalus. *Journal of Neurosurgery, 104*, 157-159.

Bergsneider, M., Peacock, W.J., Mazziotta, J.C. & Becker, D.P. (1999). Beneficial effect of siphoning in treatment of adult hydrocephalus. *Archives of Neurology, 56*, 1224–1229.

Besson, G., Ceccaldi, M., Tramoni, E., Felician, O., Didic, M. & Barbeau, E.J. (2014). Fast, but not slow, familiarity is preserved in patients with amnestic mild cognitive impairment. *Cortex, 65*, 36-49.

Birbilis, T., Matis, G., Chrysou, O., Karakosta, E., Themelidis, D. & Panopoulou, M. (2013). Metal external ventricular drainage catheters in the treatment of persistent ventriculitis - an old story made new: technical note and preliminary results. *Turkish Neurosurgery, 23*, 420-425.

Black, P.M. (1980). Idiopathic normal-pressure hydrocephalus: Results of shunting in 62 patients. *Journal of Neurosurgery, 52*, 371–377.

Boon, A.J.W., Tans, J.T., Delwel, E.J., Egeler-Peerdeman, S.M., Hanlo, P.W., Wurzer, H.A., Avezaat, C.J., De-Jong, D.A., Gooskens, R.H. & Hermans, J. (1998). Dutch normal pressure hydrocephalus study: Randomized comparison of low- and medium-pressure shunts. *Journal of Neurosurgery, 88*, 490–495.

Boop, F.A., Medhkour, A., Honeycutt, J., James, C., Cherny, W.B. & Duntsch, C. (2007). In vitro testing of current spread during ventricular catheter coagulation using diathermy. Technical note. *Journal of Neurosurgery, 106*, 165-168.

Børgesen, S.E. (1984). Conductance to outflow of CSF in normal pressure hydrocephalus. *Acta Neurochirurgica, 71*, 1–45.

Black, P.M. (1980). Idiopathic normal pressure hydrocephalus: Results of shunting in 62 patients. *Journal of Neurosurgery, 52*, 371–377.

Bradley, W.G. (2000). Normal pressure hydrocephalus: New concepts on etiology and diagnosis. *American Journal of Neuroradiology, 21*, 1586–1590.

Brean, A. & Eide, P.K. (2008). Prevalence of probable idiopathic normal pressure hydrocephalus in a Norwegian population. *Acta Neurologica Scandinavica, 118*, 48-53.

Bret, P., Guyotat, J. & Chazal, J. (2002). Is Normal pressure hydrocephalus a valid concept in 2002? A reappraisal in five questions and proposal for a new designation of the syndrome as "chronic hydrocephalus." *Journal of Neurology, Neurosurgery and Psychiatry, 73*, 9–12.

Brownlee, R.D., Dold, O.N. & Myles, S.T. (1995). Intraventricular hemorrhage complicating ventricular catheter revision: incidence and effect on shunt survival. *Pediatric Neurosurgery, 22*, 315-320.

Chapman, P.H., Cosman, E.R. & Arnold, M.A. (1990). The relationship between ventricular fluid pressure and body position in normal subjects and subjects with shunts: A telemetric study. *Neurosurgery, 26*, 181–189.

Cheatle, J.T., Bowder, A.N., Agrawal, S.K., Sather, M.D. & Hellbusch, L.C. (2012). Flow characteristics of cerebrospinal fluid shunt tubing. *Journal of Neurosurgery: Pediatrics, 9*, 191-197.

Clark, T.W., Van-Canneyt, K., Verdonck, P. (2012). Computational flow dynamics and preclinical assessment of a novel hemodialysis catheter. *Seminars in Dialysis, 25*, 574-581.

Clarke, M.J. & Meyer, F.B. (2007). The history of mathematical modeling in hydrocephalus. *Neurosurgical Focus, 22*, 1-5.

Cochrane, D.D. & Kestle, J. (2002). Ventricular shunting for hydrocephalus in children: patients, procedures, surgeons and institutions in English Canada, 1989–2001. *European Journal of Pediatric Surgery, 12*, 6–11.

Couldwell, W.T., LeMay, D.R. & McComb, J.G. (1996). Experience with use of extended length peritoneal shunt catheters. *Journal of Neurosurgery, 85*, 425-427.

Cozzens, J.W. & Chandler, J.P. (1997). Increased risk of distal ventriculoperitoneal shunt obstruction associated with slit valves or distal slits in the peritoneal catheter. *Journal of Neurosurgery, 87*, 682-686.

Crowley, R.W., Dumont, A.S., Asthagiri, A.R., Torner, J.C., Medel, R., Jane, J.A., Jane, J.A. & Kassell, N.F. (2014). Intraoperative ultrasound guidance for the placement of permanent ventricular cerebrospinal fluid shunt catheters: a single-center historical cohort study. *World Neurosurgery, 81*, 397-403.

Czosnyka, M., Czosnyka, Z., Keong, N., Lavinio, A., Smielewski, P., Momjian, S., Schmidt, E.A., Petrella, G., Owler, B., Pickard, J.D. (2007). Pulse pressure waveform in hydrocephalus: what it is and what it isn't. *Neurosurgical Focus*, 22:E2.

Del-Bigio, M.R. (1998). Biological reactions to cerebrospinal fluid shunt devices: a review of the cellular pathology. *Neurosurgery, 42*, 319–326.

Delwel, E.J., de Jong, D.A., Dammers, R., Kurt, E., van den Brink, W., Dirven, C.M. (2013). A randomised trial of high and low pressure level settings on an adjustable ventriculoperitoneal shunt valve for idiopathic normal pressure hydrocephalus: results of the Dutch evaluation programme Strata shunt (DEPSS) trial. *Journal of Neurology Neurosurgery and Psychiatry, 84,* 813-817.

Di-Rocco, C., Marchese, E. & Velardi, F. (1994). A survey of the first complication of newly implanted CSF shunt devices for the treatment of nontumoral hydrocephalus. Cooperative survey of the 1991– 1992 Education Committee of the ISPN. *Child's Nervous System, 10,* 321–327.

Dippel, D.W. & Habbema, J.D. (1993). Probabilistic diagnosis of normal pressure hydrocephalus and other treatable cerebral lesions in dementia. *Journal of the Neurological Sciences, 119,* 123–133.

Drake, J.M., Kestle, J.R., Milner, R., Cinalli, G., Boop, F., Piatt, J., Haines, S., Schiff, S.J., Cochrane, D.D., Steinbok, P. & MacNeil, N. (1998). Randomized trial of cerebrospinal fluid shunt valve design in pediatric hydrocephalus. *Neurosurgery, 43,* 294–305.

Drake, J.M., Kestle, J.R. & Tuli, S. (2000a). Cerebrospinal fluid shunt technology. *Clinical Neurosurgery, 47,* 336–345.

Drake, J.M., Kestle, J.R. & Tuli, S. (2000b). CSF shunts 50 years on—past, present and future. *Child's Nervous System, 16,* 800–804.

Drake, J.M. & Sainte-Rose, C. (1995). *The shunt book*. Cambridge: Blackwell Science.

Eide, P.K. (2006). Intracranial pressure parameters in idiopathic normal pressure hydrocephalus patients treated with ventriculo-peritoneal shunts. *Acta Neurochirurgica, 148,* 21-29.

Enger, P.O., Svendsen, F. & Wester, K. (2003) CSF shunt infections in children: experiences from a population-based study. *Acta Neurochirurgica, 145,* 243–248.

Etus, V. & Ceylan, S. (2005). The role of endoscopic third ventriculostomy in the treatment of triventricular hydrocephalus seen in children with achondroplasia. *Journal of Neurosurgery,103,* 260-265.

Etus, V. & Ceylan, S. (2005). Success of endoscopic third ventriculostomy in children less than 2 years of age. *Neurosurgical Review, 284,* 284-288.

Fachinotti, V.D., Toro, S., Sánchez, P.J., Huespe, A.E. (2015). Sensitivity of the thermomechanical response of elastic structures to microstructural changes. *International Journal of Solids and Structures, 69–70,* 45–59

Faillace, W.J. (1995). A no-touch technique protocol to diminish cerebrospinal fluid shunt infection. *Surgical Neurology, 43,* 344–350.

Ferziger, J.H., Peric, M. (2001). *Computational Methods for Fluid Dynamics.* Revised Edition. Springer, Berlin; New York.

Fox, R. & Norton, J. (2014). A novel device for the clearance and prevention of blockages within biomedical catheters. *Medical Engineering and Physics, 36,* 1526-1529.

Frawley, P. & Geron, M. (2009). Combination of CFD and DOE to analyze and improve the mass flow rate in urinary catheters. *Journal of Biomechanical Engineering, 131,* 411-426.

Galarza, M., Giménez, A., Valero, J., Pellicer, O. & Amigó, J.M. (2014). Computational fluid dynamics of ventricular catheters used for the treatment of hydrocephalus: a 3D analysis. *Child's Nervous System, 30,* 105-116.

Galarza, M., Giménez, A., Pellicer, O., Valero, J. & Amigó, J.M. (2015a). New designs of ventricular catheters for hydrocephalus by 3-D computational fluid dynamics. *Child's Nervous System, 31,* 37-48.

Galarza, M., Giménez, A., Pellicer, O., Valero, J. Martínez-Lage J.F. & Amigó, J.M. (2015). Basic cerebrospinal fluid flow patterns in ventricular catheters prototypes. *Child's Nervous System, Childs Nerv Syst. 31, 873-884*.

Galarza, M., Giménez, A., Pellicer, O., Valero, J. & Amigó, J.M. (2015b). Parametric study of ventricular catheters for hydrocephalus. *Acta Neurochirurgica (in publication).*

Galbarriatu, L., Rivero-Garvía, M., Olivares, M., Miranda, D., Pomposo, I. & Márquez-Rivas, J. (2013). Low-pressure hydrocephalus: indication for custom-made catheters? Technical report. *Acta Neurochir (Wien), 155,* 1981-1985.

Gangemi, M., Maiuri, F., Buonamassa, S., Colella, G. & De-Divitiis, E. (2004). Endoscopic third ventriculostomy in idiopathic normal pressure hydrocephalus. *Neurosurgery, 55,*129–134.

Ghajar, J.B. (1985). A guide for ventricular catheter placement. Technical note. *Journal of Neurosurgery, 63,* 985-986.

Giménez, A., Galarza, M., Pellicer, O., Valero, J. & Amigó, J.M. (2015). Influence of hole geometry on the flow distribution in ventricular catheters. *Biomedical Engineering (in publication).*

Ginsberg, H.J., Drake, J.M., Peterson, T.M. & Cobbold, R.S. (2006). Recanalization of obstructed cerebrospinal fluid ventricular catheters using ultrasonic cavitation. *Neurosurgery, 59,* 403-412.

Ginsberg, H.J., Sum, A. & Drake, J.M. (2000). Ventriculoperitoneal shunt flow dependency on the number of patent holes in a ventricular catheter. *Pediatric Neurosurgery, 33,* 7–11.

Gnanalingham, K.K., Lafuente, J., Brew, S., Thompson, D., Harkness, W. & Hayward, R. (2005). Percutaneous coagulation of choroid plexus to unblock the ventricular catheter using the Seldinger technique: preliminary report. *Surgical Neurology, 64,* 440-443.

Haase, J. & Weeth, R. (1976). Multiflanged ventricular Portnoy catheter for hydrocephalus shunts. *Acta Neurochirurgica, 33,* 213-218.

Hakim, S. (1964). *Some observations on CSF pressure: Hydrocephalic syndrome in adults with ''normal'' CSF pressure.* Doctoral dissertation, Javeriana University School of Medicine, Bogota, Colombia.

Hakim, S. (1969). Observations on the physiopathology of the CSF pulse and prevention of ventricular catheter obstruction in valve shunts. *Developmental Medicine and Child Neurology, 20,* 42-48.

Hakim, S. & Adams, R.D. (1965). The special clinical problem of symptomatic hydrocephalus with normal cerebrospinal fluid pressure. Observations on cerebrospinal fluid hydrodynamics. *Journal of the Neurological Sciences, 2,* 307-327.

Harris, C.A. & McAllister, J.P. (2011). Does drainage hole size influence adhesion on ventricular catheters? *Child's Nervous System, 27,* 1221-1232.

Harris, C.A. & McAllister, J.P. (2012). What we should know about the cellular and tissue response causing catheter obstruction in the treatment of hydrocephalus. *Neurosurgery, 70,* 1589-1601.

Harris, C.A., Resau, J.H., Hudson, E.A., West, R.A., Moon, C. & McAllister, J.P. (2010). Mechanical contributions to astrocyte adhesion using a novel in vitro model of catheter obstruction. *Experimental Neurology, 222,* 204-210.

Harris, C.A., Resau, J.H., Hudson, E.A., West, R.A., Moon, C., Black, A.D., McAllister, J.P. (2011). Reduction of protein adsorption and macrophage and astrocyte adhesion on ventricular catheters by polyethylene glycol and N-acetyl-L-cysteine. *Journal of Biomedical Materials Research, 98,* 425-433.

Hellström, P., Klinge, P., Tans, J. & Wikkelso, C. (2012). The neuropsychology of iNPH: findings and evaluation of tests in the European multicentre study. *Clinical Neurology and Neurosurgery, 114,*130-134.

Hermann, E.J., Capelle, H.H., Tschan, C.A. & Krauss, J.K. (2012). Electromagnetic-guided neuronavigation for safe placement of intraventricular catheters in pediatric neurosurgery. *Journal of Neurosurgery: Pediatrics, 10,* 327-333.

Hirsch, J.F. (1992). Surgery of hydrocephalus: past, present and future. *Acta Neurochirurgica, 116,* 155–160.

Hong, Y.J., Yoon, B., Shim, Y.S., Cho, A.H., Lim, S.C., Ahn, K.J. & Yang, D.W. (2010). Differences in microstructural alterations of the hippocampus in Alzheimer disease and idiopathic normal pressure hydrocephalus: a diffusion tensor imaging study. *American Journal of Neuroradiology. 31,* 1867-1872.

Hudgins, R.J. & Boydston, W.R. (1998). Shunt revision by coagulation with retention of the ventricular catheter. *Pediatric Neurosurgery, 29,* 57-59.

Hughes, C.P., Siegel, B.A., Coxe, W.S., Gado, M.H., Grubb, R.L., Coleman, R.E. & Berg, L. (1978). Adult idiopathic communicating hydrocephalus with and without shunting. *Journal of Neurology, Neurosurgery and Psychiatry, 41,* 961–971.

Iddon, J.L., Pickard, J.D., Cross, J.J., Griffiths, P.D., Czosnyka, M. & Sahakian, B.J. (1999). Specific patterns of cognitive impairment in patients with idiopathic normal pressure hydrocephalus and Alzheimer's disease: a pilot study. *Journal of Neurology, Neurosurgery and Psychiatry, 67,* 723-732.

Janson, C.G., Romanova, L.G., Rudser, K.D. & Haines, S.J. (2014). Improvement in clinical outcomes following optimal targeting of brain ventricular catheters with intraoperative imaging. *Journal of Neurosurgery, 120,* 684-696.

Kaufman, B.A. & Park, T.S. (1999). Ventricular anatomy and shunt catheters. *Pediatric Neurosurgery, 31,* 1-6.

Kehler, U., Langer, N., Gliemroth, J., Meier, U., Lemcke, J., Sprung, C., Schlosser, H.G., Kiefer, M., Eymann, R. & Heese, O. (2012). Reduction of shunt obstructions by using a peel-away sheath technique? A multicenter prospective randomized trial. *Clinical Neurology and Neurosurgery, 114,* 381-384.

Kehler, U., Klöhn, A., Heese, O. & Gliemroth, J. (2003). Hydrocephalus therapy: reduction of shunt occlusions using a peel-away sheath. *Clinical Neurology and Neurosurgery, 105*, 253-255.

Kestle, J., Milner, R. & Drake, J. (1999). The shunt design trial: variation in surgical experience did not influence shunt survival. *Pediatric Neurosurgery, 30*, 283–287.

Kiefer, M. (2012). Unterberg, A. The differential diagnosis and treatment of normal-pressure hydrocephalus. *Deutsches Ärzteblatt International, 109*, 15-25.

Klinge, P.M., Brooks, D.J. Samii, A., Weckesser, E., Van-Den-Hoff, J., Fricke, H., Brinker, T., Knapp, W.H. & Berding, G. (2008). Correlates of local cerebral blood flow (CBF) in normal pressure hydrocephalus patients before and after shunting--A retrospective analysis of [(15)O]H(2)O PET-CBF studies in 65 patients. *Clinical Neurology & Neurosurgery. 110*, 369-375.

Klinge, P., Marmarou, A., Bergsneider, M., Relkin, N. & Black, P.M. (2005). Outcome of shunting in idiopathic normal-pressure hydrocephalus and the value of outcome assessment in shunted patients. *Neurosurgery, 57*, 40-52.

Krauss, J.K., Droste, D.W., Vach, W., Regel, J.P., Orzaugh, M., Corremans, J.J. & Tielz, A. (1996). Cerebrospinal fluid shunting in idiopathic normal-pressure hydrocephalus of the elderly: Effect of periventricular and deep white matter lesions. *Neurosurgery, 39*, 292–300.

Larsson, A., Wikkelso, C., Bilting, M. & Stephensen, H. (1991). Clinical parameters in 74 consecutive patients shunt operated for normal pressure hydrocephalus. *Acta Neurologica Scandinavica, 84*, 475–482.

Lee, S.A., Lee, H., Pinney, J.R., Khialeeva, E., Bergsneider, M. & Judy, J.W. (2011). Development of Microfabricated Magnetic Actuators for Removing Cellular Occlusion. *Journal of Micromechanics and Microengineering, 21*, 1-35.

Lemcke, J., Meier, U., Müller, C., Fritsch, M.J., Kehler, U., Langer, N., Kiefer, M., Eymann, R., Schuhmann, M.U., Speil, A., Weber, F., Remenez, V., Rohde, V., Ludwig, H.C., Stengel, D. (2013). Safety and efficacy of gravitational shunt valves in patients with idiopathic normal pressure hydrocephalus: a pragmatic, randomised, open label, multicentre trial (SVASONA). *Journal of Neurology Neurosurgery and Psychiatry, 84*, 850-857.

Lin, J., Morris, M., Olivero, W., Boop, F. & Sanford, R.A. (2003). Computational and experimental study of proximal flow in ventricular catheters. Technical note. *Journal of Neurosurgery, 99*, 426-431.

Lind, C.R., Tsai, A.M., Lind, C.J. & Law, A.J. (2009). Ventricular catheter placement accuracy in non-stereotactic shunt surgery for hydrocephalus. *Journal of Clinical Neuroscience, 16*, 918-920.

Linninger, A.A., Xenos, M., Zhu, D.C., Somayaji, M.R., Kondapalli, S. & Penn, R.D. (2007). Cerebrospinal fluid flow in the normal and hydrocephalic human brain. *IEEE Transactions on Biomedical Engineering, 54*, 291-302.

Levitt, M.R., O'Neill, B.R., Ishak, G.E., Khanna, P.C., Temkin, N.R., Ellenbogen, R.G., Ojemann, J.G. & Browd, S.R. (2012). Image-guided cerebrospinal fluid shunting in children: catheter accuracy and shunt survival. *Journal of Neurosurgery: Pediatrics, 10*, 112-127.

Malm, J., Kristensen, B., Fagerlund, M., Koskinen, L.O. & Ekstedt, J. (1995). Cerebrospinalfluid shunt dynamics in patients with idiopathic adult hydrocephalus syndrome. *Journal of Neurology, Neurosurgery and Psychiatry, 58*, 715–723.

Malm, J., Kristensen, B., Karlsson, T., Fagerlund, M., Elfverson, J. & Ekstedt, J. (1995). The predictive value of cerebrospinal fluid dynamic tests in patients with the idiopathic adult hydrocephalus syndrome. *Archives of Neurology, 52*, 783–789.

Malm, J., Kristensen, B., Stegmayr, B., Fagerlund, M. & Koskinen, L.O. (2000). Three-year survival and functional outcome of patients with idiopathic adult hydrocephalus syndrome. *Neurology, 55*, 576–578.

Marmarou, A., Young, H.F. & Aygok, G.A. (2007). Estimated incidence of normal pressure hydrocephalus and shunt outcome in patients residing in assisted-living and extended-care facilities. *Neurosurgical Focus, 22*, 1-10.

Marmarou, A., Bergsneider, M., Relkin, N., Klinge, P. & Black, P.M. (2005). Development of guidelines for idiopathic normal-pressure hydrocephalus: introduction. INPH Guidelines, Part I. *Neurosurgery, 57*, 1-4.

Martínez-Lage, J.F., López, F., Poza, M. & Hernández, M. (1998). Prevention of intraventricular hemorrhage during CSF shunt revisions by means of a flexible coagulating electrode. A preliminary report. *Child's Nervous System, 14*, 203-206.

Mataró, M., Poca, M.A., Del-Mar-Matarín, M., Catalan, R., Sahuquillo, J. & Galard, R. (2003). CSF galanin and cognition after shunt surgery in normal pressure hydrocephalus. *Journal of Neurology, Neurosurgery & Psychiatry, 74*, 1272-1277.

McDowell, D., Story, T. (1998). New directions in materials design science and engineering. Report, Workshop Sponsored by the U.S. National Science Foundation, Georgia Institute of Technology and Morehouse College, Atlanta, GA, USA

Meier, U., Kiefer, M. & Sprung, C. (2004). Evaluation of the Miethke dual-switch valve in patients with normal pressure hydrocephalus. *Surgical Neurology, 61*, 119–128.

Milhorat, T.H. (1972). *Hydrocephalus and the cerebrospinal fluid*. Baltimore: Williams and Wilkins.

Missori, P., Paolini, S. & Currà, A. (2010). From congenital to idiopathic adult hydrocephalus: a historical research. *Brain, 133*, 1836-1849.

Mori, K. (2001). Management of idiopathic normal-pressure hydrocephalus: a multiinstitutional study conducted in Japan. *Journal of Neurosurgery, 95*, 970–973.

Mukerji, N., Cahill, J., Rodrigues, D., Prakash, S. & Strachan, R. (2009). Flow dynamics in lumboperitoneal shunts and their implications in vivo. *Journal of Neurosurgery, 111*, 632-637.

Nieuwenhuys, R., Voogd, J. & Van-Hujzen, C. (2007). *The Human Central Nervous System. 4th Ed*. Berlin: Springer.

Pattisapu, J.V., Trumble, E.R., Taylor, K.R., Howard, P.D. & Kovach, T.M. (1999). Percutaneous endoscopic recanalization of the catheter: a new technique of proximal shunt revision. *Neurosurgery, 45*, 1361-1366.

Patwardhan, R.V. & Nanda, A. (2005). Implanted ventricular shunts in the United States: the billion-dollar-a year cost of hydrocephalus treatment. *Neurosurgery, 56*, 139–145.

Payr, E. (1908). Drainage der Hirnventrikel Mittelst frei Transplantirter Blutgefasse; Bemerkungen ueber Hydrocephalus. *Archiv fur Klinische Chirurgie, 87*, 801–885.

Penn, R.D., Basati, S., Sweetman, B., Guo, X. & Linninger, A. (2011). Ventricle wall movements and cerebrospinal fluid flow in hydrocephalus. *Journal of Neurosurgery, 115*, 159-164.

Penn, R.D., Lee, M.C., Linninger, A.A., Miesel, K., Lu, S.N. & Stylos, L. (2005). Pressure gradients in the brain in an experimental model of hydrocephalus. *Journal of Neurosurgery, 102*, 1069-1075.

Petri, H.L. & Mishkin, M. (1994). Behaviorism, cognitivism, and the neuropsychology of memory. *American scientist, 82*, 30-37.

Portnoy, H.D. (1971). New ventricular catheter for hydrocephalic shunts. Technical note. *Journal of Neurosurgery, 34*, 702-703.

Prasad, A., Madan, V.S., Buxi, T.B., Renjen, P.N. & Vohra, R. (1991). The role of the perforated segment of the ventricular catheter in cerebrospinal fluid leakage into the brain. *British Journal of Neurosurgery, 5*, 299-302.

Raftopoulos, C., Deleval, J., Chaskis, C., Leonard, A., Cantraine, F., Desmytterye, F., Clarysel, S. & Brotchi, J. (1994). Cognitive recovery in idiopathic normal pressure hydrocephalus: A prospective study. *Neurosurgery, 35*, 397–405.

Raftopoulos, C., Massager, N., Baleriaux, D., Deleval, J., Clarysse, S. & Brotchi, J. (1996). Prospective analysis by computed tomography and long-term outcome of 23 adult patients with chronic idiopathic hydrocephalus. *Neurosurgery, 38*, 51–59.

Relkin, N., Marmarou, A., Klinge, P., Bergsneider, M. & Black, P.M. (2005). Diagnosing idiopathic normal-pressure hydrocephalus. INPH Guidelines, Part II. *Neurosurgery, 57*, 4-16.

Sagan, L.M., Kojder, I. & Madany, L. (2005). [Endoscopic revision of adherent ventricular catheter. Evaluation of the method]. *Neurologia i Neurochirurgia Polska, 39*, 294-299.

Sainte-Rose, C., Piatt, J.H., Renier, D., Pierre-Kahn, A., Hirsch, J.F., Hoffman, H.J., Humphreys, R.P. & Hendrick, E.B. (1991). Mechanical complications in shunts. *Pediatric Neurosurgery, 17*, 2–9.

Savolainen, S., Hurskainen, H., Paljarvi, L., Alafuzoff, I. & Vapalahti, M.P. (2002). Five-year outcome of normal pressure hydrocephalus with or without a shunt: Predictive value of the clinical signs, neuropsychological evaluation and infusion test. *Acta Neurochirurgica, 144*, 515–523.

Schaumann, A. & Thomale, U.W. (2013). Guided Application of Ventricular Catheters (GAVCA)--multicentre study to compare the ventricular catheter position after use of a catheter guide versus freehand application: study protocol for a randomized trail. *Trials, 14*, 428-436.

Schley, D., Billingham, J. & Marchbanks, R.J. (2004). A model of in-vivo hydrocephalus shunt dynamics for blockage and performance diagnostics. *Mathematical Medicine and Biology, 21*, 347-368.

Schuhmann, M.U., Sood, S., McAllister, J.P., Jaeger, M., Ham, S.D., Czosnyka, Z., Czosnyka, M. (2008). Value of overnight monitoring of intracranial pressure in hydrocephalic children. *Pediatric Neurosurgery, 44*, 269-79.

Schuhmann, M.U., Ostrowski, K.R., Draper, E.J., Chu, J.W., Ham, S.D., Sood, S., McAllister, J.P. (2005). The value of C-reactive protein in the management of shunt infections. *Journal of Neurosurgery, 103,* 223-30.

Shannon, C.N., Simon, T.D., Reed, G.T., Franklin, F.A., Kirby, R.S., Kilgore, M.L. & Wellons, J.C. (2011). The economic impact of ventriculoperitoneal shunt failure. *Journal of Neurosurgery: Pediatrics, 8,* 593-599.

Shprecher, D., Schwalb, J. & Kurlan, R. (2008). Normal pressure hydrocephalus: diagnosis and treatment. *Current Neurology and Neuroscience Reports, 8,* 371-376.

Simon, T.D., Riva-Cambrin, J., Srivastava, R., Bratton, S.L., Dean, J.M., Kestle, J.R. & Hydrocephalus Clinical Research Network. (2008). Hospital care for children with hydrocephalus in the United States: utilization, charges, comorbidities, and deaths. *Journal of Neurosurgery: Pediatrics, 1,* 131-137.

Sood, S., Canady, A.I. & Ham, S.D. (2000). Evaluation of shunt malfunction using shunt site reservoir. *Pediatric Neurosurgery, 32,* 180-186.

Sood, S., Kim, S., Ham, S.D., Canady, A.I. & Greninger, N. (1993). Useful components of the shunt tap test for evaluation of shunt malfunction. *Child's Nervous System, 9,* 157-161.

Sood, S., Kumar, C.R., Jamous, M., Schuhmann, M.U., Ham, S.D. & Canady, A.I. (2004). Pathophysiological changes in cerebrovascular distensibility in patients undergoing chronic shunt therapy. *Journal of Neurosurgery: Pediatrics, 100,* 447-453.

Sood, S., Lokuketagoda, J. & Ham, S.D. (2005). Periventricular rigidity in long-term shunt-treated hydrocephalus. *Journal of Neurosurgery, 102,* 146-149.

Sotelo, J., Arriada, N. & López, M.A. (2005). Ventriculoperitoneal shunt of continuous flow vs valvular shunt for treatment of hydrocephalus in adults. *Surgical Neurology, 63,* 197-203.

Sotelo, J., Izurieta, M. & Arriada, N. (2001). Treatment of hydrocephalus in adults by placement of an open ventricular shunt. *Journal of Neurosurgery, 94,* 873-879.

Stein, S.C. & Guo, W. (2008). Have we made progress in preventing shunt failure? A critical analysis. *Journal of Neurosurgery: Pediatrics, 1,* 40-47.

Stephensen, H., Andersson, N., Eklund, A., Malm, J., Tisell, M., Wikkelsö, C. (2005). Objective B wave analysis in 55 patients with non-communicating and communicating hydrocephalus. *Journal of Neurology Neurosurgery & Psychiatry,* 76, 965-70.

Suresh, S. & Black, R.A. (2015). Electrospun polyurethane as an alternative ventricular catheter and in vitro model of shunt obstruction. *Journal of Biomaterials Applications, 29,* 1028-1038.

Thomale, U.W., Hosch, H., Koch, A., Schulz, M., Stoltenburg, G., Haberl, E.J. & Sprung, C. (2010). Perforation holes in ventricular catheters--is less more? *Child's Nervous System, 26,* 781-789.

Torsnes, L., Blåfjelldal, V. & Poulsen, F.R. (2014). Treatment and clinical outcome in patients with idiopathic normal pressure hydrocephalus--a systematic review. *Danish Medical Journal, 61,* A4911.

Tuli, S., Drake, J., Lawless, J., Wigg, M., Math, M. & Lamberti-Pasculli, M. (2000). Risk factors for repeated cerebrospinal shunt failures in pediatric patients with hydrocephalus. *Journal of Neurosurgery, 92*, 31–38.

Tuli, S., O'Hayon, B., Drake, J., Clarke, M. & Kestle, J. (1999). Change in ventricular size and effect of ventricular catheter placement in pediatric patients with shunted hydrocephalus. *Neurosurgery, 45*, 1329-1333.

Ventureyra, E.C. & Higgins, M.J. (1994). A new ventricular catheter for the prevention and treatment of proximal obstruction in cerebrospinal fluid shunts. *Neurosurgery, 34*, 924-926.

Versteeg, H. & Malalasekra, W. (2007). *An Introduction to Computational Fluid Dynamics: The Finite Volume Method. Second Edition.* Harlow: Pearson Education Limited.

Vieweg, U., Kaden, B. & Van-Roost, D. (1996). A flexible metal ventricular catheter for treatment of complicated and protracted infections of the cerebrospinal fluid spaces: preliminary experiences. *Acta Neurochirurgica, 138*, 1431-1436.

Whitehead, W.E., Riva-Cambrin, J., Wellons, J.C., Kulkarni, A.V., Holubkov, R., Illner, A., Oakes, W.J., Luerssen, T.G., Walker, M.L., Drake, J.M. & Kestle, J.R. (2013). Hydrocephalus Clinical Research Network. No significant improvement in the rate of accurate ventricular catheter location using ultrasound-guided CSF shunt insertion: a prospective, controlled study by the Hydrocephalus Clinical Research Network. *Journal of Neurosurgery: Pediatrics, 12*, 565-574.

Whitfield, P.C., Guazzo, E.P. & Pickard, J.D. (1995). Safe removal of retained ventricular catheters using intraluminal choroid plexus coagulation. Technical note. *Journal of Neurosurgery, 83*, 1101-1102.

Williams, M.A., Razumovsky, A.Y. & Hanley, D.F. (1998). Evaluation of shunt function in patients who are never better, or better than worse after shunt surgery for NPH. *Acta Neurochirurgica Supplement, 71*, 368–370.

Wilson, T.J., Stetler, W.R., Al-Holou, W.N. & Sullivan, S.E. (2013). Comparison of the accuracy of ventricular catheter placement using freehand placement, ultrasonic guidance, and stereotactic neuronavigation. *Journal of Neurosurgery, 119*, 66-70.

Winkler, K.M., Woernle, C.M., Seule, M., Held, U., Bernays, R.L. & Keller, E. (2013). Antibiotic-impregnated versus silver-bearing external ventricular drainage catheters: preliminary results in a randomized controlled trial. *Neurocritical Care, 18*, 161-165.

Wu, Y., Green, N.L., Wrensch, M.R., Zhao, S. & Gupta, N. (2007). Ventriculoperitoneal shunt complications in California: 1990 to 2000. *Neurosurgery, 61*, 557-562.

Yamada, S.M., Kitagawa, R. & Teramoto, A. (2013). Relationship of the location of the ventricular catheter tip and function of the ventriculoperitoneal shunt. *Journal of Clinical Neuroscience, 20*, 99-101.

Yamada, S.M., Yamada, S., Goto, Y., Nakaguchi, H., Murakami, M., Hoya, K. & Matsuno, A. (2012). A simple and consistent technique for ventricular catheter insertion using a tripod. *Clinical Neurology and Neurosurgery, 114*, 622-626.

Yamamoto, M., Oka, K., Nagasaka, S. & Tomonaga, M. (1994). Ventriculoscope-guided ventriculoperitoneal shunt and shunt revision. Technical note. *Acta Neurochirurgica, 129,* 85-88.

Zemack, G. & Romner, B. (2002). Adjustable valves in normal-pressure hydrocephalus: A retrospective study of 218 patients. *Neurosurgery, 51,* 1392–1400.

Zhu, C., Yago, T., Lou, J., Zarnitsyna, V.I., & McEver, R.P. (2008). Mechanisms for flow-enhanced cell adhesion. *Annals of biomedical engineering, 36,* 604–621.

UNIVERSITAS
Miguel
Hernández

Spanish translation of the PhD dissertation Abstract and Conclusions

Resumen de la disertación de Tesis Doctoral

La hidrocefalia normotensiva (HPN) descrita por Hakim y Adams en 1965 (Hakim & Adams, 1965) fue el primer tipo tratable de demencia. Con los años pasó a denominarse Complejo Demencia Hidrocefalia, principalmente en aquellos pacientes donde predominaban los síntomas cognitivos. La derivación de líquido cefalorraquídeo (LCR) fue el primer tratamiento disponible en forma general para la hidrocefalia, incluida esta enfermedad. En los años siguientes, el entusiasmo, inicialmente acrítico, de la derivación de LCR fue disminuyendo poco a poco debido al escaso desarrollo de la tecnología en derivaciones, las bajas tasas de éxito clínico y las frecuentes complicaciones (Dippel & Habbema, 1993).

La más frecuente de las complicaciones es la obstrucción del catéter ventricular, que puede llegar entre un 50 a un 80% de las derivaciones recién insertadas (Bergsneider et al., 2006). Aunque muchos factores contribuyen a esta complicación (Harris & McAllister, 2012), la principal causa está relacionada con las características de flujo del LCR dentro del catéter, en el cerebro con hidrocefalia (Harris & McAllister, 2012, Lin, Morris, Olivero, Boop & Sanford, 2003). Un estudio sin precedentes realizado en 2003 abordó el problema de las características del flujo en los catéteres ventriculares Lin, Morris, Olivero, Boop & Sanford, 2003) mediante el uso de un programa de simulación 2-D de la dinámica de fluidos computacional (DFC). Este estudio reveló por primera vez, información importante relacionada con esta temida complicación, esto es, que la mayor parte del flujo en estos catéteres ocurre a través de sus agujeros proximales.

En la actualidad, según nuestro conocimiento, no existe ningún estudio que haya utilizado programa de simulación en 3-D de DFC para estudiar distintos modelos de catéteres actualmente en uso y de diseños de nuevos catéteres para el tratamiento de esta enfermedad.

Por lo que el objetivo principal de este trabajo es:

-Estudiar la dinámica de flujo en cinco modelos de catéteres ventriculares actualmente en uso.

-Crear cinco nuevos diseños de catéteres ventriculares que tengan diferentes distribuciones de los agujeros y diferente tamaño, según el modelo. Con la finalidad de que estas variaciones en las características geométricas de los catéteres modifiquen en forma significativa la distribución del caudal de masa líquida que entra en ellos, evitando o minimizando la obstrucción de los mismos.

-Estudiar los patrones de flujo que podemos encontrar en las distintas configuraciones de catéteres ventriculares, utilizando nuevos modelos o prototipos de estos.

-Establecer una serie de parámetros matemáticos universales que puedan ser utilizados para el desarrollo de nuevos diseños de catéteres ventriculares con una mejor dinámica de flujo.

Para lograr estos objetivos, los actuales y los nuevos modelos de catéteres ventriculares se estudiarán mediante el uso, nunca antes utilizados para ello, de un programa de simulación 3-D de dinámica de fluidos computacional. El procedimiento general para el desarrollo de un modelo de DFC implica la incorporación de las dimensiones físicas del sistema para ser estudiado en un modelo de alambrado virtual. La forma y características del modelo físico real se transforman en coordenadas dentro del espacio virtual de la computadora y se genera una rejilla de cálculo (malla). Las propiedades de los fluidos y el movimiento se calculan en cada uno de estos puntos de la cuadrícula. Después de la generación de la red, se aplican las condiciones de contorno de campo de flujo y se incluyen las propiedades termodinámicas y de transporte del fluido. Al final, un sistema de acoplamiento fuerte, no lineal, de ecuaciones de conservación diferenciales y parciales que rigen el movimiento del campo de flujo se resuelven numéricamente. Esta solución numérica describe el movimiento y las propiedades del fluido.

En conclusión, se pretende simular el funcionamiento del flujo del LCR en cinco catéteres ventriculares de uso actual y en 35 nuevos diseños de catéteres ventriculares, mediante un sistema nunca antes utilizado. Se establecerán los parámetros que influirán a lo largo de los catéteres ventriculares que permitirá que el fluido entre en el catéter de manera más uniforme a lo largo de su longitud perforada, reduciendo así la probabilidad de que este se ocluya. Este hallazgo contribuiría a un mejor tratamiento de la hidrocefalia y, dentro de ella, del complejo demencia hidrocefalia.

Palabras claves:

Complejo Demencia Hidrocefalia. Hidrocefalia de presión normal. Dinámica de fluidos computacional. Catéteres ventriculares. Características de flujo.

1. Resumen de los resultados principales

Los estudios presentados en los capítulos anteriores han demostrado que el flujo del LCR a través de catéteres ventriculares, ya sea de aquellos actualmente existentes o de prototipos de ellos pueden ser simulados con precisión por medio de DFC. Además, estos estudios dieron a conocer los patrones de flujo de LCR específicos que existen dentro de los catéteres ventriculares. Hemos llevado a cabo un estudio paramétrico en varios modelos de catéteres. Los parámetros fueron el número de segmentos de drenaje, las distancias entre ellos, su posición angular relativa, y el número y diámetro de los agujeros en cada segmento. En consecuencia hemos formulado principios generales para el diseño de nuevos catéteres ventriculares. Estos principios pueden ayudar a desarrollar nuevos catéteres con patrones de flujo homogéneo, por lo tanto, posiblemente se prolongue la vida útil de estos. Lo que sigue es una breve descripción, incluida sus conclusiones, de los capítulos anteriores; y una reflexión general sobre sus implicaciones.

1.2 Estudio 1

El tratamiento más común para la hidrocefalia sigue siendo la derivación ventrículo-peritoneal, cuya complicación más frecuente es la obstrucción del catéter ventricular, que puede llegar a un 50-80% de las derivaciones recién colocadas. Aunque muchos factores contribuyen a esto, el principal está relacionado con las características de flujo del catéter dentro del cerebro hidrocefálico. Un estudio inicial llevado a cabo por Lin, Morris, Olivero, Boop & Sanford, 2003 abordó el problema de las características del flujo en los catéteres ventriculares utilizando un programa de simulación bidimensional de dinámica de fluidos computacional (DFC), encontrando una distribución desigual del flujo a lo largo de un catéter ventricular, donde el LCR penetra en el catéter en sus agujeros proximales siendo los demás agujeros inutilizables.

En este primer trabajo, se han estudiado cinco diseños de catéter ventricular disponibles en el mercado actualmente, utilizando DFC en tres-dimensiones. Los modelos estudiados fueron un catéter de 12 agujeros, dos de 16, uno de 24 (Rivulet) y otro de 32 agujeros. El objetivo concreto de este primer trabajo fue investigar el patrón de flujo en estos catéteres.

Mediante el programa de simulación de DFC en tres-dimensiones, en este trabajo se ha podido observar que la mayor parte de la masa total de líquido fluye en la mayoría de los agujeros proximales de los catéteres. El 75 % del flujo desemboca en los dos agujeros más proximales de los catéteres de 12, 16 y 32 agujeros. Cierta uniformidad de flujo, con un 50% de flujo en los agujeros más proximales, se ha visto en el catéter de 24 agujeros tipo Rivulet. Según los datos observados, se concluye que la mayoría de los catéteres ventriculares disponibles comercialmente tienen un patrón de distribución anormal de flujo, esto es aumentado en su extremo proximal.

1.2. Estudio 2

Tomando como base el estudio de referencia realizado por Lin, Morris, Olivero, Boop & Sanford (2003), de flujo bidimensional en catéteres ventriculares (CV) a través de la dinámica de fluidos computacional (DFC), se estudió en un trabajo previo (Galarza M, Giménez A, Valero J, Pellicer O, Amigó JM, 2014) los patrones de flujo tridimensionales de cinco CV actualmente disponibles en el mercado, y se encontró que el drenaje del líquido cefalorraquídeo (LCR) se produce principalmente a través de la mayoría de los agujeros proximales de los catéteres. En este segundo estudio se diseñaron cinco prototipos de CV con características de flujo igualadas. Se estudiaron cinco prototipos por medio de dinámica de fluidos computacional (DFC) en modelos automatizados tridimensionales y se compararon los resultados de mecánica de fluidos con nuestro estudio anterior. El procedimiento general para el desarrollo de un modelo de DFC utiliza la transformación de las dimensiones físicas del sistema a ser estudiados en un modelo de alambrado virtual que proporciona las coordenadas para el espacio virtual de una malla de DFC. Variando el número de agujeros de drenaje y la relación agujero/segmento, se mejoran las características de flujo en cinco prototipos de CV. Los Modelos 1, 2 y 3 tienen un flujo que disminuye de distal a proximal. El Modelo 4 tiene un flujo inverso a los anteriores, es decir, un aumento de flujo de distal a proximal, mientras que el Modelo 5 tiene un flujo constante en todos los segmentos. Estos cinco nuevos diseños de catéteres con orificios de diámetro variable, número de agujeros variables, y distinta relación de orificio/segmento a lo largo del catéter permite que el fluido entre en el catéter de manera más uniforme a lo largo de este.

1.3. Estudio 3

Mediante el uso de la metodología de nuestros estudios anteriores, el objetivo del tercer estudio fue investigar los patrones de flujo básicos en seis prototipos de CV. El procedimiento general para el desarrollo de un modelo de DFC utiliza la transformación de las dimensiones físicas del sistema para ser estudiado en un modelo de mallado virtual que proporciona las coordenadas del espacio virtual de DFC, en este caso, un CV. De este modo los nuevos diseños de CV, con nuevas configuraciones de agujeros, fueron modelados y calculado el patrón de flujo correspondiente. Se utilizaron también otros seis CV modificados deliberadamente para la prueba experimental de inyección de tinta en vaso de agua o benchmarking test.

Mediante la variación de los parámetros específicos del diseño del catéter, del número de orificios en los segmentos de drenaje, y de la distancia de separación entre ellos, se obtuvieron tres tipos distintos de patrón de flujo en estos modelos prototipos de CV. En concreto, se observaron patrones de tipo ascendente, homogéneo, y descendente. Además se ha analizado cómo ecualizar y revertir el patrón de flujo a través de los diferentes segmentos de drenaje del CV seleccionando los parámetros apropiados. En base a esto, se concluye que el patrón de flujo en los prototipos de catéteres se determina por el número de agujeros, el diámetro del agujero, la relación orificio/segmento y la distancia entre los segmentos de los orificios. Por lo tanto, la aplicación de los principios básicos de estos diseños puede ayudar a desarrollar nuevos catéteres ventriculares con una mejor circulación del flujo, lo que podría reducir la posibilidad de que estos se vean ocluidos.

1.4. Estudio 4

En este estudio nos centramos en el análisis de los efectos de la inclinación que tiene en los agujeros de los CV, así como de los orificios cónicos y cilíndricos tienen sobre la distribución del flujo y la fuerza de fricción (shear stress). Hemos llevado a cabo simulaciones 3D computacionales para estudiar el efecto de la geometría de los agujeros en el flujo de líquido cefalorraquídeo a través de los CV. Una vez más, todas las simulaciones se realizaron utilizando el sistema utilitario OpenFoam®. En particular, tres grupos diferentes de modelos se investigaron mediante la variación de los ángulos

de inclinación de los agujeros, de los diámetros interior y exterior de los orificios y de las distancias entre los segmentos. Se encontró que los agujeros cónicos, en lugar de agujeros cilíndricos, tienen una fuerte influencia en la distribución del flujo y de disminuir ligeramente la fuerza de fricción. La inclinación de los agujeros no implica un cambio en la distribución del flujo, cuando los segmentos están suficientemente separados, pero la fuerza de fricción promedio sin duda disminuye. Los autores presentan nuevos resultados sobre el comportamiento del flujo de fluido a través de los CV en función de la geometría del agujero. Estos resultados completan el trabajo anterior sobre este tema.

1.5. Estudio 5

Después de haber encontrado tres tipos distintivos de patrón de flujo en seis prototipos de modelos de CV; para comprender mejor el patrón de flujo, hemos llevado a cabo un estudio paramétrico mediante doce modelos numéricos de catéteres ventriculares. Los parámetros elegidos fueron el número de segmentos de drenaje, las distancias entre ellos, el número y diámetro de los agujeros en cada segmento, así como su posición angular relativa. Como resultado, se formulan una serie de principios generales a ser utilizados para el diseño de nuevos catéteres ventriculares.

Principio 1. El patrón del caudal del flujo depende, de manera sensible, de las distancias entre segmentos de agujeros de la sección perforada del CV. De hecho, se puede invertir el patrón simplemente escalando hacia arriba o abajo las distancias entre los segmentos.

Principio 2. Una distribución decreciente de los diámetros de los agujeros disminuye el patrón de caudal aumentado producido por segmentos espaciados uniformemente, pero con agujeros del mismo tamaño.

Principio 3. El número de agujeros en el segmento proximal no tiene influencia significativa en el patrón de caudal de flujo.

Principio 4. Un pequeño número de segmentos en un área perforada dada, soporta un patrón de velocidad de flujo uniforme, teniendo en cuenta que las áreas de drenaje de los segmentos siguen la *Ecuación 1*.

$$A_i = A_1 exp(\lambda(d_i - d_1)), \qquad \text{(Eq. 1)}$$

Principio 5. Las rotaciones relativas de los segmentos de drenaje alrededor del eje del catéter no modifican el patrón de la velocidad de flujo.

Tras estos análisis, se proporciona una fórmula cuantitativa para lograr una distribución de la zona de drenaje por segmento garantizando un patrón de caudal de flujo relativamente homogéneo *(Eq. 1)*.

Conclusiones cautelares

Experiencias previas nos llevan a afirmar que los resultados incluidos en esta tesis tienen que ser tratados con precaución. Aunque la línea de investigación iniciada por Salomon Hakim y Raymond Adams en 1965 en el área neurológica definió las características más destacadas de HPN, esta línea abrió a su vez, una serie de áreas escondidas sobre la patogénesis, que aún no ha sido dilucidada. El Complejo Demencia Hidrocefalia es todavía una entidad poco clara.

Nuestros estudios describen principios básicos de diseño de CV que pueden ayudar a desarrollar nuevos catéteres con una mejor circulación del flujo. Sin embargo, estos modelos requieren una prueba experimental con prototipos fabricados en forma específica, y no con CV de uso actual, modificados a propósito, como los que hemos utilizado en nuestro tercer estudio. Sin duda, son necesarios además los estudios debidos de validación clínica.

Sin embargo, la metodología utilizada en todos nuestros estudios fue a través de un poderoso y eficaz sistema de simulación matemática, lo cual minimiza la posibilidad de introducir un sesgo en las muestras. Por lo que, y por otro lado, las conclusiones de este

trabajo se podrían aplicar a todos los modelos de catéteres ventriculares utilizados actualmente en el tratamiento de la hidrocefalia, y en los nuevos modelos a desarrollar.

Este trabajo, constituye el primer paso en un camino más largo, en el que queda por desarrollar y probar los nuevos prototipos de CV. Eventualmente, con el tiempo, estos nuevos catéteres también se obstruirán. Pero esto, hoy en día, no lo sabemos. Lo que sí es conocido a día de hoy es que los CV disponibles actualmente se obstruyen en aproximadamente un 50% en un plazo de dos años. Lo que hace imperativo que se tomen las medidas necesarias para mejorar su diseño y desarrollo.

UNIVERSITAS
Miguel
Hernández

Neurosurg Rev (2002) 25:205–215
DOI 10.1007/s10143-002-0208-y

REVIEW

Marcelo Galarza

Evidence of the subcommissural organ in humans and its association with hydrocephalus

Received: 17 August 2001 / Accepted: 16 January 2002 / Published online: 6 April 2002

Abstract A group of structures in the human central nervous system (CNS) represents a noteworthy dilemma for the neuroscientist, particularly to the neuroanatomist. In this paper an attempt is made by extensive review of the literature to give an account of the significance of the subcommissural organ (SCO) in humans and its possible relationship with cerebrospinal fluid (CSF) disorders. The subcommissural organ is a gland located in the diencephalic plate caudal to the pineal organ that covers the anterior part of the posterior commissure. Histologically, it is a highly differentiated ependyma. After birth, the SCO undergoes regressive changes, and in the adult human only remnants of the specialized SCO cells can be found. The Reissner's fiber (RF) may be regarded as a pure secretory product of the SCO. Only a few vertebrate species have been reported to lack an RF, namely the bat, camel, chimpanzee, and man. Nonetheless, a successful immunoreaction against a proteinaceous compound of the fetal human SCO has been performed. Recently, new interest was elicited regarding SCO and its possible implication in the pathogenesis of hydrocephalus. The objective of this review is to bring into consideration the relevance of the SCO to the neurosurgical scenario.

Keywords Subcommissural organ · Reissner's fiber · Hydrocephalus · Human

Commentaries on this paper are available at http://dx.doi.org/10.1007/s10143-002-0209-x and http://dx.doi.org/10.1007/s10143-002-0210-4

M. Galarza (✉)
Department of Anatomy and Neuroanatomy,
University of Salvador, School of Medicine,
Buenos Aires, Argentina
e-mail: Marcelo.Galarza@med.va.gov
Tel.: +1-513-5585387, Fax: +1-513-5587702

M. Galarza
Department of Neurosurgery,
University of Cincinnati Medical Center,
P.O. Box 670515, Cincinnati, OH 45267–0515, USA

Introduction

The subcommissural organ (SCO) is a small gland located in the diencephalic plate caudal to the pineal organ that covers the ventral aspect of the posterior commissure and points the opening into the cerebral (Sylvian) aqueduct. A borderline between the diencephalon (epithalamus) and the mesencephalon (pretectal area) cannot be represented with confidence in this area of the central nervous system (CNS). The SCO meets the criteria as a member of the group of circumventricular organs (CVO) [1, 2] due to its topographical location between the ventricular cerebrospinal fluid (CSF) and a special circumscribed vascular plexus (Fig. 1).

Histologically, it is a highly differentiated ependyma. The SCO cells are arranged into two layers, the ependyma and hypendyma. The ependymal cells release their secretion into the ventricular CSF; the hypendymal cells project processes to the local blood vessels and the subarachnoidal space [2]. The SCO secretes glycoproteins of high molecular mass [3]; the majority of these glycoproteins are released into the ventricular cavity, where they compact to form a threadlike configuration, the Reissner's fiber (RF) [4] (Fig. 2).

In lower vertebrates, the central canal becomes dilated at its caudal end, forming a terminal ventricle also known as the ampulla caudalis [4]. When reaching the terminal ventricle, RF glycoproteins go through some chemical modifications and form a gel and a thick mass known as the massa caudalis [5]. The glycoproteins undergo the dorsal wall of the terminal ventricle to reach spinal local blood vessels.

An anatomist at the University of Dorpat, Reissner [6], published in 1860 a monograph on the microscopic structure of the spinal cord of *Petromyzon fluviatilis*. However, it was Edinger [7] who gave the first description of the organ structure in 1892, and in 1900 Studnicka (cited in [4]), called attention to the tall ependymal cells covering the posterior commissure of *Petromyzon fluviatilis* and provided the first illustration of this structure. Sargent [8], in 1900, was the first to associate

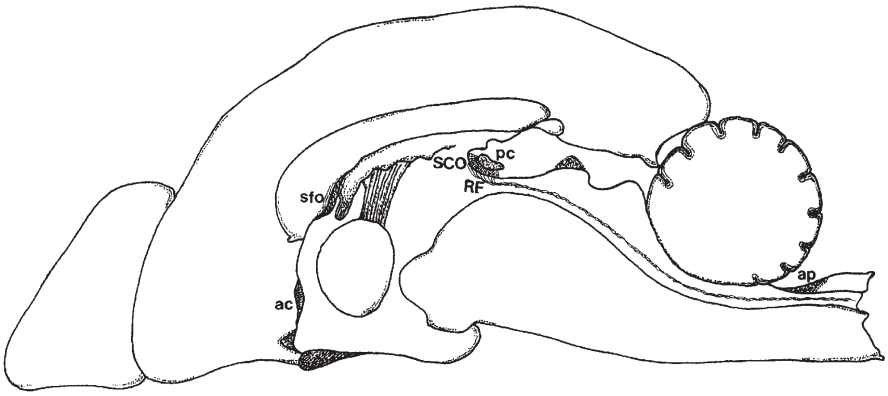

Fig. 1 Artist's illustration of a sagittal section of a mammalian brain with the circumventricular organs represented. *SCO* subcommissural organ, *RF* Reissner's fiber, *pc* posterior commissure, *ac* anterior commissure, *sfo* subfornical organ, *ap* area postrema. Based on Woollam [49]

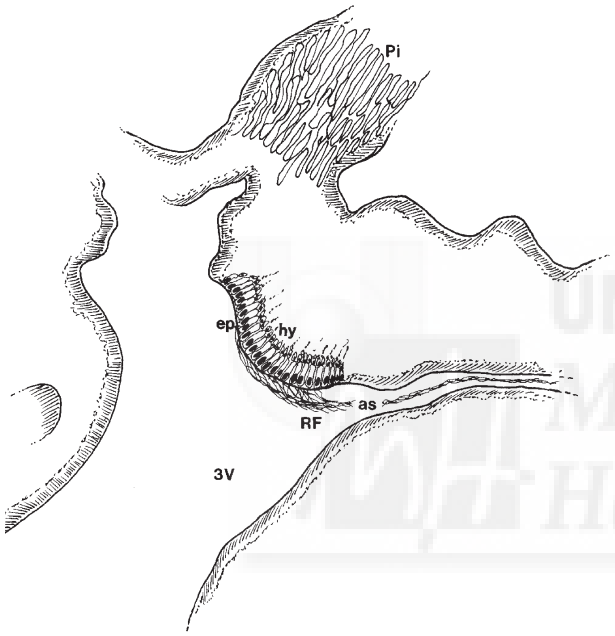

Fig. 2 Illustration showing a sagittal section of a mammalian epithalamic area. *3 V* third ventricle, *RF* Reissner's fiber, *ep* ependyma, *hy* hypendyma, *as* sylvian aqueduct, *Pi* pineal gland

RF with the area of the SCO. His publication includes an accurate schematic representation of the SCO-RF complex and represents the first jump in the knowledge of the SCO and RF. In 1910, Dendy and Nicholls [9] introduced the term subcommissural organ.

Phylogenetically, the SCO is an ancient and conserved structure. It is one of the first brain structures to differentiate during ontogeny, and in many species, including the human, it reaches its full development during embryonic life. It is sequestered within a double-barrier system, a blood-brain barrier and a CSF-SCO barrier. Some evidence suggests that the SCO may participate in different processes such as the clearance of certain elements from the CSF, the circulation of CSF, and morphogenetic mechanisms [4]. Nonetheless, the precise function of the SCO is still unknown. We will discuss the possible implications of the SCO with human hydrocephalus.

Anatomy

General and microscopic structure

Histological studies about the SCO included studies by Gabriel [10], Hofer [11], Gilbert [12], Rakic and Sidman [13], and Leonieni [14]. Some of them involved exclusively human SCO [15, 16, 17, 18]. The human SCO reaches its maximum morphological development during the fetal life [5, 19, 20, 21, 22]. After birth, the SCO undergoes regressive changes, and in the adult human only remnants of the specialized SCO cells can be found [21]. According to Palkovits [22], the human SCO remains highly differentiated during the first postnatal year (Fig. 3).

The secretory cells of the SCO are arranged into two different layers, the ependyma and the hypendyma. The SCO of most mammalian species displays the following features: ependymal cells, hypendymal secretory cells, an occasional leptomeningeal connection provided by hypendymal cells, and numerous contacts of secretory cells with blood vessels [23, 24]. The ependymal cells lack long basal processes and the hypendymal cells occur in either a scattered arrangement or clusters. In 1933, Krabbe [25] introduced the term "hypendyma" to identify a tissue layer located under the ependyma of the SCO which is characterized by numerous blood capillaries and glial cells. The degree of development of the hypendyma may vary from a few cells lying under the ependyma in lower vertebrates to a distinct subependymal layer in some mammals. In many species, hypendymal cells are also located within the posterior commissure and in the vicinity of the subarachnoidal space [4]. The hypendymal cells, like the ependymal cells, are polarized elements. In several species, junctional complexes forming rosette-like structures pack the "apical pole" of these cells. The dilated rough endoplasmic reticulum (RER) is located in the surrounding area of the nucleus, and numerous secretory granules accumulate at the pole lining the rosette cavity [26]. These granules immunoreact with

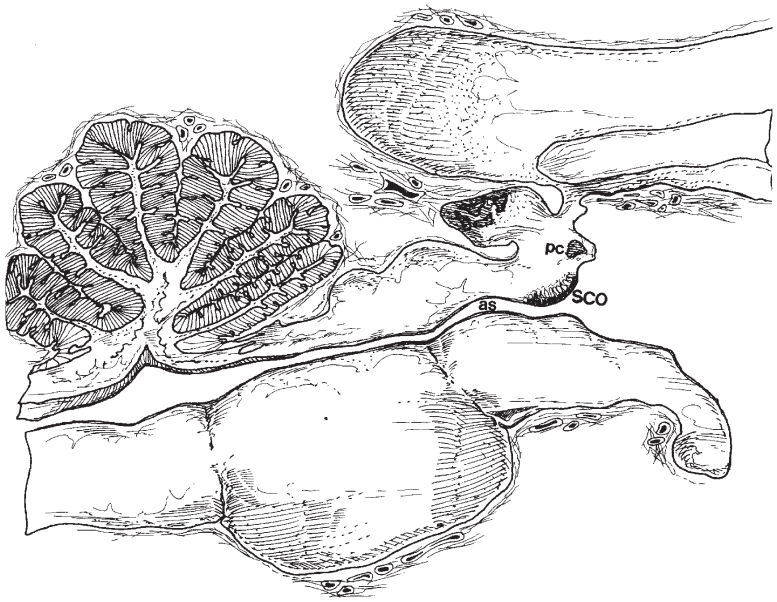

Fig. 3 Anatomic illustration based on a sagittal histological section of a human brain representing the localization of the subcommissural organ. *SCO* subcommissural organ, *as* sylvian aqueduct, *pc* posterior commissure

polyclonal and monoclonal antibodies against RF glycoproteins [4]. Nonetheless, there is no information on the destiny of the material secreted into these openings. The other cell pole of the hypendymal cells is represented by one or two processes ending on local blood vessels or on the external limiting membrane of the brain. This pole is also immunoreactive with anti-RF sera [24]. The ultrastructure of these processes and their endings is similar to that described for the processes of the ependymal cells.

High cylindrical cells form the ependymal layer of the SCO. They display an infolded nucleus with abundant euchromatin and are located in the basal cell region [4]. The cell body presents a clear zonation: perinuclear, intermediate, subapical, and apical. The distinctive zone of the SCO ependymal cells is distinguishable at the light microscopic level and has facilitated the investigation of the secretory process because different phases of this process occur in separate areas of the cell. The different processes include, namely, synthesis in the perinuclear and intermediate regions, storage of precursor forms in the RER cisternae, processing and packaging in the intermediate region, transport in the subapical region, storage of processed forms, and release in the apical region. The SCO offers a sole feature: the secretory material on release condenses first as a film on the surface of the organ and thereafter furthers packaging into RF. It is worth noting that all of these studies involved immunoreactive material that was displayed in the SCO of several species of New- and Old-World monkeys.

Irrigation and innervation

The blood capillaries supplying the SCO have characteristics that make them unique in the CNS. An attribute characterizing the capillaries of all circumventricular organs, including the SCO, is the presence of a perivascular space. Although the functional meaning of this space is not known, it has been suggested that its presence is indicative of a permeable blood-brain barrier [4]. In all circumventricular organs but the SCO, a perivascular space coexists with a fenestrated endothelium and the absence of a blood-brain barrier. The endothelium of the SCO is not fenestrated and has a tight endothelium [1, 27, 28]. Therefore, the SCO appears to have an efficient blood-brain barrier, in spite of having capillaries with a perivascular space [29]. In the SCO of mammals, the modality and degree of the structural relationships between secretory cells and blood vessels vary greatly from species to species. In the SCO of the armadillo and dog, the secretory tissue is organized as a thick, highly vascularized layer, with most of the cells oriented toward the capillaries. An opposite situation is found in the SCO of New- and Old-World monkeys, where vascular contacts are restricted to a few ependymal cells [24]. Also, the tightness of the SCO-CSF barrier to tracers administered into the ventricle varies with the species. Thus, the SCO is a unique brain structure, with its cells restricted within a double-barrier system.

Another characteristic of the SCO capillaries is the presence in the perivascular space of long spacing collagen [30]. There is no other region in the CNS endowed with long spacing collagen except for the capillaries of the human ciliary body.

Considerations on the probable mechanisms controlling the production rate and composition of the SCO secretion are based on structural findings and not on biological actions of the secretion material (RF). Only a few mechanisms appear controlling the secretory activity of the SCO. Several studies have established the existence of a dense plexus of serotonergic fibers along the basal

region of the SCO [31]. The administration of 5[3H]-HT or the specific neurotoxic destruction of the serotonergic innervation has revealed that serotonergic fibers establish well-differentiated axon-glandular synapses on the laterobasal processes of the ependymal cells [4]. Electrolytic lesions of different raphe nuclei revealed that the serotonergic innervation of the rat SCO is mainly derived from nuclei raphe centralis superior and raphe dorsalis, each nucleus contributing about one third of the input; the remainder is suggested to originate from the nucleus raphe pontis. The secretory activity of the SCO is under a strong inhibition by serotonergic fibers. The SCO of mammals during embryonic development and the SCO of adult nonmammalian species do not receive a serotonergic neural input. The role of the nonserotonergic fibers innervating the SCO is unknown [4].

Reissner's fiber composition

By isolating RF, a pure SCO secretion may be obtained. Reissner's fiber is readily obtained by perfusing the central canal of the bovine spinal cord. After the isolation of RF, the solubilization of the RF glycoproteins is obtained using various extraction procedures. Only a few vertebrate species have been reported to lack an RF, namely the bat, camel [33], chimpanzee [9], and man [2]. Sterba et al. [32] and Rodriguez et al. [24] raised polyclonal antibodies (anti-RF sera) and used them for immunocytochemical studies of the SCO-RF complex of several species. The antisera reacted specifically with the secretory material of the SCO and with RF. Ultrastructural immunocytochemistry using polyclonal and monoclonal antibodies has demonstrated strong labeling of the secretory material located in the dilated RER cisternae and the secretory granules located at the apical cell pole [33, 34]. It was also located in the vascular and leptomeningeal ependymal endings [33].

Reissner's fiber grows caudally by the addition to its cephalic end of newly released glycoproteins. It is formed by densely packed filaments 5–15 nm in diameter [4]. At its distal end, the central canal of the spinal cord becomes dilated; this dilatation is known as the terminal ventricle or ampulla caudalis. At the terminal ventricle, RF ends as an irregular mass known as massa caudalis [5]. In higher vertebrates, the microanatomy of the caudal end of the central canal shows differences with respect to that of lower vertebrates [4].

Three different spatial and temporal stages of the RF glycoproteins released into the ventricular CFS may be distinguished: pre-RF material, RF proper, and massa caudalis [26, 33]. Initially, the ependymal cells of the SCO secrete into the ventricle core-glycosylated proteins of high molecular mass. The bulk of this secretion is formed by glycoproteins that would derive from two different precursors of 540 kDa and 320 kDa and that, upon release into the ventricle aggregate, form the threadlike structure of the RF. By addition of newly released glycoproteins to its proximal end, RF grows caudally and extends along the aqueduct, fourth ventricle, and the whole length of the central canal of the spinal cord. Reissner's fiber material continuously arrives at the dilated caudal end of the central canal. When reaching the ampulla, the RF material undergoes chemical modifications, disaggregates, and then escapes through openings in the dorsal wall of the ampulla to reach local blood vessels. The SCO also appears to secrete a CSF-soluble material that is different from the RF material circulating in the ventricular and subarachnoidal CSF. Cell processes of the ependymal and hypendymal cells, containing a secretory material, terminate at the subarachnoidal space and on the very special blood capillaries supplying the SCO [4].

Other factors than the ventricular release of secretory material would be required for the formation of RF. Schoebitz et al. [35] and Oksche [21] postulated that the hydrodynamics of the aqueductal CSF plays a role in the aggregation of the secreted material in the form of a typical RF. This hypothesis is supported by the fact that hydrocephalic rats do not form distinct RF [36].

Histophysiology and functions

Attributed functions

Although the SCO-RF complex was first described a century ago, its function remains enigmatic. Several functional hypotheses have been proposed based on indirect evidence. It has been proposed that the SCO-RF complex is involved in osmoregulation [22], detoxification of the CSF, mechanoreception, and morphogenesis of the vertebral column and the spinal cord [4]. However, none of these hypotheses has been convincingly substantiated [37]. A variety of experimental designs will be discussed.

The SCO is a unique secretory structure consisting of specialized ependymal and ependyma-derived cells of neuroepithelial origin, both elements of glial lineage. In contrast to the extended apparatus of neuroendocrine, especially peptidergic neurons, the phenomenon of ependyma- or glia-related secretion appears to be restricted to a few specialized formations [4]. Because of its extensive secretory activity and the chemical properties of its secretion, this array of cells assumes, among plain ependymal and glial elements, a position similar to that of neurosecretory nerve cells among ordinary neurons. In a number of ependymal complexes, the elements possessing a secretory capacity are actually closely adjacent neurons [5]. Furthermore, granular inclusions of glial cells supposed to indicate an extended interstitial gland of the brain (as suggested by Nageotte in 1910) were recently proven to be regular cell organelles [4].

Highly vascularized CVO of the mammalian brain are the sites of increased vascular permeability for peptides and other molecules, which generally do not cross the blood-brain barrier. In the pineal, a single neurophysin (vasopressin or oxytocin) fiber has been observed occasionally. In the subfornical organ and area postrema

which do not appear to have a primary neuroendocrine function, blood-neural interactions may be important for effects of circulating peptides and other molecules on specific receptors [38]. Secretory neurons capable of elaborating neuropeptides and biogenic amines are an integral component of nervous systems. It is involved in short- and long-range communication by means of paracrine, transmitter-like, modulatory and neurohormonal types of messages. This finely adjusted activity of secretory neurons serves the control of a variety of important biological functions. Secretory pinealocytes are derivatives of pineal photoreceptors, primary sensory cells of neuronal character. In contrast to these neuron-like or paraneuronal elements, the secretory cells of the subcommissural organ are of ependymal origin [39].

The SCO has been linked to various aspects of the hydromineral metabolism, such as aldosterone secretion, volume reception, thirst, sodium excretion, and diuresis [2, 22, 40]. Corticosteroids (glucocorticoids and mineralocorticoids) have multiple actions in the CNS which are mediated via specific intracellular receptors. An important control of glucocorticoid action has been identified in peripheral tissue, that is the prereceptor metabolism by 11 beta-hydroxysteroid dehydrogenase (11beta-HSD). The functions of 11beta-HSD-1 in the CNS may relate to mood, neuronal survival, and glucocorticoid feedback. The identification of aldosterone-selective actions in the brain, i.e., on blood pressure and salt appetite predicts the presence of 11beta-HSD-2. This isozyme has very limited expression in the adult brain confined to the subregions of the brainstem and the subcommissural organ, where some aldosterone-selective actions may be mediated [41]. New evidence indicates that it may be involved in the hypertension produced by aldosterone acting on the brain [42].

The ependymal cells of the pineal recess and SCO synthesize the pineal nonapeptide hormone arginine vasotocin (AVT). It is stored in undefined cells of the pineal gland. The AVT is first released into the ventricular CSF and reaches the blood only secondarily after its absorption from CSF. It displays a diurnal rhythm in the pineal and CSF, suggesting its release into the CSF during the night in the dark. Melatonin represents its releasing hormone. The AVT is a CSF hormone whose major if not sole site of action is the brain itself [43]. The SCO has been directly implicated in the water metabolism. By using electrical stimulation of the SCO, Gilbert [44] produced increased water intake in rats.

It was hypothesized that RF glycoproteins, by binding and transporting biogenic monoamines out of the CSF, participate in the clearance of these compounds. The CSF concentration of monoamines was investigated in RF-deprived rats subjected to immunological neutralization of the SCO-RF complex. Secondly, the capacity of RF to bind monoamines in vivo was studied by injecting radiolabeled serotonin or noradrenaline into the rat CSF and by perfusing them into the CSF. After that, in vitro binding studies were performed using isolated bovine RF. The obtained findings indicate that RF binds monoamines present in the ventricular CSF and then transports them along the central canal. In the absence of RF, the CSF concentration of monoamines increases sharply [45]. All these results support the hypothesis that the SCO-RF complex participates in the clearance of monoamines from the CSF [46]. Also, the presence of sialic acid in the secretion of the SCO and RF suggested that it might participate in the detoxifying function of RF [4].

Bovine SCO-spondin was shown to be a brain-secreted glycoprotein specifically expressed in the SCO. In fact, SCO-spondin intrinsically comprises part of RF. These results indicate that SCO-spondin is an ancient ependymal secretion making part of RF that may have had an important function during the evolution of the CNS in chordates, probably involved in axonal growth and/or guidance [47].

Radiolabeled RF-glycoproteins perfused into the rat CSF were also bound to the paraventricular thalamic nucleus and the floor of the Sylvian aqueduct and of the rostral half of the fourth ventricle. Binding of the meninges of the brain and spinal cord was also noted. The labeling of the paraventricular thalamic nucleus points to a functional relationship between this nucleus and the SCO, addressing the possibility that the SCO may be a component of the circadian timing system [48].

Another theory by Woollam [49] about RF involved its possible relationship as a regulator of the choroid plexus secretion. When increased CSF production and pressure accomplish the rupture of the RF, the CSF production is out of control, thus developing human hydrocephalus. However, the human CNS lacks RF.

It seems that at the present state of knowledge, the main specific function attributed to the SCO is the hydromineral metabolism. Specific, high-affinity binding sites for atrial natriuretic factor (ANF) were identified and localized in the rat and guinea pig CNS, the cat brainstem, and the rat, guinea pig, cat, and human spinal cord using autoradiographic techniques. In guinea pig and rat, moderate concentrations were observed in the nucleus accumbens, dorsomedial and suprachiasmatic hypothalamic nuclei, paraventricular thalamic nuclei, primary olfactory cortex, and the SCO. In the brainstem of the cat and all levels of the rat, guinea pig, cat, and human spinal cord, the only site where specific binding was observed was in the pia/arachnoid. These findings suggest that ANF binding sites constitute several functional classes in the CNS as well as in a variety of other tissues, with possible implications in an integrative and/or indirect regulatory role in fluid and electrolyte balance related to the SCO in chordate [50].

Secretion of the human cerebrospinal fluid-soluble material

Bargmann [19] gave a detailed review on the early period of investigation of the SCO in a comprehensive monograph on the pineal organ. This report summarizes

certain ideas concerning the development and possible functional significance of the SCO. In the borderline area of the primordia, it is possible to delimit either of these epithalamic organs, thus providing arguments for speculations. In ontogeny, the SCO displays an early onset of its secretory activity and formation of RF [37].

Whether or not the human SCO discharges a secretory material into the CSF has been a matter of controversy. The absence of RF in the human [2, 5] has also contributed toward the ambiguity with respect to the secretory capacity of the human SCO [37]. Although the ultrastructural characteristics of the human fetal SCO points a distinct secretory activity [5], "stainable" secretory material has never been demonstrated in these SCO cells at a site other than the apical borderline. Furthermore, a representative series of antibodies which immunoreact with the SCO of virtually all vertebrate species investigated do not immunostain the SCO of man and anthropoid apes [24, 51].

Nonetheless, there is evidence that part of the SCO secretion released into the CSF remains soluble. In a lectin-histochemical study of the human fetal SCO, evidence was obtained that this organ secretes glycoproteins with a carbohydrate chain similar to that of the secretions elaborated by the SCO of other species [51]. The material released by the human SCO into the ventricle does not form a compact (pre-RF or RF) but becomes soluble in the CSF [51].

Under certain physiological conditions, such as the embryonic period (chicken, rat, and human) and under specific experimental conditions such as hydrocephalus, the SCO would secrete CSF-soluble compounds that do not form an RF, although they react with anti-RF sera [36, 37]. Furthermore, there is evidence that the SCO may secrete CSF-soluble compounds different from RF glycoproteins. Antibodies raised against "CSF-specific" glycoproteins (glycoproteins present in the CSF but missing from the plasma) obtained from the CSF of hydrocephalic children react with the human and rat SCO [37]. The detection of CSF-soluble secretory material in the CSF of the lateral ventricle and cisterna magna [37] indicates that such a material circulates in the ventricular and subarachnoidal CSF. The SCO-soluble secretion could reach any region of the CNS, because both CSF compartments are in open communication with the brain tissue.

The human fetal SCO does not immunoreact with any of the numerous polyclonal and monoclonal antibodies raised against RF-glycoproteins of animal origin. Considering the ultrastructural, lectin-histochemical, and immunocytochemical findings, the SCO of humans and the anthropoid apes secrete glycoproteins with a protein and with a carbohydrate chain similar or equal to that of RF-glycoproteins secreted by the SCO of all other species. These glycoproteins do not aggregate but become soluble in the CSF, and they still are unidentified. Evidence that these CSF-soluble proteins secreted by the human SCO corresponds to a 45-kDa compound similar or identical to transthyretin and to a protein of about 500 kDa [52].

Evidence of the subcommissural organ in humans

Phylogenetic considerations

In phylogeny, the SCO is an ancient and highly constant structure of the vertebrate brain [5, 21, 23, 24, 53]. In spite of interspecific variations in the form and fine-structural organization of its ependymal and hypendymal formations, there is a high degree of conformity concerning the location and general morphologic pattern of the SCO. It is present in the most archaic vertebrate brains. It is very prominent and active as a secretory structure already in both orders of cyclostomes, i.e., lampreys and hagfish [32, 54].

Intrinsic cavities or wide spaces containing circulating fluid (CSF or its precursors) are a fundamental prerequisite for the concentration of secretion into an RF-like structure in lower vertebrates with SCO. In this context, the rudimentary ventricular compartment (vesicle) to which the SCO of Myxine is exposed still provides the basic conditions required for the formation of a RF [54]. Concerning similar threadlike secretory structures, which occur in other sites of the central nervous system of acranian chordates (*Branchiostoma lanceolatum*) and early developmental stages of teleosts, notably, an RF-like structure has never been observed within the compact ganglia of invertebrates [37].

The presence of a pineal organ is not a necessary condition for the existence of the SCO. In the hagfish, *Myxine glutinosa*, and also in all crocodiles so far examined, in which the pineal organ is reported to be missing, the SCO is well developed and active as a secretory structure. This holds true also for mammalian species lacking a typical pineal body. Thus, in the armadillo, *Dasypus novemcinctus*, the SCO is abundant and highly active as a secretory structure [24, 55].

Only very few vertebrate species possess a poorly differentiated and barely secretory active SCO, e.g., the European hedgehog (*Erinaceus europaeus*). This is, however, not a characteristic feature of the insectivore brain; for example, the SCO of the European mole (*Talpa europaea*) is conspicuous and rich in secretory material [55]. In these cases, a particular correlation between the pineal and the SCO is not evident. The situation in primates deserves special attention. As described by Hofer et al. [11], in a representative number of species of Old- and New-World monkeys (e.g., rhesus monkey, Cebus, Ateles, Aotes) the SCO is well developed and active as a secretory structure even in mature animals [11]. Of eminent interest, however, is the situation in anthropoid apes. In very old chimpanzees, the SCO shows a reduction in height and regression of its secretory parenchyma. So far, there is no evidence of sex-dependent development [37].

Ontogenetic considerations

The SCO is a conserved brain gland present throughout the vertebrate phylum. The human SCO shows its high-

est development between the 3rd and 4th months of fetal life, followed by a gradual regression during the second half of pregnancy and a further decline after birth. Thus, in 6-year-old children, only rudiments of SCO parenchyma can be found [21]. The very early ontogenetic differentiation of the SCO secretory cells and the relatively late appearance of RF could be an indication that the immunoreactive material secreted by the early SCO cells play a role in the first developmental stages of the CNS. This possibility is supported by the appearance of RF-immunoreactive material covering the surface of the rat neuroepithelium [30] and within the floor plate cells [37] at stages prior to the differentiation of the SCO.

The SCO of human embryos offers some special characteristics. The human SCO appears in the 2nd month of intrauterine life in a 27-mm embryo, later than the posterior commissure and concurrently with the pineal gland [56]. Studies in 58 individual embryos were ranked in ascending order of the features present. The main features of stage 19 (approximately 48 days) were the cochlear nuclei, the ganglion of the nervus terminalis, and nuclei of the prosencephalic septum. Also, the appearance of the subcommissural organ, the presence of villi in the choroid plexuses of the fourth and lateral ventricles, and the stria medullaris thalami characterized this stage [57]. However, the human SCO reaches its maximum development during the embryonic period [9, 20, 21, 22]. After birth, the SCO undergoes regression, so that in the adult human only remnants of the SCO parenchyma remain [21].

During ontogeny, it is the first secretory structure of the brain to differentiate. In the human, the SCO can be morphologically distinguished in 7- to 8-week-old embryos. The SCO of 3- to 5-month-old fetuses is an active, secretory structure of the brain. However, already in 9-month-old fetuses, the regressive development of the SCO parenchyma is evident. In 1-year-old infants, the height of the secretory ependymal cells is distinctly reduced, and they are grouped in the form of islets that alternate with cuboid nonsecretory ependyma. The regression of the SCO continues during childhood, so that at the 9th year of life, the specific secretory parenchyma is confined to a few islets of secretory ependymal cells. The human fetal SCO shares the distinct ultrastructural characteristics the SCO of all other species, namely, a well-developed RER, with its cisternae dilated and filled with a filamentous material, several Golgi complexes, and secretory granules of variable size, form, and electron density [52]. The SCO of human embryos has a histochemically detectable material [5, 20, 21, 58] because the ultrastructural [5] and lectin-binding [51] properties of the SCO of human embryos evidenced that this organ secretes glycoproteins. The lack of reactivity of the human SCO to anti-RF sera should be described as having a different nature of the human SCO secretion [37]. Because the human lacks an RF, [2] it could be postulated that in this species the SCO has only kept the property to secrete a CSF-soluble material [4]. Additionally, cytokeratin-positive cell clusters were demonstrated in the infant pineal gland that may be related to ependymal cells arising from the SCO. The ependymal cells in the SCO and pineal parenchyma express the neuroectoderm-specific individual cytokeratins. Cytokeratin-positive ependymocytes additionally exhibited vimentin, as revealed by double immunofluorescence labeling. By contrast, cytokeratin positive cells were not clustered in adult pineal glands. An interesting but unexplained increase of neurofilament positive in nerve fibers was also detected [59].

Tumorally related morphology

Some recent observations suggest that chordoid glioma may represent a subtype of ependymoma whose cells resemble the highly specialized ependyma of the subcommissural organ [60]. Chordoid glioma is a rare neoplasm occurring in the human third ventricle recently described by the World Health Organization (WHO). Ultrastructurally, they showed features of ependymal differentiation for the presence of an apical pole with microvilli and a basal pole characterized, as in normal ependyma, by many hemidesmosome-like structures connecting cell membranes to the underlying basal lamina. Constant features were a submicroscopic cell body zonation (i.e., perinuclear, intermediate, subapical, and apical regions) and the presence of secretory granules [60]. These findings were similar to those described for the secretory ependymal cells of the subcommissural organ.

Association of the subcommissural organ with hydrocephalus

Alteration in cerebrospinal fluid circulation

There is evidence that the SCO-RF complex is one of the factors involved in the CSF circulation. In mammals, the predominant route of escape of CSF into blood is through the arachnoid villi. In lower vertebrates, the distal end of the central canal, known as the terminal ventricle or ampulla caudalis, represents the main site of CSF escape into blood [61]. Under normal physiological conditions, the CSF is secreted continuously, although this secretion undergoes circadian variations. Mechanisms operating at the vascular side of the choroidal cells involve sympathetic and cholinergic innervation, with the initial inhibiting and the latter stimulating CSF secretion. There are also regulatory mechanisms operating at the ventricular side of the choroidal cells, where receptors for monoamines such as dopamine, serotonin, and melatonin and for neuropeptides such as vasopressin, atrial natriuretic hormone, and angiotensin II have been identified. These compounds that are normally present in the CSF participate in the regulation of CSF secretion [46]. Although the mechanisms responsible for the CSF circulation are not fully understood, several factors are known to play a role. Both the function and the ultrastructural

arrangement of the ampulla caudalis suggest that it may be the ancestor structure of the mammalian arachnoid villi. RF-glycoproteins reaching the ampulla caudalis might play a role in the formation and maintenance of the route communicating the CSF and blood compartments. The SCO-RF complex may participate, under physiological conditions, in the circulation and reabsorption of CSF [49]. Under pathological conditions, the SCO appears to be involved in the pathogenesis of congenital hydrocephalus. Changes in the SCO have been described in all species developing congenital hydrocephalus. In these reports, the important question of whether the changes occurring in the SCO precede hydrocephalus or are a consequence of the hydrocephalic state has not been clarified. Evidence has been obtained indicating that a primary defect of the SCO-RF complex may lead to hydrocephalus. A primary and selective immunoneutralization of the SCO-RF complex during the fetal and early postnatal life leads to absence of RF, aqueductal stenosis, increased CSF concentration of monoamines, and a moderate but sustained hydrocephalus [61].

Overholser et al. [62] proposed in 1954 the hypothesis that a dysfunction of the SCO leads to aqueductal stenosis and congenital hydrocephalus. The causes of such a stenosis are not well known. The immunological blockage of the SCO-RF complex has been used to test Overholser's hypothesis. After pregnant rats had been immunized with RF glycoproteins, the mothers produced anti-RF antibodies and transferred them to the fetuses through the placenta and to the pups through the milk. The antibodies reached the brain of the fetuses and pups and blocked the SCO-RF complex. This resulted in a permanent absence of RF that was followed by stenosis of the cerebral aqueduct and then by the appearance of hydrocephalus. The chronic hydrocephalic state appeared to induce new alterations of the SCO [63].

In fact, this organ was investigated in the mutant mouse hyh developing a congenital hydrocephalus. The SCO showed signs of increased secretory activity; it released to the stenosed aqueduct a material that aggregated but it did not form an RF. A large area of the third ventricular wall differentiated into a secretory ependyma synthesizing a material similar to that secreted by the SCO [64].

Alteration in the regional tectal anatomy

Evidence suggests that certain anatomical disturbances in the regional tectal region could lead to hydrocephalus [65, 66, 67, 68]. Takeuchi et al. [65] found that the SCO and the posterior commissure were completely absent in the hydrocephalic brain of genetically modified rats. Nonetheless, the cerebral aqueduct in the hydrocephalic brain was never completely stenosed. Another study disclosed that the SCO of the congenital hydrocephalus spontaneously occurring in CWS/Idr rats was severely reduced in size and displaced at some distance from the anterior end of the cerebral aqueduct. The cerebral aqueduct was somewhat narrower at its middle region than in the normal brain [66].

It was proposed that prenatal hydrocephalus develops in the transgenic mouse as a consequence of SCO failure [66, 67]. Comparison suggests that subcommissural organ failure is the main cause of prenatal hydrocephalus observed in different strains of transgenic mice. A series of gain- or loss-of-function experiments performed in different vertebrate species have demonstrated that the engrailed genes play multiple roles during brain development. They have been implicated in the determination of the mid- and hindbrain domain, in cell proliferation and survival, in neurite formation, tissue polarization, and as an axonal pathfinder. The choroid plexus, posterior commissure, subcommissural organ, and pineal gland either fail to form or are atrophic. These defects are preceded by an increase in cell death at the dorsal midline [67].

There is only one histopathological study performed in the human SCO with hydrocephalus. Human hydrocephalic fetuses of 20 and 21 gestational weeks presented a size reduction of the subcommissural organ compared to the normal cases aged 19 and 23 gestational weeks. However, there were also alterations of the morphological components of the subcommissural organ, suggesting a direct pathogenic relationship between hydrocephalus and dysplasia of the subcommissural organ [68].

Release of CSF-soluble material from the human subcommissural organ that might have implication in hydrocephalus

In 1990, Rodriguez et al. [51] investigated the SCO of seven human fetuses 3 to 6.5 months old by means of immunocytochemistry employing three different antisera against products extracted from the bovine SCO and Reissner's fiber; the antisera were lectin binding using concanavalin A (Con A), wheat-germ agglutinin (WGA), and Limax flavus agglutinin (LFA). Sections of bovine SCO were processed simultaneously and examined for comparative purposes. The human fetal SCO displayed lectin-binding properties identical to those in the SCO of other mammals. Thus, Con A-binding sites were restricted to abundant supranuclear structures that most likely corresponded to the RER but were missing from granules located in the apical cytoplasm. The latter secretory material was strongly WGA- and LFA-positive and formed a distinct zone in the most apical portion of the ependymal cells. In contrast, this type of reactivity was missing in the adjacent cells of ependyma proper. The secretory material in the bovine SCO, especially its apical granular component, was strongly immunoreactive with the three antisera used; the human fetal SCO, however, lacked this immunoreactivity. After this study, it was postulated that the SCO of human fetuses secretes glycoproteins with a carbohydrate chain similar to and a protein backbone different from the secretions elaborated by the SCO of other vertebrate species [51].

The secretion of the SCO is primarily into the CSF [2, 5, 33]. The size of this secretion, upon release into the CSF, becomes densely packed in the form of RF. In this respect, the most convincing evidence has been gained from immunocytochemical investigations. Antibodies raised against RF extracts react specifically with RF and the secretory material stored in the SCO proper [23, 24, 32]. On the other hand, antibodies against secretory products extracted [34, 69, 70] or purified [3] from the SCO immunoreacted with RF.

The demonstration of a component of SCO secretion soluble in CSF provided the research of this brain gland with a unique and thought-provoking perspective [37]. The attractive possibility that in the human, especially in fetuses and newborn infants, the bulk of secretory material released by the SCO becomes soluble in the CSF led to the following investigation. Cerebrospinal fluid was collected weekly from ten children suffering from congenital hydrocephalus. All these CSF samples and serum samples were transferred to nitrocellulose sheets. The blots were processed for Con A and WGA binding using the lectin-antilectin method [3]. The aim of this experiment was to identify glycoproteins which might be present in the CSF and missing (or not detectable) in the serum. Four WGA-positive bands present in the CSF and missing in the serum were certainly identified; their apparent molecular weights were 235 kDa, 150 kDa, 73 kDa, and 45 kDa. They were regarded as "CSF-specific glycoproteins." The 235-, 150-, and 45-kDa bands were missing from a pool of CSF samples of adult humans. Material from each of these four bands was utilized to immunize rats, and subsequently the antisera were used for immunostaining of serial sagittal sections through the brain of human fetuses and of adult rats. The antisera against the 235- and 73-kDa bands did not immunostain any structure in either the human or rat brain. The antiserum against the 45-kDa band immunoreacted with certain structures of the fetal human brain but did not react with the rat CNS. In the fetal human brain, the anti-45-kDa serum stained the following structures: the SCO, the pineal organ, and the choroid epithelium. In the SCO, about half of the population of the ependymal cells of the SCO displayed a very distinct immunoreaction. The immunoreactive material appeared in the form of granules in the cytoplasm and filling the main portion of the cell body from the nucleus to the apical pole that generally protruded into the ventricle. Furthermore, this granular material also marked the slender basal processes projecting to and penetrating the posterior commissure [37]. In the fetal human brain, the antiserum against the 150-kDa band immunostained the same structures as the antiserum against the 45-kDa compound. In the rat, however, the antiserum against the 150-kDa band stained two structures, the glycocalyx of the choroid epithelium of all choroid plexuses and the SCO.

Cerebrospinal fluid blots from hydrocephalic children treated with the antiserum against the 45-kDa compound showed a positive immunoreaction of the 45-kDa band. As well, the fraction of IgG with an electrophoretic mobility somewhat faster than the 45-kDa compound also immunoreacted with the anti-45-kDa serum. This indicates that the latter antiserum contained antibodies against a component of the IgG molecule. However, an antihuman IgG serum did not stain any structure of the fetal brain. Thus, it seems highly probable that the immunostaining of certain structures of the human fetal brain with the antiserum against the 45-kDa band was a reaction produced by antibodies directed against a 45-kDa polypeptide present in the CSF and probably secreted by the SCO. For the first time, a successful immunoreaction against a proteinaceous compound of the fetal human SCO was performed. The fact that the antibodies exhibiting this reaction were raised against CSF-soluble glycoproteins may be taken as compelling evidence that the human SCO does include a secretory activity, resulting in a discharge of a CSF-soluble material [37].

Future perspectives

It is important to recognize that there is a supported evidence of the association of the SCO with hydrocephalus. The anatomical location of the organ leads to primary hypothesis regarding its logical association with the development of CSF disorders. Nonetheless, there is much to be further investigated at the present time.

Cerebrospinal fluid-soluble secretory material appears to circulate in the ventricular and subarachnoidal CSF, since it could be detected in the CSF from the lateral ventricles and cisterna magna. However, this was demonstrated only in lower vertebrates and not in humans. The question concerning the target site(s) for the secretory products of the SCO circulating in the CSF is open to discussion.

The availability of antisera reactive with the human SCO opens new avenues in the investigation of the SCO and CSF of fetuses and infants under normal and hydrocephalus conditions [37].

Under certain physiological conditions manifested during the embryonic period of man and also under particular experimental conditions such as hydrocephalus, the SCO secretes exclusively CSF-soluble material and does not form RF.

The human fetal SCO and probably also that of young infants appear to secrete exclusively CSF-soluble compounds. Identification in the CSF of glycoproteins that might correspond to SCO secretions appears to provide a useful analytic tool.

With hope, in the near future it will be possible to identify specific proteins related to hydrocephalus in terms of a useful indicator or, even more, accurate prognosis of cerebral injury. Other different CSF abnormalities such as external hydrocephalus or arrested hydrocephalus could be specifically defined in the context of cerebral damage.

Acknowledgement The author gratefully acknowledges Mrs. Stefania Fraccalvieri for manuscript preparation.

References

1. Hofer H (1959) Zur Morphologie der circumventriculären Organe des Zwischenhirns der Säugetiere. Verh Dtsch Zool Ges 55:202–251
2. Leonhardt H (1980) Ependym und circumventriculäre Organe. In: Oksche A, Vollrath L (eds) Neuroglia. I. Handbuch der mikroskopischen Anatomie des Menschen, vol IV, part 10. Springer, Berlin Heidelberg New York, pp 117–665
3. Nualart F, Hein S, Rodriguez EM, Oksche A (1991) Identification and partial characterization of the secretory glycoproteins of the bovine subcommissural organ-Reissner's fiber complex. Evidence for the existence of two precursor forms. Mol Brain Res 11:227–238
4. Rodriguez EM, Rodriguez S, Hein S (1998) The subcommissural organ. Microsc Res Tech 41:98–123
5. Oksche A (1969) The subcommissural organ. J Neuro Visc Relat [Suppl] 9:11–139
6. Reissner E (1860) Beiträge zur Kenntnis vom Bau des Rückenmarks von Petromyzon fluviatilis. L Arch Anat Physiol 77:545–588
7. Edinger L (1892) Untersuchungen über die vergleichende Anatomie des Gehirnes. 2. Das Zwischenhirn. Abhandl Senckenb Naturforsch Gesellsch 18:3–55
8. Sargent PE (1900) Reissner's fiber in the canalis centralis of vertebrates. Anat Anz 17:33–44
9. Dendy A, Nicholls GE (1910) On the occurrence of a mesocoelic recess in the human brain, and its relation to the SO of lower vertebrates; with special reference to the distribution of Reissner's fibre in the vertebrates series and its possible function. Anat Anz 32:496–509
10. Gabriel KH (1970) Comparative histologic studies on the subcommissural organ. Anat Anz 127:129–170
11. Hofer H, Meiniel W, Erhardt H (1980) Electron microscopic study of the origin and formation of Reissner's fiber in the subcommissural organ of Cebus apelus (Primates, Platyrrhini). Cell Tissue Res 205:295–301
12. Gilbert GJ (1956) The subcommissural organ. Anat Rec 126: 253–266
13. Rakic P, Sidamn RL (1968) Subcommissural organ and adjacent ependyma: autoradiographic study of their origin in the mouse brain. Am J Anat 122:317–336
14. Leonieni J (1968) Histophysiology of the subcommissural organ. Folia Morphol (Warsz) 27:403–418
15. Murakami M, Nakayama Y, Shimada T, Amagase N (1970) The fine structure of the subcommissural organ of the human fetus. Arch Histol Jpn 31:529–540
16. Guliants ES, Siziakina LP (1974) Histophysiology of the subcommissural organ in human prenatal ontogeny. Arkh Anat Gistol Embriol 67:87–92
17. Mollgard K, Moller M, Kimble J (1973) Histochemical investigations on the human fetal subcommissural organ. II. The "large granules". Histochemie 37:61–74
18. Mollgard K (1972) Histochemical investigations on the human foetal subcommissural organ. I. Carbohydrates and mucosubstances, proteins and nucleoproteins, esterase, acid and alkaline phosphatase. Histochemie 32:31–48
19. Bargmann W (1943) Die Epiphysis cerebri. In: Von Moellendorff W (ed) Handbuch der mikroskopischen Anatomie des Menschen, vol IV, part 4. Springer, Berlin, pp 307–502
20. Oksche A (1956) Funktionelle histologische Untersuchungen über die Organe des Zwischenhirndaches der Chordaten. Anat Anz 102:404–419
21. Oksche A (1961) Vergleichende Untersuchungen über die sekretorische Aktivität des Subkommissuralorgans und den Gliacharakter seiner Zellen. Z Zellforsch 54:549–612
22. Palkovits M (1965) Morphology and function of the subcommissural organ. Stud Biol Hung 4:1–105
23. Rodriguez EM, Oksche A, Hein S, Rodriguez S, Yulis R (1984) Spatial and structural interrelationships between secretory cells of the subcommissural organ and blood vessels. An immunocytochemical study. Cell Tissue Res 237:443–449
24. Rodriguez EM, Oksche A, Hein S, Rodriguez S, Yulis R (1984) Comparative immunocytochemical study of the subcommissural organ. Cell Tissue Res 237:427–441
25. Krabbe KH (1933) Anatomy of the subcommissural organ of the brain; review of literature. Nord Med Tidskr 6:1030–1035
26. Rodriguez EM, Oksche A, Hein S, Yulis CR (1992) Cell biology of the subcommissural organ. Int Rev Cytol 135:39–121
27. Chouaf L, Didier-Bazes M, Aguera M, Tardy M, Sallanon M, Kitahama K, Belin MF (1989) Comparative marker analysis of the ependymocytes of the subcommissural organ in four different mammalian species. Cell Tissue Res 257:255–262
28. Duvernoy H, Koritke JG (1964) Contribution a l'etude de l'angioarchitectomie des organes circumventriculaires. Arch Biol Suppl 75:693–748
29. Bouchaud C (1993) Neural inputs to the subcommissural organ. In: A Oksche, EM Rodriguez, P Fernandez-Llebrez (eds) The subcommissural organ. Springer, Berlin Heidelberg New York, pp 169–180
30. Naumann WW, Lehmann W, Debbage P (1993) The subcommissural organ and ontogenetic development of the brain. In: Oksche A, Rodriguez EM, Fernandez-Llebrez P (eds) The subcommissural organ. Springer, Berlin Heidelberg New York, pp 61–69
31. Bouchaud C, Bosler O (1986) The circumventricular organs of the mammalian brain with special reference to monoaminergic innervation. Int Rev Cytol 105:283–327
32. Sterba G, Kiessig C, Naumann W, Petter H, Kleim I (1982) The secretion of the SO. A comparative immunocytochemical investigation. Cell Tissue Res 226:427–439
33. Rodriguez EM, Oksche A, Rodriguez S, Hein S, Peruzzo B, Schoebitz K, Herrera H (1987) The subcommissural organ and Reissner's fiber. In: Gross PM (ed) Circumventricular organs and body fluids, vol II. CRC Press, Boca Raton, pp 1–41
34. Rodriguez S, Yulis CR, Siegmund I, Rodriguez EM (1985) Reissner's fiber and the wall of the central canal in the lumbosacral region of the bovine spinal cord. Cell Tissue Res 240: 649–662
35. Schoebitz K, Garrido O, Heinrichs M, Speer L, Rodriguez EM (1986) Ontogenetical development of the chick and duck subcommissural organ. An immunocytochemical study. Histochemistry 84:31–41
36. Irigoin C, Rodriguez EM, Heinrichs M, Frese K, Herzog S, Oksche A, Rott R (1990) Immunocytochemical study of the subcommissural organ of rats with induced postnatal hydrocephalus. Exp Brain Res 82:384–392
37. Rodriguez EM, Jara P, Richter H, Montecinos H, Flandez B, Wiegand R, Oksche A (1993) Evidence for the release of CSF-soluble secretory material from the subcommissural organ, with particular reference to the situation in the human. In: Oksche A, Rodriguez EM, Fernandez-Llebrez P (eds) The subcommissural organ. Springer, Berlin Heidelberg New York, pp 121–131
38. Weindl A, Sofroniew MV (1981) Relation of neuropeptides to mammalian circumventricular organs. Adv Biochem Psychopharmacol 28:303–320
39. Castaneyra-Perdomo A, Meyer G, Carmona-Calero E, Banuelos-Pineda J, Oksche A (1988) Sensory and secretory potencies and differentiations of the central nervous system. Acta Anat (Basel) 132:216–224
40. Brown DD, Afifi AK (1965) Histological and ablation studies on the relation of the subcommissural organ and rostral midbrain to sodium and water metabolism. Anat Rec 153:255–263
41. Seckl JR (1997) 11Beta-hydroxysteroid dehydrogenase in the brain: a novel regulator of glucocorticoid action? Front Neuroendocrinol 18:49–99
42. Ganong WF (2000) Circumventricular organs: definition and role in the regulation of endocrine and autonomic function. Clin Exp Pharmacol Physiol 27:422–427
43. Pavel S (1978) Arginine vasotocin as a pineal hormone. J Neural Transm Suppl 13:135–155
44. Gilbert GJ (1957) The subcommissural organ: a regulator of thirst. Am J Physiol 191:243–247

45. Rodriguez S, Caprile T (2001) Functional aspects of the subcommissural organ-Reissner's fiber complex with emphasis in the clearance of brain monoamines. Microsc Res Tech 52:564–572
46. Rodriguez S, Vio K, Wagner C, Barria M, Navarrete EH, Ramirez VD, Perez-Figares JM, Rodriguez EM (1999) Changes in the cerebrospinal-fluid monoamines in rats with an immunoneutralization of the subcommissural organ-Reissner's fiber complex by maternal delivery of antibodies. Exp Brain Res 128:278–290
47. Gobron S, Creveaux I, Meiniel R, Didier R, Dastugue B, Meiniel A (1999) SCO-spondin is evolutionarily conserved in the central nervous system of the chordate phylum. Neuroscience 88:655–664
48. Miranda E, Almonacid JA, Rodriguez S, Perez J, Hein S, Cifuentes M, Fernandez-Llebrez P, Rodriguez EM (2001) Searching for specific binding sites of the secretory glycoproteins of the subcommissural organ. Microsc Res Tech 52:541–551
49. Woollam DHM (1982) The circumventricular organs of the brain: their role as possible sites for future neurosurgery. Ann R Coll Surg Engl 64:309–317
50. Mantyh CR, Kruger L, Brecha NC, Mantyh PW (1987) Localization of specific binding sites for atrial natriuretic factor in the central nervous system of rat, guinea pig, cat and human. Brain Res 412:329–342
51. Rodriguez EM, Garrido O, Oksche A (1990) Lectin histochemistry of the human fetal subcommissural organ. Cell Tissue Res 262:105–113
52. Rodriguez EM, Oksche A, Montecinos H (2001) Human subcommissural organ, with particular emphasis on its secretory activity during the fetal life. Microsc Res Tech 52:573–590
53. Rodriguez EM, Rodriguez S, Schoebitz K, Yulis CR, Hoffmann P, Manns V, Oksche A (1989) Light – and electron – microscopic investigation of the rat subcommissural organ grafted under the kidney capsule, with particular reference to immunocytochemistry and lectin histochemistry. Cell Tissue Res 258:449–514
54. Adam H (1957) Beitrag zur Kenntis der Hirnventrikel und des Ependyms bei den Cyclostomen. Anat Anz 103:173–188
55. Hofer HO, Merker G, Oksche A (1976) Atypical forms of mammalian pineal body. Verh Anat Ges 70:97–102
56. Castaneyra-Perdomo A, Meyer G, Ferres-Torres R (1985) The early development of the human subcommissural organ. J Anat 143:195–200
57. O'Rahilly R, Muller F, Hutchins GM, Moore GW (1988) Computer ranking of the sequence of appearance of 40 features of the brain and related structures in staged human embryos during the seventh week of development. Am J Anat 182:295–317
58. Wislocki GB, Roth WD (1958) Selective staining of the human subcommissural organ. Anat Rec 130:125–130
59. Kasper M, Terpe HJ, Perry G (1990) Age-dependent pattern of intermediate filament protein expression in the human pineal gland. J Hirnforsch 31:215–21
60. Cenacchi G, Roncaroli F, Cerasoli S, Ficarra G, Merli GA, Giangaspero F (2001) Chordoid glioma of the third ventricle: an ultrastructural study of three cases with a histogenetic hypothesis. Am J Surg Pathol 25:401–405
61. Perez-Figares JM, Jimenez AJ, Rodriguez EM (2001) Subcommissural organ, cerebrospinal fluid circulation, and hydrocephalus. Microsc Res Tech 52:591–607
62. Overholser MD, Whitley JR, O'Dell BL, Hogan AG (1954) The ventricular system in hydrocephalic rat brains produced by a deficiency of vitamin B12 or folic acid in the maternal diet. Anat Rec 120:917–933
63. Vio K, Rodriguez S, Navarrete EH, Perez-Figares JM, Jimenez AJ, Rodriguez EM (2000) Hydrocephalus induced by immunological blockage of the subcommissural organ-Reissner's fiber (RF) complex by maternal transfer of anti-RF antibodies. Exp Brain Res 135:41–52
64. Perez-Figares JM, Jimenez AJ, Perez-Martin M, Fernandez-Llebrez P, Cifuentes M, Riera P, Rodriguez S, Rodriguez EM (1998) Spontaneous congenital hydrocephalus in the mutant mouse hyh. Changes in the ventricular system and the subcommissural organ. J Neuropathol Exp Neurol 57:188–202
65. Takeuchi IK, Kimura R, Matsuda M, Shoji R (1987) Absence of subcommissural organ in the cerebral aqueduct of congenital hydrocephalus spontaneously occurring in MT/HokIdr mice. Acta Neuropathol (Berl) 73:320–322
66. Takeuchi IK, Kimura R, Shoji R (1988) Dysplasia of subcommissural organ in congenital hydrocephalus spontaneously occurring in CWS/Idr rats. Experientia 44:338–440
67. Louvi A, Wassef M (2000) Ectopic engrailed 1 expression in the dorsal midline causes cell death, abnormal differentiation of circumventricular organs and errors in axonal pathfinding. Development 127:4061–4071
68. Castaneyra-Perdomo A, Meyer G, Carmona-Calero E, Banuelos PJ, Mendez-Medina R, Ormazabal-Ramos C, Ferres-Torres R (1994) Alterations of the subcommissural organ in the hydrocephalic human fetal brain. Brain Res Dev Brain Res 79:316–320
69. Meiniel R, Duchier N, Meiniel A (1988) Monoclonal antibody C1B8A8 recognizes a ventricular secretory product elaborated in the bovine subcommissural organ. Cell Tissue Res 254:611–615
70. Karoumi A, Meiniel R, Croisille Y, Belin MF, Meiniel A (1990) Glycoprotein synthesis in the subcommissural organ of the chick embryo. I. An ontogenetical study using specific antibodies. J Neural Transm Gen Sect 79:141–153

UNIVERSITAS
Miguel
Hernández

ELSEVIER

Symptomatic Supratentorial Arachnoid Cysts in Children

Marcelo Galarza, MD, Hugo B. Pomata, MD, Francisco Pueyrredón, MD, Marcelo Bartuluchi, MD, Graciela N. Zuccaro, MD, and Jorge A. Monges, MD

This study was undertaken to evaluate the clinical and radiologic long-term outcome of symptomatic primary arachnoid cysts in pediatric patients. Thirty-three children, ranging from 2 months to 17 years of age (mean age, 6 years) were treated. Craniotomy and fenestration of the cyst were used for temporal fossa and midline cysts in 24 patients (73%); later, two patients required shunt placement. Shunting device implantation was performed for cerebral convexity cysts in nine patients (27%), and two patients required a subsequent craniotomy and fenestration of the cyst. Four patients (12%) required additional surgery because of clinical progression rather than for cyst enlargement. Eleven patients (33%) experienced a cyst reduction of more than 50% compared with the original size on imaging studies. There was a significant correlation with the alleviation of symptoms ($P < 0.005$), regardless of the treatment used. Complete alleviation of symptoms was achieved in all patients after treatment, regardless of cyst reduction. Long-term follow-up of 70 ± 9.3 months demonstrated no recurrence of symptoms or progressive enlargement of the arachnoid cyst in all children.

Galarza M, Pomata HB, Pueyrredón F, Bartuluchi M, Zuccaro GN, Monges JA. Symptomatic supratentorial arachnoid cysts in children. Pediatr Neurol 2002;27: 180-185.

Introduction

Intracranial primary arachnoid cysts are benign extra-axial cerebrospinal fluid-filled cavities that are surrounded by a membrane of arachnoid mater. They can arise at any intracranial location adjacent to and variously communicating with the subarachnoid spaces and cisterns [1-3]. Surgical intervention is generally recommended to protect the patients from intracranial hypertension. Because limited information is available in different series [1,4-6] on the long-term outcome in patients treated for arachnoid cyst, we reviewed the imaging evolution and clinical outcome in a group of pediatric patients with supratentorial primary arachnoid cysts that were surgically treated at our institution.

Patients and Methods

The 33 patients presented in this report include patients with supratentorial primary arachnoid cysts who were surgically treated at the National Pediatric Hospital of Buenos Aires, Argentina from 1988 through 1997. We excluded patients who were treated nonsurgically (n = 30), patients with infratentorial cysts (n = 9), and any of the supratentorial patients with insufficient follow-up (n = 25). Patient sex was unequally represented with 21 males and 12 females, and the average age (mean ± standard deviation) was 6.3 ± 2.1 years (range = 2 months-17 years). The duration of the patients' preadmission clinical evaluation varied from 1 week to 2 years and averaged 8 ± 3.2 months.

Computed tomography (CT) and magnetic resonance imaging (MRI) represented the primary diagnostic tools, although MRI was performed in only five patients, including those with midline cysts, in one patient with fibrous dysplasia, and in one patient with a contralateral tumor. Postoperative CT scanning was performed in all patients during early (average time = 3 ± 1.1 months) and late follow-up (average time = 70 ± 9.3 months). Cyst measurement was assessed in all CT scans in the axial plane.

Surgery was performed using either a direct fenestration in 24 patients or an insertion of a shunting device in nine patients. The latter technique was primarily used in treating moderate and giant primary arachnoid cysts of the cerebral convexity, whereas the former technique was usually indicated to treat temporal and midline cysts. We implanted cyst–peritoneal shunts with a low-pressure valve (Codman, Goleta, CA) in eight patients and a ventriculoperitoneal shunt with a medium pressure valve (Codman, Goleta, CA) in one child. We performed an osteoplastic craniotomy in 24 children and after that, fenestration of the parietal and visceral wall of the cyst, with subsequent communication with the basal cerebrospinal fluid cisterns. For statistical analysis, we performed a nonparametric sign test for paired data and contingency tables for

From the Department of Neurosurgery, Hospital Nacional de Pediatría; Prof. Dr. J. P. Garrahan; Buenos Aires, Argentina.

Communications should be addressed to:
Dr. Galarza; Department of Neurosurgery; University of Cincinnati Medical Center; P.O. Box 670515; Cincinnati, OH 45267-0515.
Received January 10, 2002; accepted March 19, 2002.

PII S0887-8994(02)00414-9 • 0887-8994/02/$—see front matter

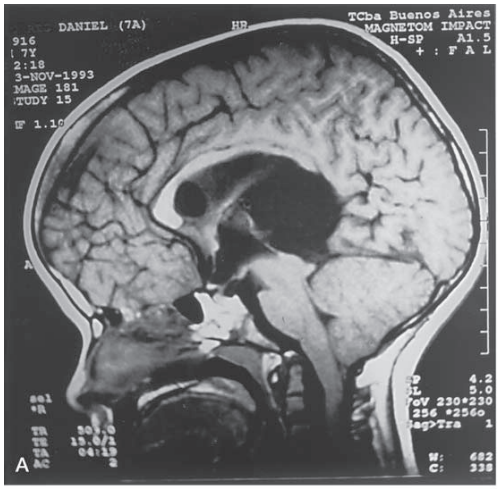

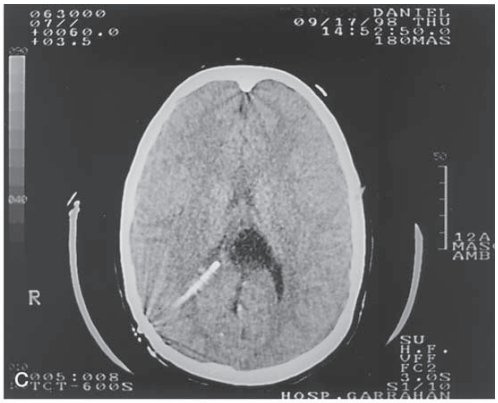

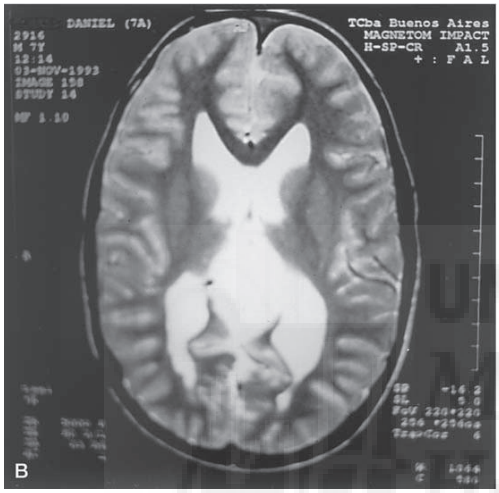

Figure 1. (A) Magnetic resonance T_1-weighted image (TR = 509 ms, TE = 15 ms) was obtained for the initial diagnostic determination of a quadrigeminal arachnoid cyst in a 7-year-old male with amblyopia and papilledema. (B) Magnetic resonance T_2-weighted image (TR = 3,000 ms, TE = 45 ms) axial view, demonstrates associated hydrocephalus to the quadrigeminal arachnoid cyst. (C) Computed tomography scan, axial view, obtained 6 years after insertion of a ventricular shunt device, demonstrates resolution of the hydrocephalus and marked reduction of the quadrigeminal arachnoid cyst.

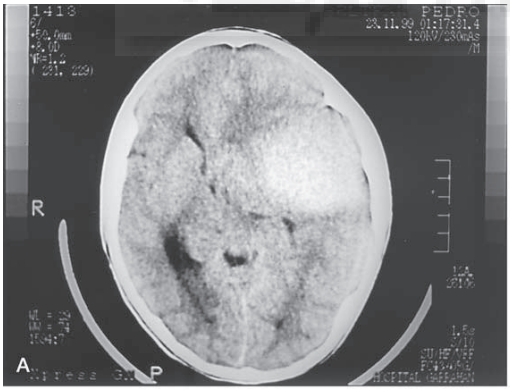

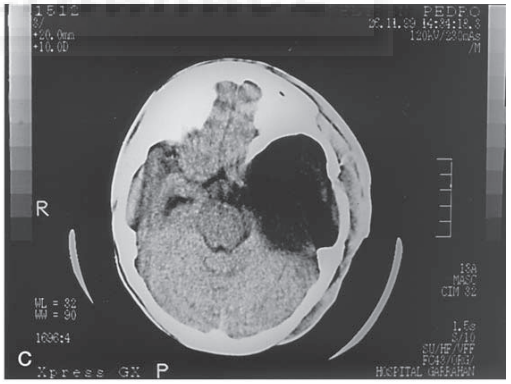

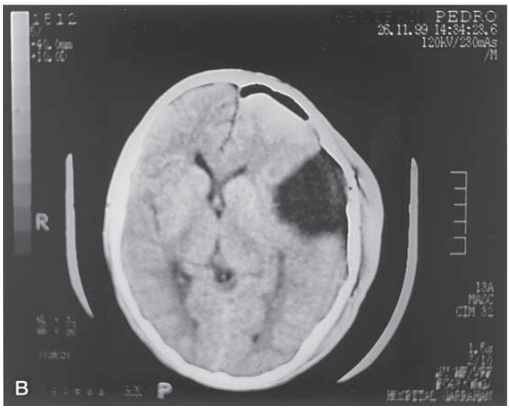

Figure 2. (A) Computed tomography scan, axial view, demonstrates gross temporal subdural hematoma in a 12-year-old male with headaches after mild head trauma. (B, C) Computerized tomography scan, axial view, performed 3 days after craniotomy and evacuation of the subdural hematoma, demonstrates an arachnoid cyst in the temporal fossa.

Table 1. Series of 33 supratentorial primary arachnoid cysts in a pediatric population

Age, Sex	Localization	Main Symptom	Other Symptoms	Treatment*	Other Relevant Medical Association
7 yr, M	Temporal type III	Macrocephaly	Developmental delay	CF	Hydrocephalus
8 yr, M	Temporal type III	Developmental I delay	Papilledema	CF	Hydrocephalus
6 yr, M	Temporal type III	Macrocephaly	Cranial asymmetry	CF	Hydrocephalus
3 yr, F	Temporal type III	Macrocephaly		SD > 50†	Hydrocephalus
17 yr, M	Temporal type III	Head trauma/incidental		CF	Bone remodeling
11 mo, F	Temporal type III	Macrocephaly		SD	
11 yr, F	Temporal type III	Head trauma/incidental		CF	Bone remodeling
2 yr, M	Temporal type III	Head trauma/incidental		CF > 50†	
17 yr, M	Temporal type III	Headache	Papilledema	CF > 50†	Subdural hematoma
12 yr, M	Temporal type III	Headache	Mild head trauma	CF	Subdural hematoma
14 yr, M	Temporal type II	Headache	Epilepsy	CF > 50†	Occipital epilepsy
9 yr, F	Temporal type II	Amblyopia	Epilepsy	CF	Acute lymphoblastic leukemia
5 yr, M	Temporal type II	Headache	Epilepsy	CF > 50†	Astrocytoma
1 yr, M	Temporal type II	Macrocephaly	Epilepsy	CF	Encephalocele
12 yr, F	Temporal type I	Amaurosis		CF > 50†	
5 yr, M	Temporal type I	Palpebral ptosis		CF > 50†	Fibrous dysplasia
4 yr, F	Temporal type I	Headache	Papilledema	CF	Bone remodeling
2 yr, M	Temporal type I	Amblyopia		CF	
8 mo, M	Giant convexity	Macrocephaly	Cranial asymmetry	SD	
2 mo, F	Giant convexity	Cranial asymmetry		CF > 50†	Bone remodeling
8 yr, M	Giant convexity	Palpebral ptosis		CF	
2 yr, F	Giant convexity	Macrocephaly	Cranial asymmetry	SD	Bone remodeling
2 yr, M	Giant convexity	Macrocephaly		SD	
13 yr, F	Giant convexity	Headache		SD	
12 yr, M	Cerebral convexity	Cranial asymmetry	Papilledema	CF	
3 mo, F	Cerebral convexity	Macrocephaly		SD > 50†	
1 yr, M	Cerebral convexity	Developmental delay	Nystagmus	CF	
14 yr, F	Cerebral convexity	Headache		SD > 50†	
10 yr, M	Cerebral convexity	Headache	Papilledema	CF	
5 yr, M	Cerebral convexity	Hemiparesis	Papilledema	CF > 50†	
7 yr, M	Quadrigeminal	Amblyopia	Papilledema	SD-VPS	Hydrocephalus/anemia
10 yr, F	Suprasellar	Amblyopia	Papilledema	CF	Hydrocephalus
1 yr, M	Suprasellar	Hemiparesis	Nystagmus	CF	Hydrocephalus

* Final treatment performed.
† Cyst reduction above 50% compared with its original size.

Abbreviations:
CF = Craniotomy and cyst fenestration
SD = Shunt device implantation
VPS = Ventriculo-peritoneal shunt

association analysis between results of clinical evaluation and initial treatment, initial and final treatment, cyst reduction and initial treatment, and cyst reduction and sex association. Results of percentage of cyst reduction, epilepsy association, and relationship between clinical manifestations with type of cyst were compared using only sign test, as appropriate. For all results, probability values less than 0.01 were considered to indicate statistical significance.

Results

Macrocephaly and cranial asymmetries were observed in the majority of infants, although headache was the main complaint in older children and, as a rule, was described as dull and always associated with vomiting. Patients with midline cysts did not present with either diabetes insipidus or precocious puberty. Interestingly, four patients also experienced epilepsy, which was not significantly associated with their primary arachnoid cysts ($P < 0.05$). Papilledema was observed in most cases, and one patient presented with acute amaurosis. Diagnosis of temporal type III cyst [3] was incidental in three patients after minor head trauma, but they later required treatment for headaches and progressive distension of the cyst. The cerebrospinal fluid-density cyst displayed well-defined margins with compression of adjacent structures without edema. Associated hydrocephalus was present in seven patients (27%) (Fig 1), and structural deformities of the skull reflecting chronic molding of the bones was present in five patients (15%). Nontraumatic intracystic subdural hematomas were detected in two patients (6%) (Fig 2). One patient presented with an associated fibrous dysplasia of the orbit, and another child presented with a history of an occipital encephalocele, which was treated after delivery. With respect to the laterality, there were 18 (55%) right-sided cysts, 12 (36%) left-sided cysts, and three (9%) midline cysts. Overall results of clinical presentation and imaging characteristics in our series are summarized in Table 1. Of the 33 patients, 11 (33%) achieved a substan-

tial cyst reduction of more than a 50% on follow-up imaging studies. Regardless of the cyst reduction on imaging studies, a satisfactory alleviation of symptoms was achieved during the first month of the postoperative period in 29 (88%) of the patients.

Craniotomy and Fenestration

A direct approach with resection and fenestration of the cyst was used in 24 patients (73%): 18 patients harbored middle fossa cysts, two patients presented with suprasellar cysts, and four patients presented with cysts of the cerebral convexity (two parietal, one frontal, and one occipital). Two children presented with suprasellar primary arachnoid cysts and hydrocephalus that, after excision and marsupialization of its wall, did not require a subsequent operation of cerebrospinal fluid shunting, either of the associated hydrocephalus or the cystic lesion. Two (8%) patients with a type III temporal cyst [3] presented with minimal progressive cyst enlargement associated with worsening of clinical symptoms within 1 month after fenestration. Therefore a shunt device was promptly inserted in both cases. Three patients with incidentally discovered type III temporal cysts required surgery for headaches and progressive distension of the cyst on subsequent CT scanning. An additional two patients presented with a subdural hematoma as a form of presentation of a temporal type III cyst and, after surgical evacuation of the hematoma, did not require further treatment. Another patient treated early in the series for a type II temporal cyst presented 4 years later with epilepsy and a cystic lesion on the contralateral temporal lobe, which was found to be a grade II astrocytoma after complete surgical resection (Table 1). No complications were encountered that were directly related to the surgeries with the exception of one patient who presented with a small subdural hematoma that was managed conservatively.

Cyst–Peritoneal Shunting

A shunting device was inserted in nine (27%) patients. Cyst–peritoneal shunting was performed in eight patients: five of whom harbored a frontotemporoparietal cyst, one had a frontotemporal cyst, and one had a giant cerebral convexity cyst (frontotemporoparieto-occipital cystic lesion). The shunting only of the associated hydrocephalus in primary arachnoid cysts has been practically abandoned; however, in a patient with a quadrigeminal region cyst and severe hydrocephalus associated with serious anemia, ventriculoperitoneal shunting was performed electively. After reduction in size of the cerebral ventricles, the volume of the cyst was also diminished (Fig 1). Hydrocephalus was present in patients with midline cysts and in four patients with type III temporal cysts. No other patient with hydrocephalus was treated beyond the management of the cyst. After insertion of the shunting device, two (22%) of the patients with frontotemporoparietal cyst underwent an elective craniotomy and fenestration of the cyst because of progressive clinical worsening without enlargement of the cyst (Table 1). Two patients (22%) of nine presented 1 month later with a shunt device infection as a result of *Staphylococcus epidermidis*, which was managed with an insertion of an external ventricular device and proper administration of antibiotics. After treatment, a new shunt device was inserted without consequences. No other complications, such as overdrainage symptoms, were recorded.

Table 2. Results of primary arachnoid cysts surgically treated: long-term outcome (average 70 months, n = 33)

a) Clinical outcome		
	Symptomatic No. (%)	**Nonsymptomatic No. (%)**
Before treatment	30 (91)	3 (9)
After treatment	0	33 (100)

b) Final surgical treatment and imaging evolution		
Cyst reduction	**CF* No. (%)**	**SD† No. (%)**
< 50%	16 (48)	6 (18)
> 50%	8 (24)	3 (9)
TOTAL	24 (72)	9 (27)

* Craniotomy and fenestration performed as final treatment in temporal, suprasellar, and minor cerebral convexity cysts.
† Shunting device inserted as final treatment in moderate and giant cerebral convexity cysts.

Postoperative Clinical Results

In one patient, persistent fever without evident infection was encountered during the early postoperative period. One patient with a known history of acute lymphoblastic leukemia presented with severe anemia. Finally, one patient presented with visual hallucinations and delirium during the early postoperative period, which required sedative medication. No other complications were appreciated. Ocular symptoms resolved in all patients after surgery. All patients are presently asymptomatic and without clinical symptoms related to the cyst after a follow-up of 3-12 years (average 70 ± 9.3 months). Long-term outcome, final surgical results, and imaging evolution are outlined in Table 2.

Associated Epilepsy

Epilepsy was present in four (12%) of 33 patients. Preoperative electroencephalographic studies and postoperative electroencephalogram studies were performed. All patients presented with a type II right temporal arachnoid cyst. Nevertheless, these epileptic patients presented with a previous known history of central nervous system disorder in addition to their temporal primary arachnoid cysts. One patient presented with acute lymphoblastic

leukemia and previous history of temporal epilepsy, although no seizures were recorded on him. In the other three patients at least two seizures were recorded: one patient with a temporal grade II astrocytoma, another with a treated occipital encephalocele, and, finally, one patient with a previous history of occipital epilepsy who presented with visual hallucinations after treatment. All patients are currently free from seizures and are being managed with antiepileptic drugs. Nonetheless, we cannot specifically assess that the primary arachnoid cysts in each patient was not at least partially responsible for the seizures.

Statistical Analysis Results

There was no association between initial treatment and clinical manifestation ($P < 0.02$), as well as between initial and final treatment ($P < 0.03$) results. Also, no association was evident between cyst reduction and initial treatment performed ($P < 0.02$). However, there was a substantially higher incidence of a second surgery with the shunt surgery compared with the craniotomy and fenestration as initial treatment, although it was not significant. Regardless of the treatment used, there was a significant correlation between alleviation of symptoms ($P < 0.005$) and surgical treatment. A higher incidence of male patients disclosed a cyst reduction of less than 50% on long-term outcome, although there was no statistically significant association between sex and cyst reduction ($P < 0.03$). Finally, no association was evident between epilepsy and primary arachnoid cysts ($P < 0.05$) or between primary clinical symptom and type of cyst ($P < 0.07$).

Discussion

In the present series, primary arachnoid cysts accounted for approximately 1.5% of all intracranial masses treated in our hospital, as well as for those described in other studies [1,3,4,6]. In our patients, and in reported series in the literature, the male sex prevalence and the young age of presentation matched that of primary arachnoid cysts as a whole [2,4,7]. Infants with primary arachnoid cysts were commonly symptomatic, although the clinical picture was rather specific: failure to thrive, irritability, developmental delay, cranial remodeling, ocular symptoms, and macrocrania. It is worth noting that primary arachnoid cysts were not associated primarily with epilepsy in our patients. All the patients who presented with seizures had other associated central nervous system disorders. Duration and presentation of clinical symptoms of cerebral dysfunction were similar with those encountered in the literature [4,5,7,8].

Radiologic diagnosis of primary arachnoid cysts was based on findings on CT and MRI. Nonetheless, as reported in the literature [9], we noted that certain primary arachnoid cysts might be confused with certain porencephalic cysts, craniopharyngiomas, holoprosencephalies, and certain forms of agenesis of corpus callosum, as well as, with those cysts originating from a defect in the hemispheral cleavage [10]. In some patients, a neuropathologic examination was required to differentiate arachnoid cysts from other cystic lesions. Biopsy and subsequent pathologic examination was assessed in all our patients treated with craniotomy and fenestration.

Our findings that treatment of arachnoid cysts resulted in an overall alleviation of symptoms with or without reduction of the cyst size on imaging studies are believed to be indicative of the development of primary arachnoid cysts as an early cerebral malformation, either with or without postnatal evolution. Many arguments provide evidence of the congenital genesis of primary arachnoid cysts: definitive prevalence in infancy and childhood, with most lesions diagnosed within the first two decades of life [1,6,7], and exceptional reports of occurrences in siblings [11]. Moreover, in the series by Menezes et al. [12], 30% of the patients had additional malformations. Multiple pathogenic theories [1-3,13,14] have been proposed to explain the progressive distension of the pathologic cavity (i.e., active fluid secretion directly by the cyst walls or fluid filtration through the lining of membranes by virtue of an osmotic gradient). A cause for acute expansion is the development of intracystic hemorrhage, which was observed in two (6%) patients from our series, although we could not determine a minor head trauma in these patients.

Therapeutic Implications

The surgical correction in our series, either shunting or excision of its wall, was nearly always aimed at controlling the increased intracranial pressure rather than controlling a progressive cyst enlargement. Controversy mainly concerns the indication for surgery in asymptomatic patients and the choice of an optimal surgical procedure. We do not perform elective treatment in asymptomatic cases with type I temporal cysts. Asymptomatic patients with small midline cysts are closely monitored to assess cyst enlargement or subsequent development of hydrocephalus. With respect to the temporal fossa, interhemispheric fissure, and cerebral convexity cysts of moderate size, the efficacy of craniotomy with direct cyst fenestration has been reported in previous studies with marked reduction on imaging studies [15,16]. Primary arachnoid cysts of infratentorial, suprasellar, and quadrigeminal location may cause a complex impairment of the cerebrospinal fluid circulation as a result of a permanent obstruction or of a defect of the fluid absorption mechanisms easily associated with concurrent hydrocephalus [2,17]. In such circumstances a fenestration into occluded and incompetent cerebrospinal fluid spaces would be useless, whereas cyst–peritoneal shunting should be the primary advisable surgical option [2,17-19]. The main advantage of shunting the cyst is that it is a relatively safe procedure compared with more difficult operations requiring craniotomy [3,20]. Nonetheless, Menezes et al. [12] reported a series of 10 children with arachnoid cysts in whom eight (89%)

of nine patients with fenestrations were free of complications. Contrarily, Ciricillo et al. [5] concluded that cyst–peritoneal shunting is the procedure of choice for arachnoid cysts in most locations, including those in the middle fossa. Of 15 patients with cysts initially treated by fenestration, 10 patients (67%) later required a shunting procedure. It should be taken into consideration that neuroendoscopic procedures have enabled cerebrospinal fluid diversion [19], especially in patients with obstructive hydrocephalus.

After surgical correction in our series, either shunting or fenestration, successful clinical results (i.e., the normalization of intracranial pressure and resolution of papill-edema) were obtained in all of the affected patients. Furthermore, the recurrence of symptoms because of refilling of the cyst was not observed in our patients in a mean follow-up of 6 years. With respect to middle fossa cysts, the efficacy of the direct fenestration has been confirmed by our experience as judged by the low rate of marked reduction in size compared with the original cyst. We believe that the failure of the cyst to diminish after surgery may be also a result of failure of a dysgenetic brain to re-expand. Only eight (24%) of 24 patients treated with craniotomy and fenestration presented a reduction of more than 50% from the original size of the cyst on postoperative CT scanning (Table 2). None of these patients presented a total collapse of the cyst after craniotomy; however, total disappearance of the cyst was observed only in three (9%) patients, all of whom had cerebral convexity cysts treated with shunting. We also compared the two therapeutic methods based on the original cyst size. In an early hypothesis, we had considered that the shunting device technique might be more adept at treating large cysts. However, no difference was observed after treatment between the two methods in relation to the cysts' size. Undoubtedly, it seems that the postoperative reduction of the cyst does not correlate with the improvement of clinical symptoms. It is worth noting that one limitation of our study is that we did not gather information on shunting devices systems (i.e., free-valve devices compared with low-pressure valves or medium-pressure valves). In addition, we did not assess the number, size, and anatomic locations of the fenestrations performed on the cysts. We also did not perform volumetric imaging measures to objectively compare before treatment and after treatment cyst size.

Conclusions

Although an appreciable cyst reduction on imaging studies may not be obtained after surgery, it seems that this does not correlate with the clinical improvement in a long-term follow-up. It is unusual that additional surgeries will be required to control progressive enlargement or symptoms of cerebral dysfunction after initial treatment. At an average follow-up interval of 6 years, none of these patients exhibited cyst-related symptoms; however, the majority of patients still exhibit a similar size of the initial untreated cyst on imaging studies. We emphasize that critical and accurate clinical evaluation of the child, as well as a correct interpretation of the imaging studies, are critically necessary to indicate whether further surgeries are warranted.

References

[1] **Aicardi** J, Bauman F. Supratentorial extra-cerebral cysts in infants and children. J Neurol Neurosurg Psychatry 1975;38:57-68.

[2] **Di Rocco** C, Caldarelli M. Suprasellar arachnoidal cysts. In: Raimondi AJ, Choux M, Di Rocco C, eds. Intracranial cyst lesions. Berlin: Springer-Verlag, 1993:113-28.

[3] **Galassi** E, Gaist G. Dynamics of intracranial cyst formation and expansion. In: Raimondi AJ, Choux M, Di Rocco C, eds. Intracranial cyst lesions. Berlin: Springer-Verlag, 1993:53-77.

[4] **Choux** M, Raybaud C, Pinsard N, Hassoun J, Gambardelli D. Intracranial supratentorial cysts in children, excluding tumor and parasytic cysts. Child Brain 1978;4:15-32.

[5] **Ciricillo** SF, Cogen PH, Harsh GR, Edwards MSB. Intracranial arachnoid cysts in children. A comparison of the effects of fenestration and shunting. J Neurosurg 1991;74:230-5.

[6] **Naidich** TP, McLone DG, Radkowski MA. Intracranial arachnoid cysts. Pediat Neurosci 1986;12:112-22.

[7] **Leo** JS, Pinto RS, Hulvat GF, Epstein F, Kricheff II. Computed tomography of arachnoid cysts. Radiology 1979;130:675-80.

[8] **Galassi** E, Gaist G, Giuliani G, Pozatti E. Arachnoid cysts of the middle cranial fossa: Experience with 77 cases treated surgically. Acta Neurochir (Wien) 1988;42:201-9.

[9] **Rao** K, Gunadi IK, Diaconis JN. Interhemispheric intradural cyst. Case report. J Comput Assist Tomogr 1982;6:1167-71.

[10] **Aoki** N. Cyst of the septum presenting as hemiparesis. Childs Nerv Syst 1986;2:326-8.

[11] **Handa** J, Okamoto K, Sato M. Arachnoid cysts of the middle cranial fossa: Report of bilateral cysts in siblings. Surg Neurol 1981;16: 127-30.

[12] **Menezes** AH, Bell WE, Perret GE. Arachnoid cysts in children. Arch Neurol 1980;37:168-72.

[13] **Krawchenko** J, Collins GH. Pathology of an arachnoid cyst. J Neurosurg 1979;50:224-8.

[14] **Rengachary** SS, Watanabe I. Ultrastructure and pathogenesis of intracranial arachnoid cysts. J Neuropathol Exp Neurol 1983;40:61-83.

[15] **Anderson** FM, Segall HD, Caton WL. Use of computerized tomography scanning in supratentorial arachnoid cysts. J Neurosurg 1979;50:333-8.

[16] **Harsh** GR, Edwards MSB, Wilson CB. Intracranial arachnoid cysts in children. J Neurosurg 1986;64:835-42.

[17] **Raimondi** AJ, Shimoji T, Gutierrez FA. Suprasellar cysts: Surgical treatment and results. Childs Brain 1980;7:57-72.

[18] **Kaplan** BJ, Mickle JP, Pakhurst R. Cystoperitoneal shunting for congenital arachnoid cysts. Childs Brain 1985;11:304-11.

[19] **Miyajima** M, Arai H, Okuda O, Hishii M, Nakanishi H, Sato K. Possible origins of suprasellar arachnoid cysts: Neuroimaging and neurosurgical observations in nine cases. J Neurosurg 2000;93:62-7.

[20] **Raffel** C, McComb JG. To shunt or to fenestrate: Which is the best surgical treatment for arachnoid cysts in pediatric patients. Neurosurgery 1988;23:338-41.

Transcranial Doppler in infantile cerebrospinal fluid disorders: clinical validity

Marcelo Galarza and Jorge A. Lazareff

Section of Pediatric Neurosurgery, Division of Neurosurgery, University of California at Los Angeles, Los Angeles, CA, USA

The present study was designed to investigate a possible relationship between transcranial Doppler sonography (TCD) parameters with infantile hydrocephalus and other types of cerebrospinal fluid (CSF) abnonnalities, i.e. *arrested hydrocephalus and essential ventriculomegaly. TCD parameters in the major arteries of the circle of Willis were studied in hydrocephalic children (n=12) before and after insertion of a ventricular shunt device. ft was correlated with TCD parameters of children with CSF disorders (n=13), in whom no surgery was performed. Also, TCD parameters were assessed in control cases (n =10). Mean values for medial cerebral artery (MCA) flow velocities were higher in the essential ventriculomegaly (75.3814.1) and in the control group (73.93 1 3.4) compared with hydrocephalic children (64.131 5.3). All hydrocephalic children had a higher mean MCA pulsatility index (RI) (1.08 0.13) and resistance index (RI) (0.641 0.17) values than the essential ventriculomegaly group (PI: 1.03 10.48; RI: 0.63 10.13) and the control group (PI: 0.841 0.32; RI: 0.571 0.23). Analysis of al! TCD parameters disclosed its usefulness only after a particular and thorough evaluation of the TCD results with special emphasis in the clinical correlation of every case.* [Neurol Res 2004; **26:** 4094131

Keywords: Hydrocephalus; arrested hydrocephalus; ventriculomegaly; pulsatility index; resistance index; transcranial Doppler sonography

INTRODUCTION

TCD is commonly accepted as a noninvasive method for evaluation of cerebral blood flow velocities (CBFV) in the major arteries of the polygon of Willis. Preliminary reports suggest that TCD readings in the middle cerebral artery (MCA) also may correlate with intracranial pressure (ICP) elevation in patients with hydrocephalus[1-4]. Several authors[5-7] have described the use of TCD ultrasonography to examine the effects of treatments aimed at decreasing ICP and improving brain perfusion in infants with the previously mentioned clinical conditions. However, certain cases with ventriculomegaly on imaging studies and no clinical symptoms of raised ICP are believed to be indicative of patients with arrested hydrocephalus (usually older pediatric patients without marked cerebral atrophy on imaging studies) or, on the other hand, patients with essential ventriculomegaly (usually children with associated systemic diseases and with marked cerebral atrophy on imaging studies). In those particular cases, controversy continues regarding whether or not they require surgical treatment. The proposed relationship between TCD parameters and infantile hydrocephalus or other CSF abnormalities, with or without clinical symptoms of raised ICP, has not been clearly established in clinical settings, where the variability of TCD readings and additional factors influencing CBFV and ICP are encountered. Hence, this study was designed to evaluate a possible correlation of TCD parameters with different types of CSF disturbances in a pediatric population. A group consisting of normal children was used as control.

Correspondence and reprint requests to: Marcelo Galarza, MD, Department of Neurosurgery, Sinai Grace Hospital, Detroit Medical Center, Wayne State University, 6071 W Outer Drive, Detroit, MI 48235, USA. [Mgalarza@neurosurgery.wayne.edu] Accepted for publication October 2003.

MATERIALS AND METHODS

Three different groups of children underwent TCD assessments. The first group consisted of 12 hydrocephalic patients, seven boys and five girls between the ages of 1 month and 17 years (mean 3.5 years ± 5 years standard deviation). These patients presented clinical symptoms of raised ICP, such as increasing head circumference, bulging fontanel le or forced downward gaze of the eyes, among others. All presented hydrocephalus secondary to stenosis of the Sylvian aqueduct except for two patients with hydrocephalus secondary to nnyclomen ingocele, and all were treated with insertion of a ventricular peritoneal shunt device that included a distal slit valve (Medtronic PS Medical, Goleta, CA, USA). Computed tomography (CT) scanning was performed in this group, before and after ventricular shunt implantation. In addition, a second group of 13 patients was analyzed who presented with essential ventriculomegaly or arrested hydrocephalus on imaging studies without clinical symptoms of raised ICP. This group consisted of six boys and seven girls, range of age 2 months to 6 years (mean 1.5 years ±1.7 years standard deviation) with the following diagnoses: congenital heart disease *(n=1),* id iopath ic arrested hydrocephalus *(n=8),* id iopath ic essential ventriculomegaly *(n=2),* essential ventriculomegaly with benign macrocrania *(n=2).* The control group consisted of five boys and five girls, range of age 4 months to 15 years (mean 5.7 years ± 5 years standard

10.1179/016164104225016010

deviation), without clinical symptoms of raised ICP and hydrocephalus on imaging studies, as well as an absent clinical history of cardiac or pulmonary disease. Approval of this study was obtained from the Human Protection Committee of the hospital. Informed written consent was obtained by a parent, or legal guardian, prior to participation in this study. TCD examination of the basal cerebral arteries was performed 5 ± 3 days before and 12 ± 5 days after insertion of the shunt device in the hydrocephalic group. With a 2-5 MHz phased-array transducer using color flow Doppler sonography, the anterior cerebral artery (ACA), medial cerebral artery (MCA) and posterior cerebral artery (PCA) were identified in the temporal window and anterior fontanelle. Using the depth of the range gate, the flow direction and the characteristic TCD spectra aided identification of the vessels. To minimize inter-investigator bias one clinician carried out all TCD measurements. The peak systolic (VS), end-diastolic (VD), and mean (VM) blood flow velocities in the right and left MCA were nneasured, and the Gosling pulsatility index (PI) and Pourcelot resistance index (RI) were calculated according to the equations

$$PI = \frac{VS - VD}{VM}$$

and

$$RI = \frac{VS - VD}{VS}$$

Also the VM of the right and left ACA and PCA, as wel I as the PI and RI of the ACA were determined. There was no statistically significant difference between the values for the left and the right MCA, ACA, PCA. Reference values for normal flow velocities and TCD indices were established in the group of 10 control children. Linear regression methods and differences investigated possible correlations between all TCD readings among the three groups by the paired Student's t-test. Statistical significance was set at the 5°/0 level ($p < 0.05$).

RESULTS

Findings of the TCD parameters in the hydrocephalic group, essential ventriculomegaly group and the control group are I isted in *Table 1.* The mean values for systolic, mean and end-diastolic MCA flow velocities were higher in the essential ventriculomegaly group. The mean blood flow velocities in the ACA disclosed negative values for retrograde flow and an elevated value in the essential ventriculomegaly group. The mean PCA blood flow velocities showed no difference between the essential ventriculomegaly group and the control group, whom disclosed the highest values *(Figure 1).* All hydrocephalic children had higher mean MCA PI and RI values than the essential ventriculomegaly group and the control group. However, no difference was noted in the PI and RI of the ACA between the hydrocephalic group and the essential ventriculomegaly group. In the hydrocephalic group, an increase in PI and RI value was seen post-operatively in the MCA and ACA *(Figure 2).* Comparison of the TCD data among all groups did not demonstrate statistically significant differences (data not shown).

When comparing the PI and RI data in the hydrocephalic group alone *(Table 2),* six patients (four boys and two girls, mean age 8 months ±14), had higher parameters after shunt insertion (Subgroup 1) and six hydrocephalic children (three boys and three girls, mean age 6 nnonths ± 25) showed lower values after surgery (Subgroup 2). Initial post-operative TCD studies were done within the first two days in Subgroup 1 and within the first month in Subgroup 2. A correlation was noted between post-operative normalized TCD parameters and delayed time of TCD study, though these results were not significant. Follow up CT showed controlled hydrocephalus in all patients. No difference was noted among them regarding age, clinical presentations, and mean time interval of post-operative TCD study.

DISCUSSION

The presented TCD parameters from children with hydrocephalus, essential ventriculomegaly and arrested hydrocephalus revealed a poor correlation between TCD indices and clinical settings. In fact, a lack of uniformity in the Doppler indices was revealed in the hydrocephalic group after shunt device insertion. However, when analyzed individually, the TCD paranneters were demonstrated to be useful for each patients' follow-up.

In 1982, Aaslid *et al.8* reported the results of noninvasive transcranial Doppler investigations of blood flow velocities in the middle, anterior, and posterior cerebral

Table 1: Mean results of TCD parameters in a group of hydrocephalic children, essential ventriculomegaly and control group. Velocities: cm sec-1

Group	Vm MCA	Vs MCA	Vd MCA	Vm ACA	Vm PCA	PI MCA	RI MCA	PI ACA	RI ACA
Pre-op	64.13	101.19	39.69	-45.94	31.69	1.08	0.64	0.92	0.62
SD	5.3	6.9	5.2	5.2	0.4	0.13	0.17	0.52	0.32
Post-op	62.06	101.56	36.06	-36.43	36.68	1.16	0.65	1.01	0.65
SD	5.7	6.7	5.2	5.2	1.1	0.27	0.26	0.42	0.21
Nonsurg	75.38	117.19	44.51	-57.61	39.80	1.03	0.63	0.92	0.62
SD	4.1	5.5	1.6	3.7	1.8	0.48	0.13	0.33	0.58
Control	73.93	108.11	45.48	-48.48	39.61	0.84	0.57	0.82	0.56
SD	3.4	2.5	4.2	5.6	2.2	0.32	0.23	0.12	0.12

ACA, anterior cerebral artery; MCA, media! cerebral artery; PCA, posterior cerebral artery; Pre-op, pre-operative results in the hydrocephalic group; Postop, post-operative results in the hydrocephalic group; Nonsurg, nonsurgical essential ventriculomegaly group; SD, standard deviation; Vm, mean flow velocity; Vs, systolic flow velocity; Vd, diastolic flow velocity; PI, pulsatility index; RI, resistance index.

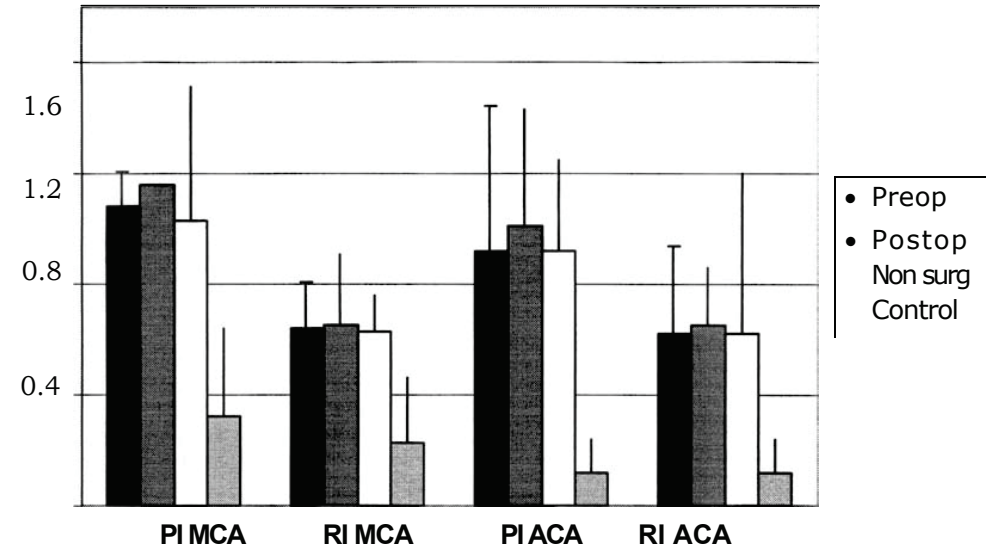

Figure 1: Mean, systolic, diastolic cerebral flow velocities in a group of hydrocephalic children, essential ventriculomegaly and in a control group as assessed with TCD. Velocities: cm sec-1

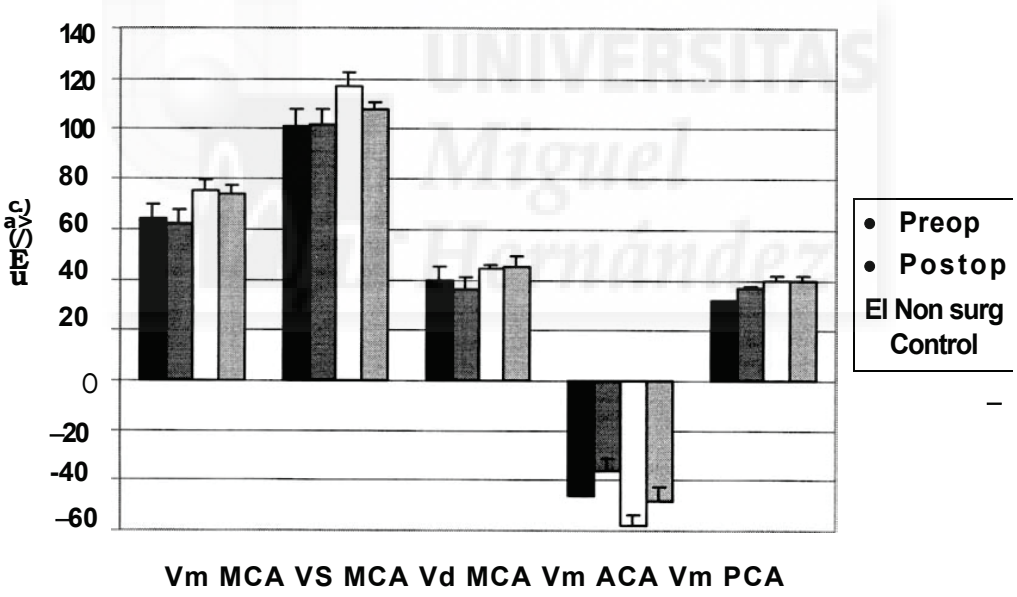

Figure 2: TCD pulsatility index and Resistance index in a group of hydrocephalic children, essential ventriculomegaly and in a control group. ACA, anterior cerebral artery; MCA, medial cerebral artery; PCA, posterior cerebral artery; Preop, pre-operative results in the hydrocephalic group; Postop, post-operative results in the hydrocephalic group; Non surg, nonsurgical essential ventriculomegaly group; SD, standard deviation; Vm, mean flow velocity; Vs, systolic flow velocity; Vd, diastolic flow velocity. PI: pulsatility index; RI, resistance index

arteries respectively. In the past, ultrasonography of the intracerebral vessels in newborns and infants was performed using duplex sonography through the open fontanelle. TCD parameters of all basal cerebral arteries can now be assessed through the temporal bone window. However, TCD u ltrasonography in the pediatric population is different than that in the adults, requiring another set of normative velocity values including different recording depths. According to De Witt *et al.9* description of the normal values, the side-to-side difference of blood velocities is remarkably low, despice a larger inter-individual than intra-individual variability of flow velocities and considerable changes with age. Nonetheless, investigations in children of all ages showed correlations were best among MCA mean flow velocity and peak systolic flow velocity1°.

Table 2: mean pulsatility and resistance index (±SD) results in children with hydrocephalus treated with a shunt. See Results for explanations

	PI	SD	RI	SD
Subgroup 1				
Pre-shunt	1.02	± 0.29	0.62	± 0.3
Post-shunt	1.37	± 0.17	0.72	± 0.18
Subgroup 2				
Pre-shunt	1.48	± 0.21	0.71	± 0.2
Post-shunt	0.94	± 0.13	0.58	±0.12

Elevation of ICP in infants, resulting from hydrocephalus, leads to brain damage through hypoperfusion[11-13], mainly due to diastolic hypoperfusion. The Gosling PI and the Pourcelot RI are the most commonly employed indices in hydrocephalic patients. Both indices are ratios, designed to minimize the error in estimating the true velocity as a result of varying angle of insonation. This is important especially in hydrocephalus where the vascular anatomy is distorted by the enlarged ventricles[14]. An increased PI can result from an increase in end diastolic flow velocity (VD). Therefore the significant fall in pulsatility following CSF drainage is due to a significant increase in VD. These suggest that the PI and RI may be a reliable reflection of the distal cerebrovascular contraction status[2]. Since the arterioles and capillaries at their pre-capillary sphincter provide 80°/0-90°/0 of vascular resistance", TCD is a gross diagnostic method in the evaluation of hydrocephalus, because it only evaluates the blood flow velocities in the basal arteries (i.e. MCA/ACA), which is a function of the upstreann arterioles. There is a need to evaluate the status of arterioles, anatomically and physiologically, in order to assess real perfusion disturbances. PET and SPECT nneasurements of cerebral blood flow (CBF) are not feasible and easy to perform. TCD values can 'mirror' the functionality of the arterioles based on the measured parameters in basal arteries. Hence, we suggest that TCD could be useful as an accessory bol in the long-term evaluation of the function of a ventricular shunt system. Changes of TCD parameters can then indicate changes in ICP or vascular reactivity, if other reasons for TCD changes are excluded.

Controversies exist regarding the clinical validity of the TCD parameters in the assessment of pediatric hydrocephalus. Accord ing to Westra *et al.*[7], a higher RI is found in children with hydrocephalus and need of CSF diversion, but its series included patients with a variety of associated neurological disorders. In another TCD study" following surgery in a congenital hydrocephalic group and in a hydrocephalic group due to tuberculous meningitis were compared. The fall in PI following CSF diversion seen in congenital hydrocephalus did not occur in children with hydrocephalus due to tuberculous meningitis, especially when complicated by cerebral infarcts. More compelling conclusions were suggested in other studies. Jindal and Mahapatral [7] found that a fall in pulsatility index correlated well with decrease in ventricle size, concluding that TCD could be used as simple bedside test for the assessment of shunt function. In a study by Goh and Minnsm, it was found that stable ventriculomegaly was associated with normal pulsatility, and the cerebral blood flow velocity parameters changed significantly following CSF drainage by tapping or shunting the hydrocephalus. The authors concluded that cerebral blood flow velocity is currently one of the best ways of assessing the need of CSF diversion and monitoring subsequent shunt function. Our results do not support these conclusions. Moreover, we believe that shunt monitoring must be subjected to a thorough and critical evaluation in every particular clinical context.

Although most studies found increased pulsatility in children with progressive hydrocephalus, Grant *et al."* found no significantly raised RI values in patients with progressive hydrocephalus. Anderson and Mawk[2°] reported increased pulsatility in only 30% of their hydrocephalic children requiring shunting. Hanlo et al.[21] concluded that the present Doppler indices are inadequate for monitoring the complex intracranial dynamic responses in patients with raised ICP because the correlation between PI or RI and ICP in long-term simultaneous recordings was generally poor. The risk of obtaining false positive or false negative PI or RI values in short term nneasurements was also dennonstrated al that time. Our results showed no significant differences among results in the TCD parameters in our evaluated groups, nonetheless, the TCD parameters proved to be valuable when correlated with clinical presentation and su rgical h istory.

In the essential ventriculomegaly group the TCD parameters showed a trend lo higher mean arterial velocities and to lower PI and RI compared with the hydrocephalic group, though none of the results were significantly different. Essential ventriculomegaly is closely associated with cortical atrophy. In fact, we do not know if essential ventriculomegaly or arrested hydrocephalus are, in a certain manner, secondary to a late compensatory mechan ism arising from chronic hypoperfusion. Cerebral perfusion during the early developmental-pre-natal period of the brain is normally unknown. In that way, we may assume that all diagnosed CSF disorders should be treated in the earliest period, before its evolution to either arrested hydrocephalus or essential ventriculomegaly. We accept as true that we should not permit the brain's evolution to atrophy or ventricular arrestment dueto its 'plasticity', in this case, secondary to hypoperfusion.

Ursino *et* ai.[22] dennonstrated in a mathematical model that in cases with defective autoregulation, the mean velocity and velocity amplitude decrease linearly with decreasing CPP, but the PI still increases in a way similar to that observed patients with preserved autoregulation. The patterns clearly showed that the Gosling PI were almost equally sensitive to ICP changes, because they exhibit similar percentage variations in the entire pressure range. In contrast the Pourcelot RI appeared much less sensitive to ICP than the others. On the other hand, in an experimental study, Czosnyka *et al.*[23] found that PI, although being widely used is one of the nnost ambiguous variables ever used in cerebrovascular hemodynamic studies. First, it is highly dependent on arterial pressure pulsatility. A high systolic-diastolic difference

of arterial pulse pressure increases PI directly. Moreover, PI depends on many factors like heart rate, cerebral perfusion pressure, arterial carbon dioxide concentration, cerebral resistance and compliance of big vessels. In the clinical study by Hanlo *et al.21,* the correlations between PI or RI and ICP in long-term simultaneous recordings, was generally poor. Also, the risk of obtaining false positive or false negative measurements was demonstrated. Interestingly, in this study TCD results among the hydrocephalic group disclosed that some children presented higher pulsatility values after shunting device insertion and some others hydrocephalic children presented normalized pulsatility values after surgery. However, all patients presented without signs and symptoms related to high ICP and all showed controlled hydrocephalus on imaging studies. These controversial TCD results could lead to erroneous conclusions if analyzed in general.

Because of the wide range of reference values and an overlap between normal and abnormal values, the usefulness of PI and RI measurements lies in their employment on an individual basis, particularly in terms of patients follow-u[p1,21.] A noteworthy assessment of each case is mandatory for proper pediatric CSF disorder and shunt functionality evaluation. A general prospective concerning diagnosis or prognosis of patients with various CSF disorders presentations is not possible on the basis of TCD results.

CONCLUSION

TCD in children with CSF disorders is a highly valuable accessory study when evaluating in an individual context. Previous Doppler studies in infantile hydrocephalus have reported inconsistent conclusions on the significance of PI and RI, in regard to intracranial hemodynamics. Both PI and RI are influenced by many extracranial factors and have a wide range of reference values. When assessing the results in the hydrocephalic group we disclosed children that presented post-operative nonexpected TCD parameters like a higher PI, nonetheless they were all clinically intact and presented imaging studies with controlled hydrocephalus. There is a need to evaluate the long-term outcome in the post-operative group, as well as in the nonsurgical group for final assessing of TCD discrepancies. It can be concluded that these preliminary results of Doppler indices are useful if applicable in a thorough clinical evaluation of each case.

ACKNOWLEDGEMENTS

The authors gratefully acknowledge Dr Martin Schuhmann for valuable recommendations in the preparation of the manuscript, and to Brenda Rimsky RN, for providing patient's information.

REFERENCES

1 Chadduck WM, Seibert JJ. Intracranial Duplex Doppler: Practical uses in pediatric neurology and neurosurgery. *I Child Neurol* 1989; **4:** 77-86

2 Goh D, Minns RA, Hendry GMA, Thambyayah M, Steerrs AJW. Cerebrovascular resistive index assessed by Duplex Doppler sonography and its relationship to intracranial pressure in infantile hydrocephalus. *Pediatr Radiol* 1992; **22:** 246-250

3 Norelle A, Fisher AQ, Flannery AM. Transcranial Doppler: Noninvasive method to monitor hydrocephalus. *I Child Neurol* 1989; **4:** 87-90

4 Sanker P, Richard KE, Weigl HC, Klug N, van Leyen K. Transcranial Doppler Sonography and intracranial pressure monitoring in children and juveniles with acute brain injuries or hydrocephalus. *Child Nerv Syst* 1991; **7:** 391-393

5 Taylor GA, Madsen JR.: Neonatal hydrocephalus: Hemodynamic response to fontanele compression — Correlation with intracranial pressure and need for shunt placement. *Radiology* 1996; **201:** 685-670

6 Taylor GA, Phillips MD, Ichord RN. Intracranial compliance in infants: Evaluation with Doppler US. *Radiology* 1994; **191:** 787-792

7 Westra SJ, Lazareff JA, Curran JG, Sayre JW, Kawamoto H. Transcrahial Doppler ultrasonography to evaluate need for cerebrospinal fluid drainage in hydrocephalic children. *Ultrasound Med* 1998; **17:** 561-569

8 Aaslid R, Markwalder TH, Nomes H.: Noninvasive transcranial Doppler ultrasound recording flow velocity in basal cerebral arteries. *I Neurosurg* 1982; **57:** 769-774

9 De Witt DL, Rosengart A, Teal PA. Transcranial Doppler ultrasonography: Normal values. In: Babikion LV, Wechsler LR, eds. *Transcranial Doppler Ultrasonography,* St. Louis, MO: Mosby, 1993: pp. 29-37

10 Bode **H.**, ed. *Pediatric Applications of Transcranial Doppler Sonography,* Vienna: Springer-Verlag, 1988

11 Deeg KH, Rupprecht T, Zeilinger G. Doppler sonographic classifIcation of brain edema in infants. *Pediatr Radiol* 1990; **20:** 509-512

12 Fisher AQ, Livingstone JN. Transcranial Doppler and real time sonography in neonatal hydrocephalus. *I Child Neurol* 1989; **4:** 64-70

13 Hill A, Volpe JJ. Decrease in pulsatility flow in the anterior cerebral arteries in the infantile hydrocephalus. *Pediatrics* 1982; **69:** 4-8

14 Finn JP, Quin MW, Hall-Craggs MA, Kendall BE. Impact of vessel distortion on transcranial Doppler velocity measurements: correlation with magnetic resonance imaging. *I Neurosurg* 1990; **73:** 572-575

15 Ziljstra WG. Physiology of the cerebral circulation. In: Minderhoud JM, ed. *Cerebral Blood Flow, Basic Knowledge and Clinical Implications,* Amsterdam: Excerpta Medica, 1981: pp. 34-55

16 Nadvi SS, Van Dellen JR, Gouws E. Transcranial Doppler ultrasonography in hydrocephalic children with tuberculous meningitis. *Neurosurg* 1995; **9:** 519-526

17 Jindal A, Mahapatra AK. Correlation of ventricular size and transcranial Doppler finding before and after ventricular peritoncal shunt in patients with hydrocephalus: A prospective study. / *Neurol Neurosurg Psychiatry* 1998; **65:** 269-271

18 Goh D, Minns RA. Intracranial pressure and cerebral arterial flow velocity indices in childhood hydrocephalus: Current review. *Childs Nerv Syst* 1995; 11: 392-396

19 Grant EG, White EM, Schellinger D, Choyke PL, Sarcone AL. Cranial Duplex sonography of the infant. *Radiology* 1987; **163:** 177-185

20 Anderson JC, Mawk JR. Intracranial arterial duplex Doppler waveform analysis in infants. *Childs Nerv Syst* 1988; **4:** 144-148

21 Hanlo PW, Gooskens RH, Nijhuis IJ, Faber JA, Peters RJ, van Huffelen AC, Tulleken CA, Willemse J. Value of transcranial Doppler indices in predicting raised ICP in infantile hydrocephalus. A study with review of the literature. *Childs Nerv Syst* 1995; 11: 595-603

22 Ursino M, Giulioni M, Lodi CA.: Relationships among cerebral perfusion pressure, autoregulation, and transcranial Doppler waveform: A modeling study. *Neurosurg* 1998; **89:** 255-266

23 Czosnyka M, Richards HK, Whitehouse HE, Pickard JD. Relationship between transcranial Doppler-determined pulsatility index and cerebrovascular resistance: An experimental study. *I Neurosurg* 1996; **84:** 79-84

UNIVERSITAS
Miguel
Hernández

MIN/975/10.10.2006/Macmillan

M. Galarza[1]
P. Peretta[1]
R. Gazzeri[4]
G. Cinalli[1]
M. Forni[2]
I. Morra[2]
P. Ragazzi[1]
S. Sandri[3]

Spinal Cord Gliomas and Hydrocephalus: Utility of Neuroendoscopy

Original Article

Abstract

Objective: The aim of this study is to report on the role of neuroendoscopy during the management of hydrocephalus that led to the diagnosis of intracranial tumoral dissemination and the subsequent finding of a spinal cord glioma. **Methods and Results:** We present two children each with an intramedullary astrocytoma that presented initially with hydrocephalus without spinal cord symptoms. In both cases leptomeningeal gliomatous dissemination was asserted during routine endoscopy for the management of hydrocephalus. The diagnosis of a cervical and a lower thoracic intramedullary tumor was made soon after on magnetic resonance imaging. **Conclusions:** Spinal cord MRI with contrast should be considered initially in selected cases of hydrocephalus without evident diagnosis. The intraoperative diagnosis of gliomatous dissemination and secondary hydrocephalus due to unrecognized spinal cord gliomas was possible, in our experience, with the routine use of the neuroendoscope.

Key words

Spinal cord glioma · tumoral dissemination · neuroendoscopy · hydrocephalus · cerebrospinal fluid

Introduction

Intramedullary tumors of the spinal cord in childhood are usually of low grade [1,2] and are frequently found in the cervical [3,4] and cervicothoracic regions [2,5,6]. They present with symptoms and signs of spinal cord tumor [1,2,4,6–11]. In rare cases intraspinal tumors can manifest at first with hydrocephalus without a spinal cord syndrome [10–13]. Mechanisms of hydrocephalus proposed include altered cerebrospinal fluid absorption from increased cerebrospinal fluid protein [4,14], associated hyperproteinorrhachia and arachnoiditis, with basal blockage of the cerebrospinal fluid pathways [15,16]. The hydrocephalus seems to be unrelated to the level, location or the pathology of the spinal lesion [4]. Metastatic seeding of an intramedullary astrocytoma in children has been reported on a few occasions [2,12,13]. The efficacy of neuroendoscopy in cases of obstructive hydrocephalus is widely recognized and its applications include also performing biopsies in tumoral [17–19] and non-tumoral lesions [20,21], in the supratentorial [17,22] and infratentorial [20,21,23] compartment. However, the role of endoscopic procedures in cases of communicating hydrocephalus is controversial [17,19,22].

We report two cases of low-grade diffuse infiltrating intramedullary astrocytoma that manifested with clinical hydrocephalus and cranial tumor dissemination to the third and fourth ventricle

Affiliation
[1]Division of Neurosurgery, Children Hospital of Turin, Turin, Italy
[2]Department of Pathology, Children Hospital of Turin, Turin, Italy
[3]Department of Oncology, Children Hospital of Turin, Turin, Italy
[4]Department of Neurosurgery, San Giovanni-Addolorata Hospital, Rome, Italy

Correspondence
Marcelo Galarza, M.D. · Division of Neurosurgery · Villa Maria Cecilia Hospital · 48010 Cotignola RA · Italy · Tel.: + 39/0545/21 71 11 · Fax: + 39/0545/21 72 01 · E-mail: galarza.marcelo@gmail.com

Bibliography
Minim Invas Neurosurg 2006; 00: 1–6 © Georg Thieme Verlag KG · Stuttgart · New York
DOI 10.1055/s-2006-955066
ISSN 0946-7211

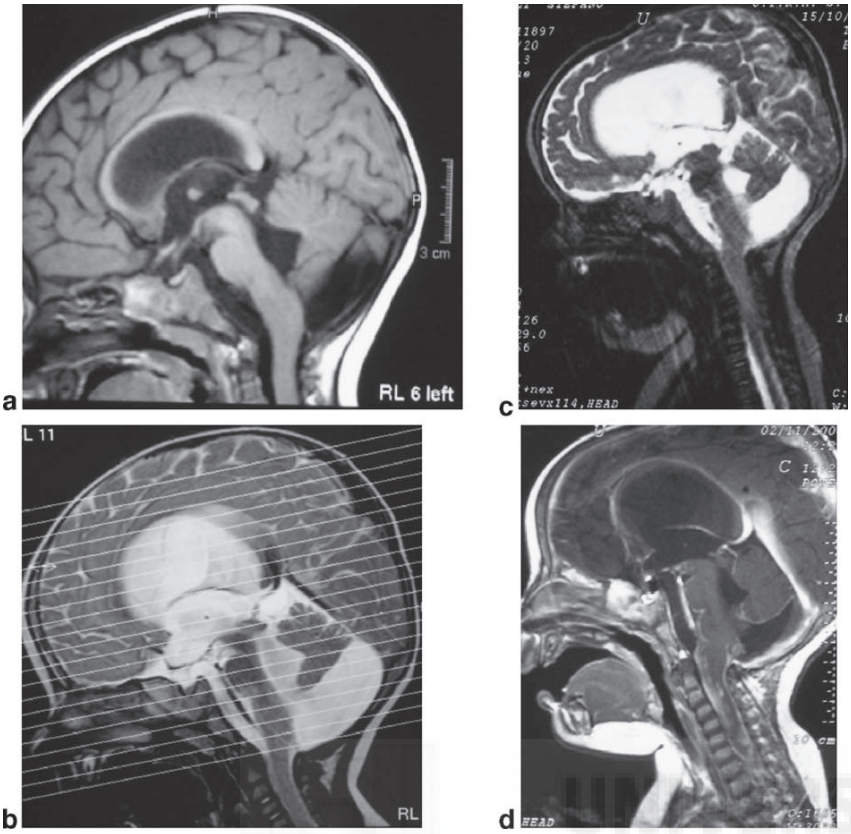

Fig. **1** **a** Cerebral sagittal T_1-weighted MR image showing a 3-cm, well-delineated cyst in the posterior fossa and hydrocephalus. **b** Cerebral sagittal T_2-weighted MR preoperative endoscopic image showing progression of the hydrocephalus. **c** Cerebral and cervical sagittal T_2-weighted MR image showing the cervical spinal swelling cord up to the C5 suggesting the diagnosis of an intraspinal tumor. **d** Sagittal T_1-weighted MR images with gadolinium injection performed after tumor operation. Note the significant progression of ventricular and meningeal neoplastic dissemination and lack of control of hydrocephalus.

without symptoms of spinal cord tumor. Direct visualization of tumoral dissemination was achieved during endoscopy for treatment of the hydrocephalus. We review the literature and discuss the role of neuroendoscopy for not only the treatment, but also for the initial diagnosis in cases of unrecognized secondary hydrocephalus.

Case Reports

Case 1

A 7-month-old boy with an uncomplicated prenatal history was admitted to our department with projectile vomiting, irritability and bulging fontanelle. On admission, his parents reported a progressive change of mood and behavior during the last 2 months. A cerebral magnetic resonance imaging (MRI), showed a communicating ventriculomegaly, wide cerebral subarachnoid spaces, a partial agenesis of the vermis with a posterior fossa cyst in apparent communication with the fourth ventricle, and no signs of transependymal reabsortion or brain edema (Figs. **1a** and **b**). A cine-flow MRI demonstrated enlarged ventricles and no CSF flow on the posterior fossa. An attempted third ventriculostomy disclosed a non-clear CSF hence an external ventricular drain (EVD) was inserted. The amount of CSF drainage was 120 mL in 24 hours. CSF examination demonstrated hypercellularity, elevated protein but no atypical cells. The EVD was the converted to a ventriculoperitoneal (VP) shunt. After that, the patient presented with normotensive fontanelle and evident motor weakness of the upper extremities and decreased spontaneous movements in the lower extremities. A new MRI without contrast showed no change in the ventricular and subdural spaces, but an enlarged non-communicating posterior fossa cyst in close proximity with an upper hypointense cervical spinal cord (Fig. **1c**). In an attempt to communicate the cyst, the subsequent neuroendoscopic approach to the posterior fossa revealed a cyst with turbid fluid content and a soft edematous leptomeningeal tissue at the level of the bulbomedullary junction. Endoscopic biopsy of the suspicious lesion and intraoperative smear disclosed a possible gliomatous origin. The endoscopic burr hole was changed to a limited inferior suboccipital craniectomy. A soft, suckable and heterogeneous tumor was found and partially resected under the microscope using an ultrasonic aspirator. This was then confirmed by a cranial and spinal MR image with contrast showing a heterogeneously enhanced tumor in the cervical spinal cord down to the C6 level along with diffuse subependymal dissemination from the anterior pons down to the conus medullaris (Fig. **1d**). The postoperative course was complicated with respiratory insufficiency and a tracheostomy was made.

Microscopic examination showed a glial tumor with mucinous background with microcysts. Solid areas, mainly perivascular, showed fibrillary and elongated cells. GFAP was strongly positive. MIB-1 was focally elevated up to 8 %. In some areas of the neoplasia, an ependymal lining was still present covering the bulging tumor. Based on these features, the lesion was considered to be a low-grade pylocytic astrocytoma with diffuse meningeal dissemination (see Fig. **3a**).

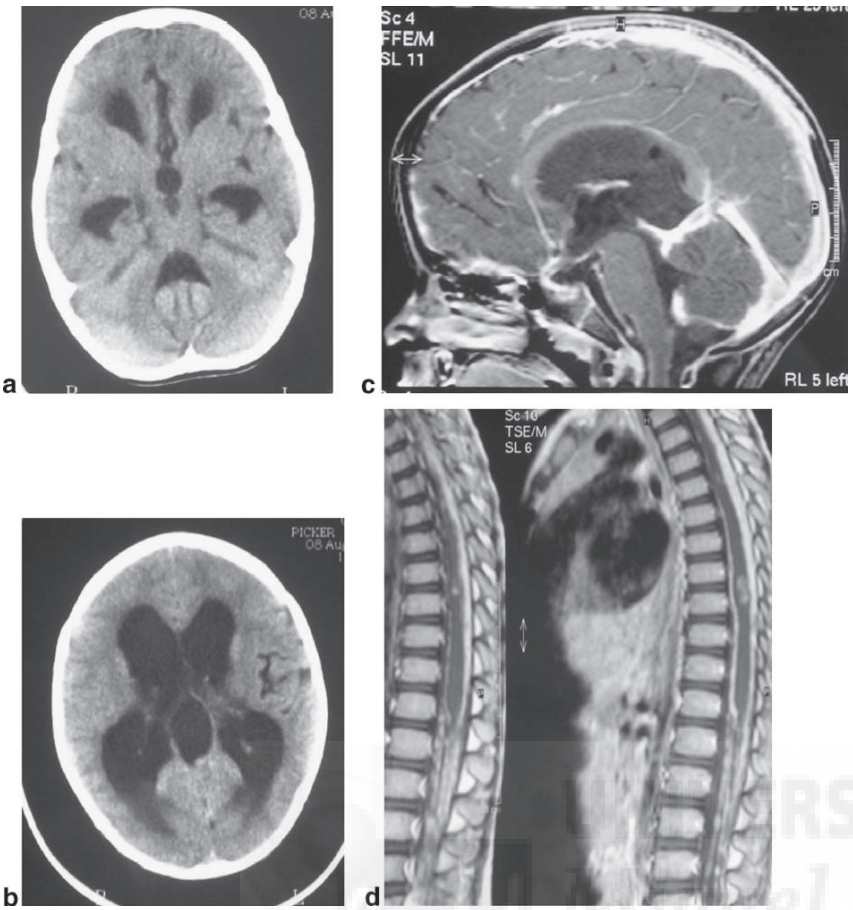

Fig. **2** **a** and **b** Cerebral CT images at that time of the first clinical manifestation in June 2004, no intracranial lesion was evident, only a communicating hydrocephalus. **c** Cranial metastatic spread at the time of the intramedullary tumor progression along the ventricles as well as frontobasally is depicted in sagittal images. **d** The initial intramedullary tumor at T8/9 is shown on sagittal T_1-weighted contrast-enhanced MR images from July 2004.

The patient's postoperative condition was unchanged. A protocol of chemotherapy was discussed with the parents. Just before it started, the child presented with rapidly progressive respiratory and neurological deterioration, sepsis, multi-organ failure and died. The parents refused an autopsy.

Case 2

This 2-year-old boy presented with a two-month history of irritability, abdominal pain, inconsistent divergent strabismus and onset of projectile vomiting during the last two days before admission to our division. The neurological examination revealed also a decreased level of consciousness, evident macrocephaly (CC 54 cm, above 2 SD) and four-limbic ataxia. A non-contrast head CT disclosed a wide hydrocephalus (Figs. **2a** and **b**). He had no relevant medical history except a long labor delivery. A third ventriculostomy was performed on an emergency basis. During the procedure, CSF was clear but the floor of the third ventricle was found to be covered with subependymal excrescences. An endoscopic biopsy of the lesions disclosed a gliomatous origin. Fenestration of the floor did not control the hydrocephalus and, two days later, a VPS was inserted.

Brain-spinal contrast MRI revealed an intramedullary focal lesion at the thoracic 8 and 9 segment with diffuse leptomenigeal spinal and basal cerebral enhancement (Figs. **2c** and **d**). This lesion was approached through a T8 laminotomy. A soft and heterogeneous tumor was found and a biopsy was performed under the operative microscope.

Leptomenigeal biopsies consisted of tiny laminar fragments. Microscopic analysis disclosed collagen depositions with small and ill-defined nests of cells. Immunohistochemistry was positive for GFAP and negative for EMA and vimentin, confirming the glial origin of the infiltrating cells. MIB-1 staining was limited to the nests of infiltrating cells. A labelling index was not calculated due to the limited extension of the present neoplastic nests. Ultrastructural analysis on fragments fixed for EM revealed collagen depositions, fibroblastic elements, many necrotic cells and sporadic elements with glial differentiation. The final diagnosis was non-anaplastic astrocytoma with diffuse meningeal dissemination (Fig. **3b**).

At the time of writing, the patient is still alive 18 months after the diagnosis. He has remained on chemotherapy protocol treatment for the last 3 months with well-preserved neurological functions except for his slight paraparesis.

Discussion

We present two patients with hydrocephalus related to a spinal cord glioma during the clinical management of which a neu-

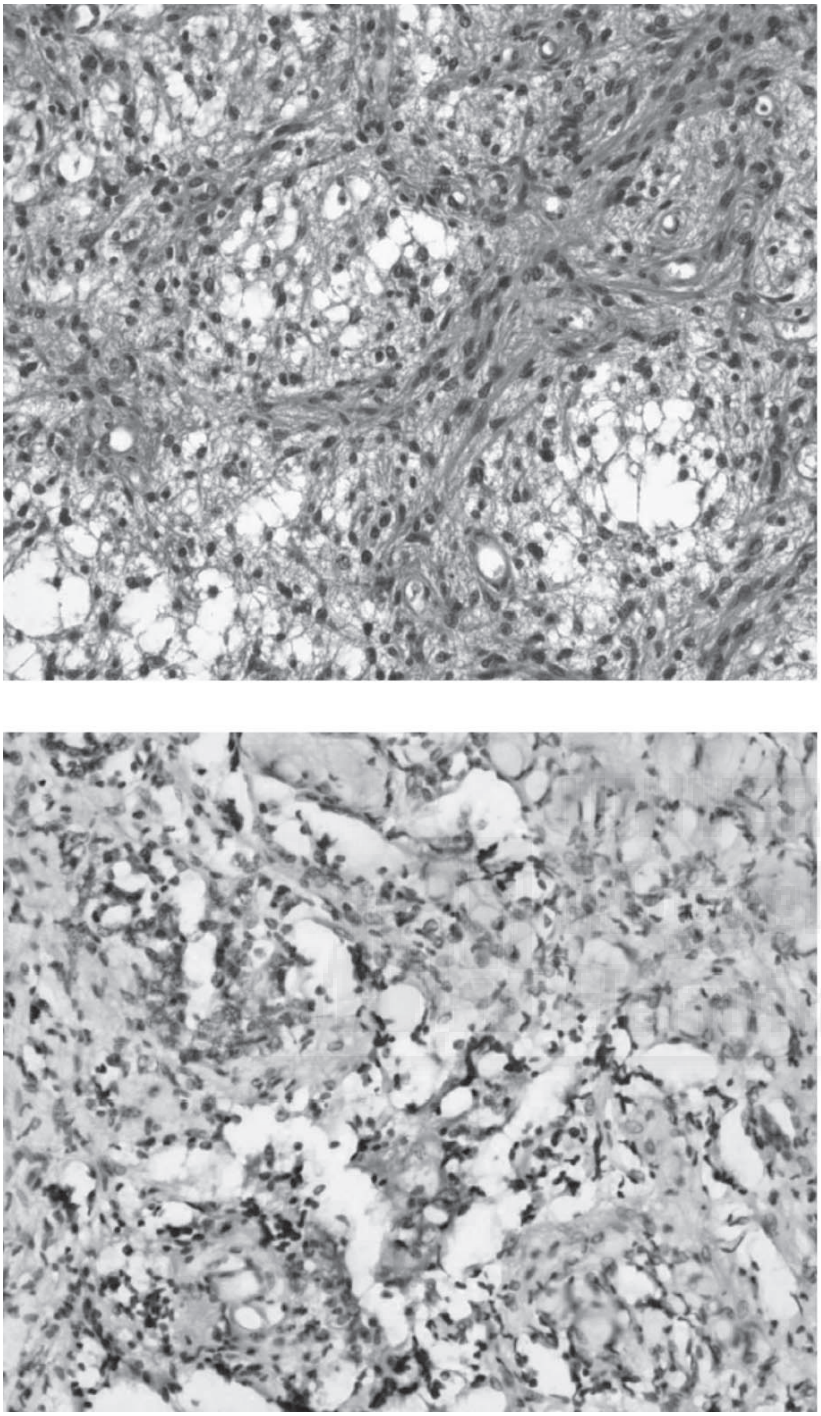

Fig. **3** Pathology: **a** H&E staining, **b** GFAP staining.

roendoscopic examination was conducted. The points made in our report are:

- Spinal cord tumors may rarely present only with symptoms of hydrocephalus.
- Metastatic seeding of a spinal cord tumor to the cranial CSF space may rarely be seen at presentation.
- In those cases of non-obstructive hydrocephalus where the etiological diagnosis is obscure, endoscopic inspection at the time of third ventriculostomy or even prior to the insertion of ventriculoperitoneal shunt, may yield diagnostic findings.

Neurological findings

Pain is the most common presenting symptom in patients with intramedullary tumors; with weakness, gait deterioration, torticollis also being frequently reported [8,10]. The cervical spine is the region of the spine most affected [1,2,3,5]. The apparent early absence of spinal cord symptoms in children harboring intramedullary tumors is explained by lack of specificity of clinical and neurological findings [4,10]. As well, in infants, the neurological examination is usually deferred until the appearance of a blunt neurological deficit. One of our patients was an

infant and other a child, but both cases initially manifested only with hydrocephalus without gross spinal cord symptoms. Although papilledema and raised intracranial symptoms have been reported in about 12.5 % of cases of spinal cord tumors [13], it is rare to find them presenting only with symptoms of raised intracranial pressure [7]. Our cases presented initially with hydrocephalus, and the gross symptoms of the spinal cord developed in one case thereafter.

Spinal tumors and hydrocephalus

Reported spinal tumors with hydrocephalus are intramedullary, intradural and extradural neoplasms [6]. The most frequent association is with low-grade intramedullary astrocytoma [1, 2, 8], but other reported spinal neoplasms included anaplastic astrocytomas [13], gangliogliomas [11], neurinomas [12], malignant schwanomas [15], ependymomas [8, 12], granulomas [12]. Rifkinson et al [2]. reported a series of 25 (15 %) patients, mostly children that developed symptomatic hydrocephalus, from an original series of 171 spinal tumors; of them, thirteen patients had malignant tumors, complicated by increased intracranial pressure with hydrocephalus; of the remaining, 12 developed symptomatic hydrocephalus, after diagnosis of benign spinal tumors. In the same report [2], the authors noted that the presence of hydrocephalus in patients with malignant intramedullary astrocytomas was associated with a shorter survival rate than in those patients with high-grade tumors but without hydrocephalus, seemingly because of rapid tumor progression; while the associated ventriculomegaly with benign spinal cord gliomas did not influence the long-term prognosis. In our cases, at the last follow-up, one child is under a chemotherapy protocol and neurologically stable, while the infant died after respiratory problems due to a rapid progressive tumor.

As seen from previous reports [1, 2, 4], hydrocephalus occurs with greater frequency in children than in adult patients and often requires a shunt. Theories that have been proposed to explain the association of spinal tumors with hydrocephalus, include that of Bamford and Labadie [14] which proposed that the abnormal presence of fibrinogen and its transformation into fibrin at the level of the basal cisterns and Pacchioni's granulation that may alter CSF hydrodynamics. As well, Maurice-Williams and Lucey [15] suggested that the resulting leptomeningeal fibrosis might predispose the secondary implantation of neoplastic elements in the subarachnoid spaces of the brain. Both mechanisms are sufficient to induce communicating hydrocephalus and also explain the cranial dissemination and seeding of tumoral cells. Other proposed hypotheses include an increase in CSF viscosity due to elevated fluid protein content [16]; obliteration of the cisterna magna because of a cranial extension of the tumor [6]; and obstruction of the spinal subarachnoid pathways of CSF resorption [1, 4].

In our cases, cranial tumoral seeding was directly visualized during neuroendoscopy.

Cranial dissemination of spinal cord tumors

Spinal dissemination of primary intracranial tumors is frequent and through the CSF pathways, a similar mechanism of tumor cell dissemination may add to the inverse situation of cranial seeding of a primary spinal neoplasm [1]. Cranial seeding occurs most frequently in association with a tumor recurrence or malignant transformation [13]. Astrocytomas are infiltrating neoplasms and gross total resection is occasionally possible in the pediatric population. The role of radical resection of low-grade fibrillary astrocytomas of the spinal cord in children has not been definitively demonstrated in the literature [1–5, 8, 13]. The outcome for low-grade astrocytomas is better in children than in adults [1, 2]. Malignant tumors have dreary outcomes and surgery in these patients serves only to provide a diagnosis [8, 13]. Our cases were defined as diffuse infiltrating intramedullary low-grade astrocytomas. The prognosis in cases of primary diffuse infiltrating astrocytoma is not yet defined in clinical settings. These tumors, although benign in pathological appearance, can present with a diffuse dissemination from the initial diagnosis.

Third ventriculostomy and communicating hydrocephalus

Reports indicate that third ventriculostomy is a most effective treatment in cases of obstructive hydrocephalus caused by aqueductal stenosis, posterior fossa and brainstem tumors and other space-occupying lesions [17–20, 22, 23]. The technique is less effective in cases with communicating hydrocephalus [18, 19, 22]. For these patients neuroendoscopy has an effect in selected cases, preferably with confirmed CSF circulation studies [22]. The efficacy of endoscopy to treat cases with secondary hydrocephalus due to neoplastic dissemination of central nervous system tumors is not clearly evident in the literature [19, 22]. Routine placement of a VP shunt is the standard practice in these cases [3, 13]. While in patients with tumoral CSF dissemination at the initial presentation, third ventriculostomy, by controlling hydrocephalus, permits chemotherapy to be undertaken prior to tumor resection [19]. By avoiding insertion of a VP shunt, one may prevent intraperitoneal or systemic tumoral seeding. Our patients had hydrocephalus of the communicating type and we failed to control it following third ventriculostomy; both cases later required insertion of a VP shunt. However, neuroendoscopy was particularly useful for the intraoperative recognition of the cause of the hydrocephalus, that later led to the diagnosis of a spinal cord tumor. In unrecognized cases of secondary hydrocephalus, it is possible to avoid deferral in the correct diagnosis with the routine use of the endoscope.

The cases reported are not similar, as in case 1 the diagnostic endoscopic examination was not a ventriculoscopy but rather an endoscopic retrocerebellar cystoscopy. Also, in both cases, after abnormal tissue was found in the third ventricle and the retrocerebellar cyst, the diagnosis was made on subsequent spinal surgery and the MRI.

While cranial and spinal cord MRI with contrast is not considered in the initial diagnostic work-up in pediatric cases of so-called idiopathic hydrocephalus, after this preliminary experience, in our opinion it should be considered initially in selected cases of hydrocephalus without an evident diagnosis.

References

[1] Cinalli G, Sainte-Rose C, Lellouch-Tubiana A, Sebag G, Renier D, Pierre-Kahn A. Hydrocephalus associated with intramedullary low-grade

glioma. Illustrative cases and review of the literature. J Neurosurg 1995; 83: 480–485
[2] Rifkinson-Mann S, Wisoff JH, Epstein F. The association of hydrocephalus with intramedullary spinal cord tumors: a series of 25 patients. Neurosurgery 1990; 27: 749–754
[3] Prasad VS, Basha A, Prasad BC, Reddy DR. Intraspinal tumor presenting as hydrocephalus in childhood. Childs Nerv Syst 1994; 10: 156–157
[4] Schijman E, Zuccaro G, Monges JA. Spinal tumors and hydrocephalus. Childs Brain 1981; 8: 401–405
[5] Gelabert M, Bollar A, Paseiro MJ, Allut AG. Hydrocephalus and intraspinal tumor in childhood. Childs Nerv Syst 1990; 6: 110–112
[6] Oi S, Raimondi AJ. Hydrocephalus associated with intraspinal neoplasms in childhood. Am J Dis Child 1981; 135: 1122–1124
[7] Caviness JA, Tucker MH, Pia SK, Tam DA. Hydrocephalus as a possible early symptom in a child with a spinal cord tumor. Pediatr Neurol 1998; 18: 169–171
[8] Houten JK, Weiner HL. Pediatric intramedullary spinal cord tumors: special considerations. J Neurooncol 2000; 47: 225–230
[9] Jooma R, Hayward RD. Upward spinal coning: impaction of occult spinal tumors following relief of hydrocephalus. J Neurol Neurosurg Psychiatry 1984; 47: 386–390
[10] Kudo H, Tamaki N, Kim S, Shirataki K, Matsumoto S. Intraspinal tumors associated with hydrocephalus. Neurosurgery 1987; 21: 726–731
[11] Miller G, Towfighi J, Page RB. Spinal cord ganglioglioma presenting as hydrocephalus. J Neurooncol 1990; 9: 147–152
[12] Neau JP, Roualdes G, Bataille B, Boissonnot L, Muckensturm B, Salles M, Bontoux D, Gil R, Lefevre JP. [Intracranial hypertension and hydrocephalus caused by spinal cord tumors. Apropos of 3 cases]. Neurochirurgie 1987; 33: 216–219
[13] Purohit AK, Dinakar I, Sundaram C, Ratnakar KS. Anaplastic astrocytoma of the spinal cord presenting with features of raised intracranial pressure. Childs Nerv Syst 1990; 6: 113–115
[14] Bamford CR, Labadie EL. Reversal of dementia in normotensive hydrocephalus after removal of a cauda equina tumor. Case report. J Neurosurg 1976; 45: 104–107
[15] Maurice-Williams RS, Lucey JJ. Raised intracranial pressure due to spinal tumors: 3 rare cases with a probable common mechanism. Br J Surg 1975; 62: 92–95
[16] Zavala LM, Adler JR, Greene CS, Winston KR. Hydrocephalus and intraspinal tumor. Neurosurgery 1988; 22: 751–754
[17] Bakshi A, Patir R, Bakshi A, Banerji AK. A multifunctional, modified rigid neuroendoscopic system: clinical experience with 83 procedures. Technical note. J Neurosurg 2003; 99: 421–425
[18] Macarthur DC, Buxton N, Punt J, Vloeberghs M, Robertson IJ. The role of neuroendoscopy in the management of brain tumors. Br J Neurosurg 2002; 16: 465–470
[19] Sainte-Rose C, Cinalli G, Roux FE, Maixner R, Chumas PD, Mansour M, Carpentier A, Bourgeois M, Zerah M, Pierre-Kahn A, Renier D. Management of hydrocephalus in pediatric patients with posterior fossa tumors: the role of endoscopic third ventriculostomy. J Neurosurg 2001; 95: 791–797
[20] Gangemi M, Maiuri F, Colella G, Sardo L. Endoscopic surgery for large posterior fossa arachnoid cysts. Minim Invasive Neurosurg 2001; 44: 21–24
[21] Matula C, Reinprecht A, Roessler K, Tschabitscher M, Koos WT. Endoscopic exploration of the IVth ventricle. Minim Invas Neurosurg 1996; 39: 86–92
[22] Feng H, Huang G, Liao X, Fu K, Tan H, Pu H, Cheng Y, Liu W, Zhao D. Endoscopic third ventriculostomy in the management of obstructive hydrocephalus: an outcome analysis. J Neurosurg 2004; 100: 626–633
[23] Schroeder HW, Oertel J, Gaab MR. Endoscope-assisted microsurgical resection of epidermoid tumors of the cerebellopontine angle. J Neurosurg 2004; 101: 227–232

Original Paper

Pediatric Neurosurgery

Pediatr Neurosurg 2010;46:442–449
DOI: 10.1159/000327220

Received: February 14, 2011
Accepted: March 7, 2011
Published online: May 3, 2011

Cerebral Anomalies and Chiari Type 1 Malformation

Marcelo Galarza[a] Juan F. Martínez-Lage[a] Steven Ham[b] Sandeep Sood[b]

[a]Regional Service of Neurosurgery, 'Virgen de la Arrixaca' University Hospital, Murcia, Spain;
[b]Department of Neurosurgery, Children's Hospital of Michigan, Detroit, Mich., USA

Key Words
Cerebellar tonsillar ectopia · Chiari type 1 malformation · Cerebral dysgenesis · Hydrocephalus · Congenital central nervous system malformations · Craniovertebral junction

Abstract
Objective: To analyze the association of diverse cerebral anomalies in a series of pediatric patients with cerebellar tonsillar ectopia. ***Methods:*** We reviewed the medical records of 60 children diagnosed with Chiari type 1 malformation (CM1), of these, 20 patients (11 boys and 9 girls; mean age 7.2 years, range 2–16 years) had an associated cerebral anomaly. Symptoms of tonsillar ectopia evolved over a mean of 12 months (range 3 months to 4 years). Syringomyelia was present in 5 cases. All patients underwent a posterior fossa decompression. ***Results:*** Disclosed anomalies included: congenital hydrocephalus (n = 11), cervicomedullary kinking (n = 5), focal cerebral heterotopia with epilepsy (n = 4), partial agenesis of the corpus callosum (n = 4), hypoplastic brain stem (n = 2), holoprosencephaly (n = 1), and subcortical dysplasia in the context of neurofibromatosis type 1 (n = 1). Other malformations included: subcortical hamartoma associated with neurofibromatosis type 1, craniofacial dysmorphism secondary to Noonan syndrome, congenital occipital plagiocephaly, os odontoideum, craniofacial cleft, juvenile rheumathoid arthritis with platybasia, and osteogenesis imperfecta with bathrocephaly and scoliosis. ***Conclusion:*** Craniocerebral anomalies in children treated for CM1 may be found consistently. The association of hydrocephalus, which was the most common anomaly in this cohort, with cerebellar tonsillar ectopia may contribute to a poor outcome in regard to tonsillar herniation symptoms.

Introduction

According to Sarnat [1], dysgenesis or malformation are synonymous terms that refer to any tissue that is imperfectly developed during embryonic or fetal life. The term includes heterotopia, hamartoma, dysplasia and hypoplasia collectively and may refer to global disorders in which the entire organ is malformed or to focal abnormalities within an otherwise normal organ.

Chiari [2] initially described cerebellar tonsillar ectopia as 'alterations in the cerebellum resulting from cerebral hydrocephalus'. These features were demonstrated in a 'relatively large percentage of cases of chronic congenital hydrocephalus but never without hydrocephalus or in cases of acute or later-developing hydrocephalus'. More recently, Chiari type 1 malformation (CM1) in pediatric

KARGER

Fax +41 61 306 12 34
E-Mail karger@karger.ch
www.karger.com

1016–2291/10/0466–0442$26.00/0

Accessible online at:
www.karger.com/pne

Marcelo Galarza, MD, MSc
Regional Service of Neurosurgery
Hospital Universitario Virgen de la Arrixaca
ES–30120 Murcia (Spain)
Tel. +34 968 369 489, E-Mail marcelo.galarza@carm.es

series has also been associated with congenital hydrocephalus [3].

On the other hand, reported cerebral dysgeneses in association with CM1 include cortical dysplasia with epilepsy [4, 5], corpus callosum dysgenesis [6], cervicomedullary kinking [7], tectal beaking [3], brain stem hypoplasia [7] and forking of the aqueduct [3]. Other reported associated anomalies comprise: primary arachnoid cyst [1], aplasia of the temporal fossa [8], cerebral manifestations of neurofibromatosis type 1 [9], craniosynostosis [10–12], Noonan syndrome [13, 14], otopalatodigital syndrome [15], and a variety of craniovertebral junction abnormalities [16–18].

Tonsillar ectopia is the hallmark of CM1 but, as long as there are broader and detailed series on pediatric CM1, the association with other anomalies may be more common, as has been reported in previous articles [1, 3, 19].

We conducted a retrospective analysis of associated cerebral dysgeneses from an original surgical series of 60 children diagnosed with CM1 [16]. We categorized the associated anomalies and examined the patients' surgical outcomes regarding cerebellar tonsillar herniation symptoms.

Clinical Material and Methods

Sixty children had surgical treatment for relieving symptoms of CM1. A retrospective analysis of surgical outcome was reported extensively [16]. Twenty of them, 11 boys and 9 girls, with a mean age of 7.2 (range 2–16) years had an associated hydrocephalus or feature of cerebral dysgenesis. The patients' main characteristics are summarized in table 1.

The most common clinical complaint associated with CM1 was pain limited to the occipitocervical region. Irritability was seen in 2 nonverbal patients associated with upper extremity weakness. Four children presented with ataxia in conjunction with either vocal cord paralysis or staring spells. Mean clinical evolution was 12 months with a range from 3 months to 4 years. The last patient developed nuchalgia and was diagnosed with hydrocephalus and callosal agenesis. Psychomotor delay was found in 2 children (patients No. 4 and 16), mental delay in 2 (patients No. 10 and 20) and attention-deficit disorder in 2 further patients (patients No. 13 and 15).

Cerebral magnetic resonance (MR) imaging disclosed a cerebellar tonsil descent into the cervical canal that reached the posterior arch of C1 in 15 patients and the lamina of C2 in 5 patients. Preoperative cine phase-differential mode MR imaging was performed in 12 patients that demonstrated impaired or absent flow at the posterior foramen magnum in all cases. Five patients had syringomyelia, involving the cervical cord in 4 and the cervicothoracic region in 1. A right thoracic scoliosis was diagnosed in 2 children (patients No. 13 and 20).

Table 1. Association of cranial and cerebral dysgeneses in a series of 20 pediatric patients with CM1

Patient No.	Age years/sex	Preoperative clinical evolution	Main clinical complaint	Cerebral anomaly or dysgenesis	Other associated malformation	Syringomyelia
1	6/m	12 months	nuchalgia	hydrocephalus	no	no
2	10/f	12 months	nuchalgia	cervicomedullary kinking	os odontoideum	no
3	12/m	12 months	nuchalgia	hydrocephalus	no	no
4	10/f	4 years	ataxia	cervicomedullary kinking	hypoplastic brain stem, mild basilar invagination	no
5	15/m	12 months	ataxia	hydrocephalus	Noonan syndrome	cervicothoracic
6	6/f	12 months	nuchalgia	hydrocephalus	no	no
7	8/m	12 months	nuchalgia	temporal arachnoid cyst	platybasia, cervicomedullary kinking	cervical
8	4/m	3 months	nuchalgia	cervicomedullary kinking	hypoplastic brain stem, displaced vermis	no
9	5/f	12 months	nuchalgia	callosal agenesis	no	no
10	7/f	2 years	ataxia	cortical dysgenesis	facial cleft	cervical
11	16/f	12 months	nuchalgia	hydrocephalus	cortical dysplasia and epilepsy	no
12	6/m	12 months	ataxia	callosal agenesis	cervicomedullary kinking, tectal beaking	no
13	4/m	2 years	nuchalgia	subcortical hamartoma	neurofibromatosis type 1	cervical
14	4/f	12 months	nuchalgia	temporal arachnoid cyst	occipital plagiocephaly	no
15	7/m	4 years	tremors	hydrocephalus	callosal agenesis, cortical dysplasia and epilepsy, tectal beaking	no
16	2/m	12 months	upper extremity weakness	hydrocephalus	holoprosencephaly, cortical dysplasia and epilepsy, callosal agenesis, tectal beaking	no
17	2/f	12 months	upper extremity weakness	hydrocephalus	no	no
18	4/m	12 months	nuchalgia	hydrocephalus	no	no
19	7/m	4 years	nuchalgia	hydrocephalus	cortical dysplasia and epilepsy	cervical
20	9/f	12 months	nuchalgia	hydrocephalus	basilar invagination, batrocephaly, scoliosis	no

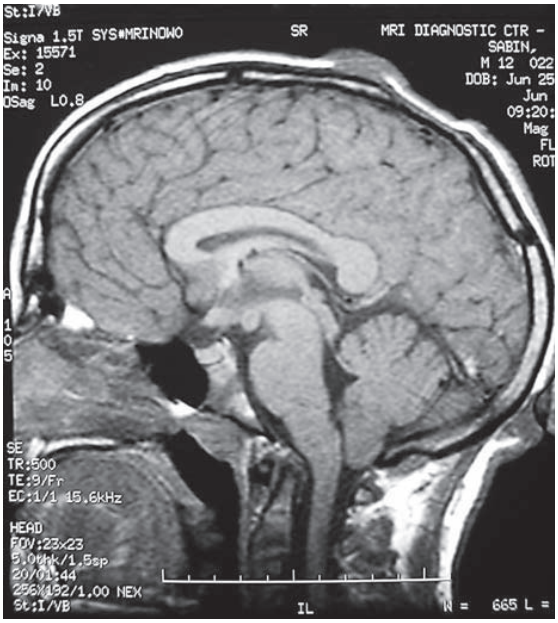

Fig. 1. Child No. 13 with a subcortical hamartoma associated with multiple scalp neurofibromas in the context of neurofibromatosis type 1 and CM1.

Eleven patients underwent ventriculoperitoneal shunting at the time of diagnosis of congenital hydrocephalus. Surgery for the CM1 included a suboccipital decompression with additional cadaveric pericardium duraplasty (n = 16) and suboccipital decompression with tonsillectomy and duraplasty (n = 4) in cases of syringomyelia. Additional syringosubarachnoid shunting was performed in 2 cases during the CM1 surgery.

Results

Congenital hydrocephalus was the most common anomaly associated with cerebellar tonsillar ectopia (n = 11) (table 2). Associated cerebral dysgenesis in our patients included cervicomedullary kinking (n = 5), focal cortical dysplasia with epilepsy (n = 4), partial agenesis of the corpus callosum (n = 4), tectal beaking (n = 3), hypoplastic brain stem (n = 2), forking of the aqueduct (n = 2), basilar invagination (n = 2) and temporal primary arachnoid cyst (n = 2). Other malformations included: upward displaced vermis, holoprosencephaly, subcortical hamartoma associated with neurofibromatosis type 1 (fig. 1), Noonan syndrome, occipital plagiocephaly, os odontoideum (fig. 2), craniofacial cleft, juvenile rheumatoid arthritis

Table 2. Clinical outcome and categorization of associated cranial and cerebral anomaly or dysgenesis in a series of 20 pediatric patients with CM1

Patient No.	Length of follow-up, years	Anomaly likely responsible for tonsillar ectopia	Number of dysgeneses	Last shunting for hydrocephalus	Other surgical treatment
1	1	hydrocephalus	single	LPS	no
2	3	no	multiple	N/A	C1-2 fusion
3	10	hydrocephalus	single	VPS	no
4	2	no	multiple	N/A	no
5	1	hydrocephalus	multiple	VPS	syringosubarachnoid shunt
6	2	hydrocephalus	single	VPS	no
7	1	platybasia	multiple	N/A	no
8	1	no	multiple	N/A	no
9	1	no	single	N/A	no
10	1	craniofacial dysmorphia	multiple	N/A	craniofacial repair
11	1	hydrocephalus	multiple	VAS	no
12	2	no	multiple	N/A	no
13	2	no	multiple	N/A	no
14	1	no	multiple	N/A	occipital reshaping
15	2	hydrocephalus	multiple	VAS	no
16	3	hydrocephalus	multiple	VPS	no
17	1	hydrocephalus	single	VPS	no
18	2	hydrocephalus	single	VPS	no
19	3	hydrocephalus	multiple	LPS	syringosubarachnoid shunt
20	1	hydrocephalus	multiple	VPS	craniofacial repair

Hydrocephalus, craniofacial or primary bone disorders were considered likely responsible for the cerebellar tonsillar herniation development. LPS = Lumboperitoneal shunt; VPS = ventriculoperitoneal shunt; VAS = ventriculoatrial shunt.

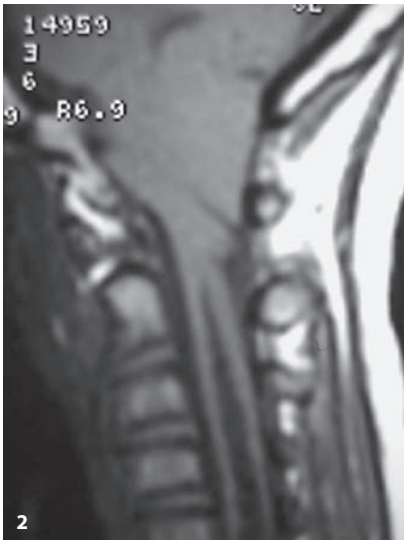

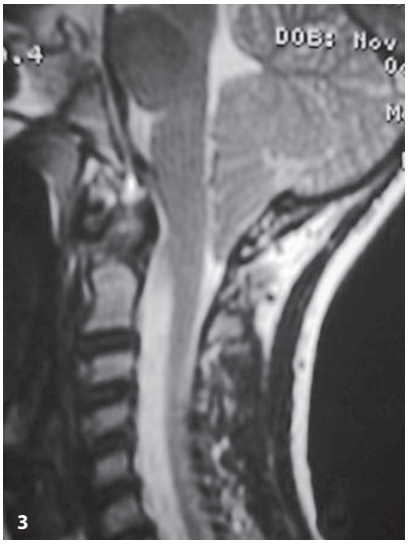

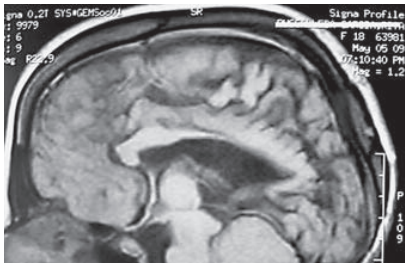

Fig. 2. Child No. 2 with os odontoideum and CM1; he later required C1/C2 arthrodesis.
Fig. 3. Child No. 7 has juvenile rheumatoid arthritis with secondary platybasia and CM1.

Fig. 4. Child No. 15 with partial callosal agenesis and beaked tectum in the context of hydrocephalus and CM1.

with platybasia (fig. 3), and osteogenesis imperfecta with bathrocephaly and scoliosis. Partial corpus callosum agenesis was seen associated with tectal beaking (fig. 4).

Of the initial 60 children treated for CM1 [16], 33% had cerebral anomalies, with 13 children having hydrocephalus or another anomaly that may have contributed to cerebellar tonsillar ectopia. Multiple dysgeneses were found in 14 patients.

All patients with congenital hydrocephalus were initially treated with a ventriculoperitoneal shunt, and 8 of them presented 4–15 years later with symptoms and imaging findings of tonsillar ectopia with (n = 2) or without syrinx. In patients initially diagnosed with both CM1 and hydrocephalus (patients No. 16, 17 and 18), imaging follow-up included head CT and brain MR imaging performed 2–4 months after shunting that showed resolution of hydrocephalus and ruled out shunt malfunction. However, the cerebellar tonsils failed to return to a normal position that was accompanied by a lack of patients' clinical improvement regarding nuchalgia or hand weakness. Accordingly, the children were submitted to posterior fossa decompression. We excluded those cases of hydrocephalus with secondary tonsillar ectopia on imaging studies that after shunting did not require surgery for tonsillar herniation.

Regarding Chiari symptoms, after a mean follow-up of 3 (range 1–10) years, total clinical recovery was seen in 4 children, and although these children had no hydrocephalus, they had other multiple cerebral dysgenetic features. Partial clinical improvement occurred in 16 patients who ameliorated in regard to ataxia, weakness and tremor. Of them, 4 children had some persisting nuchalgia at the time of evaluation for Chiari symptoms, which constituted their main clinical presentation. Three had shunted hydrocephalus with working shunts on imaging scanning, and 1 was found to have an indenting os odontoideum.

Additional shunt revisions were required in 5 of the 11 children with hydrocephalus after CM1 surgery, 4 children needing multiple revisions.

Complications occurred in 2 patients. Patient No. 10 developed a cerebrospinal fluid leakage that was treated with wound exploration and reclosure. Patient No. 12 had an intraoperative bleeding from the occipital sinus and presented a central cord syndrome during the immediate postoperative period; although on follow-up his cord syndrome had resolved, he had persisting ataxia.

In the cases treated with the tonsillar technique, no arachnoid adhesions were observed.

The syringomyelia was resolved in 4 children, as was evidenced at the first or second postoperative spinal MR imaging performed 5–8 months after surgery. Patient No. 5 who had a significant cervicothoracic syringomyelia received an additional syrinx shunt. Motor deficits in this

patient improved immediately after surgery, in spite of the fact that there was a decrease in syrinx size only at 1-year follow-up MR imaging. The clinical symptoms of patient No. 19 were cured as was his syrinx on follow-up imaging. Scoliosis, which was present in 2 cases, remained stable and accordingly spine surgery was not warranted.

Other surgical treatments included craniofacial repair in the child with osteogenesis imperfecta and bathrocephaly, and in another one with a facial cleft. A child with nonpositional occipital plagiocephaly underwent occipital reshaping. A 10-year-old girl with nuchalgia who was found to have a congenital os odontoideum along with C1-C2 instability was submitted to a C1-C2 posterior fusion after CM1 surgery; she barely improved from her nuchalgia at follow-up.

Cine phase-differential mode MR imaging was performed in 12 patients who had persistence of symptoms. A bidirectional pulsating cerebrospinal fluid flow around the basal cisterns was seen in all cases, anterior to the spinal cord and in the region of the foramen of Magendie.

Discussion

We have reported a cohort of 20 children treated for symptoms of CM1 that have associated other craniocerebral anomalies. Several types of dysgeneses were present in these patients. We classified these anomalies in two groups: hydrocephalus and other dysgeneses, in an attempt to better categorize this association.

Congenital hydrocephalus was the most common anomaly. Yet, we have also disclosed anomalies like focal cortical dysplasia, partial agenesis of the corpus callosum and brain stem abnormalities, cervicomedullary kinking, midbrain deformities, hypoplastic brain stem, and forking of the aqueduct. Nonetheless, all these found brain stem anomalies are more common in Chiari type 2 than in CM1 patients [1]. A malformation in which a CM1 is seen in combination with brain stem herniation through the foramen magnum has been named Chiari type 1.5 [3, 20]. Cervicomedullary kinking, found in 5 children, was the most common brain stem anomaly, while other defects included brain stem hypoplasia and forking of the aqueduct. Midbrain deformity, often found in Chiari type 2 patients [7], was seen in a further 3 cases and a displaced vermis in another child. Callosal dysgenesis consisting of hypoplastic splenium and rostrum of the corpus callosum was reported in these patients [6], and we also found 4 cases with a partial corpus callosum agenesis, mainly of its anterior third. As previously reported [1, 19] and according to our observations, some children presenting with lower cranial nerve dysfunction did not ameliorate even after adequate decompression of the posterior fossa as shown on cerebrospinal fluid flow studies, as may happen with some patients with Chiari malformation type 2. This fact may be due to a primary or secondary structural damage of the brain stem nuclei themselves. To our knowledge, there have been no previous reports on intrinsic brain stem dysgeneses occurring in CM1 patients. We failed to report on any other combined Chiari type 2 malformations such as tethered cord, myelodysplasia, or enlarged massa intermedia, though we found all other shared features.

Cerebral and Cranial Dysgeneses

CM1 evolving with seizures or neurodevelopmental deficits, or both, has been previously reported [21]. CM1 patients with seizures had been shown to have hypoperfusion on imaging studies that may represent the functional expression of cerebral microdysgenesis [5]. CM1 cases with mental retardation, speech delay, and epilepsy have been reported as a possible specific disorder [4]. Four children in our series had focal cortical dysplasia associated with epilepsy; one of them was diagnosed with motor-mental developmental delay and the other with an attention-deficit disorder; but we failed to disclose a specific speech disorder in these children.

Subcortical hamartoma associated with neurofibromatosis type 1 was seen in one of our CM1 patients. An association of this kind has been previously documented [3, 9].

Noonan syndrome is a relatively common, but genetically heterogeneous autosomal dominant malformation syndrome. Proportionate short stature, a dysmorphic face, and congenital heart defects constitute the characteristic features of this entity [14]. There are 3 reported cases of Noonan syndrome with CM1 [13], and we describe a fourth instance of this association.

CM1 cases with skull and spine anomalies, such as oxycephaly [11], metopic ridging [12], bone dysplasias including acro-osteolysis, basilar invagination [22] and various vertebral anomalies [10] have also been reported. Craniosynostosis involving the posterior sagittal suture results in a characteristic skull deformity known as bathrocephaly, which is marked in the posterior scalp by a prominent stair. We have observed a child with this feature. Also, we operated another case with marked deformity due to congenital occipital plagiocephaly. Menezes [18] described primary craniovertebral anomalies, such

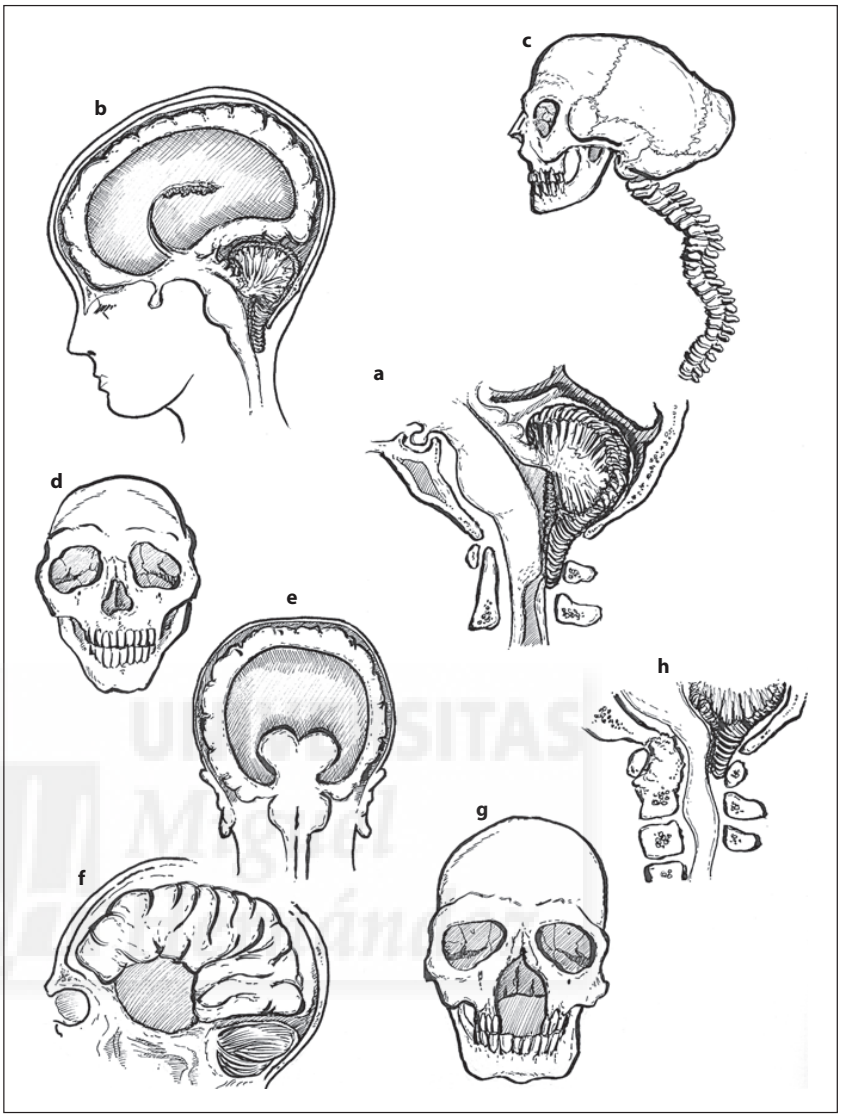

Fig. 5. Artistic depiction of dysgeneses associated with cerebellar tonsillar ectopia (**a**). Hydrocephalus (**b**) was the most common anomaly that may be considered directly related to tonsillar herniation causation. Others included: bathrocephaly and scoliosis secondary to osteogenesis imperfecta (**c**), craniofacial dysmorphism secondary to Noonan syndrome (**d**), alobar holoprosencepahly (**e**), large primary arachnoid cysts (**f**), craniofacial cleft (**g**) and juvenile rheumatoid arthritis with secondary platybasia (**h**).

as proatlas remnants, atlas assimilation and vertebral segmentation defects. We also disclosed 3 cases of basilar invagination, a case of os odontoideum and another of cervical segmentation defect with associated scoliosis. While the principal pathological characteristic is a reduction in posterior cranial fossa volume in patients who had both basilar invagination and Chiari malformation [17, 22, 23], a small posterior fossa may also indicate fourth occipital sclerotome abnormalities [18].

Extensive craniofacial and vertebral abnormalities, including aplasia of the floor of the left middle fossa and posterior cranial fossa, and articulation of the left mandibular condyle with the basal temporal lobe were described in a patient with CM1 [8]. These anomalies could represent a specific disorder of the para-axial mesoderm. Similarly, the association of otopalatodigital syndrome type 2 and CM1 has also been reported [15]. In this regard, 1 of our patients had a craniofacial cleft and 2 other a temporal primary arachnoid cyst.

Associated Dysgenesis and Clinical Outcome Regarding CM1 Symptoms

Isolated cerebral dysgenesis was seen in 6 children in our series. Five had hydrocephalus and 1 a partial ante-

rior callosal agenesis. Two of them improved partially after surgery (patients No. 12 and 17). Multiple cerebral dysgeneses were noted in 14 children and 4 without hydrocephalus completely recovered from their symptoms after CM1 surgery, while the remaining ones showed partial improvement. Patient No. 10 was completely cured of her ataxia and her cervical syrinx was resolved after CM1 surgery. This patient also underwent craniofacial repair for a facial cleft. Fourteen patients required additional procedures, namely ventricular shunting, syrinx shunting, craniofacial repair, spinal fusion and craniostenosis repair.

Although an extensive discussion regarding surgical outcome is beyond the scope of this article, additional surgery was not, per se, a factor contributing to a poor outcome of tonsillar herniation symptoms, mainly because the majority of these patients required initial shunting or shunt revision for treatment of their hydrocephalus. Eventually, patients with hydrocephalus or with multiple cerebral dysgeneses will have a fair clinical outcome in regard to tonsillar herniation symptoms. Nevertheless, other than hydrocephalus, no other anomaly had an influence on the resolution of syringomyelia or cerebellar symptoms.

Hydrocephalus and Cerebral Dysgeneses

We categorized these cases as having hydrocephalus (fig. 5), when the anomaly was probably responsible for the development of cerebellar tonsillar ectopia, or as having other dysgeneses, when the dysgenesis was liable to be independent of the cerebellar tonsillar ectopia causation; however, they may be linked because of an underlying predisposition to dysgenesis, such as occurs in neurofibromatosis type 1. A familial predisposition to CM1 was previously reported in an extensive series [22]. Indeed, the term dysgenesis may not be accurate in describing a cytoarchitecturally normal brain with hydrocephalus.

Hydrocephalus, as previously documented by Chiari [2] and others [3], was the most common associated cerebral anomaly in this cohort. A first group was classified as having hydrocephalus with secondary tonsillar ectopia. These patients required later posterior fossa decompression because of persisting clinical and imaging findings of persisting tonsillar ectopia, even after successful treatment of hydrocephalus. A second group of 8 children, with long-term shunted hydrocephalus, may have a subsequent posterior fossa shrinking with a secondary tonsillar herniation [19, 23]. This may be an acquired condition rather than a congenital one. However, we do not know if these patients also had cerebellar tonsillar ectopia at the time of diagnosing hydrocephalus because of lacking MR imaging studies in newborns at that time. We excluded those cases of hydrocephalus with secondary tonsillar herniation or syringomyelia on MR imaging studies that after shunting did not warrant surgery for tonsillar herniation or syrinx symptoms (n = 32).

Our patient population may reflect a significant tertiary care referral bias for CM1 and hydrocephalus. It is, therefore, unlikely that this selected group reflects the natural history or clinical patterns of cerebellar tonsillar ectopia and hydrocephalus in the pediatric population.

Also, we disclosed many dysgenetic features that are more commonly seen in patients with Chiari type 2 malformation, i.e. tonsillar ectopia with myelomeningocele. Most features in this group were associated brain stem anomalies.

One relative caveat is that our patients were preselected, so it remains uncertain how frequently the dysgenetic findings actually are present in CM1 patients. Our quest was directed towards a surgical series, to categorize different cerebral and cranial dysgeneses associated with CM1, and to indicate that this link is probably more usual than previously described. Even though, this hypothesis must be supported with a sizeable, nonselected group of patients, from multicenter recruitment.

References

1 Sarnat HB: Cerebral Dysgenesis: Embryology and Clinical Expression. New York, Oxford University Press, 1992, pp 333–348.
2 Chiari H: Über Veränderungen des Kleinhirns infolge von Hydrocephalie des Grosshirns (in German). Dtsch Med Wschr 1891; 17:1172–1175.
3 Tubbs RS, McGirt MJ, Oakes WJ: Surgical experience in 130 patients with Chiari I malformation. J Neurosug 2003;99:291–296.
4 Grosso S, Scattolini R, Paolo G, Di Bartolo RM, Morgese G, Balestri P: Association of Chiari I malformation, mental retardation, speech delay, and epilepsy: a specific disorder? Neurosurgery 2001;49:1099–1104.
5 Iannetti P, Spalice A, De Felice Ciccoli C, Bruni O, Festa A, Maini CL: Seizures in paediatric Chiari type I malformation: the role of single-photon emission computed tomography. Acta Paediatr 2002;91:313–317.
6 Sener RN: Chiari I malformation associated with callosal dysgenesis and ectopic neurohypophysis. Comput Med Imaging Graph 1995;19:487.
7 Hunter JV, Youl BD, Moseley IF: MRI demonstration of midbrain deformity in association with the Chiari malformation. Neuroradiology 1992;34:399–401.

8 Mesiwala AH, Shaffrey CI, Gruss JS, Ellenbogen RG: Atypical hemifacial microsomia associated with Chiari I malformation and syrinx: further evidence indicating that Chiari I malformation is a disorder of the paraaxial mesoderm. Case report and review of the literature. J Neurosurg 2001;95:1034–1039.
9 Battistella PA, Perilongo G, Carollo C: Neurofibromatosis type 1 and type I Chiari malformation: an unusual association. Childs Nerv Syst 1996;12:336–338.
10 Lin KY, Gampper TJ, Jane JA Sr: Correction of posterior sagittal craniosynostosis. J Craniofac Surg 1998;9:88–91.
11 Renier D, Cinalli G, Lajeunie E, Arnaud E, Marchac D: Oxycephaly, a severe craniosynostosis. Apropos of a series of 129 cases (in French). Arch Pediatr 1997;4:722–729.
12 Tubbs RS, Elton S, Blount JP, Oakes WJ: Preliminary observations on the association between simple metopic ridging in children without trigonocephaly and the Chiari I malformation. Pediatr Neurosurg 2001;35:136–139.
13 Colli R, Colombo P, Russo F, Sterpa A: Type 1 Arnold Chiari malformation in a subject with Noonan syndrome (in Italian). Pediatr Med Chir 2001;23:61–64.
14 Holder-Espinasse M, Winter RM: Type 1 Arnold-Chiari malformation and Noonan syndrome. A new diagnostic feature? Clin Dysmorphol 2003;12:275.
15 Hung PC, Wang HS, Lui TN: Association of oto-palato-digital syndrome type II and Arnold-Chiari I malformation in an infant. Brain Dev 1999;21:488–490.
16 Galarza M, Sood S, Ham S: Impact of surgical strategies in Chiari type I malformations: analysis in 60 patients. Childs Nerv Syst 2007:32:121–125.
17 Goel A, Bhatjiwale M, Desai K: Basilar invagination: a study based on 190 surgically treated patients. J Neurosurg 1998;88:962–968.
18 Menezes AH: Primary craniovertebral anomalies and the hindbrain herniation syndrome (Chiari I): data base analysis. Pediatr Neurosurg 1995;23:260–269.
19 Lazareff JA, Galarza M, Gravori T, Spinks TJ: Tonsillectomy without craniectomy for the management of infantile Chiari I malformation. J Neurosurg 2002;97:1018–1022.
20 Tubbs RS, Iskandar BJ, Bartolucci AA, Oakes WJ: A critical analysis of the Chiari 1.5 malformation. J Neurosurg 2004;101 (2 suppl):179–183.
21 Brill CB, Gutierrez J, Mishkin MM: Chiari I malformation: association with seizures and developmental disabilities. J Child Neurol 1997;12:101–106.
22 Milhorat TH, Chou MW, Trinidad EM, et al: Chiari I malformation redefined: clinical and radiographic findings for 364 symptomatic patients. Neurosurgery 1999;44:1005–1017.
23 Stovner LJ, Bergan U, Nilsen G, Sjaastad O: Posterior cranial fossa dimensions in the Chiari I malformation: relation to pathogenesis and clinical presentation. Neuroradiology 1993;35:113–118.

Neurosurg Rev
DOI 10.1007/s10143-010-0262-9

ORIGINAL ARTICLE

Posterior fossa arachnoid cysts and cerebellar tonsillar descent: short review

Marcelo Galarza · Antonio López López-Guerrero · Juan F. Martínez-Lage

Received: 23 November 2009 / Revised: 7 March 2010 / Accepted: 8 March 2010

Abstract The objective of this study was to analyze the association of cerebellar tonsillar descent and syringomyelia in patients with posterior fossa arachnoid cysts. We reviewed the medical records of ten patients (mean, age 33; range, 24–49 years) diagnosed with posterior fossa arachnoid cyst and tonsillar descent. Symptoms evolved over a mean of 12 months (range, 6 months to 3 years). Syringomyelia was present in six cases. Six patients underwent a suboccipital craniectomy, three cases underwent an additional C1 laminectomy, and a further case had a limited craniectomy and tonsillar reduction. Three patients were also treated for hydrocephalus: one with a ventriculoperitoneal shunt and two with endoscopic third ventriculostomy. Two patients had conservative treatment. The posterior fossa arachnoid cysts were located at the vermis-cisterna magna (n=4), the cerebellar hemispheres (n=2), the cerebellopontine angle (n=3), and the quadrigeminal cistern (n=1). A patient with achondroplasia showed features of platybasia. Associated malformations included craniofacial dysmorphism in a patient diagnosed of trichorhinophalangeal syndrome and a case with a primary temporal arachnoid cyst. After a mean follow-up of 2 years (range, 3 months to 5 years), four patients showed resolution of their neurological symptoms, and two exhibited persisting ocular findings. Headaches and nuchalgia improved in four cases and persisted in four. Syringomyelia was resolved in four patients and improved in two. Patients harboring a posterior fossa arachnoid cyst may evolve with acquired Chiari malformation and syringomyelia. Initial management should be directed to decompressing the foramen magnum and should include the resection of the arachnoid cyst's walls. A wait-and-see attitude can be implemented in selected cases. In our experience, hydrocephalus should be properly addressed before treating the arachnoid cyst.

Keywords Chiari type 1 malformation · Arachnoid cyst · Cerebellum · Posterior fossa · Cerebral dysgenesis · Hydrocephalus · Syringomyelia · Tonsillar descent

Introduction

Chiari malformation type I (CM-1) is a congenital disorder resulting from a faulty development of the paraxial mesoderm [16, 17]. It is characterized by a reduced volume of the posterior fossa and by the caudal displacement of the cerebellar tonsils through the foramen magnum into the cervical canal [6, 8]. Syringomyelia has been associated with many intracranial and spinal anomalies. CM-1 malformation and syringomyelia present with clinical manifestations of posterior fossa or foramen magnum involvement, i.e., head and neck pain, retro-ocular pain, cerebellar signs, cranial nerve dysfunction, sleep apnea, and respiratory difficulty, or with those of spinal cord compression such as loss of fine movements, dysesthesias, dissociated sensory loss, sensory level, spasticity, scoliosis, or sphincteric disturbances. Nonetheless, supratentorial and posterior fossa mass lesions, such as tumors or arachnoid cysts, may also result in tonsillar herniation with or without syringomyelia [5]. Obstruction of cerebrospinal fluid (CSF) flow may lead to an increased pulse pressure within the spinal canal that may force the entry of CSF into the spinal cord [19]. There have been several reports of large

M. Galarza (✉) · A. L. López-Guerrero · J. F. Martínez-Lage
Regional Service of Neurosurgery,
"Virgen de la Arrixaca" University Hospital,
El Palmar,
30120 Murcia, Spain
e-mail: marcelo.galarza@carm.es

Published online: 18 May 2010

arachnoid cysts in the posterior fossa associated with syrinx [2, 4, 7, 9, 11, 18–22, 24, 25].

Arachnoid cysts are benign collections of CSF that develop as the result of an abnormal duplication of the arachnoid membranes during brain development. They may lead to symptoms according to their location, but more often, their symptoms are unspecific [10]. Whether these two malformations are concomitant rather than caused by the presence of one of them is not clear. Obstruction of CSF flow is most commonly caused by the Chiari malformation and by crowding of the posterior fossa structures. A different mechanism has been proposed that attributes the development of tonsillar herniation and syringomyelia to the push exerted by a retrocerebellar arachnoid cyst [4, 14, 15]. The aim of this paper is to report a series of adult patients with CM-1 associated with the presence of an extra-axial cerebellar cyst, six of them with associated syringomyelia, and discuss its management.

Clinical material and methods

Included in this survey were ten patients (seven male and three female), with mean age of 33 (range, 23–49) years, who presented with clinical and imaging findings of a tonsillar descent together with a posterior fossa arachnoid cyst. We reviewed these individuals' medical records in regard to symptoms and signs, neuroimaging findings, and operation charts (n=8) when applicable. The degree of tonsillar herniation, arachnoid cyst location and size, and the presence of hydrocephalus and of associated brain and osseous anomalies were investigated in the neuroimaging studies. Preoperative cranial and spinal magnetic resonance (MR) findings were reviewed and compared with those obtained along the patients' follow-up. Evolution and outcomes of the study group were obtained from the patients' medical records or by clinical revision at the outpatient clinic and classified in worsened, unchanged, improved, and complete recovery.

Results

Patients' characteristics and management

The patients' most common clinical complaint was headache, which was limited to the occipito-cervical region in two fof them. Retro-ocular pain was seen in two instances. Individuals with upper-extremity weakness had, in addition, dizziness or strabismus. One patient, diagnosed with a cervicothoracic syrinx and hydrocephalus, evolved with nuchalgia. Other symptoms included vertigo, nystagmus, acuphenos, and loss of hands' fine movements. No patient had a relevant medical history, such as prenatal infections, head trauma, or postnatal meningitis. The patients' main characteristics are summarized in Table 1 (Figs. 1, 2, 3, 4, 5, 6, 7, 8, 9, and 10).

Cranial MR imaging disclosed cerebellar tonsil descent into the cervical canal that reached the posterior arch of C-1 in four patients, the lamina of C-2 in other three cases, and the tectorial membrane in three remaining cases. Six patients had syringomyelia that involved the cervical cord (n=3) or the cervicothoracic region (n=3). Cine phase-differential mode MR imaging was not performed in our patients.

Of the three patients with hydrocephalus, two initially underwent endoscopic third ventriculostomy and the other ventriculoperitoneal shunting. Surgery for the tonsillar herniation included suboccipital decompression with duraplasty (n=5), with additional C1 posterior arch resection (n=3) and limited suboccipital decompression with tonsillectomy and duraplasty (n=1). Fenestration with ample resection of the cyst wall was done in five cases. No syringo-subarachnoid shunting was performed. The initial surgical technique employed was dictated from the main clinical manifestation and, regarding the posterior fossa, according to the surgeon's particular preference. Two patients with chronic headaches had a small cerebellopontine angle cyst and were treated conservatively with oral analgesics. Tonsillar descent in these two patients reached the posterior atlanto-occipital ligament in one case and the posterior arch of C1 in the other, and both had no syrinx. They had normal somatosensory and visual evoked potentials, normal ocular fundi and audiograms. Diffusion-weighted mode and contrast-enhanced MR and computed tomography (CT) imaging excluded the diagnosis of an epidermoid cyst. The patients' mean clinical evolution was 12 months with a range from 6 months to 3 years.

Posterior fossa lesions in our patients included vermian/mega cisterna magna (n=4), cerebellopontine angle (n=3), quadrigeminal cistern (n=1), and hemispheric cerebellar (n=2) arachnoid cysts. Other malformations included temporal primary arachnoid cyst, achondroplasia with platybasia, and craniofacial dysmorphism in the context of trichorhinophalangeal syndrome.

Mean follow-up time was 2 years (range, 6 months to 5 years). One patient with hydrocephalus and achondroplasia was initially treated with a ventriculoperitoneal shunt. Imaging follow-up, including CT and MR, in this patient, performed 8 months after surgery, showed resolution of hydrocephalus. The cerebellar tonsils returned to a normal position, which was accompanied by improvement of clinical symptoms. In another patient, who initially underwent a third ventriculostomy, the cerebellar tonsils returned to a normal position; her syrinx improved along with her clinical symptoms (Fig. 10). In another patient, firstly submitted to

Table 1 Clinical characteristics of ten adult patients with posterior fossa arachnoid cysts and Chiari type 1 malformation

Patient & Figure No.	Age (yrs)/Sex	Preoperative Clinical Evolution	Main Complaint	PFAC/Cerebral dysgenesis	Other clinical manifestation	Tonsillar Level descent/Preoperative Syringomyelia
1	45/M	6 months	Ataxia	Quadrigeminal	Nistagmus	C1/no
2	37/M	6 months	Frontal headaches	Midline/Hydrocephalus Platybasia	Ambliopia Achondroplasia	C1/cervical
3	39/M	3 years	Nuchalgia	Midline/Hydrocephalus	Strabismus UE weakness	C2/cervico-thoracic
4	26/M	18 months	Nuchalgia	Hemispheric	Retro-ocular pain UE weakness Dizziness	C2/cervical pre-syrinx
5	36/M	2 years	Dizziness	Midline	Nuchalgia TRP syndrome	C2/cervico-thoracic
6	33\M	3 years	Vertigo	Hemispheric/Temporal arachnoid cyst	Nuchalgia Acuphenos,	Occipital/no
7	27/M	1 year	Dizziness	Midline	Nuchalgia	C1/cervical
8	49/F	3 years	Frontal headaches	Cerebellopontine angle	Retro-ocular pain Dizziness UE weakness	C1/no
9	24/F	3 years	Frontal headaches	Cerebellopontine angle	Dizziness	Occipital/no
10	35/F	2 years	Dizziness	Cerebellopontine angle Hydrocephalus	Nuchalgia	Occipital/cervical-thoracic

PFAC posterior fossa arachnoid cyst, *C* cervical, *UE* upper extremity, *TRP* trichorhinophalangeal

third ventriculostomy, the cerebellar tonsils failed to return to a normal position, and this was accompanied by a lack of clinical improvement. Accordingly, this patient underwent surgery for his posterior fossa arachnoid cyst and tonsillar descent.

Clinical evolution and outcomes

The patients' clinical outcomes are summarized in Table 2. Five patients experienced a total clinical recovery: two with cerebellar hemispheric cysts, two with a vermian pouch and one with a quadrigeminal plate cyst. One of these patients had hydrocephalus and achondroplasia, while the other had a temporal arachnoid cyst. Three of them referred resolution of their headaches, while the other two referred to have ameliorated substantially.

A partial clinical improvement occurred in the remaining five individuals. These patients improved in regard to dizziness, ataxia, upper limb weakness, hand fine movements, and tremor. One of them had persisting strabism with resolved hydrocephalus and syrinx. All of these cases referred persisting headaches, which constituted their main clinical symptom at presentation. There were no surgical complications among our patients.

Regarding neuroimaging findings, syringomyelia was resolved in four patients and improved in two, as was evidenced at their first or second postoperative spinal MR performed 5 to 8 month after surgery. Patient 5, who had trichorhinophalangeal syndrome, presented with a significant cervicothoracic syringomyelia. This patient's motor deficits improved immediately after surgery, although a decrease in syrinx size was not appreciated until the MR study performed 1 year later.

Illustrative case report

A 38-year-old man presented with headaches, right arm weakness, and sensory loss to pain and temperature on his right hand of 24 month evolution. He also referred having had three episodes of drop attacks. On physical examination, the patient had a bilateral sixth cranial nerve paresis and loss of hearing on the left side. Motor strength and ability were diminished on his upper extremity, but there was no atrophy. Deep reflexes could not be elicited on the right arm. There was also dissociated hypoesthesia on his right arm and shoulder. MR showed a retrocerebellar arachnoid cyst, descent of the cerebellar tonsils, and a syringomyelic cavity extending from C2 to T6 together with hydrocephalus (Fig. 3). The patient underwent an endoscopic third ventriculostomy, after which the headaches markedly improved. A 6-month postoperative cerebral MRI study showed marked reduction of hydrocephalus but his posterior fossa cyst, cerebellar tonsil descent, and syringomyelia were

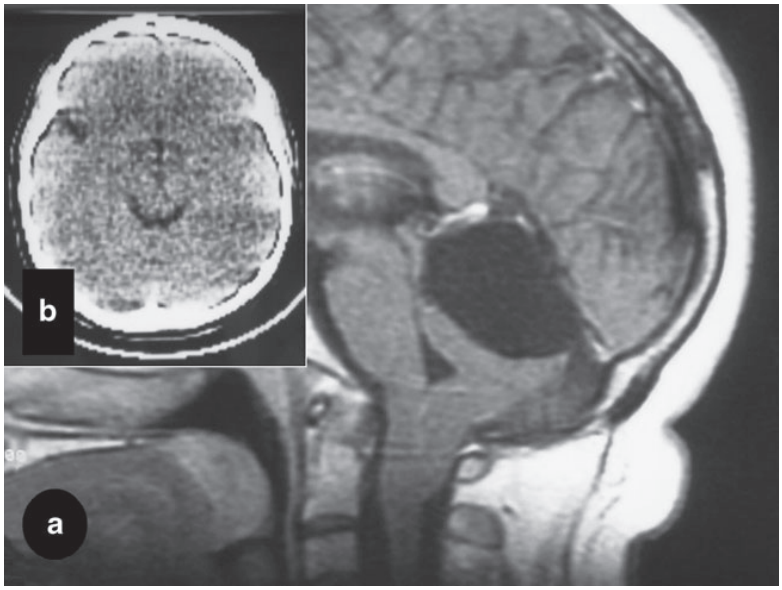

Fig. 1 **a** Patient 1. preoperative T1 sagittal MRI of a quadrigeminal posterior fossa arachnoid cyst compressing the upper vermis of the cerebellum and provoking secondary CM1 and **b** the same patient's CT scan made in the 1980s because of headaches without evidence of an arachnoid cyst

unchanged. The patient underwent a suboccipital craniectomy and Cl laminectomy with ample removal of the arachnoid cyst's walls. The dura mater was closed with a dural graft. Histopathological study of the excised tissues showed flattened cells of meningothelial origin on a loose fibrous wall with normal vessels. The patient made an uneventful recovery and, at 10-month follow-up visit, his objective neurological examination remained unchanged, although he had gained some strength on his right hand. A control MR showed normalization of the cerebellar tonsils' position and a significant shrinkage of the cervicothoracic syringomyelic cavity.

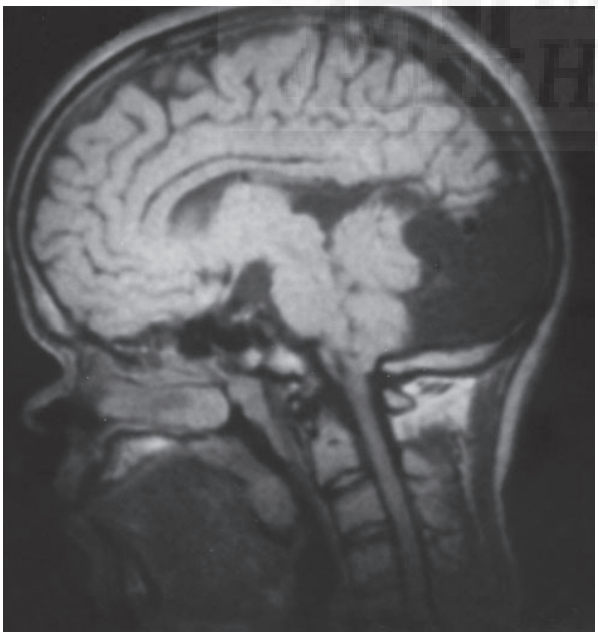

Fig. 2 Patient 2. MRI T1 sagittal shows in a patient with achondroplasia, hydrocephalus, and platybasia, a midline posterior fossa arachnoid cyst and associated Chiari I malformation. This patient had resolution of hydrocephalus, cervical syrinx, and Chiari symptoms after insertion of a VP shunt

Discussion

We report on ten patients in whom a posterior fossa arachnoid cyst was found associated with clinical and imaging findings of tonsillar heniation and syringomyelia in more than half of them. Two of our cases have been previously reported [14, 15]. Hans Chiari [8] described in 1891 this anomaly as one of the four types of hindbrain malformations. Evidence supports the hypothesis that the main problem in the Chiari I malformation is a posterior cranial fossa of smaller than normal volume [19]. The posterior fossa originates by endochondral ossification of the cartilaginous scaffold that forms the cranial base as well as the first four somites that model the occipital bone [4]. Marin-Padilla and Marin-Padilla [13] attributed the origin of the Chiari malformation to a primary defect in the development of the basicranium. Based on dynamic MRI studies, Oldfield et al. [19] proposed that the descended tonsils obstruct the CSF flow to and from the spinal compartment at the foramen magnum, thus explaining the appearance of syringomyelia. Several reports have documented tonsillar herniation and syringomyelia in a variety of conditions, including supra- and infratentorial tumors,

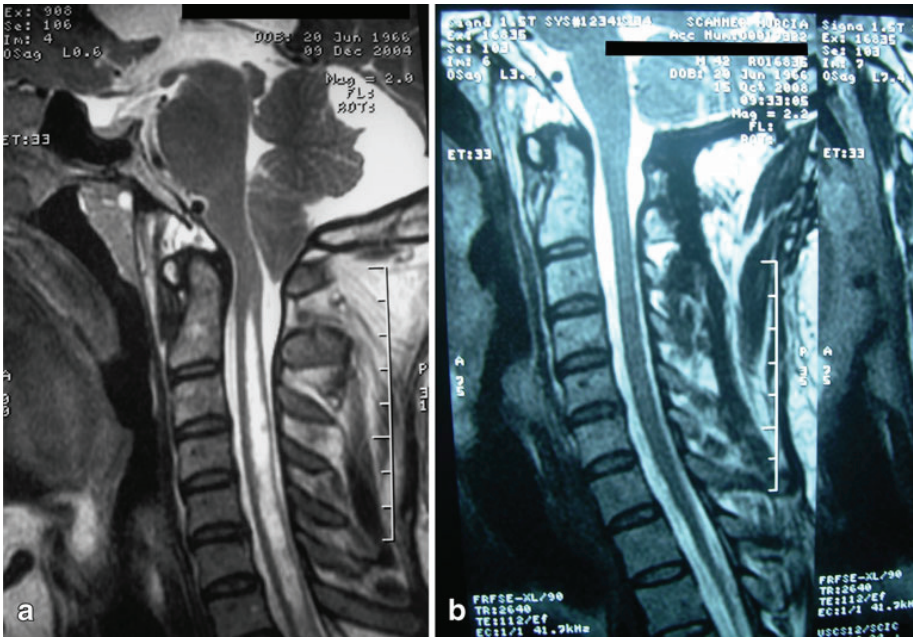

Fig. 3 **a** Patient 3. Preoperative T2 sagittal MRI image showing a midline posterior fossa arachnoid cyst associated with Chiari I malformation and syrinx from C2 to T1. This patient had a third ventriculostomy for hydrocephalus, before treating the posterior fossa with surgery (**b**)

pseudotumor cerebri, craniosynostosis, cranio-encephalic disproportion, overdrainage of CSF, or spinal CSF drainage [1, 2, 6]. Hence, in cases of so-called "acquired" Chiari malformation, it seems that there is a pressure gradient across the cranial and spinal compartments. According to one theory, syringomyelia results from obstruction to CSF flow at the foramen magnum and at the outlets of the fourth ventricle [1–3, 12].

We may assume that most, if not all, of our patients have an "acquired" CM-1. We cannot affirm that tonsillar descent is acquired, rather than we suggest it might constitute a combination with a developmental origin. The posterior fossa cyst in most of the presented cases appears to be the precipitating factor, as it presses down the lower part of the cerebellum through the foramen magnum. On the other side, we had cases with relatively small cysts of the cerebellopontine angle (cases 8–10), in whom the pressure exerted by the pouch, probably, was not sufficient to lead to CM-1.

Posterior fossa arachnoid cyst, syrinx, and hydrocephalus

The average delay in diagnosis of a Chiari malformation is 5 years after the onset of symptoms, leaving ample time for

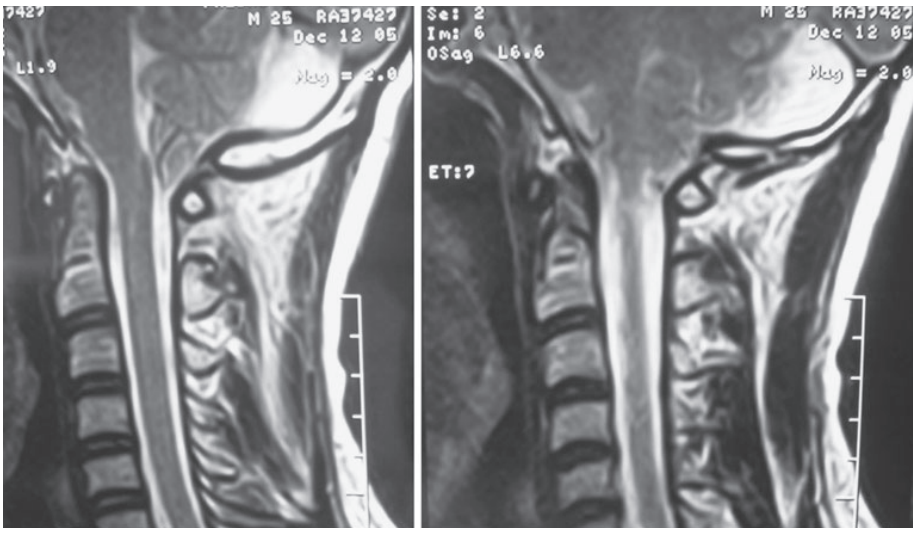

Fig. 4 Patient 4. T2 sagittal MRI of a preoperative image of a hemispheric posterior fossa arachnoid cyst, cervical presyrinx state, and CM1

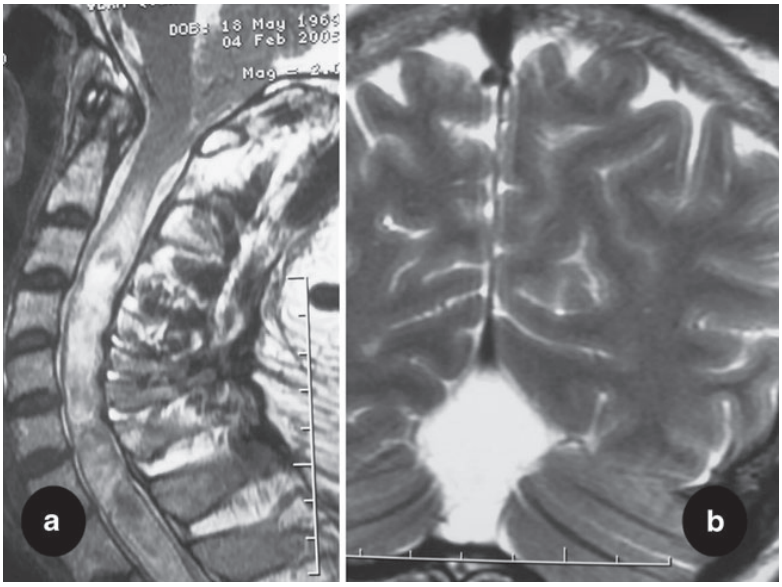

Fig. 5 **a** Patient 5. T2 sagittal showing a midline posterior fossa arachnoid cyst, Chiari I malformation, and significant cervicothoracic syrinx. **b** T2 coronal sequence of the same patient. Although the cyst was relatively small, after posterior fossa decompression and cyst fenestration, the patient improved his syrinx state

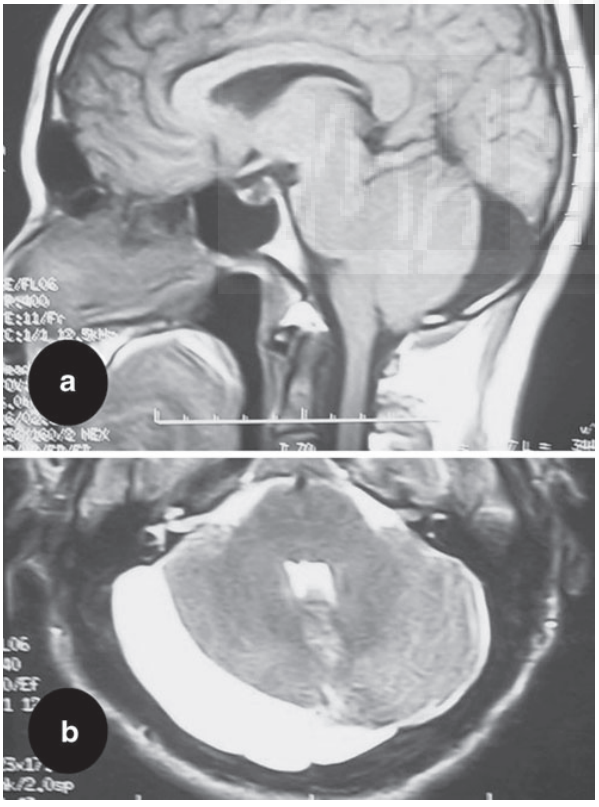

Fig. 6 **a** Patient 6. T1 axial MRI of an hemispheric posterior fossa arachnoid cyst. Note the important mass effect compressing right cerebellar hemisphere. **b** Same patient, an T2 sagittal image showing a secondary CM1

the development of syrinx formation [7]. Although an extensive discussion regarding the origin of syrinx is beyond the scope of this paper, we found 15 reported cases of syringomyelia in association with diverse cystic conditions of the posterior cranial fossa. Cystic lesions included congenital primary arachnoid cysts, Dandy–Walker malformation, Blake's pouch cyst, and posttraumatic CSF pouches [2, 4, 7, 9, 11, 18–22, 24]. However, all these instances were case reports. Tubbs et al. [23] reported two cases of mega cisterna magna in a series of pediatric CM-1. In previous documented cases, the obstruction to normal CSF flow through the foramen magnum was due to blockage caused by the cyst wall itself, and all manifested with coexistent syringomyelia [2, 4, 7, 9, 11, 18–22, 24, 25]. The reported cases with both CM-1 and posterior fossa cysts have been managed with a variety of procedures, including foramen magnum decompression, with or without cyst removal [4, 7, 9, 11, 20, 22, 24, 25], cysto-peritoneal shunting [21], or endoscopic cyst fenestration [18]. In addition, ten of these patients had hydrocephalus of varied severity that might have contributed to the formation of the syrinx. In our series, six cases had syringomyelia, and three of them hydrocephalus. After posterior fossa decompression along with cyst wall resection, insertion of a ventriculoperitoneal shunt (VPS), or third ventriculostomy, the syringomyelic cavity had improved or completely resolved.

Milhorat et al. [16] reviewed a series of 364 symptomatic patients with CM-1, and 43 of these patients had a familial history of CM-1 or syringomyelia, which suggests a genetic transmission. We had two patients with a strong genetic trait, namely, trichorhinophalangeal syndrome type

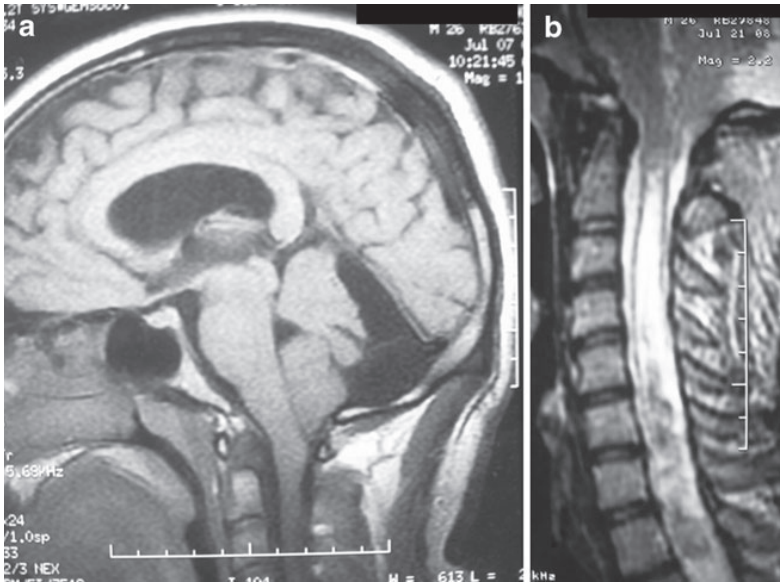

Fig. 7 **a**, **b** Patient 7. Preoperative T1 and T2 sagittal MRI image showing a midline posterior fossa arachnoid cyst associated with Chiari I malformation and syrinx from C2 to C6

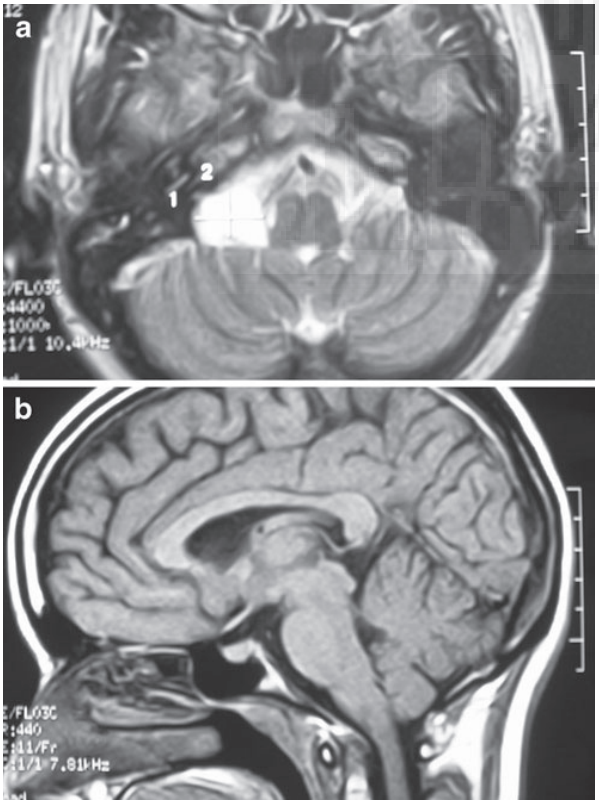

Fig. 8 **a** Patient 8. T2 axial image showing an arachnoid cyst in the right cerebellopontine angle and in sagital T1 sequence (**b**), the associated Chiari malformation with no syrinx. This patient was treated conservatively

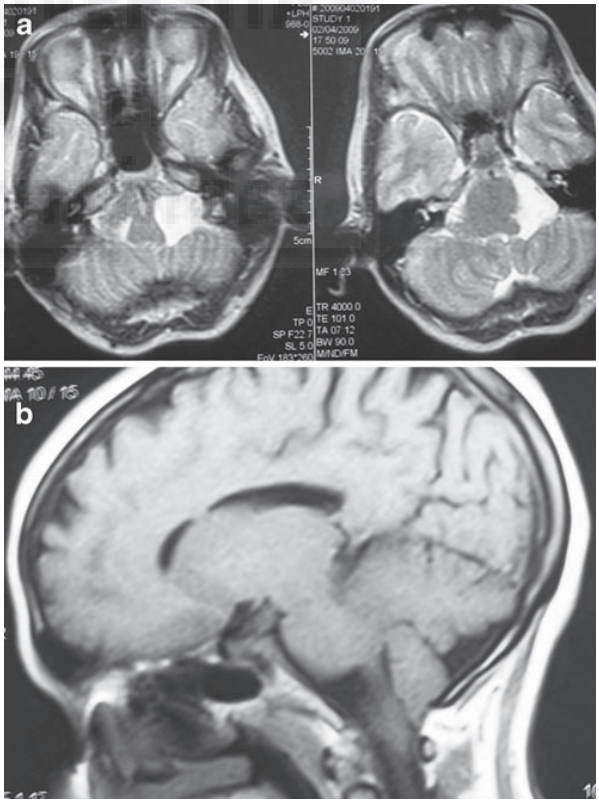

Fig. 9 **a** Patient 9. T2 MRI axial left cerebellopontine angle arachnoid cyst compressing brainstem and **b** its asssociated C1 Chiari malformation in T1 sagittal sequence

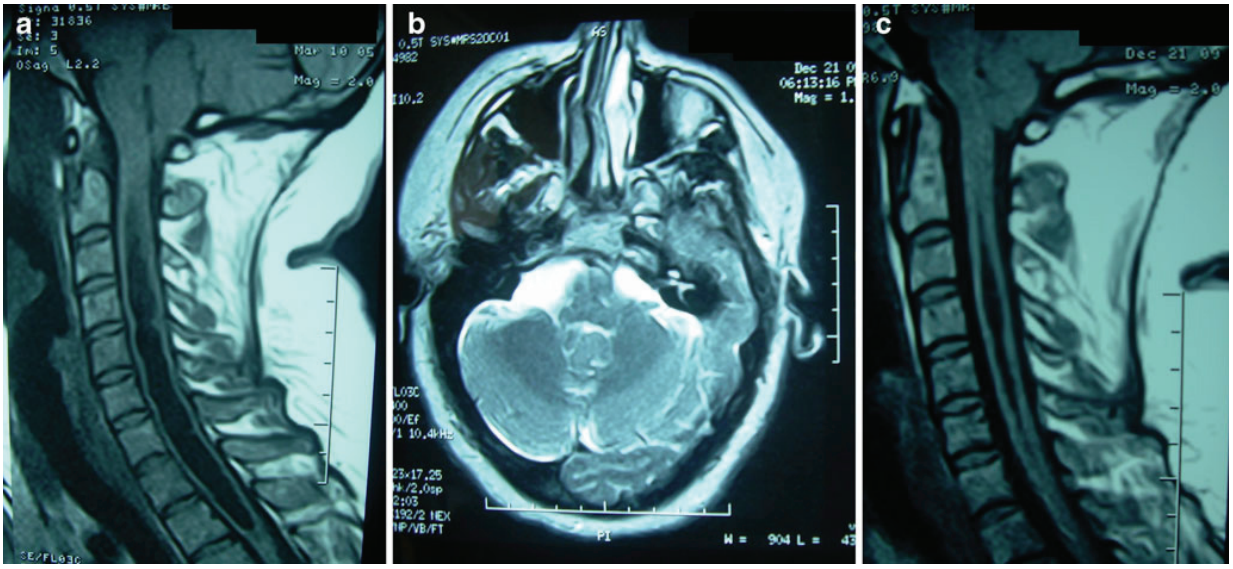

Fig. 10 **a** Patient 10. Preoperative T2-weighted MRI showing a cerebellopontine angle arachnoid cyst (**b**), tonsillar descent, and significant cervical syrinx formation on sagittal sequence. The patient had hydrocephalus (not shown). After a third ventriculostomy (**c**), it is evident the shrinking of the cervical syrinx along with upward movilization of the tonsils, with the PFAC remaining intact

I and achondroplasia. Patients with achondroplasia in all age groups generally have a small cranial base, whereas the rest of the skull is normal in size. This volume discrepancy may predispose patients to anomalous formation of the posterior fossa and of the foramen magnum, thus creating a smaller than normal posterior fossa. In our patient with achondroplasia and hydrocephalus, VPS was sufficient to resolve both the CM-1 and the syringomyelia. In another case with achondroplasia reported by Bauer et al. [4], the obstacle to CSF circulation through the foramen magnum was due to acquired Chiari malformation that, in turn, seemed to originate from the cerebellar displacement exerted by the push of the retrocerebellar arachnoid cyst. Chiari malformation and syringomyelia in our other cases

Table 2 Surgical and conservative treatment and evolution of clinical characteristics in patients with posterior fossa arachnoid cysts associated with Chiari type 1 malformation

Patient number	Length of follow-up	Surgical treatment of PFAC and CM1	Treatment for hydrocephalus	Outcome	Headaches evolution	Syrinx evolution
1	3 years	Bone decompression/fenestration	–	Total recovery	–	–
2	1 year	None	VPS	Persisting ambliopia	Resolved	Resolved
3	5 year	Bone decompression/fenestration/duraplasty/C1 resection	Third ventriculostomy	Persisting strabism	Persisting nuchalgia	Resolved
4	3 year	Bone decompression/fenestration/duraplasty/C1 resection	–	Total recovery	Improved nuchalgia	Resolved
5	2 year	Bone decompression/fenestration/duraplasty/C1 resection	–	Total recovery	Persisting headaches	Improved
6	6 months	Bone decompression/fenestration/duraplasty/ tonsillar reduction	–	Total recovery	Improved nuchalgia	–
7	6 months	Bone decompression/fenestration	–	Total recovery	Improved nuchalgia	Resolved
8	3 years	None	–	Some dizziness	Persisting headaches	–
9	6 months	None	–	Some dizziness	Persisting headaches	–
10	3 years	None	Third ventriculostomy	Total recovery	Improved	Improved

must have been the consequence of the pressure exerted by the retrocerebellar cyst, as demonstrated by the resolution of the tonsillar descent and the syringomyelia following osseous decompression and surgical excision of the cyst walls.

As in other instances of hydrocephalus-associated syringomyelia, the initial treatment for hydrocephalus, in our patients, was aimed at alleviating the raised intracranial pressure and to prevent the risk of acute cerebellar herniation that can occur during the posterior fossa procedure, while the second operation consisted of a foramen magnum decompression with ample fenestration of the cysts.

We had included headaches as a clinical relevant factor for these patients. In the series by Helland and Wester [10], 11 out of 13 surgically treated posterior fossa arachnoid cyst presented with headaches, and only one of them had a poor clinical outcome after surgery. Two of our patients complained of retro-ocular pain—a symptom that could be attributed to stretching of the inferior portion of the tentorium by the crowded cerebellum. This feature resolved after surgery in one case, and in another, it was improved after conservative treatment. Certainly, chronic and persisting headaches hardly disappear totally after posterior fossa decompression.

We acknowledge that a shortcoming of our paper is the lack of preoperative CSF flow studies. However, in all our operated cases, we could verify the restoration of the CSF flow by direct inspection during the procedure through the open dura mater. In addition, the decrease in the volume of the syrinx after removal of the cyst walls and duraplasty, as shown by repeat neuroimaging studies, seems to indicate improvement in the CSF flow at the foramen magnum.

The presence of syringomyelia, the level of tonsillar descent, and the cyst size constitute key factors at the time of deciding surgical treatment. Syringomyelia alone constitutes a main indication for surgery. Interestingly, we have also documented the progressive enlargement of a quadrigeminal arachnoid cyst in one of our patients, until reaching a clinically significant size, during a 25-year follow-up time (Fig. 1). Three cases of relatively small cerebellopontine angle arachnoid cysts are being treated conservatively. We believe that a wait-and-see conduct can be indicated in selected cases that evolve with subtle clinical symptoms and have no syringomyelia. From our literature review and from our observations, it is obvious that patients with syringomyelia or CM-1 must be managed in an individualized manner. The pathogenetic factors, such as the presence of a posterior fossa arachnoid cyst and the coexistence with hydrocephalus, should be taken into account. This should tailor surgical treatment accordingly.

References

1. Alden TD, Ojemann JG, Park TS (2001) Surgical treatment of Chiari I malformation: indication and approaches. Neurosurg Focus 11(1), article 2
2. Arunkumar MJ, Korah I, Chandy MJ (1998) Dynamic CSF flow study in the pathophysiology of syringomyelia associated with arachnoid cysts of the posterior fossa. Br J Neurosurg 12:33–36
3. Banna M (1988) Syringomyelia in association with posterior fossa cysts. AJNR 9:868–873
4. Bauer AM, Mueller DM, Oró JJ (2005) Arachnoid cyst resulting in tonsillar herniation and syringomyelia in a patient achondroplasia. Case report. Neurosurg Focus 19(5):E14
5. Batzdorf U (1991) Syringomyelia related to abnormalities at the level of the craniovertebral junction. In: Batzdorf U (ed) Syringomyelia: current concepts in diagnosis and treatment. Williams & Wilkins, Baltimore, pp 22–23
6. Bertrand G (1973) Dynamic factors in the evaluation of syringomyelia and syringobulbia. Clin Neurosurg 20:322–333
7. Cano G, Anderson M, Kutschbach P, Borden Saris S (1993) Hydromyelia associated with posterior fossa. Surg Neurol 40:512–515
8. Chiari H (1895) Uber die veränderungen der kleinhirns, der Pons und der medulla oblongata in folge von congenitaler hydrocephalie des grosshirns. Denkschr Akad Wissensch Math Naturw Cl 63:71–116
9. Conti C, Lunardi P, Buzzao A, Liccardo G, Fraioli B (1993) Syringomyelia associated with hydrocephalus and Blake's pouch cyst. Spine 28:E279–E283
10. Helland CA, Wester K (2007) A population-based study of intracranial arachnoid cysts. Clinical and radiological outcome following surgical cyst decompression in adults. J Neurol Neurosurg Psychiatry 78:1129–1135
11. Jain R, Sawlani V, Phadke R, Kumar R (1993) Retrocerebellar arachnoid cyst with syringomyelia: a case report. Neurol India 48:81–83
12. Lee EJ, Yoon SH, Cho KH, Sim SY (2004) Syringomyelia as a sequelae of the 4th ventricular dilatation traumatic hydrocephalus and cerebellar atrophy. J Korean Neurosurg Soc 36:242–245
13. Marín-Padilla M, Marin-Padilla TM (2004) Morphogenesis of experimentally induced Arnold–Chiari malformation. Neurol Sci 50:29–55
14. Martínez-Lage JF, Almagro MJ, de San R, Pedro J, Ruiz-Espejo A, Felipe-Murcia M (2007) Regression of syringomyelia and tonsillar herniation after posterior fossa arachnoid cyst excision. Case report and literature review. Neurocirugia (Astur) 18:227–231
15. Martínez-Lage JF, Ruiz-Espejo A, Encarna-Guillen E, Almagro MJ (2008) Posterior fossa arachnoid cyst, tonsillar herniation, and syringomyelia in trichorhinophalangeal syndrome Type I. J Neurosurg 109:746–750
16. Milhorat TH, Chou MW, Trinidad EM et al (1999) Chiari I malformation redefined: clinical and radiographic findings for 364 symptomatic patients. Neurosurgery 44:1005–1017
17. Nishikawa M, Sakamoto H, Hakuba A et al (1997) Pathogenesis of the Chiari malformation: a morphometric study of the posterior cranial fossa. J Neurosurg 86:40–47
18. Nomura S, Akimura T, Imoto H, Nishizaki Suzuki M (2002) Endoscopic fenestration of posterior fossa arachnoid cyst for the treatment of presyrinx myelopathy. Case report. Neurol Med Chir (Tokyo) 42:452–454
19. Oldfield EH, Muraszko K, Shawker TH, Patronas NJ (1994) Pathophisiology of syringomyelia associated with Chiari I malformation of the cerebellar tonsils. Implications for diagnosis and treatment. J Neurosurg 80:3–15

20. Owler BK, Halmagyi GM, Brennan J, Besser M (2004) Syringomyelia with Chiari malformation: 3 unusual with implications for pathogenesis. Acta Neurochir (Wien) 146:1137–1143
21. Shinoda S, Tanaka K, Kawaguchi K (1998) A huge retrocerebellar arachnoid cyst with syringomyelia: case report. No Shinkei Geka 26:363–367 (Jpn)
22. Tokime T, Okamoto S, Yamagata S, Konishi S (1997) Syringomyelia associated with a posterior fossa cyst. Illustration of two cases. J Neurosurg 86:907
23. Tubbs RS, McGirt MJ, Oakes WJ (2003) Surgical experience in 130 pediatric patients with Chiari I malformation. J Neurosurg 99:291–296
24. Wakamoto H, Kobayashi K (1996) Syringomyelia associated with posterior fossa cyst: a case report. No Shinkei Geka 24:939–943 (Jpn)
25. Zager EL, Ojemann RG, Poletti CE (1990) Acute presentation of syringomyelia. Report of three cases. J Neurosurg 72:133–138

Comments

Ernst Delwel, Rotterdam, The Netherlands

The authors are to be complimented with their detailed description of ten patients with arachnoid cysts in the posterior fossa, combined with tonsillar herniation and, in six cases, syringomyelia.

They explain their arguments to choose between the different surgical approaches very well, and this is useful information. Treatment options are CSF shunting, removal of the arachnoid cyst, endoscopic procedures, and foramen magnum decompression besides a wait-and-see policy.

One question is still not solved: should we consider the arachnoid cyst and tonsillar herniation as a causal relationship or a concomitant circumstance. In other words, is the tonsillar herniation caused by the push of the space-occupying arachnoid cyst in the posterior fossa or are the cyst and the tonsillar herniation part of one congenital abnormality?

Since this question seems yet to be unsolved, the term secondary tonsillar herniation caused by a space-occupying arachnoid cyst in the posterior fossa seems to be the most appropriate description rather than using the term (acquired) Chiari malformation, as the term Chiari malformation refers to a limited volume of the posterior fossa on a congenital base.

Knut Wester, Bergen, Norway

In this brief review and small series of cases, Galarza et al. discuss the combination of posterior fossa arachnoid cysts (AC) and descent of the cerebellar tonsils through the foramen magnum, thus mimicking Chiari malformation type I. Interestingly, six of their patients also developed syringomyelia, most likely due to the compression of the content in the most caudal part of the posterior fossa.

An obvious question, as also raised by the authors, is whether the two malformations are concomitant or whether one of them (cerebellar descent) is caused by the other (AC). It is not surprising that any space-occupying lesion in the posterior fossa, arachnoid cysts included, may cause the tonsils to protrude through the foramen magnum. In true Chiari I malformations, the posterior fossa volume is assumed to be too small for the normal content. In the cases presented here, it reversely seems as if the normal-sized posterior fossa is filled with a content that is too voluminous and that this disproportion between the available space and the content is the cause of the cerebellar descent. However, a concomitance cannot be ruled out completely on the basis of the authors' findings; a considerable proportion of their patients (3 and 4) had relatively small cysts, mostly in the cerebellopontine (CP) angle, which hardly can explain the cerebellar descent.

We have in our department operated a considerable amount of posterior fossa cysts. In retrospect, we believe that some of these "cysts" in fact were not cysts at all, but megacisterna magnas. As a consequence of that, we now investigate such possible "false cysts" with CT scanning after intrathecal contrast instillation whenever we are in doubt about the nature of a large fluid assembly over the cerebellar hemispheres. If the fluid only represents a large cisterna magna, it will be filled immediately with contrast medium and appear bright white if the patient has been lying with the head down for only a minute, whereas the contrast will not enter the fluid compartment so rapidly if it is a true cyst.

After having read the present report, I believe we will abandon this invasive procedure as the first choice and instead look for a cerebellar descent on an MRI, as a megacisterna magna hardly causes this phenomenon.

It seems natural to assume that the present patients' problems and complaints were caused by the presence of the cyst in the posterior fossa. It was therefore somewhat surprising to learn that the authors preferred *not* to attack the posterior fossa pathology in as much as five of their ten patients. These patients were either not operated at all (two patients) or with a CSF diversion as the only (two patients) or the first operation (one patient). Personally, I believe I would have attacked the posterior fossa first, including the two patients with CP angle cysts. They both had persisting headache and dizziness. After having decompressed more than 20 CP angle cysts, it is our experience that these patients have a complete or near-complete relief of such symptoms.

Child's Nerv Syst (2002) 18:15–18
DOI 10.1007/s00381-001-0544-1

ORIGINAL PAPER

Anthony A. Virella
Marcelo Galarza
Michael Masterman-Smith
Rafael Lemus
Jorge A. Lazareff

Distal slit valve and clinically relevant CSF overdrainage in children with hydrocephalus

Received: 1 April 2001
Revised: 26 October 2001
Published online: 25 January 2002

A.A. Virella · M. Galarza
M. Masterman-Smith · R. Lemus
J.A. Lazareff (✉)
Division of Neurosurgery,
Pediatric Neurosurgery,
University of California
at Los Angeles (UCLA)
School of Medicine, Box 957039,
Los Angeles, CA 90095–7039, USA
e-mail: jlazareff@mednet.ucla.edu
Tel.: +1-310-2066677
Fax: +1-310-7942147

Abstract *Introduction:* Distal slit valve (DSV) is a system designed for the treatment of hydrocephalus. It has been assumed that, by dispensing with an anti-siphon (AS) mechanism, the DSV induces a set of clinical symptoms associated with fluid overdrainage in patients. Nonetheless, there is no published evidence to support this assumption. *Materials and methods:* Thus, to determine whether such an association is valid, we reviewed the records of 101 hydrocephalic patients (150 procedures) who had DSVs placed at our institution. The records of 40 hydrocephalic patients (69 procedures) in whom anti-siphon devices (AS) were placed were also reviewed. *Results:* One DSV patient presented with slit ventricle syndrome (SVS) and low intracranial pressure (ICP). No DSV patients had postoperative subdural collection. One AS patient had a postoperative subdural collection. Thirty-one DSV patients (31%) each required one revision, and 8 (8%) required more than one revision. Twelve AS patients (30%) required one revision and 8 AS patients (20%) required more than one revision. No significant differences were found between the DSV and AS groups in number of revisions, infections or overdrainage. *Conclusion:* We did not find a direct correlation between clinically relevant CSF overdrainage and DSV.

Keywords Distal slit valve · Pediatric hydrocephalus · Slit ventricle syndrome

Introduction

Numerous shunt devices have been designed for the treatment of hydrocephalus [18], the distal slit valve (DSV), introduced in 1974, being just one of them. Its design is simple, with a valve mechanism limited to a series of slits at the tip of the peritoneal catheter. Several years after the development and active utilization of the DSV and other valve types, a series of clinical syndromes, such as persistent headaches in shunted children, were attributed to rapid outflow of cerebrospinal fluid (CSF) [7, 8, 13, 14, 17, 25]. Following this, the routine use of the DSV fell out of favor and other, more elaborate, designs that included an anti-siphon mechanism (AS) were given preference.

To the best of our knowledge there has been no study that has directly linked the use of DSV with an increased incidence of clinically relevant CSF overdrainage. At our institution we have been utilizing the DSV since 1993. In order to increase our understanding of the clinical manifestations of CSF overdrainage and the putative use of DSV, we evaluated our experience with the use of the DSV to determine the incidence of slit ventricle syndrome (SVS) and extra-axial fluid collections in our patients.

Materials and methods

We reviewed the medical and surgical records of the pediatric patients who had a DSV placed as their first ventriculoperitoneal

shunt (VPS; Codman) at the UCLA Medical Center between 1993 and December 1999. We identified 101 patients, in whom 150 DSV shunt-related procedures were performed (group 1). For comparison, we also identified and reviewed the records of 40 pediatric patients in whom 69 AS shunt-related procedures were performed (Delta level 1, Medtronics, Radionics) (group 2).

The information gathered from these records included the age of the patient at the time of the operation, the etiology of hydrocephalus, and the specifics of the shunt failure. Patients were classified by primary cause of hydrocephalus, age at the time of their shunt procedure, the number of revisions and, in the DSV group, by the presence or absence of collapsed ventricles at follow-up.

In 80 group 1 patients we had radiographic images obtained an average of 4 months after shunt insertion. The patients did not present signs or symptoms of shunt failure. In those images we calculated the frontal-to-occipital horn ratio (FOR) as described in the literature [16]. In brief, the FOR is obtained by measuring the widest distances across the frontal horns and the occipital horns. The average of these measurements is then divided by the largest biparietal diameter.

Results

The etiologies of hydrocephalus for both groups are presented in Table 1. The age range of our patients for both groups was similar and extended from newborn to 17 years. It should be noted that this was a retrospective study and therefore random assignment to groups was not possible.

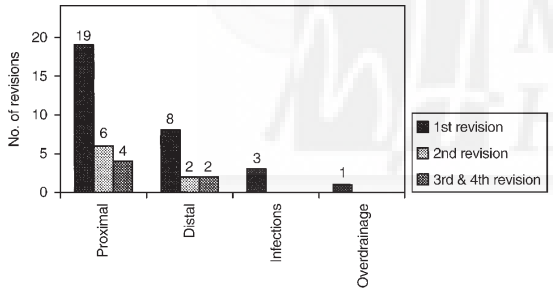

Fig. 1 Site of shunt failures in 31 hydrocephalic children treated with distal slit valves (DSV)

Thirty-one patients (31%) in the DSV group required a single shunt revision, and 8 (8%) required a second revision. Of the latter, 6 (6%) required a third shunt revision. Twelve patients (12/40, 30%) in group 2 required a single shunt revision, and 8 required a second revision (8/40, 20%). Only 1 patient in the AS group required a third revision. The intraoperative findings in 31 patients undergoing DSV shunt revisions are shown in Fig. 1. Of the 20 patients in group 2 who had a shunt malfunction, 16 had proximal dysfunction, 2 were distal, 1 outgrew the length of the peritoneal catheter, and 1 had a proximal and distal shunt obstruction. Three patients in group 1 (2.9%) and 4 patients in group 2 (4/40, 10%) developed shunt infection. They were treated according to the standard protocol. There was no statistically significant difference between the respective groups (Chi-square, $P<0.05$) regarding shunt revision and shunt infection (Table 2).

One patient had persistent headaches, and an intracranial pressure monitor (ICP) was therefore placed. It determined that she had negative ICP. Subsequently the DSV was removed and a shunt system with an anti-siphon device (Radionics) was placed, and her symptoms improved thereafter. On the imaging review, collapsed or silt-like ventricles were observed in 38 (47.5%) patients

Table 1 Etiology of infantile hydrocephalus in 101 distal slit valve (DSV) shunt patients and 40 patients with anti-siphon (AS) devices

Etiology	No. of patients		Percentage	
	DSV	AS	DSV	AS
Congenital	33	19	32	48
Tumor	22	7	21	17
IVH-PHH	20	2	20	5
Meningomyelocele	18	1	18	2
Meningitis	6	3	6	8
Arteriovenous malformation	0	2	0	5
Other/unknown etiology	2	6	2	15
Total	101	40	100	100

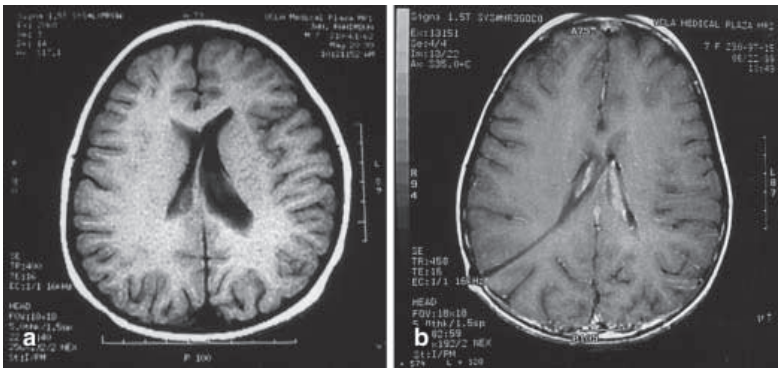

Fig. 2 **a** T1-weighted MR image of noncollapsed ventricles in a shunted patient. **b** T1-weighted MR image of collapsed ventricles in a shunted patient. Both images obtained while patient asymptomatic

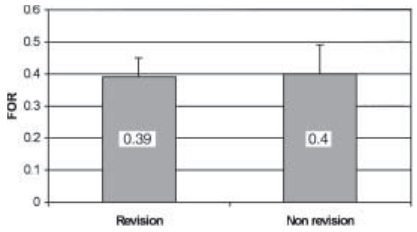

Fig. 3 Frontal-to-occipital horn ratio (FOR) in asymptomatic DSV-treated hydrocephalic patients. The FOR is obtained by measuring the widest distances across the frontal horns and the occipital horns. The average of these measurements is then divided by the largest biparietal diameter

Table 2 Number of patients with shunt failure and infection according to shunt group. No statistical significant difference was demonstrated

Type of shunt	Failures (*n*)			Infection (*n*)	
	None	1	2	No	Yes
DSV	62	31	8	98	3
AS	20	12	8	36	4

and noncollapsed ventricles were seen in 30 (37.5%) patients (Fig. 2). We noted dysmorphic ventricles in the other 12 (15%) cases. Congenital hydrocephalus was the primary diagnosis in 17 (45%) of the 38 patients with collapsed ventricles. Of the 80 patients with imaging reviews, 16 (42.1%) patients with collapsed ventricles and 8 (26.6%) patients with noncollapsed ventricles required at least one shunt revision.

The mean FOR ratio was calculated for the DSV patients with noncollapsed ventricles (Fig. 3). Of the patients with collapsed ventricles on imaging studies, only 1 developed the so-called slit ventricle syndrome as defined in previous reports [8, 17]. No extra-axial fluid collections were observed in any of the images studied.

Discussion

The DSV has been loosely associated with an elevated risk of CSF overdrainage. However, to the best of our knowledge, there is no published evidence that supports this assumption. In our series we observed that the development of clinical symptoms associated with CSF overdrainage is independent of AS mechanism utilization.

The overdrainage phenomenon includes the development of slit-like small ventricles, extra-axial fluid collection, and isolated unilateral ventricles. In some patients the collapsed lateral ventricles may lead to a clinical and radiological entity known as slit-ventricle syndrome (SVS). The incidence of SVS has not been well documented, because of variations in the way it is defined, but it was estimated in most series to be about 3–5% [3, 7, 8, 13, 15] of shunted cases. Slit-like ventricles are revealed by CT scan in at least one-third of all successfully shunted patients and their presence by itself does not constitute the SVS [12]. McLaurin and Olivi [17] defined SVS as including a slit-like appearance of the shunted ventricle on CT scans, a characteristic clinical manifestation of cyclic vomiting, headaches, and intermittent symptoms lasting for several days with slow refilling of the pumping device after manual compression. Epstein et al. [8] believed that the SVS is not a pathologic entity, but a common occurrence in children with shunts, which does not ordinarily cause symptoms or an increased incidence of malfunction. Other studies, however, support the concept of a pathologic state, such as decreased brain compliance [6], subependymal gliosis [6, 19], and hydrodynamic changes with decreased ependymal flow [19]. With reference to our findings, it is worth emphasizing that the observations above reported were recorded in patients who had more than one shunt system (Holter, Pudenz), and none of them had a DSV placed.

Although the follow-up radiological studies in our patients were performed only 4 months after surgery, we assume that a rapid drainage of CSF from the lateral ventricles would have had occurred by then. It is thus possible that the phenomena of low ICP following CSF overdrainage may not be related to the diversion of CSF alone. A recent study [1] in 20 patients demonstrated that even in the absence of CSF drainage, chronically shunted patients displayed a fall in ICP when assuming an upright position and that the venous volume changes may have a greater role in the postural pressure changes than does CSF shift.

In our series, 38 (47.5%) of the 80 patients whose films were reviewed demonstrated slit ventricles. However, only 1 of them experienced the SVS secondary to overdrainage, with subsequent low ICP. These findings are consistent with other studies [10, 17, 20] that led to the conclusion that only a minority of patients with radiographic evidence of slit or collapsed ventricles will become symptomatic. Furthermore, Hahn et al. [11] showed a radiographic slit ventricle in 50% of their patients in whom the double distal slit valve was utilized, whereas only 8.5% of these patients developed SVS and required shunt revision.

DSVs have been associated with an increased incidence of obstruction [11, 22, 23]. In some studies, a peritoneal catheter with a DSV increased the risk of obstruction more than the open-ended peritoneal catheter [22]. A retrospective study [23] led to the conclusion that proximal nonslit valve shunts become obstructed less often than shunts with DSVs. The most common form of failure was obstruction of the ventricular catheter, which was initially

associated with a collapsed ventricle [7, 8, 13]. Our shunt failure rate of 31% was consistent with those in other publications and independent of the type of shunt utilized [2, 5, 7, 8, 13, 14, 15, 17, 23]. Recently, a review of a Delta valve system [4] that has an integrated siphon control device showed a failure rate similar to ours and demonstrated that its performance was more or less the same as that of other differential pressure valves. In the present study, the primary infection rate of 2.9% in the DSV group was lower than the reported rates of infections observed [9, 14, 21, 22, 24]. The use of single-unit shunts and shorter operative times probably contributed to the relatively low infection rates seen in our series of patients.

Although a perfect shunt has not been developed, the results of our study reveal that the shunt with a DSV is cost-effective and relatively easy to install, and it was not associated with an increased incidence of shunt malfunctions compared with other series. Shorter operative times resulted in better patient outcomes, such lower infection rates, as seen in our patients.

Interestingly, the syndromes attributed to CSF overdrainage were not prevented by the routine use of AS shunt systems. Thus, the role that CSF overdrainage may have in the development of such conditions as slit ventricle syndrome needs to be re-examined.

References

1. Barami K, Sood S, Ham SD, Canady AI (2000) Postural changes in intracranial pressure in chronically shunted patients. Pediatr Neurosurg 33:64–69
2. Blount JP, Campbell JA, Haines SJ (1993) Complications in ventricular cerebrospinal fluid shunting. Neurosurg Clin N Am 4:633–656
3. Czosnyka Z, Czosnyka M, Richards HK, Pickard JD (1998) Posture-related overdrainage: comparison of the performance of 10 hydrocephalus shunts in vitro. Neurosurgery 42:327–334
4. Davis SE, Levy ML, McComb JG, Sposto R (2000) The delta valve: how does its clinical performance compare with two other pressure differential valves without antisiphon control? Pediatr Neurosurg 33:58–63
5. Drake JM, Kestle JR, Milner R, Cinalli G, Boop F, Piatt J, Haines S, Schiff SJ, Cochrane DD, Steinbok P, MacNeil N (1998) Randomized trial of cerebrospinal fluid shunt valve design in pediatric hydrocephalus. Neurosurgery 43:294–303
6. Engel M, Carmel P, Chutorian AM (1979) Increased intraventricular pressure without ventriculomegaly in children with shunts: “normal volume” hydrocephalus. Neurosurgery 5:549–552
7. Epstein FJ, Marlin AE, Wald A (1978) Chronic headache in the shunt-dependent adolescent with nearly normal ventricular volume: diagnosis and treatment. Neurosurgery 3:351–355
8. Epstein FJ, Lapras C, Wisoff JH (1988) ’Slit-ventricle syndrome': etiology and treatment. Pediatr Neurosci 14:5–10
9. George R, Leibrock L, Epstein M (1979) Long-term analysis of cerebrospinal fluid shunt infections. A 25-year experience. J Neurosurg 51:804–811
10. Gruber R, Glaser F (1986) Effect of the anti-siphon device (ASD) on the function of various hydrocephalus drainage systems in the child. Z Kinderchir 41:327–334
11. Hahn YS (1994) Use of the distal double-slit valve system in children with hydrocephalus. Child’s Nerv Syst 10:99–103
12. Hirayama A (1982) Slit ventricle – a reluctant goal of ventriculoperitoneal shunt. Monogr Neural Sci 8:108–111
13. Holness RO, Hoffman HJ, Hendrick EB (1979) Subtemporal decompression for the slit-ventricle syndrome after shunting in hydrocephalic children. Child’s Brain 5:137–144
14. Ignelzi RJ, Kirsch JM (1975) Follow-up analysis of ventriculoperitoneal and ventriculoatrial shunts for hydrocephalus. J Neurosurg 42:679–682
15. Kiekens R, Mortier W, Pothmann R, Bock WJ, Seibert H (1982) The slit-ventricle syndrome after shunting in hydrocephalic children. Neuropediatrics 13:190–194
16. Kulkarni AV, Drake JM, Armstrong DC, Dirks PB (1990) Measurement of ventricular size: reliability of the frontal and occipital horn ratio compared to subjective assessment. Pediatr Neurosurg 31:65–70
17. McLaurin RL, Olivi A (1987) Slit-ventricle syndrome: review of 15 cases. Pediatr Neurosci 13:118–124
18. Nulsen FE (1951) Treatment of hydrocephalus by direct shunt from ventricle to jugular vein. Surg Forum 2:399–403
19. Oi S, Matsumoto S (1986) Morphological findings of postshunt slit-ventricles in experimental canine hydrocephalus: aspects of causative factors of isolated ventricles and slit-ventricle syndrome. Child’s Nerv Syst 2:179–184
20. Portnoy HD, Schulte RR, Fox JL, Croissant PD, Tripp L (1973) Anti-siphon and reversible occlusion valves for shunting in hydrocephalus and preventing post-shunt subdural hematomas. J Neurosurg 38:729–738
21. Renier D, Lacombe J, Pierre-Kahn A, Sainte-Rose C, Hirsch JF (1984) Factors causing acute shunt infection. Computer analysis of 1174 operations. J Neurosurg 61:1072–1078
22. Sainte-Rose C (1989) Shunt failure. Concepts Pediatr Neurosurg 9:7–20
23. Sainte-Rose C, Piatt JH, Renier D, Pierre-Kahn A, Hirsch JF, Hoffman HJ, Humphreys RP, Hendrick EB (1991) Mechanical complications in shunts. Pediatr Neurosurg 17:2–9
24. Venes JL (1976) Control of shunt infection. Report of 150 consecutive cases. J Neurosurg 45:311–314
25. Walsh JW, James HE (1982) Subtemporal craniectomy and elevation of shunt valve opening pressure in the management of small ventricle-induced cerebrospinal fluid shunt dysfunction. Neurosurgery 10:698–703